

Porous Titanium for Biomedical Applications

Development, Characterization and Biological Evaluation

JiaPing Li

Members of the committee:

Chairman: Prof. Dr. W. Kruijer (University of Twente)
Promotor: Prof. Dr. K. de Groot (University of Twente)
Prof. Dr. C.A. van Blitterswijk (University of Twente)

Assistant promotor: Dr. J.R. de Wijn (University of Twente)

Members: Prof. Dr. J. Feijen (University of Twente)
Prof. Dr. J. D. de Bruijn (Queen Mary University of London)
Prof. Dr.S.K. Bulstra (UMC Groningen)
Dr. G.J.V.M. van Osch (ERASMUS MC. Rotterdam)
Dr. C. Otto (University of Twente)

Porous titanium for biomedical applications: Development; characterization and biological evaluation.

JiaPing Li

PhD Thesis, University of Twente, Enschede, The Netherlands

ISBN: 978-90-365-2479-7

This publication and research was sponsored by Camimplants, IsoTis Orthobiologics, PoroGen B.V. and Anna Fonds (Leiden, NL)



Het Anna Fonds
steunt onderzoek van
het menselijk steun- en
beveiligingsapparaat



cam implants



Copyright © J.P. Li, Enschede, The Netherlands, 2004. Neither this book nor its parts may be reproduced without written permission of the author.

Printed by: WPS, Zutphen, The Netherlands.

Cover designed by: Zhao Fu

POROUS TITANIUM FOR BIOMEDICAL APPLICATIONS

**DEVELOPMENT, CHARACTERIZATION AND BIOLOGICAL
EVALUATION**

DISSERTATION

to obtain
the doctor's degree at the University of Twente,
on the authority of the rector magnificus,
prof.dr. W.H.M. Zijm,
on account of the decision of the graduation committee,
to be publicly defended

on Wednesday March 21th 2007, at 13.15

by

JiaPing Li

Born on October 23th, 1965
in Anhui, China

Promoters: Prof. Dr. Klaas de Groot
Prof. Dr. Clemens A. van Blitterswijk

Co-promotor: Dr. Joost. R. de Wijn

My son and my wife
My parents

List of Publications

This thesis was based on the following publications:

Peer reviewed papers

J. P. Li, S. H. Li, C. A. van Blitterswijk and K. de Groot. Factors having influence on the rheological properties of Ti6Al4V slurry. *J Mater Sci Mater Med.* 2004 Sep;15(9):951-8.

J. P. Li, S. H. Li, C. A. van Blitterswijk, K. de Groot. A novel porous Ti6Al4V: characterization and cell attachment. *J Biomed Mater Res A.* 2005 May; 73 (2):223-233.

Habibovic P, **Li J**, van der Valk CM, Meijer G, Layrolle P, van Blitterswijk CA, de Groot K. Biological performance of uncoated and octacalcium phosphate-coated Ti6Al4V. *Biomaterials.* 2005 Jan;26(1):23-36.

J. P. Li, Joost R. de Wijn, C. A. Van Blitterswijk and K. de Groot. Porous Ti6Al4V scaffolds directly fabricated by 3D fibre deposition technique: effect of nozzle diameter. *J Mater Sci Mater Med.* 2005 Dec;16(12):1159-63.

Jia Ping Li, Joost R. de Wijn, Clemens A. van Blitterswijk and Klaas de Groot. Porous Ti₆Al₄V scaffold directly fabricating by rapid prototyping: Preparation and in vitro experiment. *Biomaterials.* V 27(8), 2006 Mar, P 1223-1235.

J. P. Li, S. H. Li, C. A. van Blitterswijk and K. de Groot. Cancellous bone from porous Ti6Al4V by multiple coating techniques. *J Mater Sci Mater Med.* 2006 Feb;17(2):179-85.

Y.Liu, **J.P.Li**, E.B. Hunziker and K.de Groot, Incorporation of Growth Factors into Medical Devices via Biomimetic Coatings. *Phil.Trans.R.Soc.A*, (2006) 364, P233-248.

J. P. Li, J. R. de Wijn, C A. van Blitterswijk and K. de Groot. The effect of scaffold architecture on properties of direct 3D fiber deposition porous Ti6Al4V for orthopaedic implants. Submitted to *J Biomed Mater Res A*.

J. P. Li , P. Habibovic, M. van den Doel, C. E. Wilson, J. de Wijn, C. A. van Blitterswijk and K. de Groot. Bone ingrowth in porous titanium implants produced by 3D fiber deposition. *Biomaterials*, in press.

JiaPing Li, Pamela Habibovic, Clayton E. Wilson, Joost de Wijn, Clemens A. van Blitterswijk and Klaas de Groot. Biological performance of porous composite implants based on titanium alloy and biphasic calcium phosphate ceramic: in vivo study in goats. Submitted to *Biomaterials*.

Patents

J. P. Li, P. Layrolle, K. de Groot. Porous metals and metal coatings for implants. WO 02/066693.

Selected abstracts

J. P. Li, C A. Van Blitterswijk and K. de Groot. Porous titanium with reticulate structure for orthopaedic implant. 10th world conference on Titanium. Volume V, 3157-3164. Hamburg. Germany. 2003.

J. P. Li, J. R. de Wijn, C A. Van Blitterswijk and K. de Groot. In vitro study of MC3T3-E1 cells on porous Ti6Al4V scaffolds fabricated using a 3D fiber deposition technique. 19th European Conference on Biomaterials. Sorrento, Italy, 2005.

J. P. Li, J. R. de Wijn, C A. Van Blitterswijk and K. de Groot. Porous Ti6Al4V scaffolds directly fabricated by 3D fiber deposition technique. 19th European Conference on Biomaterials. Sorrento, Italy, 2005.

J. P. Li, J. R. de Wijn, C A. Van Blitterswijk and K. de Groot. Ectopic bone formation by goat bone marrow cells cultured on different porous Ti6Al4V scaffold. 20th European Conference on Biomaterials. Sorrento, Italy, 2005.

J. P. Li, C. Wilson, J.R.Wijn, C.A Van Blitterswijk, K.De Groot. Comparison of porous Ti6Al4V scaffold made by 3D fiber deposition and 3D printed mould. 20th European Conference on Biomaterials. Nantes, France, 2006.

J. P. Li, J. R. de Wijn, C A. Van Blitterswijk and K. de Groot. Comparison of porous Ti6Al4V made by sponge replication and directly 3D fiber deposition and

cancellous bone. Key Engineering Materials Vols. 330-332 (2007) pp. 999-1002.

J. P. Li, C. Wilson, J. R. deWijn, C.A. van Blitterswijk, K.De Groot. Fabrication of porous Ti6Al4V with designed structure by rapid prototyping technology. Key Engineering Materials Vols. 330-332 (2007) pp. 1293-1296.

Table of Contents

Introduction	1
Chapter 1	
General introduction and Aims.....	3
Part I Development of a Novel Porous Titanium Alloy by Sponge Replication	37
Chapter 2	
Factors of influences on the rheological properties of titanium alloy slurry.....	39
Chapter 3	
A novel porous Ti6Al4V: characterization and cell attachment	57
Chapter 4	
Improvement of mechanical properties of porous titanium alloy.....	77
Part II Development of Porous Titanium Alloy by Rapid Prototyping	91
Chapter 5	
Porous Ti6Al4V scaffold directly fabricated by rapid prototyping: preparation and in vitro experiment	93
Chapter 6	
Porous Ti6Al4V scaffolds directly fabricated by 3D fiber deposition technique: effect of nozzle diameter.....	117
Chapter 7	
The effect of scaffold architecture on properties of direct 3D fiber deposition porous Ti6Al4V for bone tissue engineering and orthopaedic implants.....	127

Part III Biological Properties of Porous Titanium Scaffold	147
Chapter 8	
Comparison of porous titanium alloy made by sponge replication and 3D fiber deposition	149
Chapter 9	
Bone ingrowth in porous titanium alloy implants produced by 3D fiber deposition.	161
Chapter 10	
Bone tissue reconstruction using porous titanium alloy combined with biphasic calcium phosphate ceramic: in vivo study in goats.....	183
General discussion	207
Chapter 11	
General discussion and future perspectives.....	209
Summary	221
Samenvatting	224
Acknowledgements	227
Curriculum Vitae	229

The background of the slide is a close-up photograph of a white, porous material with a complex, interconnected lattice structure. The material has numerous irregular, oval-shaped holes of varying sizes, creating a honeycomb-like appearance. The lighting is soft, highlighting the texture and depth of the material.

Introduction

Chapter 1
General introduction and Aims

Chapter 1

General introduction and Aims

1. Metallic biomaterial as bone graft substitute

1.1. Bone graft substitute

At present, the most widely used clinical therapies for bone replacement and regeneration employ autologous- and allogeneic bone grafts. It is well known that autologous bone graft is considered to be the golden standard in, for instance, spinal fusions, i.e. for achieving a bony bridge between transverse processes. However, treatments with both autografts and allografts exhibit a number of limitations. The harvest of the autologous graft requires an additional invasive surgical procedure that may lead to donor site morbidity, chronic post-operative pain, hypersensitivity and infection [1-5]. Another important drawback of the use of autograft is the limited availability. Unlike autologous bone, allogeneic grafts are widely available and do not require an additional surgery on the patient. However, allogeneic bone has to undergo processing techniques such as lyophilization, irradiation or freeze-drying to remove all immunogenic proteins in order to avoid any risk of immunogenic reaction [6]. In turn, these processing techniques have a negative effect on osteoinductive and osteoconductive potential of allograft [7], which consequently decreases its biological performance as compared to autograft [8].

Due to disadvantages of natural bone grafts, the use of synthetic biomaterials for orthopaedic reconstructive surgery as a means of replacing autografts and allografts is of increasing interest and a large number of scientific reports confirm this trend. Calcium-phosphate based biomaterials, such as ceramics and cements, and polymeric biomaterials are attractive as they can be produced in such a way that they mimic the mineral composition and/or structure of bone. However, although ceramics show excellent corrosion resistance and good bioactive properties, porous ceramic structures, as they are available today, are limited to non load-bearing applications [9,10], due to their intrinsic brittleness. Likewise, porous polymeric systems are deemed to be ductile with insufficient rigidity and inability to sustain the mechanical forces present in bone replacement surgery.

Metals have so far shown the greatest potential to be the basis of implants for long-term load-bearing orthopaedic applications, owing to their excellent

mechanical strength and resilience when compared to alternative biomaterials, such as polymers and ceramics. Particularly, titanium and its alloys have been widely used in orthopedic and dental devices because of their excellent mechanical properties and biocompatibility [11,12].

1.2. Background on metallic biomaterials

Metallic biomaterials have the longest history among various biomaterials. Medical use of metals aroused in India several thousand years ago, evolved in Europe with the rise of Western science and medicine, as well as in North America as the frontiers expanded and the cities grew [11]. In 1950's, stainless steel was first successfully used as an implant material in the surgical field [13]. Then, vitallium, a cobalt-based alloy was put into practical use. Titanium is the "newest" metallic biomaterial and, together with stainless steels and cobalt-based alloys, one of the most frequently used metals in biomedical applications.

The extensive use of metallic alloys is related to the availability and success at the beginning of the last century of several different alloys made of the noble metals. Clinical studies with implants made of iron (Fe), cobalt (Co), chromium (Cr), titanium (Ti), and tantalum (Ta) have demonstrated that these metals and their alloys can effectively be manufactured and safely be used as orthopedic implants. The mechanical, biological, and physical properties of these materials play a significant role in their longevity.

Metals designed to be applied as substitute for bone grafts have to fulfill certain requirements:

- 1: A good corrosion resistance to avoid degradation in the biological environment.
- 2: Biocompatibility. such as no toxic, no injurious or allergic reaction on biological systems occurs.
- 3: Adequate mechanical properties such as high fatigue strength and a Young's modulus similar to that of human bone are necessary to avoid fracture and stress-shielding.
- 4: In order to achieve the sake of cost-saving and good processability, materials need to be relatively easy to process by e.g. like casting, deformation, welding or brazing.
- 5: And last but not least, the availability is an important factor in choice of a material for biomedical applications.

In general, physical properties play an important role only in the case of special functional applications as in heart pacemaker electrodes. Good chemical and biological properties are a prerequisite for application in orthopaedic and maxillofacial surgery. The most important mechanical properties for highly loaded implants such as hip endoprostheses are fatigue strength and Young's modulus.

Based on specific properties such as corrosion resistance and biocompatibility, metals and alloys which are suitable for orthopedic and maxillofacial surgery can be divided into four groups:

1. Stainless steels (e. g. DIN/ISO 5832-1 or AISI 316L)
2. CoCr-alloys (cast DIN/ISO 5832-4 or wrought DIN/ ISO 5832-6)
3. Cp-Ti (commercially pure Ti, DIN/ISO5832-2) or Ti alloys such as Ti6Al4V (DIN/ISO 5832-3)
4. Ta

- **Stainless steel**

Nowadays, stainless steel is a frequently used biomaterial for internal fixation devices because of a favorable combination of mechanical properties, corrosion resistance and cost effectiveness when compared to other metallic implant materials. Surgical stainless steel alloys (316L) made with varying amounts of Fe, Cr, and nickel (Ni), which were developed in 1950s, are presently being used for manufacturing of prostheses. The low carbon and high chromium contents improve corrosion resistance by passivation and decrease adverse tissue responses and metal allergies. The passive layer is not as robust as in Ti and CoCr alloys. Biocompatibility of stainless steel has been proven by successful clinical studies for decades. However, due to the relatively high Ni content (10–14%) stainless steel implants may cause negative tissue reactions and dermatitis [14]. Therefore, new Ni-free austenitic stainless steels with excellent mechanical properties and biocompatibility have been developed [15].

Metallurgical requirements are stringent to ensure sufficient corrosion resistance, non-magnetic response and satisfactory mechanical properties [15]. In orthopedic and trauma surgery, stainless steel is mainly used when stiffness is required. The ductility of stainless steel is higher than that of cp Ti, because of its hexagonal crystal structure. This makes contouring of stainless steel plates easier, compared to Ti plates [16]. Therefore, reconstruction plates made of stainless steel are favored in acetabular and pelvic surgery and at some other anatomical locations. Still, fatigue failure and corrosion rates higher than occur in Ti make it a poor candidate for the production of modern joint replacement implants.

As far as mechanical properties are concerned, shortcomings of stainless steel have also been described. In the case of internal fixation of fractured bones by means of bone-plates fastened to bone on its tensile surface, an on-going concern has been the excessive stress-shielding of the bone by the exceedingly stiff stainless-steel plates (15).

- **Cobalt –chromium alloys**

The use of CoCr alloys for surgical applications is mainly of interest for orthopedic knee-, shoulder- and hip prostheses prosthesis [17]. Implants made of Co, Cr and

molybdenum (Mo) allow for the production of very hard implants and possess a high corrosion resistance in body fluids [17]. Co-based alloys (e.g. CoCrW, CoCrMo) have a Young's modulus of about 250 ± 10 GPa as well as a high wear resistance.

Although somewhat less biocompatible than chemical pure titanium (cp Ti), Co-based alloys have advantages in joint arthroplasty due to high corrosion and wear resistance. The femoral components of most knee arthroplasties are, therefore, made of Co-based alloys [18].

However, CoCr alloys are among the least ductile when metals for biomedical applications, which makes them difficult to manufacture. CoCr alloys also have high moduli of elasticity. As a result, considerable stress shielding and thigh pain were observed in the first generation of biologically fixed femoral hip implants made of Co alloys.

- **Titanium and titanium alloys**

Ti and some of its alloys are used as biomaterials for dental and orthopaedic applications. The most common grades are cp Ti and the Ti6Al4V alloy, originally designed for aerospace applications.

Cp titanium was introduced as an implant material in medicine in 1965 and was first used for manufacturing bone plates and screws. Cp Ti has a high corrosion resistance and an outstanding biocompatibility [19]. Ti derives its resistance to corrosion from the formation of a solid oxide layer with a thickness of around 3-7 nm [20]. This oxide layer forms spontaneously on the implant surface in presence of oxygen. The passivation by the oxide layer [21] is robust and persistent under physiological conditions and corrosion currents in normal saline are very low: 10^{-8} A.cm⁻². Ti implants remain virtually unchanged in appearance after implantation. Although Ti offers superior corrosion resistance, it is not as stiff or strong as steels or Co-Cr alloys.

The biomechanical properties of cp Ti mostly depend on the amount of trace elements present in the alloy. Four grades of cp Ti for medical applications are distinguished. This grading is based upon the amounts of nitrogen, carbon, hydrogen, iron and oxygen (ISO 5832-2). Increasing amounts of trace elements elevate tensile strength but reduce the ductility.

Ti plates, used for osteosynthesis, offer less stress-shielding to bone tissue as compared to other metals, because of their low Young's modulus [16]. Therefore, Ti is an ideal biomaterial for plates and screws used for fracture treatment. Nevertheless, the ductility of Ti is low as compared to stainless steel, because of its crystal structure which makes contouring of Ti plates relatively difficult [16].

To further improve the mechanical strength of Ti implants, Ti alloys have been developed. The most common one is Ti6Al4V. This Ti alloy has the greatest

commercial potential and is widely used in load-bearing orthopedic implants due to its relatively good fatigue resistance and biological passivity [22]. Implant sensitivity to Ti alloys occurs very seldom [23], despite the presence of components such as vanadium which are described to be cytotoxic [24]. In vivo studies have shown that Ti6Al4V has similar biological compatibility as vanadium-free Ti alloys [25].

It has been shown that cp Ti and Ti alloys perform better in cell culture experiments with human osteoblasts as compared to stainless steel and Co-based alloys [26]. The improved viability and osteogenic differentiation rate of human osteoblasts on cp Ti and Ti alloys indicate an improved biocompatibility as compared to stainless steel and CoCr alloys [26]. Therefore, for uncemented knee and hip arthroplasties, Ti alloys may be favorable implant materials. Additionally, Ti alloys have successfully been used for intramedullary rods, spinal clamps, self-drilling bone screws and other implants [24]. Cp Ti in combination with Ti alloys does not induce galvanic corrosion response, which makes the combination of the two materials possible. Satisfying biocompatibility, a low level of corrosion, and the modulus of elasticity closer to that of bone as compared to other metals have yielded excellent long-term results with Ti and Ti alloy implants.

- **Tantalum**

Ta is also remarkably resistant to corrosion and has been used as an ingredient in super alloys, principally in aircraft engines and spacecraft, although 50% of its current use is in the form of powder metal for manufacturing transistors and capacitors. Ta has only recently been used for the production of bone graft substitutes. Ta can be fabricated in a highly porous form, which has a modulus of elasticity closer to that of bone than stainless steel or the CoCr alloys. Recent use of Ta has been in the form of a honeycombed structure that is very porous and conducive to bone ingrowth [27-29]. It is currently available in several forms for bridging bone defects, but its use in the manufacture of femoral stems has yet to occur. Ta appears to be a promising metal for use in acetabular reconstruction, but long-term studies need to be conducted.

1.3. Mechanical properties

The applicability of various material types in orthopaedic and maxillofacial surgery largely depends on their mechanical properties. Table 1 shows that metallic materials are suitable for bearing virtually every kind of load depending on their specific properties, while ceramics can only be highly loaded by compression stresses.

Table 1 Applicability of biomaterials to different types of mechanical loads [11,30]

Type of loading	Metals	Ceramics	Polymers
Static			
Tension	suitable	Not suitable	Suitable only under low stresses
Compression	suitable	suitable	Suitable only under low stresses
Bending	suitable	Not suitable	Suitable only under low stresses
Torsion	suitable	Not suitable	Suitable only under low stresses
Dynamic			
Tension compression	suitable	Not suitable	Suitable only under low stresses
Pulsating tension	suitable	Not suitable	Suitable only under low stresses
Pulsating compression	suitable	suitable	Suitable only under low stresses
Impact	suitable	Not suitable	

Table 2 Mechanical properties of different biomaterials [11]

Type of biomaterials	Density (g/cm ³)	ultimate tensile strength [MPa]	Young's Modulus (GPa)	fatigue strength ^a [MPa]	elongation at fracture [%]
Metals					
CrNi-steels	7.8	490 - 690	200	200 - 250	> 40
CoCr-alloys	8.5	800 - 1200	230	550 - 650	8 ± 40
cp-Ti	4.5	390 ± 540	100	150 ± 200	22 ± 30
Ti6Al4V	4.5	930 ± 1140	105	350 ± 650	8 ± 15
Ceramics					
Al ₂ O ₃	3.2	350		0/400 ^b	<1
Zr O ₂	3.5	350-400		0/450 ^b	<1
Polymer					
PMMA	1.2	24-28		20-30	<1
UHMWPE	1.4	37-46		16	
Cortical bone		80-150	7-30		

^a Rotating bending fatigue

^b Compression/compression

Table 2 summarizes mechanical properties of different biomaterials. High ultimate tensile and fatigue strength combined with sufficient elongation at fracture can be seen for both CoCr- and Ti alloys. Stainless steels show reduced tensile and fatigue strength but higher ductility. The pure metals Ti, Ta and niobium have reduced strength properties but high values for elongation at fracture. Zirconia ceramic has a higher toughness and fatigue strength than alumina ceramic. The

mechanical properties of polymers are poor under tensile and compression stresses. Therefore, ceramic and polymers are only applicable in special parts of constructions, such as in hip prosthesis heads or cups. Metallic materials offer a wide range of mechanical properties so that a suitable selection according to the mechanical requirements is possible.

A comparison of the biofunctionality of various alloys shows the exceptional properties of Ti and its alloys due to their low Young's modulus (Fig. 1).

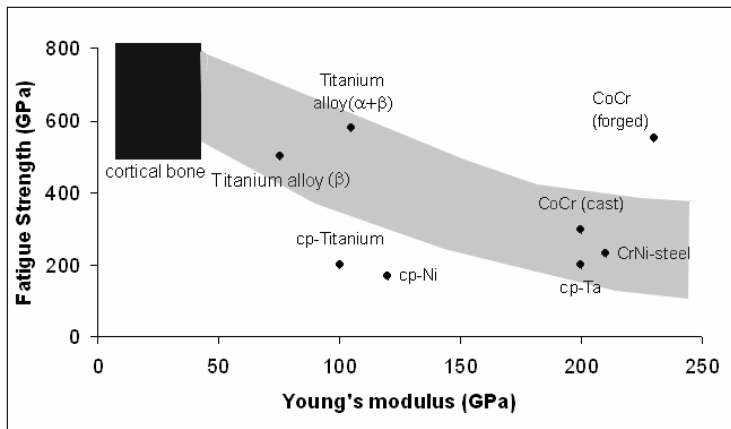


Fig. 1. Biofunctionality of metallic biomaterials [1]

From the biomechanical point of view, it is desirable to have a Young's modulus comparable to that of bone in order to achieve a good load transfer from the implant into the bone, leading to a continuous stimulation of new bone formation [31]. A further reduction of Young's modulus of Ti alloys can be achieved by alloying with β -stabilizing elements. For example, the alloy Ti30Ta which belongs to the group of near β -Ti alloys shows a reduction of Young's modulus of 80% as compared to cp Ti.

In order to provide a modulus comparable to that of compact (10 - 15 GPa) and cancellous bone (0.5 - 5 GPa), porous sintered implants are required. The reduction of Young's modulus as a function of the porosity can be calculated by means of equation [32]:

$$E_p = E_0 (p)^{3/2}$$

Where E_p is the Young's modulus of the porous sintered material, E_0 the modulus of the bulk material and p the porosity. Figure 2 shows Young's moduli for different porous sintered biomaterials as a function of their porosity. It can be seen that with alumina ceramic, even with a porosity of 40%, no modulus comparable to that of bone can be achieved. In contrast, Ti shows a low Young's modulus, close to that of bone even with relatively low values of porosity.

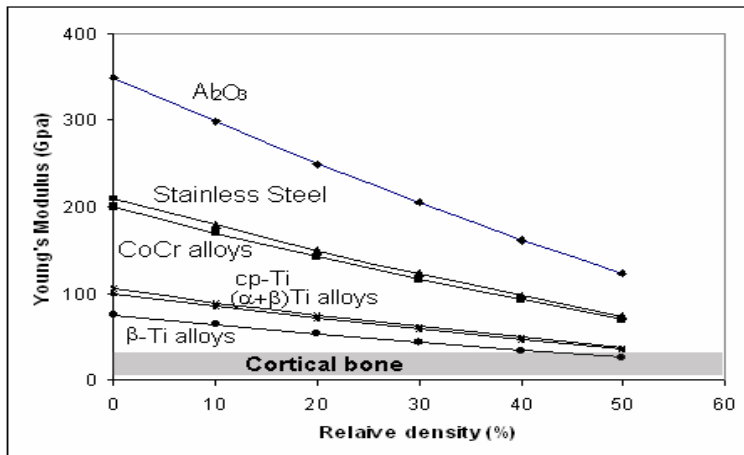


Fig.2 Young's moduli of different materials as a function of their porosity

Most metallic biomaterials have a significantly higher (2 to 4 times) density and are much stiffer (5 to 10 times) than human bone. Too much stiffness and weight tend to create undesirable conditions leading to stress shielding, bone resorption and atrophy. Density of Ti and its alloys is significantly lower than that of other metallic materials (Table 2) making Ti based implants lighter than similar implants made of stainless steel or CoCr alloys.

Up to now most implants Ti based are used in dense form, although with dense forms, problems, such as interfacial instability within host tissues, biomechanical mismatch of elastic constant and lacking biological anchorage for tissue ingrowth, may occur [33,34]. In general, joint replacement failure is rarely due to the mechanical failure of materials, such as fatigue fracture of the implant. A more common cause of arthroplasty failure is aseptic loosening of the implant. This occurs several years after the implant has been in situ and functioning reasonably [11]. Requirements for highly loaded endosseous implants such as hip endoprostheses include, in addition to sufficient mechanical properties, a good load transfer from the implant into the bone in order to stimulate the formation of new bone, leading to good long term implant integration. A reduction of Young's modulus to a value similar to that of the bone provides this isoelastic behavior.

2. Implant- tissue interface and reliable implant fixation

Regarding the long-term load-bearing implant, a successful performance requires reliable anchoring of implants into host tissue. For orthopaedic and dental implants, this means secure fixation to bone. Reliable implant fixation can be achieved by

use of surface modification or by introduction of porosity that allows mechanical interlocking between bone and implant.

There exist a number of surface modification processes. These include machined macroscopic anchorage elements such as threads, vents, fins and surface grooves or serrations as well as microscopic surface features that can be formed by: 1) removal of material from an implant surface through grit blasting, chemical or ion etching of the device, and 2) application of a porous coating or porous bulk materials. The three dimensional open porous structure is particularly suitable for implant fixation since porous surfaces provide biological anchorage for the surrounding bony tissue via the ingrowth of mineralised tissue into the pore space [35-39].

During the past 30 years, porous metallic orthopaedic implants have been used for fixation purposes. Investigations using porous metallic implants were initiated in the late 1960s and the early 1970s. In 1968, Hirschhorn was the first to report on the fabrication of a porous metal (a CoCr alloy) for use as an implant material [40]. One year later, Lueck et al. reported on manufacturing and implantation of a porous material consisting of pure Ti fibres [41]. During the early 1970s, Welsh, Galante, Pilliar and Cameron [42-52] developed porous metal coatings, which were further developed by Bobyn and others [41,42,53-56]. These dual-structured implants were prepared using particulate based methods (sintered metal powders or fibers), which yielded a porous surface around a solid-machined or cast metallic core. On the basis of clinical results and of histological evidence obtained from retrieved implants, these porous implants revealed to be biologically fixed by the ingrowth of bony- or other tissue. The ingrowth of bone into the porous structure ensured a good transfer of mechanical forces.

There are two types of porous implants: dense implants with porous surface and completely porous (porous bulk) implants.

3. Fabrication of porous titanium and titanium alloys

3.1. Conventional methods for producing porous titanium

Unlike Al, porous Ti is difficult to be produced from the liquid state, due to its high melting point and high contamination susceptibility. Existing processes are therefore based on powder metallurgy. A number of processes have been applied to produce porous Ti and Ti alloy implants. Generally these different methods can be classified as follows:

(1) Particle sintering

Porous surfaced coatings and porous bulk materials can be produced by sintering of uniformly sized beads under isostatic pressing or loose packing [57,58]. The

volume fraction of porosity is associated with the degree of particle interconnectivity and particle size and can be controlled by process variables such as compacted powder density, sintering temperature and time, and alloying additions. This method results in: (i) a low porosity (generally less than 50%), (ii) difficult to control pore size, which is depending on shape and size of the particles and (iii) incompletely interconnected pores.

(2) Fiber and wire mesh

Galante et al. [43] first reported on the implantation in animals of sintered fiber metal composites consisting of short Ti fibers. The procedure is similar to particle sintering with the difference that instead of particles, fibers or wire mesh are used. The major disadvantage of the metal fiber sintered porous coatings compared to the coatings made by powder metallurgy techniques is that fibers must be compacted to a form prior to sintering. It is therefore difficult to coat complex shapes that do not allow compaction forces to be applied directly on the fibers. Another disadvantage of this method is a sometimes occurring inadequate coating-substrate contact due to insufficient fiber compaction. In addition, the porosity of metal fiber coatings is limited to 30–50% by volume, which directly limits bone ingrowth.

(3) Space holder method

Porous surfaced coating and bulk Ti can also be fabricated by mixing Ti powder with an organic space holder followed by the compaction (e.g. uniaxial or isostatic) of the mix to form a green body. The space holder is made of carbamide powder or ammonium hydrogen carbonate [59-61]. This organic material is subsequently removed by thermal treatment, leaving a porous metallic scaffold. The pore size can be controlled by selecting a suitable size of organic spacer particles. The disadvantages of this method are the difficulty to remove large quantities of the space holder material from the compacted mix and to control the interconnectivity of the pores.

(4) Plasma spraying

Hahn and Palich first described a Ti plasma-sprayed coating for fabricating porous-coated implants [62]. They used Ti hydride powders fed into a plasma flame, whereby the decomposed Ti was deposited onto an appropriate substrate. In general, Ti powder is sprayed onto the surface of an implant under reduced pressure condition in an inert gas chamber at a high temperature. This yields a coating with an irregularly shaped porous surface. Plasma spraying was also used to make bulk Ti implants and implants with [63] a gradual change in porosity from the substrate-coating interface to the coating surface [64,65]. The drawbacks of plasma spraying are the poor interconnectivity of the pores and a relatively small pore size.

(5) Combustion synthesis

A recently developed method of producing high purity porous alloys and in particular NiTi alloys is a process known as combustion synthesis [66-68]. In combustion synthesis particle fusion is obtained through an extremely rapid self-sustaining exothermic reaction between Ti and Ni powder to form an intermetallic compound. An advantage of this fabrication process is the high purity of the resulting foams, which is largely due to the expulsion of volatile impurities under the extremely high temperatures in the process. The drawback of this method is that it is difficult to control the pore size, pore interconnectivity and the amount of Ni.

(6) Foaming by H₂O₂

In this method, Ti powder is mixed with an organic solvent to make a Ti slurry, to which H₂O₂ is subsequently added to act as a foaming agent. The pore size and porosity can be adjusted by the dosage of H₂O₂ [69]. Limitation of the method is the inability to control the porosity and interconnectivity.

(7) Electrical discharge sintering

This method is similar to powder sintering, with the difference that in electrical discharge sintering method. Sintering of powder is achieved by combination of electrical discharge with rapid heating and pressure application. Unlike conventional sintering techniques of Ti and Ti alloy powders, that require maintaining a high sintering temperature (1200–1400°C) in high vacuum (<10⁻⁴ Pa) for a long time (18-38hrs) [70], electrical discharge sintering process is performed in a relatively short period of time.

(8) Argon expansion process

In this processing technique, compressed argon gas is entrapped in a Ti body during heat-compaction of Ti powders; the resulting argon bubbles are then expanded by exposure to a high temperature [71,72], where the densified Ti matrix rapidly creeps. .

A brief description and comparison of methods to produce porous Ti and its alloys are summarized in Table 1. Porous Ti produced using different techniques has shown good clinical successes [73,74]. However, from the overview above, it is obvious that there is room for improvement in the existing production methods.

Table 1: Overview of merits and drawbacks of the porous Ti and Ti alloys made by powder metallurgy

Method	Material	Advantages	Drawbacks
Pressure shaping	Ti beads [75-77]	<ul style="list-style-type: none"> • Relatively simple to produce; • Interconnected pores; • Narrow pore size distribution; 	<ul style="list-style-type: none"> • Low porosity (<45%); • Pore size as function of particle size;
	Ti mesh [43,44,78,79]	<ul style="list-style-type: none"> • Interconnected pores 	<ul style="list-style-type: none"> • Relatively difficult to produce; • Low porosity;
	Ti powder+ space holder [59]	<ul style="list-style-type: none"> • Relatively simple method; • Porosity up to 80%; • Controllable pore size and porosity; 	<ul style="list-style-type: none"> • Difficult to control pore interconnectivity; • Many closed pores;
Pressureless shaping	Ti beads [33,80]	<ul style="list-style-type: none"> • Easy to produce; • Interconnected pores; • Narrow pore size distribution; 	<ul style="list-style-type: none"> • Low porosity (<45%); • Pore size as function of particle size;
Special shaping -Plasma spray	Ti powder [56,63]	<ul style="list-style-type: none"> • Commercially most successful for surface-coating; 	<ul style="list-style-type: none"> • Lack of interconnected pores; • Small pore size; • Variable porosity;
Combustion synthesis	Ti powder and Ni powder [66-68]	<ul style="list-style-type: none"> • No binder to remove; 	<ul style="list-style-type: none"> • Low interconnective pore size;
Foaming by H ₂ O ₂ [69]	Ti powder	<ul style="list-style-type: none"> • Relatively simple method; 	<ul style="list-style-type: none"> • Low porosity; • Non-controllable pore size; • Poor pore interconnectivity;
Electrical discharge sintering [70]	Ti powder	<ul style="list-style-type: none"> • Fast sintering; 	<ul style="list-style-type: none"> • Pore size as function of the particle size;
Argon expansion process [71,72]	Ti powder		<ul style="list-style-type: none"> • Low porosity; • Poor pore interconnectivity;

3.2. A novel technique to produce porous titanium and its alloys: positive sponge replication

Recently, we have developed a novel type of porous Ti6Al4V implant using a positive sponge replication method as shown in Fig.3. Briefly, commercially available polyurethane foams are dipped into Ti6Al4V slurry. The excess slurry is then removed by a press roller. The dipping-pressing process is repeated until all the struts of the polyurethane foam are coated with the Ti-alloy slurry. After drying, the samples are heated in argon to 500°C to burn out the foam. Finally, the metal bodies are sintered in a vacuum furnace (10^{-5} mbar) at 1250°C with a holding time of two hours.

The advantages of fabricating porous Ti6Al4V using this method include a closely controlled size of both pores and pore interconnection, and a virtually completely interconnected porous structure (Fig. 4A). The porous structure resembles that of human cancellous bone (Fig. 4B). Open pores with the diameter of several hundred micrometers, and an interconnecting porous provide sufficient space for vessels [81] and bone tissue ingrowth [82,83]. Besides the interconnected macropore structure, micropores exist in the walls of macropores (Fig.4C). These small pores are formed by fusion of powder particles during sintering process and are interconnected, which is crucial for the circulation of body fluids supplying the necessary nutrients and mineral ions for biological functions. The micropores range from 1 to 13 μ m in diameter. Several studies have shown that this microarchitecture plays an important role in bone formation and growth [84,85].

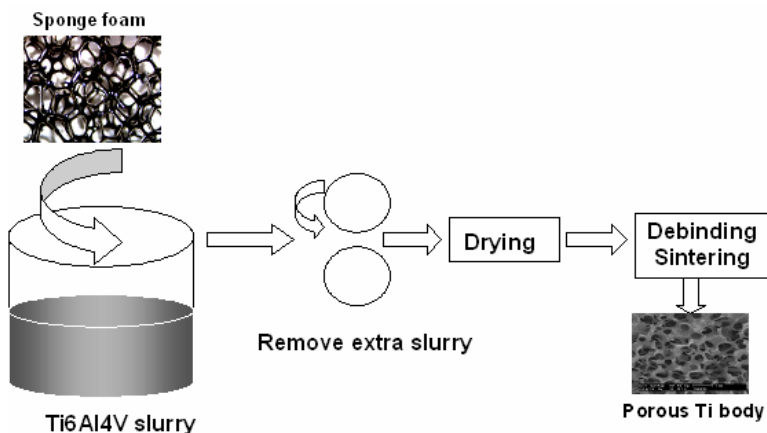


Fig.3 The Process of porous Ti alloy production by positive sponge replication

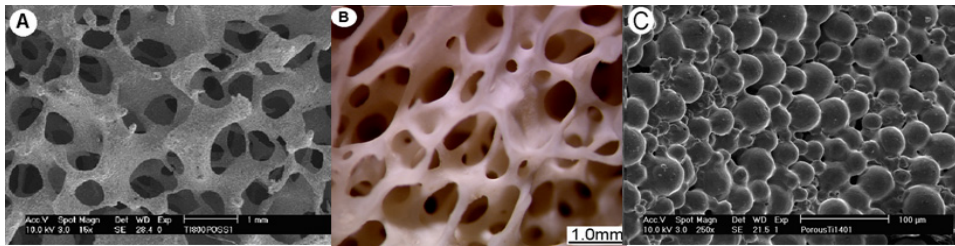


Fig.4 The macrostructure of porous Ti alloy (A) and cancellous bone (B), and the microstructure of porous Ti alloy (C)

3.3. Fabrication of titanium and titanium alloys porous structures by rapid prototyping

Various imperfections of the conventional techniques to produce metallic porous structures, such as the inability to closely control structural properties of the final product have encouraged the use of a rapid prototyping (RP) technology [86]. Since the 1980s RP technologies have emerged as a revolutionary manufacturing process with inherent capability to rapidly make objects in virtually any shape. RP, combining computer aided design (CAD) with computer aided manufacturing (CAM), has the distinct advantage of being able to build objects with predefined micro- and macrostructure [87,88]. This property gives RP the ability to make scaffolds and orthopedic implants with controlled hierarchical structures [89-94]. Until now RP method was primarily used for producing porous polymers and ceramics [95-100]. The transfer of RP technologies to metal materials is an important challenge. So far, only a few investigators were successful in producing metal scaffolds for orthopaedic and maxillofacial applications by RP [101-103]. Two methods have been applied to produce metal scaffolds: 1) indirectly casting molten metal or metal powder slurry into a mold that was made using RP [101,102,104] and 2) direct metal deposition using electrical beam sintering [103,105,106].

Recently, 3D fiber deposition (3DF) (using a "Bioplotter" , Envisiontec GmbH, Germany), a RP technology, for the first time, was successfully applied to directly produce porous Ti alloy scaffolds with fully interconnected porous networks, and highly controllable porosity and pore size (Fig.5). A key feature of this RP technology is the three dimensional dispensing at room temperature of a string of Ti6Al4V slurry to produce a porous Ti6Al4V scaffold made of layers of directionally aligned fibers using a computer controlled process. After deposition and air drying, the final scaffolds are obtained by sintering at 1200⁰C under high vacuum. By controlling fiber spacing, layer thickness and fiber lay down pattern, the desired pore size, pore shape and porosity can be achieved. By changing the dispensing

nozzle size, the fiber diameter can be adjusted. 3D fiber deposition therefore allows the production of scaffolds with various shapes with unlimited geometric freedom. 3DF is a time and material saving process through the direct manufacturing from 3D-CAD data. The efficiency of this technique was demonstrated by produce a prototype of an acetabular cup for total hip replacement (Chapter 7). 3D fiber deposition was found to provide good control and reproducibility of the desired degree of porosity and 3D structure. The 3D fiber deposition Ti offers flexibility and versatility to fabricate and improve scaffolds to better mimic the architecture and properties of natural bone and meet the requirements of orthopedic and dental implants.

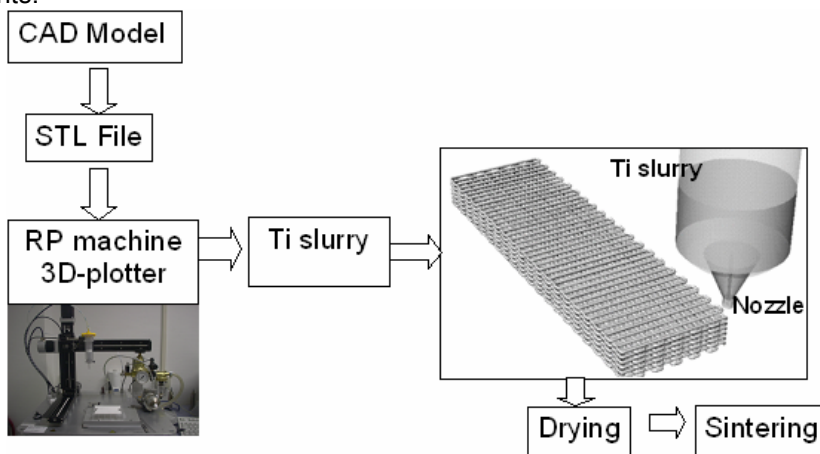


Fig.5 Process of making porous Ti alloy using 3D fiber deposition

4. Potential problems with porous surfaced and porous bulk implants

4.1. Stress shielding

When compared with bone, metal alloys used in prostheses have a non matching elastic modulus. This can result in adverse bone remodeling at the interface between the prosthetic and natural components. For the long term, maintenance of bone in close proximity to the implant surface is important in order to provide the desirable implant functionality. This requires the establishment of physiologically acceptable stresses in the implant-supporting host bone. Excessively high or low stresses will result in bone loss and associated loss of implant stability. It has been suggested that when bone loss is excessive it can compromise the long-term clinical performance of the prosthesis [107], by causing implant migration, aseptic loosening, fractures around the prosthesis, and technical problems during revision surgery [107]. In a study by Bobyn in dogs in which the effect of hip stem stiffness

of femoral prostheses on stress-related bone resorption [108] was investigated, more cortical bone formation was found in case of prostheses with flexible stems. Pilliar reported on possible bone loss in conditions of as a result of an abnormal mechanical stresses around the implant: where either very low stresses may result in bone loss due to disuse atrophy while very high stresses can cause microfracture and subsequent resorption of bone in contact with the implant [109]. In a number of studies, bone remodeling around implants was reported [110-123]. Prenderghast et.al [124-128] gave a general discussion on fracture healing and cell differentiation pathways (shown in Fig.6, reproduced from [124]). It was shown that how tissue differentiation could be controlled by mechanical variables, such as strain and interstitial fluid flow, and also how the time period during which tissue differentiation takes place depends on loading history. Fig. 6 shows with decreasing shear strain, different types of tissue are formed: when shear strain is high, fibrous tissue is formed; at an intermediate strain cartilage formation takes place while bone formation takes place at low strain stresses. When strain stresses are very low, bone starts resorbing.

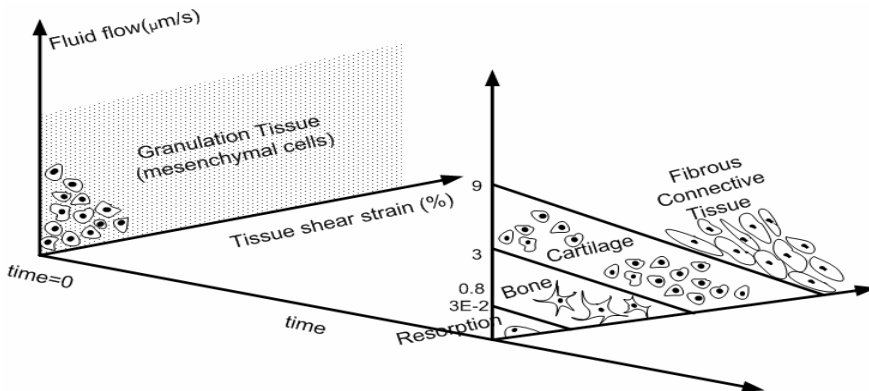


Fig.6 The hypothesis of tissue differentiation by biomechanical factors [124].

Therefore, the use of implants with low stiffness is expected to result in less extensive stress shielding and bone resorption. Lower stiffness can be achieved by fabricating implants out of materials with low Young's modulus. With elastic moduli which are at least half lower than those of Co-based implant alloys, Ti and its alloys are appropriate for reducing the extent of stress shielding. However, compared to bone, the Young's modulus of Ti and its alloys are still high. Introducing porosity into metallic implants is a way to further reduce stress-shielding between the implant and bone. Young's modulus decreases with increasing porosity of the material. The development of bone-implant integration through bone ingrowth into

the porous surface region can provide a means for effective force transfer between implant and bone.

4.2. Fatigue strength

A major issue with the use of porous implants in highly loaded applications is the detrimental effect of porous structure on the fatigue strength of the implant. Bulk porous implants and implants with porous surface coatings are less resistant to fatigue strength resulting in lower fatigue endurance. Studies have shown that both Co-Cr and Ti6Al4V alloys experience drastic reductions in fatigue strength when coated with a porous metal surface [129,130]. It has been shown that the fatigue strength of porous coated Ti6Al4V alloy equals approximately one third of that of the solid alloy with equivalent shape due to stress concentrations between the coating and its solid base. It is essential that this effect is considered and accounted for by the design of the porous-surfaced Ti implants. Similar reductions in fatigue strength occur for textured (i.e. grit blasted, plasma spray-coated, ion-etched) Ti alloy surfaces.

Attempts to improve fatigue strength after sintering of the implant include various heat treatments, such as hydrogenation-dehydrogenation treatments or sintering at temperatures below phase transformation. Cook et al. showed that approximately 15% improvement in fatigue properties of porous Ti6Al4V could be achieved through post-sintering heat treatment. However, using heat treatment to recover the fatigue strength has limited effect since it is the macroporosity of the implant rather than the microstructure of the material that causes the drastic reduction in fatigue strength. The most practical approaches to date involve an appropriate design of implants to 1) ensure that stresses are maintained below the fatigue endurance limit of porous-surfaced samples and 2) avoid porous surface regions at implant surfaces subjected to high tensile stresses.

4.3. Metal ion release

Mechanical interlocking by bone or connective tissue of an implant surface to give secure implant fixation is the primary reason for use of porous surfaced implant designs. However, a consequence of forming porous surface or porous implant is a large increase of the implant surface area. For example, sintered beads surfaced implant can have a surface area that is five times larger than as machined or as cast implant surfaces of similar shape. Since corrosion rates are directly related to the implant surface area, high rates of metal release and possible accumulation of metal corrosion products both locally and systemically could be expected with porous surfaced or porous bulk implants.

Enhanced metal ion release can increase the probability of metal sensitization and associated allergic responses as well as the susceptibility to tumor formation [131]. Porous implants have shown higher corrosion rates when tested in vitro as compared to conventional non porous-coated implants [64,65]. However, in an in vivo study in rabbits, analysis of blood and tissue samples during a two-year implantation period did not demonstrate any significant increase in retained alloy elements (Ti, Al, V with Ti alloy implants and Co, Cr, Mo with CoCrMo implants). Atomic absorption spectroscopy of blood samples collected from patients with porous-surfaced dental implants for the over implantation periods of 3 years gave similar results. The question of the long term host response to such implants remains an important issue requiring proper clinical follow-up studies.

5. Characteristics of porous titanium for orthopedic implants

Several factors may affect ingrowth of bone into pores of metallic implants, such as the porous structure itself (pore size, pore shape, porosity and interconnectivity), duration of implantation, biocompatibility, implant stiffness, micromotion between the implant and adjacent bone etc. [54,132-135].

5.1. Cell and tissue response

The adherence of cells to the biomaterial surface is a prerequisite for tissue integration. New bone formation after implantation depends on whether the surface of the implant promotes cell attachment, proliferation, differentiation and production of extracellular matrix. Using human bone-marrow cell cultures, Wilke et al. [136] have demonstrated clear differences in cell proliferation, cell differentiation and the production of extracellular matrix between hydroxyapatite, Ti and a CrMoCo alloy. Hydroxyapatite surfaces yielded the best results, followed by Ti and CrCoMo. Compared to stainless steel and Co-based alloys, cp Ti and Ti alloys performed better in cell culture experiments with human osteoblasts and other relevant cell types [137]. A number of studies showed porous titanium and its alloys to be favorable for cell attachment, proliferation and differentiation [137-142]}. Lowenberg et al. [143] reported that surface chemistry can affect the attachment and orientation of cells in vitro, and suggested that this parameter can be modified by applying relevant biological components onto the surface.

5.2. Surface geometry characteristics

A number of in vivo studies have revealed the conditions for bone ingrowth and establishment of a rigid and secure implant fixation [34,53,55,82,144-147]. By using different methods, macro- and microporous metallic implants made of Ti

[41,43,44], CoMoCr alloy [42,51,135] and stainless steel [142,148], with a pore size varying from 50 μm to 500 μm , were produced. General agreement exists that bone ingrowth rate is higher in implants with pore sizes larger than 100 μm [53,149,150]. Two studies [53,133] suggested that the optimum pore size range lies between 50 μm & 300 μm . Pores with a diameter smaller than 50 μm or larger than 300 μm led to slower bone ingrowth as assessed by implant bone interface shear strength measurements. However, Bobyn et al. [53,54] showed effective bone ingrowth into porous coatings with pore sizes down to 50 μm , and Itälä et al. [151] demonstrated the formation of an osteonal bone structure in pores with the diameter as small as 50 μm . When the pore size was increased above 1 mm, an increasing tendency for the formation of fibrous tissue was observed [152]. It was reported that porous implant should have a preferred pore size of 100-400 μm for bone ingrowth in an as short time period as possible [153-155] [53]. The effect of pore size on the strength of fixation has been investigated in canine model [108], using pores ranging in size from below 50 μm to 800 μm . In studies examining pore diameters lower than 100 μm the increasing pore size was associated with increasing strength of fixation [42,150]. In most studies no relationship between strength of fixation and pore size was found for pores with a size between 150 μm and 400 μm [53,156,157]. Most porous coated prostheses currently undergoing clinical trials have pores with a size ranging between 100 to 500 μm based on animal studies, although the optimal pore size for the implantation in humans is yet to be defined [158,159].

Previous studies did not show significant difference in biologic response as a function of pore shape [103,160]. However, Sumner et al. [161] reported different rates of bone ingrowth for powder- and fiber made Ti coating. While more bone was found in metal powder based implants after 1 month of implantation, after 6 months, fiber based implants exhibited more bone formation.

The choice of porosity degree of implants is usually a compromise between maintaining mechanical strength of the implant and providing adequate opportunity for tissue ingrowth. Recently it has been recognized that another critical factors for bone ingrowth is the size of interconnecting pores [28,63,162-171].

5.3. Implant stability / micromotion

An important factor determining bone ingrowth into porous implants is the degree of initial stability within the host bone. With a sufficient initial stability of the implant, the early tissue that infiltrates leads to either (1) direct bone formation within the pores, or, (2) appositional bone growth from the adjacent bone into the porous region [172]. Initial implant movement relative to host bone can result in infiltration by a non-mineralised fibrous connective tissue layer, inhibiting bone

formation within, or ingrowth into the pores [173], which is in agreement with the biomechanical hypothesis of micromotion and flow determining the differentiation of mesenchymal stem cells in the percolating body fluids as discussed in section 1.4.1 [110,124,126-128]. Complete absence of micromotions will lead to resorption. Burke [174] demonstrated that micromotion of 75 μm induced fibrous tissue ingrowth. Micromotion of 40 μm allowed the formation of woven bone within a porous Ti wire surface. In another study, bone ingrowth was observed in situations where the relative displacement was less than 28 μm , but when the displacements were greater than 150 μm , only mature connective tissue provided the fixation [175]. In a canine total hip (THA) model bone ingrowth was observed in the femoral components that had an initial micromotions of 56 μm [159]. Pilliar's group suggested that relative movements at the implant-bone interface that are greater than 50 μm can inhibit the osteogenic process at the implant surface thereby slowing down the rate of bone ingrowth and impairing implant fixation. With relative movements above this value, fibrous tissue formation and ingrowth or fibrous tissue encapsulation may result. This is unacceptable for most orthopaedic and dental implant situations in which rigid implant fixation is required. Therefore, the initial stability achieved at the implant bone interface following implantation is a strong determinant of this type of biological fixation.

The amount of bone ingrowth into porous implant also depends on an optimal primary stability. From a clinical perspective this primary stability can vary depending on implant design variables (cross-sectional geometry, means of additional fixation, mismatch in implant/bone stiffness), implantation technology variables (accuracy of tools for rasping, reaming, drilling, sawing), surgical technique variables (accuracy of utilization of the implantation technology) and patient variables (bone quality, bone defects). Thus, porous implants and associated procedures should be designed to promote 1) good initial implant fit and 2) as rapid as possible bone ingrowth [176].

5.4. Interface distances

The lack of a direct and continuous interface contact between the porous surface and the host bone also has a negative effect on bone ingrowth and the eventual strength of fixation of the implant. The reasons for poor contact may be the design of the implant or surgical instruments as well as the surgical technique. Numerous gap models with a controlled gap and a stable implant have demonstrated the inhibiting effect of gap size on bone ingrowth and strength of fixation [135,177,178]. In a non weight bearing study in dogs gap sizes of 2 mm, 1 mm and 0.5 mm were investigated [179]. The results suggested that the increase of the gap size had a negative effect on both bone ingrowth and strength of fixation. Clinically, these

studies imply the importance of accomplishing direct implant-bone contact by the right surgical technique.

6. Aims and approach of this thesis

It has been shown in the literature that the architecture of a porous implant has a great effect on the ingrowth of bone into the pore space [180,181]. For instance, the optimal pore size for bone ingrowth is between 100 and 500 μm , and the pores must be interconnected in order to maintain the vascular system required for continuing bone development. The three dimensional open porous structure is particularly important for implant fixation by tissue ingrowth [35,182].

This thesis mainly focuses on achieving two goals: (1) Developing new methods to fabricate porous Ti and Ti alloys for bone graft substitutes and (2) investigating biological behavior of different scaffolds to address influences of various chemical, physical and structural parameters on their performance in the role of bone graft substitute in orthopaedic and maxillofacial surgery.

Chapters 2-4 (Part I) describe the development of a new porous Ti6Al4V scaffold by sponge replication method. In chapter 2, influence of rheological properties of Ti6Al4V slurry on the final properties of the porous material were addressed in terms of Ti6Al4V powder size, organic thickening agents (binders), dispersants, concentration of powder and pH values. Chapter 3 aims at characterizing of porous Ti6Al4V produced by sponge replication method with regard to its porous structure, mechanical properties, chemical composition, phase compositions, and cell attachment behavior. Chapter 4 deals with further improvements of porous Ti6Al4V in order to achieve a better resemblance with cancellous bone in terms of porous structure and mechanical properties.

Chapters 5-7 (Part II) describe the development of a new RP technique to fabricate porous Ti6Al4V scaffolds based on 3D fiber deposition. In chapter 5, the optimization of properties of the Ti6Al4V slurry and parameters of 3D fiber deposition are described. Chapter 6 addresses the effect of the fiber diameter on the mechanical properties of the resulting scaffolds. In Chapter 7, the design of scaffolds with different structures by changing fiber spacing and fiber orientation is described as well as the influences of different architectures on mechanical properties and permeability of the scaffold.

Chapter 8 is dedicated to a comparison between the sponge replication and 3D fiber deposition Ti6Al4V scaffolds. In chapter 9, an in vivo study in goats is presented in which the influence of pore geometry on osteoconductive properties of 3D fiber deposition Ti6Al4V scaffolds is investigated. Finally, in chapter 10, an in vivo evaluation of the composite scaffolds consisting of porous Ti6Al4V and biphasic calcium phosphate ceramic is described.

Reference

1. Brown KL, Cruess RL. Bone and cartilage transplantation in orthopaedic surgery. A review. *J Bone Joint Surg Am* 1982;64(2):270-9.
2. Damien CJ, Parsons JR. Bone graft and bone graft substitutes: a review of current technology and applications. *J Appl Biomater* 1991;2(3):187-208.
3. Lane JM, Tomin E, Bostrom MP. Biosynthetic bone grafting. *Clin Orthop Relat Res* 1999(367 Suppl):S107-17.
4. Arrington ED, Smith WJ, Chambers HG, Bucknell AL, Davino NA. Complications of iliac crest bone graft harvesting. *Clin Orthop Relat Res* 1996(329):300-9.
5. Mendicino RW, Leonheart E, Shromoff P. Techniques for harvesting autogenous bone graft of the lower extremity. *J Foot Ankle Surg* 1996;35(5):428-35.
6. Brantigan JW, Cunningham BW, Warden K, McAfee PC, Steffee AD. Compression strength of donor bone for posterior lumbar interbody fusion. *Spine* 1993;18(9):1213-21.
7. Lane JM, Sandhu HS. Current approaches to experimental bone grafting. *Orthop Clin North Am* 1987;18(2):213-25.
8. Prolo DJ, Rodrigo JJ. Contemporary bone graft physiology and surgery. *Clin Orthop Relat Res* 1985(200):322-42.
9. Kalita SJ, Bose S, Hosick HL, Bandyopadhyay A. Development of controlled porosity polymer-ceramics composite scaffolds via fused deposition modeling. *Mater Sci and Eng (C)* 2003;23:611-620.
10. Zhang R, Ma PX. Poly(a-hydroxyl acids)/hydroxyapatite porous composites for bone-tissue engineering. I. Preparation and morphology. *J Biomed Mater Res* 1999;44:446-455.
11. Frosch KH, Stumer KM. Metallic Biomaterials in Skeletal Repair. *European Journal of Trauma* 2006;2:149-159.
12. Long M, Rack HJ. Review Titanium alloys in total joint replacement 杧 materials science perspective. *Biomaterials* 1998;19:1621-1639.
13. NIINOMI M. Recent Metallic Materials for Biomedical applications. *METALLURGICAL AND MATERIALS TRANSACTIONS A* 2002;33A:477-481.
14. Kanerva L, Forstrom L. Allergic nickel and chromate hand dermatitis induced by orthopedic metal implant. *Contact Derm* 2001;44:103-104.
15. Disegi JA, Eschbach L. Stainless steel in bone surgery. *Injury* 2000;31(Suppl 4):2?.
16. Ganesh VK, Ramakrishna K, Ghista DN. Biomechanics of bone-fracture fixation by stiffness-graded plates in comparison with stainless-steel plates. *Biomed Eng Online* 2005;4:46.
17. Marti A. Cobalt-base alloys used in bone surgery. *Injury Int J Care Injured* 2000;31:18-21.

18. Pellengahr C, Mayer W, Maier MI. Resurfacing knee arthroplasty in patients with allergic sensitivity to metals. *Arch Orthop Trauma Surg* 2003;123:139.
19. Ortrun EMP. Unalloyed titanium alloys for implants in bone surgery. *Injury Int J Care Injured* 2000;31:783.
20. Textor M. Titanium in medicine. Berlin & Heidelberg: Springer-verlag; 2001. 171-230 p.
21. Ratner BD. Titanium in medicine. Berlin & Heidelberg: Springer-verlag; 2001. 1-12 p.
22. Guillemot F. Recent advances in the design of titanium alloys for orthopedic applications. *Expert Rev Med Devices* 2005;2:741.
23. Schuh A, Thomas P, Kachler W. Allergic potential of titanium implants. *Orthopadec* 2000;34:327-333.
24. Disegi JA. Titanium alloys for fracture fixation implants. *Injury Int J Care Injured* 2000;31(14-17).
25. Perren SM, Geret V, Tepic M. Quantitative evaluation of biocompatibility of vanadium free titanium alloys. Amsterdam: Elsevier; 1986. 397..
26. Hendrich C, Noth U, Stahl U. Testing of skeletal implant surfaces with human fetal osteoblasts. *Clin Orthop Relat Res* 2002;394:278-289.
27. Barrere F, van der Valk CM, Meijer G, Dalmeijer RA, de Groot K, Layrolle P. Osteointegration of biomimetic apatite coating applied onto dense and porous metal implants in femurs of goats. *J Biomed Mater Res* 2003;67B(1):655-65.
28. Bobynd JD, Stackpool GJ, Hacking SA, Tanzer M, Krygier JJ. Characteristics of bone ingrowth and interface mechanics of a new porous tantalum biomaterial. *J Bone Joint Surg Br* 1999;81(5):907-14.
29. Krygier JJ, Bobynd JD, Poggie RA. Mechanical characterization of a new porous tantalum biomaterial for orthopaedic reconstruction.; 1999; Sydney, Australia.
30. Athanasou NA. The pathology of joint replacement. *Curr Diagnostic Pathol* 2002;8:262.
31. McGovern TE, Black J, Jacobs JJ. In vivo wear of Ti-6Al-4V femoral heads: a retrieval study. *J Biomed Mater Res* 1996;32:447-457.
32. Gibson LJ, Ashby MF. Cellular solids: structure and properties. Cambridge: Cambridge University Press; 1997.
33. Pilliar RM. Powder metal-made orthopedic implants with porous surface for fixation by tissue ingrowth. *Clin Orthop* 1983(176):42-51.
34. Pilliar RM, Cameron HU, Welsh RP, Binnington AG. Radiographic and morphologic studies of load-bearing porous-surfaced structured implants. *Clin Orthop* 1981(156):249-57.
35. Murray GA, Semple JC. Transfer of tensile loads from a prosthesis to bone using porous titanium. *J Bone Joint Surg Br* 1981;63-B(1):138-41.

36. Maniatopoulos C, Pilliar RM, Smith DC. Threaded versus porous-surfaced designs for implant stabilization in bone-endodontic implant model. *J Biomed Mater Res* 1986;20(9):1309-33.
37. Maniatopoulos C, Pilliar RM, Smith DC. Evaluation of shear strength at the cement-endodontic post interface. *J Prosthet Dent* 1988;59(6):662-9.
38. Maniatopoulos C, Pilliar RM, Smith DC. Evaluation of the retention of endodontic implants. *J Prosthet Dent* 1988;59(4):438-46.
39. Pilliar RM, Cameron HU, Macnab I. Porous surface layered prosthetic devices. *Biomed Eng* 1975;10(4):126-31.
40. Hirschhorn JS, Reynolds JT, Korstoff E. Powder metallurgy fabrication of cobalt alloy surgical implant materials. New York: Plenum Press; 1969.
41. Lueck RA, Galante JO, Rostoker W, Ray RD. Development of an open pore metallic implant to permit attachment to bone. *Surg Forum* 1969;20:456-457.
42. Welsh RP, Pilliar RM, Macnab I. Surgical implants. The role of surface porosity in fixation to bone and acrylic. *J Bone Joint Surg Am* 1971;53(5):963-77.
43. Galante J, Rostoker W, Lueck R, Ray RD. Sintered fiber metal composites as a basis for attachment of implants to bone. *J Bone Joint Surg Am* 1971;53(1):101-14.
44. Galante J, Rostoker W. Fiber metal composites in the fixation of skeletal prosthesis. *J.Biomed.Mater.Res.* 1973;4:43-61.
45. Cameron HU, Jacob R, Macnab I, Pilliar RM. Use of polymethylmethacrylate to enhance screw fixation in bone. *J Bone Joint Surg Am* 1975;57(5):655-6.
46. Cameron HU, Pilliar RM, Bobyn D, Prendergast W. Studies on ultrasonic removal of implants and the effect of ultrasound on bone. *Acta Orthop Belg* 1979;45(5):595-602.
47. MacGregor DC, Wilson GJ, Lixfeld W, Pilliar RM, Bobyn JD, Silver MD, Smardon S, Miller SL. The porous-surfaced electrode: a new concept in pacemaker lead design. *J Thorac Cardiovasc Surg* 1979;78(2):281-91.
48. MacGregor DC, Wilson GJ, Scully HE, Lixfeld W, Bobyn JD, Pilliar RM, Silver MD. Improved thromboresistance of mechanical heart valves with endothelialization of porous metal surfaces. *Surg Forum* 1979;30:239-41.
49. Pilliar RM, Cameron HU, Binnington AG, Szivek J, Macnab I. Bone ingrowth and stress shielding with a porous surface coated fracture fixation plate. *J Biomed Mater Res* 1979;13(5):799-810.
50. Cameron H, Macnab I, Pilliar R. Porous surfaced Vitallium staples. *S Afr J Surg* 1972;10(2):63-70.
51. Cameron HU, Macnab I, Pilliar RM. A porous metal system for joint replacement surgery. *Int J Artif Organs* 1978;1(2):104-9.
52. Ryan G, Pandit A, Apatsidis DP. Fabrication methods of porous metals for use in orthopaedic applications. *Biomaterials* 2006;27(13):2651-70.

53. Bobyn JD, Pilliar RM, Cameron HU, Weatherly GC. The optimum pore size for the fixation of porous-surfaced metal implants by the ingrowth of bone. *Clin Orthop* 1980(150):263-70.
54. Bobyn JD, Pilliar RM, Cameron HU, Weatherly GC, Kent GM. The effect of porous surface configuration on the tensile strength of fixation of implants by bone ingrowth. *Clin Orthop* 1980(149):291-8.
55. Bobyn JD, Wilson GJ, MacGregor DC, Pilliar RM, Weatherly GC. Effect of pore size on the peel strength of attachment of fibrous tissue to porous-surfaced implants. *J Biomed Mater Res* 1982;16(5):571-84.
56. Hahn H, Palich W. Preliminary evaluation of porous metal surfaced titanium for orthopedic implants. *J Biomed Mater Res* 1970;4(4):571-7.
57. Pilliar RM. P/M Processing of Surgical Implants: Sintered Porous Surfaces for Tissue-to-Implant Fixation. *International Journal of Powder Metallurgy* 1998;34(8):33-45.
58. Liao J, Zhang B. *Porous Materials of Powder Metallurgy: Metallurgy Industry Press, China; 1978.*
59. Matin B, Cornelia S, Bronkremer HP, Baur H. High-porosity Titanium, Stainless Steel, and Superalloy Parts. *Advance Engineering Materials* 2000;2(4):196-199.
60. Wen C, Yamata Y, Mabuchi M. Processing and mechanical properties of autogenous titanium implant materials. *J Mater Sci:in medicine* 2002;13:397-401.
61. Wen CE, Shimojima K, Yamada Y, Chino Y, Hosokawa H, Mabuchi M. Novel Titanium Foam for Bone Tissue Engineering. *Journal of Materials Research* 2002;17(10):2633-2639.
62. Hahn H, Palich W. Preliminary evaluation of porous metal surfaced titanium for orthopedic implants. *J Biomed Mater Res* 1970;4:571-577.
63. Fujibayashi S, Neo M, Kim HM, Kokubo T, Nakamura T. Osteoinduction of porous bioactive titanium metal. *Biomaterials* 2004;25(3):443-50.
64. Yang YZ, Tian JM, Tian JT, Chen ZQ, Deng XJ, Zhang DH. Preparation of graded porous titanium coatings on titanium implant materials by plasma spraying. *J Biomed Mater Res* 2000;52:333-337.
65. Thieme M, Wieters KP, Bergner F, Scharnweber D, Worch H, Ndop J. Titanium powder sintering for preparation of a porous functionally graded material destined for orthopaedic implants. *J Mater Sci Mater Med* 2001;12:225-131.
66. Assad M, Jarzem P, Leroux MA, Coillard C, Chernyshov AV, Charette S, Rivard CH. Porous titanium-nickel for intervertebral fusion in a sheep model: Part 1. Histomorphometric and radiological analysis1. *J Biomed Mater Res* 2003;64B(2):107-20.
67. Assad M, Chernyshov AV, Jarzem P, Leroux MA, Coillard C, Charette S, Rivard CH. Porous titanium-nickel for intervertebral fusion in a sheep model: Part 2. Surface analysis and nickel release assessment. *J Biomed Mater Res* 2003;64B(2):121-9.

68. Assad M, Chernyshov A, Leroux MA, Rivard CH. A new porous titanium-nickel alloy: part 2. Sensitization, irritation and acute systemic toxicity evaluation. *Biomed Mater Eng* 2002;12(4):339-46.
69. Zhang Q, Liu X, Chen J, Zhang X. Fabrication of porous titanium and biomimetic deposition of calcium phosphate. *Key Engineering Materials* 2003;240-241:89-92.
70. Asaoka K. Mechanical properties and biomechanical compatibility of porous titanium for dental implants. *J Biomed Mater Res* 1985;19(6):699-713.
71. Dunand DC, Teisen J. Superplastic foaming of titanium and Ti-6Al-4V. 1998. *Conf Proc Biomater*. p 231.
72. Davis NG, Teisen J, Schuh C, Dunand DC. Solid-state foaming of titanium by superplastic expansion of argon-filled pores. *J Mater Res* 2001;16:1508-1539.
73. Pilliar RM. Porous-surfaced metallic implants for orthopedic applications. *J Biomed Mater Res* 1987;21(A1 Suppl):1-33.
74. Pilliar RM, Deporter DA, Watson PA, Todescan R. The endopore implant-enhanced osseointegration with a sintered porous- surfaced design. *Oral Health* 1998;88(7):61-4.
75. Oliveira MV, Pereira LC, Cairo CAA. Porous Structure Characterization in Titanium Coating for Surgical Implants. *Materials Research* 2002;5(3):269-273.
76. Oh IH, Nomura N, Masahashi N. Mechanical properties of porous titanium compacts prepared by powder sintering. *Scripta Materialia* 2003;49:1197-1202.
77. Wu BD, Cui YF. Research on Porous Titanium for Medical Implant Material. *Rare Metal Materials Engineering* 1988;4.
78. Ducheyne P, Willems G, Martens M, Helsen J. In vivo metal-ion release from porous titanium-fiber material. *J Biomed Mater Res* 1984;18(3):293-308.
79. Kuo KN, Gitelis S, Sim FH. Segmental replacement of long bones using titanium fiber metal composite following tumor resection. *Clin Orthop* 1983;176:108-114.
80. Engh CA. Hip arthroplasty with a Moore prosthesis with porous coating. *Clin. Orthop* 1983;176:52-66.
81. Joschek S, Nies B, Krotz R, Goferich A. Chemical and physicochemical characterization of porous hydroxyapatite ceramics made of natural bone. *Biomaterials* 2000;21(16):1645-58.
82. Egli PS, Muller W, Schenk RK. Porous hydroxyapatite and tricalcium phosphate cylinders with two different pore size ranges implanted in the cancellous bone of rabbits. A comparative histomorphometric and histologic study of bony ingrowth and implant substitution. *Clin Orthop* 1988(232):127-38.
83. Guillemin G, Meunier A, Dallant P, Christel P, Pouliquen JC, Sedel L. Comparison of coral resorption and bone apposition with two natural corals of different porosities. *J Biomed Mater Res* 1989;23(7):765-79.

84. Cerroni L, Filocamo R, Fabbri M, Piconi C, Caropreso S, Condo SG. Growth of osteoblast-like cells on porous hydroxyapatite ceramics: an in vitro study. *Biomol Eng* 2002;19(2-6):119-24.
85. Schwartz Z, Boyan BD. Underlying mechanisms at the bone biomaterial interface. *J Cell Biochem* 1994;56:340-347.
86. Yang S, Leong KF, Du Z, Chua CK. The design of scaffolds for use in tissue engineering. Part II. Rapid prototyping techniques. *Tissue Eng* 2002;8(1):1-11.
87. Sachlos E, Czernuszka JT. Making tissue engineering scaffolds work. Review: the application of solid freeform fabrication technology to the production of tissue engineering scaffolds. *Eur Cell Mater* 2003;5:29-39; discussion 39-40.
88. Sachlos E, Reis N, Ainsley C, Derby B, Czernuszka JT. Novel collagen scaffolds with predefined internal morphology made by solid freeform fabrication. *Biomaterials* 2003;24(8):1487-97.
89. Webb PA. A review of rapid prototyping (RP) techniques in the medical and biomedical sector. *J Med Eng Technol* 2000;24(4):149-53.
90. Hollister SJ. Porous scaffold design for tissue engineering. *Nat Mater* 2005;4(7):518-24.
91. Yeong WY, Chua CK, Leong KF, Chandrasekaran M. Rapid prototyping in tissue engineering: challenges and potential. *Trends Biotechnol* 2004;22(12):643-52.
92. Hutmacher DW, Sittinger M, Risbud MV. Scaffold-based tissue engineering: rationale for computer-aided design and solid free-form fabrication systems. *Trends Biotechnol* 2004;22(7):354-62.
93. Hutmacher DW. Scaffolds in tissue engineering bone and cartilage. *Biomaterials* 2000;21(24):2529-43.
94. Hutmacher DW. Scaffold design and fabrication technologies for engineering tissues-state of the art and future perspectives. *J Biomater Sci Polym Ed* 2001;12(1):107-24.
95. Seitz H, Rieder W, Irsen S, Leukers B, Tille C. Three-dimensional printing of porous ceramic scaffolds for bone tissue engineering. *J Biomed Mater Res B Appl Biomater* 2005;74B(2):782-788.
96. Tan KH, Chua CK, Leong KF, Naing MW, Cheah CM. Fabrication and characterization of three-dimensional poly(ether-ether-ketone)/hydroxyapatite biocomposite scaffolds using laser sintering. *Proc Inst Mech Eng [H]* 2005;219(3):183-94.
97. Dhariwala B, Hunt E, Boland T. Rapid prototyping of tissue-engineering constructs, using photopolymerizable hydrogels and stereolithography. *Tissue Eng* 2004;10(9-10):1316-22.
98. Chua CK, Leong KF, Tan KH, Wiria FE, Cheah CM. Development of tissue scaffolds using selective laser sintering of polyvinyl alcohol/hydroxyapatite biocomposite for craniofacial and joint defects. *J Mater Sci Mater Med* 2004;15(10):1113-21.

99. Wilson CE, de Bruijn JD, van Blitterswijk CA, Verbout AJ, Dhert WJ. Design and fabrication of standardized hydroxyapatite scaffolds with a defined macro-architecture by rapid prototyping for bone-tissue-engineering research. *J Biomed Mater Res A* 2004;68(1):123-32.
100. Zein I, Hutmacher DW, Tan KC, Teoh SH. Fused deposition modeling of novel scaffold architectures for tissue engineering applications. *Biomaterials* 2002;23(4):1169-85.
101. Curodeau A, Sachs E, Caldarise S. Design and fabrication of cast orthopedic implants with freeform surface textures from 3-D printed ceramic shell. *J Biomed Mater Res* 2000;53(5):525-35.
102. Melican MC, Zimmerman MC, Dhillon MS, Ponnambalam AR, Parsons JR. Three-dimensional printing and porous metallic surfaces: a new orthopedic application. *J Biomed Mater Res* 2001;55(2):94-202.
103. Hollister S, Lin C, Saito E, Schek R, Taboas J, Williams J, Partee B, Flanagan C, Diggs A, Wilke E and others. Engineering craniofacial scaffolds. *Orthod Craniofac Res* 2005;8(3):162-73.
104. Wu M, Tinschert J, Augthun M, Wagner I, Schadlich-Stubenrauch J, Sahm PR, Spiekermann H. Application of laser measuring, numerical simulation and rapid prototyping to titanium dental castings. *Dent Mater* 2001;17(2):102-8.
105. Mazumder J, Dutta JD, Kikuchi N, Ghosh A. Closed loop direct metal deposition:art to part. *Optics and Lasers in Engineering* 2000;34:397-414.
106. Mazumder J, Qi H. Fabrication of 3D components by laser-aided direct metal deposition. In: Thomas Schriempf J, editor; 2005; San Jose, CA, USA. p 38-59.
107. Pilliar RM. Porous biomaterials. New York: Pergamon Press Cambridge, MA: The MIT Press; 1990. 312-319.
108. Bobynd JD, Pilliar RM, Binnington AG, Szivek JA. The effect of proximally and fully porous-coated canine hip stem design on bone modeling. *J Orthop Res* 1987;5(3):393-408.
109. Pilliar RM, Deporter DA, Watson PA, Valiquette N. Dental implant design--effect on bone remodeling. *J Biomed Mater Res* 1991;25(4):467-83.
110. Kelly DJ, Prendergast PJ. Mechano-regulation of stem cell differentiation and tissue regeneration in osteochondral defects. *J Biomech* 2005;38(7):1413-22.
111. Moghaddas H, Stahl SS. Alveolar bone remodeling following osseous surgery. A clinical study. *J Periodontol* 1980;51(7):376-81.
112. Carter DR. Mechanical loading histories and cortical bone remodeling. *Calcif Tissue Int* 1984;36 Suppl 1:S19-24.
113. Luedemann RE, Thomas KA, Cook SD. Bone remodeling associated with a flexible femoral intramedullary implant. *Biomater Med Devices Artif Organs* 1986;14(3-4):181-94.

114. Parfitt AM. Bone remodeling and bone loss: understanding the pathophysiology of osteoporosis. *Clin Obstet Gynecol* 1987;30(4):789-811.
115. Sumner DR, Turner TM, Urban RM, Galante JO. Experimental studies of bone remodeling in total hip arthroplasty. *Clin Orthop Relat Res* 1992(276):83-90.
116. Reeve J, Zanelli JM, Garrahan N, Bradbeer JN, Wand JS, Moyes ST, Roux JP, Smith T. Bone remodeling in hip fracture. *Calcif Tissue Int* 1993;53 Suppl 1:S108-12.
117. McGowan JA. Osteoporosis: assessment of bone loss and remodeling. *Aging (Milano)* 1993;5(2):81-93.
118. Parfitt AM. Bone remodeling, normal and abnormal: a biological basis for the understanding of cancer-related bone disease and its treatment. *Can J Oncol* 1995;5 Suppl 1:1-10.
119. Sychterz CJ, Engh CA. The influence of clinical factors on periprosthetic bone remodeling. *Clin Orthop Relat Res* 1996(322):285-92.
120. Rubin C, Gross T, Qin YX, Fritton S, Guilak F, McLeod K. Differentiation of the bone-tissue remodeling response to axial and torsional loading in the turkey ulna. *J Bone Joint Surg Am* 1996;78(10):1523-33.
121. Robling AG, Castillo AB, Turner CH. Biomechanical and Molecular Regulation of Bone Remodeling. *Annu Rev Biomed Eng* 2006.
122. Hartman GA, Cochran DL. Initial implant position determines the magnitude of crestal bone remodeling. *J Periodontol* 2004;75(4):572-7.
123. Power J, Loveridge N, Lyon A, Rushton N, Parker M, Reeve J. Bone remodeling at the endocortical surface of the human femoral neck: a mechanism for regional cortical thinning in cases of hip fracture. *J Bone Miner Res* 2003;18(10):1775-80.
124. Prendergast PJ, Huiskes R, Soballe K. ESB Research Award 1996. Biophysical stimuli on cells during tissue differentiation at implant interfaces. *J Biomech* 1997;30(6):539-48.
125. Prendergast P, Taylor D. Stress analysis of the proximo-medial femur after total hip replacement. *J Biomed Eng* 1990;12:379-382.
126. Huiskes R, Van Driel WD, Prendergast PJ, Soballe K. A biomechanical regulatory model for periprosthetic fibrous-tissue differentiation. *J Mater Sci Mater Med* 1997;8(12):785-8.
127. Duda GN, Maldonado ZM, Klein P, Heller MO, Burns J, Bail H. On the influence of mechanical conditions in osteochondral defect healing. *J Biomech* 2005;38(4):843-51.
128. Ramamurti BS, Orr TE, Bragdon CR, Lowenstein JD, Jasty M, Harris WH. Factors influencing stability at the interface between a porous surface and cancellous bone: a finite element analysis of a canine in vivo micromotion experiment. *J Biomed Mater Res* 1997;36(2):274-80.
129. Black J. Systemic effects of biomaterials. *Biomaterials* 1984;5:11-18.

130. Seah KHW, Thampuran R, Teoh SH. The influence of pore morphology on corrosion. *Corrosion Sci* 1998;40:547-56.
131. Banhart J. Manufacture, characterisation and application of cellular metals and metal foams. *Progr Mater Sci* 2001;46:559-632.
132. Simmons CA, Valiquette N, Pilliar RM. Osseointegration of sintered porous-surfaced and plasma spray-coated implants: An animal model study of early postimplantation healing response and mechanical stability. *J Biomed Mater Res* 1999;47(2):127-38.
133. Clemow AJ, Weinstein AM, Klawitter JJ, Koeneman J, Anderson J. Interface mechanics of porous titanium implants. *J Biomed Mater Res* 1981;15(1):73-82.
134. Katz JL, Pilliar RM, Berkowitch J, Christel P, Higham P, Kempeneers R, Knox GF, Scott I, Sudanese A. Biomechanical stability and design. Stiffness and remodeling. *Ann N Y Acad Sci* 1988;523:283-6.
135. Cameron HU, Pilliar RM, Macnab I. The rate of bone ingrowth into porous metal. *J Biomed Mater Res* 1976;10(2):295-302.
136. Wilke A, Landgraff M, Orth J, Kienapfel H, Grissand P, Franke R. Human bone marrow cell cultures: a sensitive method for determination of the biocompatibility of implant materials. *ATLA* 1999;27:137-151.
137. Muller U, mwinkelried TI, Horst M, Sievers M, Graf-Hausner U. DO HUMAN OSTEOBLASTS GROW INTO OPEN-POROUS TITANIUM? *Cell European Cells and Materials* 2006;11:8-15.
138. Lowenberg BF, Pilliar RM, Aubin JE, Fernie GR, Melcher AH. Migration, attachment, and orientation of human gingival fibroblasts to root slices, naked and porous-surfaced titanium alloy discs, and zircalloy discs in vitro. *J Dent Res* 1987;66(5):1000-5.
139. Li JP, de Wijn JR, Van Blitterswijk CA, de Groot K. Porous Ti6Al4V scaffold directly fabricating by rapid prototyping: preparation and in vitro experiment. *Biomaterials* 2006;27(8):1223-35.
140. Li JP, Li SH, Van Blitterswijk CA, De Groot K. A novel porous Ti6Al4V: Characterization and Cell attachment. *J.Biomed.Mat.Res* 2005;73A:223-233.
141. El Sayegh TY, Pilliar RM, McCulloch CA. Attachment, spreading, and matrix formation by human gingival fibroblasts on porous-structured titanium alloy and calcium polyphosphate substrates. *J Biomed Mater Res* 2002;61(3):482-92.
142. Ducheyne P. In vitro corrosion study of porous metal fibre coatings for bone ingrowth. *Biomaterials* 1983;4(3):185-91.
143. Lowenberg BF, Pilliar RM, Aubin JE, Sodek J, Melcher AH. Cell attachment of human gingival fibroblasts in vitro to porous-surfaced titanium alloy discs coated with collagen and platelet-derived growth factor. *Biomaterials* 1988;9(4):302-9.
144. Pilliar RM. Porous surfaced endosseous dental implants: fixation by bone ingrowth. *Univ Tor Dent J* 1988;1(2):10-5.

145. Ikeda N, Kawanabe K, Nakamura T. Quantitative comparison of osteoconduction of porous, dense A-W glass-ceramic and hydroxyapatite granules (effects of granule and pore sizes). *Biomaterials* 1999;20(12):1087-95.
146. Liu D-M. Influence of Porosity and Pore Size on the Compressive Strength of Porous Hydroxyapatite Ceramic. *Ceramics International* 1997;23:135-139.
147. Tsuruga E, Takita H, Itoh H, Wakisaka Y, Kuboki Y. Pore size of porous hydroxyapatite as the cell-substratum controls BMP-induced osteogenesis. *J Biochem (Tokyo)* 1997;121(2):317-24.
148. Ducheyne P, Martens M, Aernoudt E, Mulier J, De Meester P. Skeletal fixation by metal fiber coating of the implant. *Acta Orthop Belg* 1974;40(5-6):799-805.
149. Anderson RC, Cook SD, Weinstein AM, Haddad RJ, Jr. An evaluation of skeletal attachment to LTI pyrolytic carbon, porous titanium, and carbon-coated porous titanium implants. *Clin Orthop Relat Res* 1984(182):242-57.
150. Robertson DM, Pierre L, Chahal R. Preliminary observations of bone ingrowth into porous materials. *J Biomed Mater Res* 1976;10(3):335-44.
151. Itala AI, Ylanen HO, Ekholm C, Karlsson KH, Aro HT. Pore diameter of more than 100 microm is not requisite for bone ingrowth in rabbits. *J Biomed Mater Res* 2001;58(6):679-83.
152. Bobyn JD, Miller GJ. *Orthopaedic Basic Science*. Chicago: American academy of orthopaedic surgeons; 1994.
153. Daculsi G, Passuti N. Effect of the macroporosity for osseous substitution of calcium phosphate ceramics. *Biomaterials* 1990;11:86-7.
154. Chang BS, Lee CK, Hong KS, Youn HJ, Ryu HS, Chung SS, Park KW. Osteoconduction at porous hydroxyapatite with various pore configurations. *Biomaterials* 2000;21(12):1291-8.
155. Blokhuis TJ, Termaat MF, den Boer FC, Patka P, Bakker FC, Haarman HJTM. Properties of Calcium Phosphate Ceramics in Relation to Their In Vivo Behavior. *Journal of Trauma-Injury Infection & Critical Care*. 2000;48(1):179-188.
156. Cook SD, Walsh KA, Haddad RJ, Jr. Interface mechanics and bone growth into porous Co-Cr-Mo alloy implants. *Clin Orthop Relat Res* 1985(193):271-80.
157. Cook SD, Kay JF, Thomas KA, Jarcho M. Interface mechanics and histology of titanium and hydroxylapatite-coated titanium for dental implant applications. *Int J Oral Maxillofac Implants* 1987;2(1):15-22.
158. Jasty M, Bragdon CR, Zalenski E, O'Connor D, Page A, Harris WH. Enhanced stability of uncemented canine femoral components by bone ingrowth into the porous coatings. *J Arthroplasty* 1997;12(1):106-13.
159. Jasty M, Krushell R, Zalenski E, O'Connor D, Sedlacek R, Harris W. The contribution of the nonporous distal stem to the stability of proximally porous-coated canine femoral components. *J Arthroplasty* 1993;8(1):33-41.

160. Collier JP, Mayor MB, Chae JC, Surprenant VA, Surprenant HP, Dauphinais LA. Macroscopic and microscopic evidence of prosthetic fixation with porous-coated materials. *Clin Orthop Relat Res* 1988(235):173-80.
161. Sumner DR, Turner TM, Urban RM, Galante JO. Bone ingrowth into titanium fiber metal and bead surface in a total hip arthroplasty model.; 1986; New Orleans. p 342.
162. Takemoto M, Fujibayashi S, Neo M, Suzuki J, Matsushita T, Kokubo T, Nakamura T. Osteoinductive porous titanium implants: effect of sodium removal by dilute HCl treatment. *Biomaterials* 2006;27(13):2682-91.
163. Nishikawa M, Myoui A, Ohgushi H, Ikeuchi M, Tamai N, Yoshikawa H. Bone tissue engineering using novel interconnected porous hydroxyapatite ceramics combined with marrow mesenchymal cells: quantitative and three-dimensional image analysis. *Cell Transplant* 2004;13(4):367-76.
164. Okii N, Nishimura S, Kurisu K, Takeshima Y, Uozumi T. In vivo histological changes occurring in hydroxyapatite cranial reconstruction--case report. *Neurol Med Chir (Tokyo)* 2001;41(2):100-4.
165. Tadic D, Beckmann F, Schwarz K, Epple M. A novel method to produce hydroxyapatite objects with interconnecting porosity that avoids sintering. *Biomaterials* 2004;25(16):3335-40.
166. Woodfield TB, Van Blitterswijk CA, De Wijn J, Sims TJ, Hollander AP, Riesle J. Polymer scaffolds fabricated with pore-size gradients as a model for studying the zonal organization within tissue-engineered cartilage constructs. *Tissue Eng* 2005;11(9-10):1297-311.
167. Malda J, Woodfield TB, van der Vloodt F, Wilson C, Martens DE, Tramper J, van Blitterswijk CA, Riesle J. The effect of PEGT/PBT scaffold architecture on the composition of tissue engineered cartilage. *Biomaterials* 2005;26(1):63-72.
168. Bloebaum RD, Bachus KN, Momberger NG, Hofmann AA. Mineral apposition rates of human cancellous bone at the interface of porous coated implants. *J Biomed Mater Res* 1994;28(5):537-44.
169. Schliephake H, Neukam FW, Klosa D. Influence of pore dimensions on bone ingrowth into porous hydroxylapatite blocks used as bone graft substitutes. A histometric study. *Int J Oral Maxillofac Surg* 1991;20(1):53-8.
170. Harris WH, Jasty M. Bone ingrowth into porous coated canine acetabular replacements: the effect of pore size, apposition, and dislocation. *Hip* 1985:214-34.
171. van Eeden SP, Ripamonti U. Bone differentiation in porous hydroxyapatite in baboons is regulated by the geometry of the substratum: implications for reconstructive craniofacial surgery. *Plast Reconstr Surg* 1994;93(5):959-66.
172. Spector M. Bone ingrowth into porous polymers. Boca Raton: CRC Press; 1982. 55 p.
173. Cameron HU, Pilliar RM, MacNab I. The effect of movement on the bonding of porous metal to bone. *J Biomed Mater Res* 1973;7(4):301-11.

174. Burke DW, Bragdon CR, O'Connor DO. Dynamic measurement of interface mechanics in vivo and the effect of micromotion on bone ingrowth into a porous surface device under controlled loads in vivo. *Trans Orthop Res Soc* 1991;16:103.
175. Pilliar RM, Lee JM, Maniopoulos C. Observations on the effect of movement on bone ingrowth into porous- surfaced implants. *Clin Orthop* 1986(208):108-13.
176. Andreykiv A, Prendergast PJ, van Keulen F, Swieszkowski W, Rozing PM. Bone ingrowth simulation for a concept glenoid component design. *J Biomech* 2005;38(5):1023-33.
177. Bobyn JD, Wilson GJ, Mycyk TR, Klement P, Tait GA, Pilliar RM, MacGregor DC. Comparison of the porous-surfaced with a totally porous ventricular endocardial pacing electrode. *Pacing Clin Electrophysiol* 1981;4(4):405-16.
178. Sandborn PM, Cook SD, Spires WP, Kester MA. Tissue response to porous-coated implants lacking initial bone apposition. *J Arthroplasty* 1988;3(4):337-46.
179. Dalton JE, Cook SD. Influence of implant location on the mechanical characteristics using the transcortical model. *J Biomed Mater Res* 1995;29(1):133-6.
180. Chen PQ, Turner TM, Ronnigen H, Galante J, Urban R, Rostoker W. A canine cementless total hip prosthesis model. *Clin Orthop* 1983(176):24-33.
181. Landon GC, Galante JO, Maley MM. Noncemented total knee arthroplasty. *Clin Orthop* 1986(205):49-57.
182. Bobyn JD, Cameron HU, Abdulla D, Pilliar RM, Weatherly GC. Biologic fixation and bone modeling with an unconstrained canine total knee prosthesis. *Clin Orthop* 1982(166):301-12.

The image is a scanning electron micrograph (SEM) showing a porous titanium alloy structure. The structure consists of interconnected, irregular, porous walls forming a network of interconnected voids. The walls appear to have a fine, fibrous texture. A scale bar at the bottom left indicates a length of 1 mm. Technical parameters are listed on the left side of the image.

Part I

Development of a Novel Porous Titanium Alloy by Sponge Replication

Chapter 2

Factors of influences on the rheological properties of titanium alloy slurry

Chapter 3

A novel porous Ti6Al4V: characterization and cell attachment

Chapter 4

Improvement of mechanical properties of porous titanium alloy

Acc.V Spot Magn
10.0 kV 3.0 15x

Det WD Exp
SE 28.4 0

TI8000POSS1
1 mm

Chapter 2

Factors of influences on rheological properties of titanium alloy slurry

J.P. Li¹, J.R. de Wijn¹, C.A. van Blitterswijk¹, K. de Groot^{1,2}

¹Institute for Biomedical Technology, University of Twente, The Netherlands.

²CAM Implants. B.V, The Netherlands.

Abstract

A highly porous Ti6Al4V was produced using a porous polymeric sponge and Ti6Al4V slurry. However, the rheological properties of Ti6Al4V slurry appeared to be the key issue in the preparation of porous Ti6Al4V. In this study, factors having influence on the rheological properties of Ti6Al4V slurry were addressed in detail. Ti6Al4V powders, organic thickening agents (binders), dispersants, concentration of powder and pH values were optimized with regard to the rheological properties of Ti6Al4V slurry. The results showed that Ti6Al4V powder with a mean diameter of 45µm and spherical shape is beneficial for preparation of Ti6Al4V slurry. Binders with two ingredients, which decompose at different temperatures, have the advantage to keep the shape after debinding. The optimized procedure, based on the findings, made it possible to produce highly porous Ti6Al4V with reticulate porous structure. Porous Ti6Al4V produced using this technique is expected to be a promising bone graft substitute for orthopaedic and dental implant.

Key words: Ti6Al4V powder, slurry, viscosity, porous, rheological properties

1. Introduction

In the biomedical fields, recently, there is an increasing interest in fabricating porous scaffolds that mimic the structure of human bone, because porous structure allows the ingrowth of new tissue and the transport of the body fluids. For instance, pore characteristics of porous biomaterials are essential for bone grafting materials to achieve good bone in-growth and attachment to tissues. To obtain porous biomaterials that have proper pore size, good morphology and interconnectivity, quite many methods have been applied. For example, to produce porous calcium phosphate ceramics which have a porous structure similar to that of bone, the following methods have been addressed: 1) duplicating a coral skeleton [1,2]; 2) keeping the bovine cancellous bone structure [3,4]; 3) foaming ceramics from slurry [5,6]; 4) freeze-drying an aqueous slurry [7]; 5) impregnating a porous polymeric sponge which is subsequently pyrolyzed [8]. Among the methods mentioned, the last method is quite often used. Compared with other methods, this method can easily generate an open, three-dimensional porous structure, which is comparable to that of human cancellous bone. However this method requires a good knowledge of the rheological properties of slurry.

Although porous calcium phosphate ceramics are good bone graft substitutes because of their osteoconductive and even osteoinductive property [9-12], their inherently low mechanical strength limits their applications to non-load-bearing sites. For bone repair or replacement in load-bearing sites, such as vertebral fusion, porous biomaterials with satisfactory mechanical properties are needed, and thus development of porous metals is an important aspect in biomaterial science for hard tissue repair or replacement.

In the past years, titanium and its alloy have been widely used as implant materials under load-bearing conditions in orthopedics and dental implantology because of their relatively low modulus, superior biocompatibility and corrosion resistance [13]. Due to the importance of porous structure of biomaterials in hard tissue replacement, titanium or its alloy has also been produced in porous forms, and widely used in biomedical prostheses [14], such as hip joint and dental implant coating etc. In general, porous titanium or its alloy could be produced by traditional powder metallurgical technique, such as sintering loose powder, powder compaction and fiber pressing [14-19]. However, since porous metals made by such methods have a low porosity (<45%) and a pore size limited by the particle shape and size, porous metals obtained by these methods are not comparable to human cancellous bone that has a porosity of about 75% and a pore size from 100 μ m to 600 μ m.

To improve the porosity and porous structure of porous titanium or its alloy, the method of polymeric sponge replication was firstly introduced to make porous

Ti6Al4V [20]. Earlier, this method was used to make porous calcium phosphate (CaP) ceramics as discussed in several publications [21-23], but there are no reports in the literature to use this method for porous Ti6Al4V. The procedure itself is simple. Ti6Al4V slurry prepared from Ti6Al4V powders and binders was coated onto a polymeric foam, thereafter the foam construction was subjected to drying, pyrolyzing, and sintering with a special process to remove polymeric foam and binders. After a final sintering at a high temperature and high vacuum, a porous Ti6Al4V was produced. Two key steps are included to produce porous Ti6Al4V: preparation of Ti6Al4V slurry and removal of foam struts and final sintering. The rheological behavior of slurry becomes the most important parameter in doing so. It is, therefore, of great practical importance to achieve good rheological characterisation of slurry to coat the uniform Ti6Al4V slurry on the foam struts and to keep sponge's shape after the removal of sponge struts.

The objective of this work is to study the influence on the rheological behavior of Ti6Al4V slurry: (a) particle size, particle morphologies and their distributions, (b) kinds and contents of the binders and dispersants, (c) other relevant variables such as powder concentration, pH value, and air bubbles, and at the end, to achieve Ti6Al4V slurry, which is suitable to make porous Ti6Al4V with porosity and pore size similar to those of human cancellous bone.

2. Materials and methods

2.1. Raw materials

Three commercially available Ti6Al4V powders were employed in this study, which are TC4P2-325, TC4P2-200 [Bongen Titanium (China) Co, Ltd], and TC4-325 [China Baoji Titanium Powder Factory]. The chemical composition of Ti6Al4V powders are listed in Table 1 as compared with the ISO5832 standard requirements

Table 1 Chemical composition of Ti6Al4V powder

Element(wt%)	Al	V	N	H	O	C	Fe	Si	Ti
TC4P2-325	6.47	4.08	0.025	0.008	0.183	0.02	0.12	0.04	Bal
TC4P2-200	6.47	4.09	0.025	0.008	0.175	0.02	0.12	0.04	Bal
TC4-325	6.5	4.2	0.04	0.01	0.20	0.05	0.2	0.04	Bal
ISO5832	5.5- 6.8	3.5- 4.5	0.05	0.015	0.20	0.08	0.3	0.04	Bal

Other materials used in this study are Polyethylene glycol1500 (PEG1500, Fluka Chemie GmbH, Germany), Polyethylene glycol4000 (PEG4000, Fluka Chemie GmbH, Germany), Methylcellulose (MC, Fisher Scientific B.V, The Netherlands),

ammonia (25% ammonia solution, Merck), 1-octanol (ACROS ORGANICS, USA), dolipix (Aschimmer & Schwarz GmbH, Germany) and polyethylene foam 3.31R45 (Calligen Europe B.V, The Netherlands).

The shape of different Ti6Al4V powders was analysed under environmental scanning electron microscope (ESEM, XL-30, Philips, Eindhoven, The Netherlands). Particle sizes were measured with the working principle of incoherent light diffraction (CRYSTALSIZER®).

Thermogravimetric analyses (TGA, Perkin Elmer, software of Pyris windows) were performed on PEG4000 and MC in order to know their thermal behavior.

2.2. General analysis methods

Sediment speed: Sedimentation of different Ti6Al4V slurries was tested in volumetric flasks with the same volume. The initial level (L1) of slurry was recorded, after an interval time, the level (L2) of slurry was recorded. The speed of sediment was indicated as $\Delta L / \Delta T$, where $\Delta L = L1 - L2$.

Viscosity: The rheological behavior of Ti6Al4V slurries was measured at room temperature by viscometer (Brookfield engineering labs DV-II+ viscometer) with interval time at a speed of 20 rpm with a RV5 spindle.

pH Value: The pH value of slurry was measured at room temperature by a pH meter (Portamess PHM 85, Knick, Germany).

2.3. Experimental procedures

The Ti6Al4V slurry served as a model to study the influence of Ti6Al4V powder (particle size, particle shape and concentrations), binders (type and concentration), dispersant, pH value and air bubbles.

The components of Ti6Al4V slurries for different purposes varied but were prepared in a similar way. Firstly, demineralised water was mixed with binders by stirring for 1h, Ti6Al4V powders were subsequently added to the solution and stirred for 1.5 h. Then Dolapix, ammonia solution and 1-octanol were added to the slurry and stirring was maintained for 1h to obtain the final Ti6Al4V slurry.

2.3.1. Influence of Ti6Al4V shape and size of powders on rheological behaviour

The influence of Ti6Al4V powders on rheological behaviour of their slurries was characterized by measuring sediment speed and viscosities of different Ti6Al4V slurries with 70wt% powders (TC4P2-325, TC4P2-200, TC4-325) and 2%wt MC in water.

2.3.2. Influence of type and concentration of binders on rheological behaviour

Firstly, the viscosities of PEG1500, PEG4000 and Methylcellulose were tested in 2wt% aqueous solutions. Then the influences of PEG1500, PEG4000 and Methylcellulose on slurries were tested in Ti6Al4V slurries with 70wt% powder (TC4P2-325), 1wt% dolapix, 1wt% amonina, 1wt% 1-octanol, 2wt% of PEG1500, PEG4000 and Methylcellulose separately with regard to the viscosities. Finally, the influence of PEG4000 and MC concentrations on the viscosities of Ti6Al4V slurries were tested on the Ti6Al4V slurries with 70wt% powder (TC4P2-325), 1wt% dolapix, 1wt% amonina, 1wt% 1-octanol and different concentration of PEG4000 and MC respectively.

2.3.3. Influence of concentration of powder on rheological behaviour

The influence of Ti6Al4V powder concentrations on the viscosity of Ti6Al4V slurry was investigated on the slurries with 50% to 85wt% powder (TC4P2-325), 3.0wt% PEG4000, 0.5wt% MC, 1.0wt% dolapix, 1.0wt% amonina and 1.0wt% 1-octanol.

2.3.4. Influence of dispersant on rheological behaviour

The influence of dispersant (Dolapix) concentrations on the viscosity of Ti6Al4V slurry was tested on the slurry containing 75wt% Ti6Al4V powder (TC4P2-325), 3.0wt% PEG4000, 0.5wt% MC, 1.0wt% amonina, 1.0wt% 1-octanol and Dolapix at concentrations from 0.25 wt% to 2.0wt%.

2.3.5. Influence of pH value on rheological behaviour

To test the influence of pH value on the viscosity of Ti6Al4V slurry, ammonia was dropped into the slurry with 75wt% powder (TC4P2-325), 1.0wt% dolapix, 1.0 wt% 1-octanol and 2wt% PEG4000 to adjust the pH value and meanwhile viscosity and sediment speed of slurry were measured.

2.3.6. Influence of Air bubbles

Three different methods were used to eliminate bubbles: 1) Static curing, 2) Chemicals removal and 3) Vibration. Experiments were performed on the slurry with 75wt% Ti6Al4V powder, 3.0wt% PEG4000, 0.5wt% MC, 1.0wt% Dolapix and 1wt% ammonia. The viscosity of slurry with / without air bubbles was measured.

2.3.7. Preparation of a porous Ti6Al4V

Optimised slurry was obtained with regard to the components in Table 2, and a porous Ti6Al4V was made of such optimised slurries. Firstly, polyurethane (PU) foam was dipped into the slurry. The dipping process was repeated until all the struts of the PU foam were coated with Ti6Al4V slurry. The extra slurry was then removed by using a pressing-rolling to achieve a well-distributed coating on the struts of foam. Thereafter the raw porous body was first dried for 3 hrs at 80°C and then for 24hrs at room temperature. Subsequently, the samples were heated to burn out foam (50°C/h to 500°C under flow argon) and sintered in high vacuum furnace at 1250°C with holding time of 2hrs. The porous Ti6Al4V body was observed with ESEM.

Table2 Chemical composition of Ti6Al4V slurry

Ingredient	Wt%
Demi water	18.5
PEG4000	3.0
Dolapix	1.0
Ammonia	1.0
Methylcellulose	0.5
1-octanol	1.0
Ti6Al4V powder	75.0

3. Results

3.1. Powder shape and size

Under ESEM, Ti6Al4V powders showed different particle shapes and sizes (Fig.1). Both TC4P2-325 and TC4P2-200 particles are spherical, but TC4P2-200 has a bigger particle size than those of TC4P2-325 and TC4-325. TC4-325 is similar to TC4P2-325 in particle size but has an irregular shape. Particle size distribution of Ti6Al4V powders is shown in Fig.2. The majority of TC4P2-325 and TC4-325 size (~72%) is between 20-40 μm , while the majority of TC4P2-200 size (~66%) is between 40-80 μm . The particle size of TC4P2-325 and TC4-325 are almost the same, but the particle size of TC4P2-200 is bigger than that of TC4P2-325 and TC4-325.

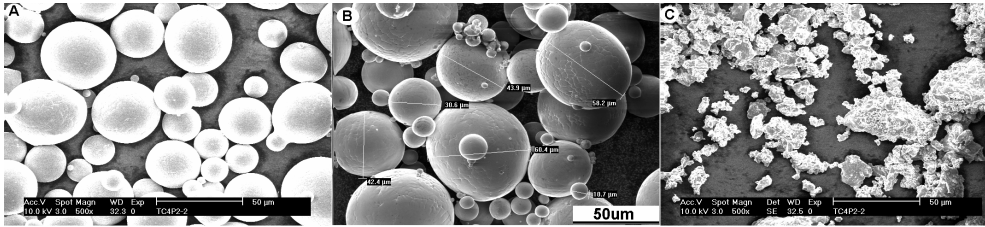


Fig.1 Particle shape and size of Ti6Al4V powders under ESEM A) TC4P2-325; B) TC4P2-200; C) TC4-325

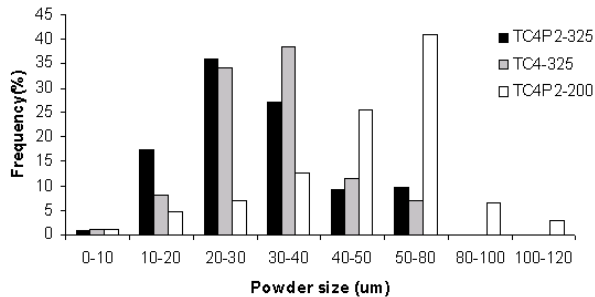


Fig.2 Size distributions of Ti6Al4V particles in different powders

The sediment speed of three kinds of slurries is displayed in Fig.3A, and the viscosity of different Ti6Al4V slurries is shown in Fig.3B. Considering different Ti6Al4V slurries, no significant difference in viscosity was observed, but their sediment speeds were significantly different. TC4-325 sediments are faster than TC4P2-200 than TC4P2-325.

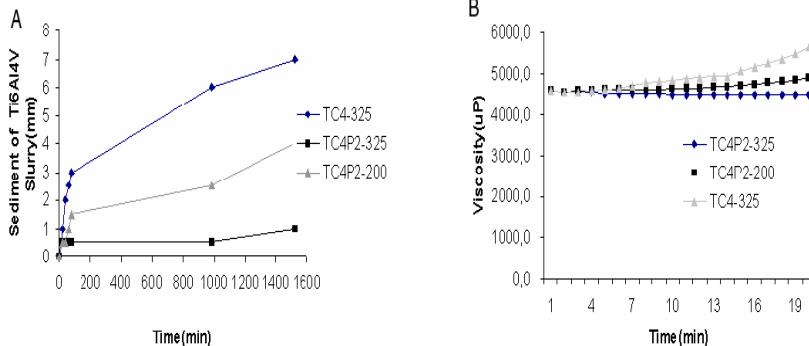


Fig.3 Influence of Ti6Al4V powder types on the rheological properties of titanium alloy slurries

- (A) Sediment of Ti6Al4V powders with time in the slurries having 70wt% powder, and 2.0wt% MC
- (B) Influence of powders on the viscosity of Ti6Al4V slurries (70wt% powder, 1.0wt% MC) as the function of time

3.2. Influence of the binders

The viscosities of PEG1500, PEG4000 and Methylcellulose aqueous solution (2.0 wt %) is shown in Fig 4A. It was shown that with the same concentration (2.0 wt %) of PEG1500, PEG4000 and Methylcellulose, Methylcellulose aqueous solution has much higher viscosity than that of PEG1500 and PEG4000. Although PEG1500 and PEG4000 aqueous solution have a similar viscosity in water, they behave differently in Ti6Al4V slurry. As shown in Fig.4B, different binders in the same Ti6Al4V slurry resulted in different viscosity of the slurries. Ti6Al4V slurry with MC still has a higher viscosity than the slurries with PEG1500 or PEG4000. Obviously and most importantly, the viscosity of Ti6Al4V slurry with PEG1500 was not stable and increased with time.

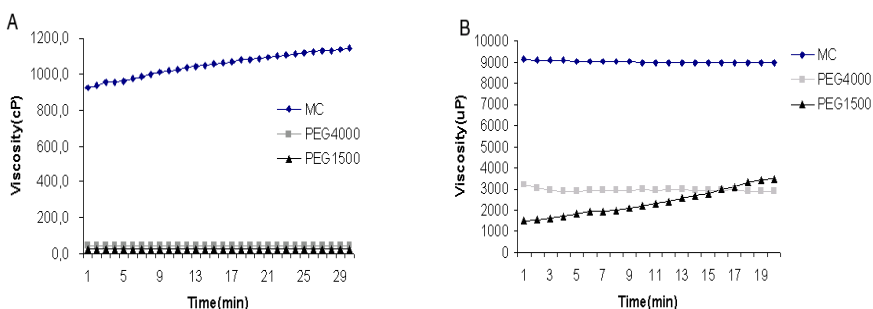


Fig.4 Influence of binders on the viscosity of Ti6Al4V slurries

- (A) Viscosities of PEG1500, PEG4000 and MC aqueous solution (2.0wt% in water);
 (B) Influence of binders on the viscosity of Ti6Al4V slurries (2.0wt% binder MC, 70wt%TC4P2-325 powder, 1.0wt% Dolapix, 1.0wt% ammonia and 1.0wt% octanol).

The binders firstly adjust the viscosity of the Ti6Al4V slurry to obtain suitable slurries, and secondly help to keep the shape of the green bodies, but at the end they were debinded at a high temperature. Fig. 5 showed that decomposition of PEG4000 and MC under nitrogen. PEG4000 started to decompose at 150°C and MC started to decompose at 300°C.

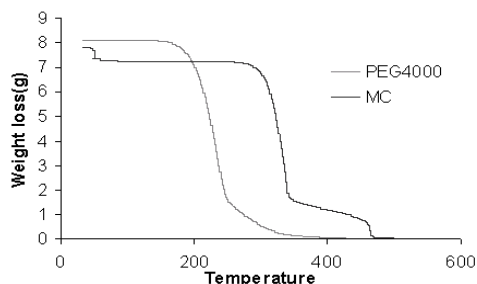


Fig.5 TGA curves of PEG4000 and MC

Not only has the type of the binders, but also the concentrations influenced the Ti6Al4V slurries. The viscosity of Ti6Al4V slurry increased with both PEG4000 (Fig. 6A) and MC (Fig. 6B).

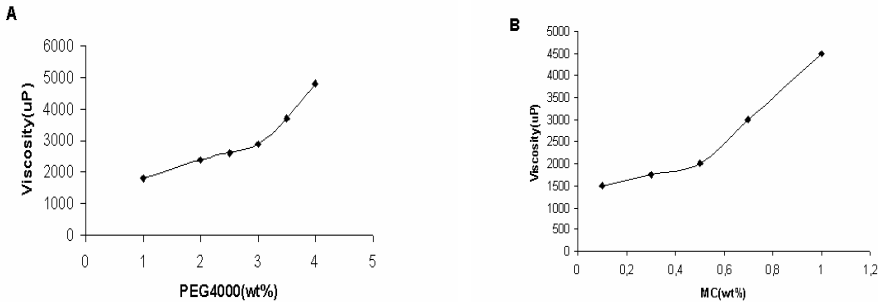


Fig.6 Influence of binder concentration on the viscosity of Ti6Al4V slurry (70wt% TC4P2-325 powder, 1.0wt% Dolapix, 1.0wt% ammonia and 1.0wt% 1-octanol) varied with different the amount of binder. (A) PEG4000; (B) MC

3.3. Powder concentration

In addition to the particle shapes and particle sizes, the concentration of the Ti6Al4V powder in the slurries influences the viscosity: the higher the powder concentration, the higher the viscosity (Fig. 7). The viscosity of the Ti6Al4V slurry increased slightly from 50wt% to 75wt% of TC4P2-325, but increased sharply when concentration was above 75 wt%.

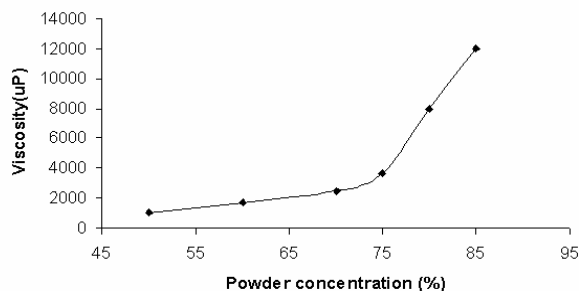


Fig.7 Change of the viscosity of Ti6Al4V slurry with TC4P2-325 powder concentration (3.0wt% PEG4000 and 0.5%MC, 1.0wt% Dolapix, 1.0wt% ammonia and 1.0wt% octanol).

3.4. Dispersant

Fig.8 shows the viscosity versus the amount of dispersant (Dolapix). A concentration of approximately 1.0wt % Dolapix allowed the achievement of

slurries containing 75wt% powder with the lowest viscosity, further increase of Dolapix increased the slurry viscosity.

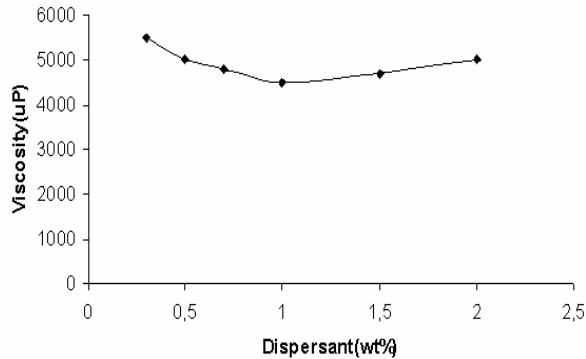


Fig.8 Viscosity of Ti6Al4Vslurry as function of dispersant (Dolapix) concentrations (75wt%TC4P2-325 powder, 3.0wt% PEG4000 and 0.5%MC, 1.0wt% ammonia and 1wt% octanol).

3.5. pH value

The pH of the slurry also influences the viscosity and the sediment speed of Ti6Al4V slurry (Fig.9). The viscosity remains stable between pH8 to pH10, decreases sometimes with further increase of the pH, while the slurry with a pH value of 10.7 has the lowest viscosity (Fig. 9A). The influence of pH on sediment speed was not in one tendency, low agglomeration occurs at pH 10.7 in the Ti6Al4V slurry (Fig. 9B).

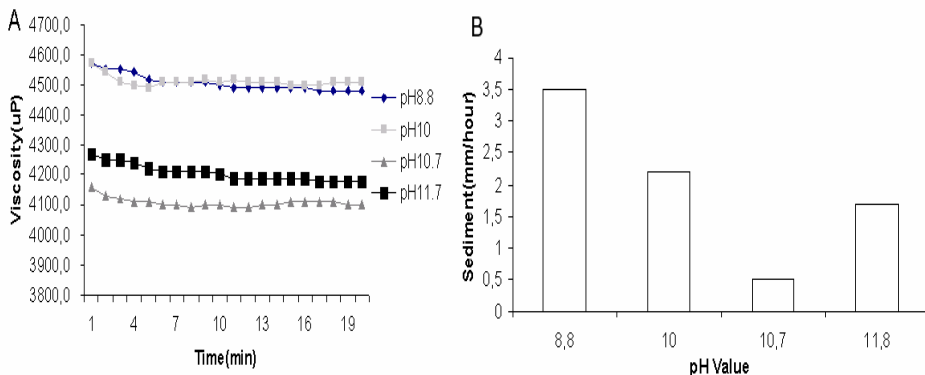


Fig.9 Influence of pH value

- (A) Viscosity of Ti6Al4V slurry with different pH as the function of time (75wt%TC4P2-325 powder, 3.0wt% PEG4000 and 0.5%MC, 1.0wt% ammonia and 1.0wt% octanol).
- (B) Sediment speed of Ti6Al4V slurry with different pH.

3.6. Air bubbles

The existence of air bubbles in slurry is detrimental to coat Ti6Al4V slurry on struts of foam and results in a variety of microstructure defects such as cracks, pores on the wall and other large flaws. Table 3 shows air bubbles are affected by different treatments. Chemicals removal is an effective method, followed by vibration. Static curing is not an effective one, air bubbles are still found on the surface of slurry after one-hour static curing.

Table3 Air bubbles corresponding procedures of treatment and time

Method\Time	10min	30min	60min
Static curing	+++	++	+
Vibration	++	+	-
Chemical	+	-	-

'+++': A lot of air bubbles on the surface; '++': some of air bubbles; '+': a few of air bubbles; '-': no air bubbles were seen on the surface

The influence of air bubbles on the viscosity of slurry is shown in Fig.10. The viscosity of slurry is slightly higher after removal of air bubbles.

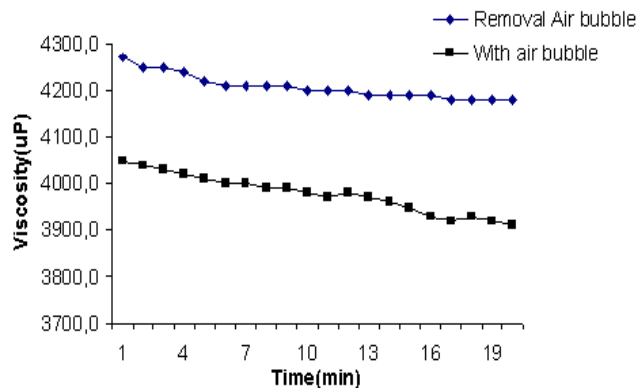


Fig.10 Change of the viscosity of Ti6Al4V slurry with the removal of air bubbles as the function of time (75wt%TC4P2-325 powder, 3.0wt% PEG4000 and 0.5%wtMC, 1.0wt% ammonia and 1.0wt% octanol).

3.7. Porous Ti6Al4V

Fig.11 showed the porous structures of porous Ti6Al4V fabricated with a polymeric sponge and optimised Ti6Al4V slurry. The porous structure was similar to the structure of the original polymeric sponge with interconnected pores.

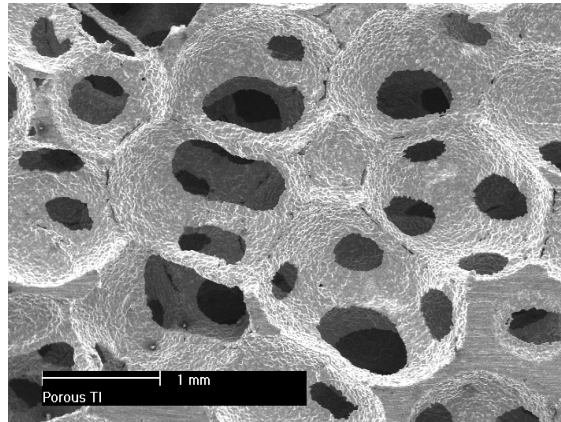


Fig.11 Porous Ti6Al4V as observed under ESEM.

4. Discussion

Slurry preparation, debinding and final sintering are the key steps in the preparation of porous Ti6Al4V by polymeric sponge replication. The rheological behavior of Ti6Al4V slurry is a key in the preparation of suitable Ti6Al4V slurry, similar to already published articles concerning the rheological behaviour of different calcium phosphate ceramic slurries [24-26]. In general, the Ti6Al4V slurry must be fluid enough to enter, fill, and uniformly coat the sponge network and subsequently remain sufficient viscous as to adhere on the struts. The viscosity is an important parameter to characterize the rheological behavior of Ti6Al4V slurry. When viscosity is high, the slurry is sticky and it is difficult to flow and to remove extra slurry after impregnation of sponge to achieve homogenous coating. On the other hand, if the viscosity of the slurry is low, the slurry is thin and only limited amounts of Ti6Al4V were coated on the struts, with the consequence that it is subsequently difficult to maintain the shape of the green porous Ti6Al4V body after the sponge foam was burned out.

In order to obtain suitable Ti6Al4V slurry to make a porous Ti6Al4V, factors that having influences on Ti6Al4V slurry were studied step by step in this study.

4.1. Ti6Al4V powders

Ti6Al4V powder was found to be one of the important factors having influence on the rheological behavior of Ti6Al4V slurry. Three Ti6Al4V powders were tested, and they performed differently. Firstly, the sediment speed differed for each powders, TC4-325 deposited in the slurry quicker than TC4P2-200, while TC4P2-325 deposited slower than other two Ti6Al4V powders in the slurry (Fig. 3A). Secondly, the viscosity changed differently with powders. The viscosity of TC4-325

slurry increased with time, so did the viscosity of TC4P2-200 slurry, although not as quick as the viscosity of TC4-325 slurry. However, the viscosity of TC4P2-325 slurry remained stable with time (Fig.3B). The performance of different powders in slurries was caused by shape and size of their particle. Having smaller particle size and similar particle size distribution (Fig.2) but different particle shape, TC4-325 and TC4P2-325 had different sediment speed. Having irregular particle shapes (Fig.1C), TC4-325 deposited in the slurry fast, but having spherical shape (Fig.1A), TC4P2-325 deposited in the slurry slowly (Fig.3A). The particle shape affected not only the sediment speed of the powders in the slurry but also the viscosity of the slurry. The spherical particle shape was helpful to keep the viscosity of the slurry stable with time, as compared the viscosity of TC4-325 slurry and TC4P2-325 slurry (Fig.3B). Although the spherical particle shape was in general useful in slurry preparation, the particle size was still a matter. Having same particle shape as TC4P2-325 (Fig. 1A and 1B), but bigger particle size (Fig. 2), TC4P2-200 deposited faster than TC4P2-325 (Fig.3A). Meanwhile, the viscosity of TC4P2-200 slurry (having big particle size) increased with time (Fig. 3B). Having spherical particle shape and small particle size, TC4P2-325 deposited in slurry slowly and the viscosity of its slurry remained almost stable with time. Since stable Ti6Al4V slurry is what is being looked for, TC4P2-325 was chosen as a standard powder to analyse other factors and for future use. Beside the particle shape, particle size and size distributions, Ti6Al4V powders influence their slurries with their concentrations, as shown in Fig.7, the viscosity increased with TC4P2-325 powder, slowly from 50wt% to 75wt%, but sharply when TC4P2-325 powder was more than 75wt%.

4.2. Binders

Careful selection of Ti6Al4V powder was important but not enough for preparation of Ti6Al4V slurry. Binders, which on the one hand allow Ti6Al4V powder to suspend in the slurry and to further adjust the rheological behavior (namely the viscosity) of the slurry on the other hand, were needed. It is clear that the binders should be carefully selected. The binders should not react chemically to Ti6Al4V powder and could be removed from green body without contamination of porous Ti6Al4V body. Meanwhile, the binders should adjust the viscosity of Ti6Al4V slurry to suitable degree. Three materials were tested as binders with the TC4P2-325 slurry. At the same concentrations, MC aqueous solution had a high viscosity, while PEG1500 and PEG4000 aqueous solution had low viscosity separately (Fig. 4A). Not only in the aqueous solutions, was same trend found in Ti6Al4V slurry. At the same concentration, MC gave higher viscosity than PEG1500 and PEG4000 in the Ti6Al4V slurry (Fig. 4B). Differently but most importantly, the viscosity of the

Ti6Al4V slurry with MC and PEG4000 remained stable with time, but the viscosity of the Ti6Al4V slurry with PEG1500 increased with time (Fig.4B). The results suggested the influence of binder types on the rheological behavior of Ti6Al4V slurry. Since PEG1500 resulted in un-stable Ti6Al4V slurry, it was therefore not a good binder material and may not be used in the preparation of Ti6Al4V slurry. Binders influenced the rheological behavior of Ti6Al4V slurry with both their types and their concentrations. As shown in Fig. 6, the viscosity of Ti6Al4V slurry increased with the concentrations of both MC (Fig.6A) and PEG4000 (Fig.6B).

4.3. Dispersant, pH value and air bubbles

Besides Ti6Al4V powders and binders, dispersant materials were used in the preparation of Ti6Al4V slurry in order to prevent the aggregations of Ti6Al4V particles and therefore to achieve a homogenous Ti6Al4V slurry. Dolapix was often used as a dispersant in slurry preparation [27,28]. Dolapix influenced the viscosity of Ti6Al4V slurry with its concentrations (Fig.8). A concentration of 1.0wt% dolapix resulted in lower viscosity, as compared with more or less concentration of dolapix.

It's known that pH helps the fluidity of slurries for slip casting [29]. In this study, ammonia was used to adjust the viscosity of Ti6Al4V slurry. The viscosity of slurry varied with different pH value (Fig.9A). The slurry has the lowest speed of sediment when pH value is about 10.7(Fig.9b). The reason may be given as follows. Normally, Ti6Al4V powder has an oxide surface layer. In the aqueous solution, the oxide surface of Ti6Al4V powder released OH^- , which gives a rise to a net surface charge. According to theory of the electrical double layer [30], the zeta potential surrounding the Ti6Al4V particles increased with the increase of pH due to increased surface charge density, and hence the repulse force between particles increased. Thereafter, less agglomeration occurred in the slurry with the decrease of viscosity.

Besides the fluidity of the Ti6Al4V slurry, air bubbles have impact on the homogeneity of the final slurry coating on the porous forms. Some study showed the air bubble would affect the density of slurry [31]. Our experiment shows that the viscosity of slurry was influenced by air bubbles as well. Viscosity of the slurry increased with removal of air bubbles (Fig.10).

Keeping the influence of Ti6Al4V powders, binders, dispersant, pH and air bubbles in mind, Ti6Al4V slurry was optimised with a concentration of 75wt% TC4P2-325 powder, 3.0wt%PEG4000 and 0.5wt%MC, 1.0wt% dispersant, 1.0wt% ammonia and 1.0wt% 1-octanol. This slurry was homogeneous without any clusters of particles, had a stable viscosity of 3000-5000uP, a pH value of 10.5, and did not have obvious air bubbles. It had a good rheological behavior for the

impregnation of sponge. When sponge was dipped into slurry and the extra slurry can be easily removed by pressing-rolling to achieve distribute coating. After debinding and sintering, the porous Ti6Al4V with sponge structures was successfully obtained (Fig.11).

In general, the optimisation of the slurry hereby mainly based on the rheological behaviour of Ti6Al4V slurry, but on the other hand, some factors, having possible influence on the properties of the final porous Ti6Al4V, were also taken into consideration in the optimisation. Powder with spherical shape and small size was selected for use. On the one hand, this kind of powder gave good rheological behaviour of the slurry; on the other hand, by providing relatively large surface area, this powder ensured a higher powder concentration (75wt%) as compared to other metals slurry such as stainless steel (60wt%)[32], and may eventually give a higher mechanical strength of the final porous Ti6Al4V, because of a high concentration of powder in the slurry, more powder could be coated. Furthermore, the small particles may easily create microstructures on the macropore surface which may be helpful to improve the biological performance of the porous Ti6Al4V [11,12].

It should be noted that titanium or Ti6Al4V is a very reactive metal and can react with nitrogen, oxygen and carbon to form titanium compounds. The formation of titanium compounds would affect sintering of porous Ti6Al4V and the mechanical strength of the final porous Ti6Al4V. So, the choice of binders, dispersant and other components in the slurry should be very carefully to avoid any chemical reactions. The most likely step that may cause compound formation was debinding, the removal of the binders. Removal of binder is usually carried out by solvent or thermal extraction methods. Considering the process of porous Ti6Al4V, besides the removal of binders, the foam had to be removed from the green body at the same time, so the thermal extraction was selected as a debinding method. For the thermal extraction, usually it is effective to remove binders and foam, but it is easy to generate carbon residue and other compounds due to chemical reaction [33]. Several groups have reported the way in which a polymer degrades under heating in an inert atmosphere [34,35]. The thermal decomposition of a polymer is explained by a chain depolymerisation and a random decomposition[36]. It is suggested that binders, which are pyrolysed by the mechanism of a chain depolymerisation, are used to reduce the impurity content [36]. Low-density polyethylene is decomposed by a chain depolymerisation. It can be seen by TGA results, during the debinding stage, PEG4000 and MC firstly debinded at 150°C and 300°C respectively, after heating above 500°C, only little PEG4000 and MC were left and therefore reduce the possibility to form possible compound in the final sintering at a high temperature (1250°C). PEG4000 and MC, as binders, on the

one hand, reduce the possible compound formation, on the other hand, due to their different decomposition temperature, PEG4000 and MC helped to keep the shape of the green body. Because PEG4000 firstly decomposed, and then MC as a binder was still left to remain the original shape of the green body under the high temperature.

4. Conclusion

By studying the influences of Ti6Al4V powders, binders, dispersant, pH value and air bubbles on the rheological behaviour of Ti6Al4V slurry, Ti6Al4V slurry was optimised as a composition of 75wt% Ti6Al4V powder (TC4P2-325), 3.0 wt%PEG4000, 0.5wt% MC, 1.0wt% Dolapix, 1wt% ammonium solution and 1wt% 1-octanol . By using the optimised Ti6Al4V slurry, a porous Ti6Al4V was successfully produced by the impregnation of polymeric sponge.

5. Acknowledgements

This study was financially supported by IsoTis S.A. The authors gratefully thank Dr. Yuan and Dr. Li for their helpful discussion.

References

1. Roy DM, Eysel W, Dinger D. Hydrothermal synthesis of various carbonate containing calcium hydroxyapatite. *Mater Res Bull* 1974;9(35-39).
2. Roy DM, Linnehan SK. Hydroxyapatite Formed from Coral Skeletal Carbonated by Hydrothermal Exchange. *Nature* 1974;247:220-222.
3. Hing KA, Hing SM, Bonfield W. Characterization of porous hydroxyapatite. *J Mater Sci Mater Med* 1999;10:135-145.
4. Valenti P. Sinus grafting with porous bone mineral (Bio-Oss) for implant placement: A 5 year study on 15 patients. *Int J Periodontics and Restorative Dent* 2000;20(3):245-253.
5. Rejda BV, Peelen JG, De Groot K. Tricalcium phosphate as a bone substitute. *J Bioen* 1977;1:93-97.
6. Ryszkewitch E. Compression strength of porous sintered alumina and zirconia. *J Am Ceram Soc* 1953;36:65.
7. Fukasawa T, Deng ZY, Ando M, Goto Y. Pore structure of porous ceramics synthesized from water-based slurry by freeze-dry process. *J Mater Sci* 2001;36:2523-2527.
8. Woyansky JS, Scott CE, Minnear WP. Processing of porous ceramics. *Am Cera Soc Bul* 1992;71:1674-1682.

9. Cornell CN, Lane JM. Current understanding of osteoconduction in bone regeneration. *Clin Orthop* 1998(355 Suppl):S267-73.
10. Gosain AK, Song L, Riordan P, Amarante MT, Nagy PG, Wilson CR, Toth JM, Ricci JL. A 1-year study of osteoinduction in hydroxyapatite-derived biomaterials in an adult sheep model: part I. *Plast Reconstr Surg* 2002;109(2):619-30.
11. Yuan H, Kurashina K, de Bruijn JD, Li Y, de Groot K, Zhang X. A preliminary study on osteoinduction of two kinds of calcium phosphate ceramics. *Biomaterials* 1999;20(19):1799-806.
12. Yuan H, de Bruijn JD, Zhang X, van Blitterswijk CA, de Groot K. Bone induction by porous glass ceramic made from Bioglass (45S5). *J Biomed Mater Res* 2001;58(3):270-6.
13. Lemons JE, Lucas LC. Properties of biomaterials. *J Arthroplasty* 1986;1(2):143-7.
14. Bobyn JD, Pilliar RM, Cameron HU, Weatherly GC. The optimum pore size for the fixation of porous-surfaced metal implants by the ingrowth of bone. *Clin Orthop* 1980(150):263-70.
15. Bobyn JD, Pilliar RM, Binnington AG, Szivek JA. The effect of proximally and fully porous-coated canine hip stem design on bone modeling. *J Orthop Res* 1987;5(3):393-408.
16. Cameron HU, Pilliar RM, Macnab I. The rate of bone ingrowth into porous metal. *J Biomed Mater Res* 1976;10(2):295-302.
17. Galante J, Rostoker W, Lueck R, Ray RD. Sintered fiber metal composites as a basis for attachment of implants to bone. *J Bone Joint Surg Am* 1971;53(1):101-14.
18. Pilliar RM, Cameron HU, Macnab I. Porous surface layered prosthetic devices. *Biomed Eng* 1975;10(4):126-31.
19. Pilliar RM. Powder metal-made orthopedic implants with porous surface for fixation by tissue ingrowth. *Clin Orthop* 1983(176):42-51.
20. Li JP, Li SH, Van Blitterswijk CA, De Groot K. A novel porous Ti6Al4V: Characterization and Cell attachment. *J.Biomed.Mat.Res* 2005;73A:223-233.
21. Jun YK, Kim WH, Kweon OK, Hong SH. The fabrication and biochemical evaluation of alumina reinforced calcium phosphate porous implants. *Biomaterials* 2003;24(21):3731-9.
22. Ramay HR, Zhang M. Preparation of porous hydroxyapatite scaffolds by combination of the gel-casting and polymer sponge methods. *Biomaterials* 2003;24:3293-3302.
23. Berry DJ, Sutherland CJ, Trousdale RT, Colwell CW, Jr., Chandler HP, Ayres D, Yashar AA. Bilobed oblong porous coated acetabular components in revision total hip arthroplasty. *Clin Orthop* 2000(371):154-60.
24. Lelievre F, Bernache-Assollant D, Chartier T. Influence of powder characteristics on the rheological behaviour of hydroxyapatite. *J.Mater.Sci:in Medicine* 1996;7:489-494.

25. Liu DM. Preparation and characterisation of porous hydroxyapatite Bioceramic via a slip-casting route. *Ceramics International* 1998;24:441-446.
26. Tian JT, Tian JM. Preparation of porous hydroxyapatite. *J. Mater.Sci* 2001;36:3061-3066.
27. Li SH, De Wijn JR, Layrolle P, De Groot K. Synthesis of macroporous hydroxyapatite scaffolds for bone tissue engineering. *J Biomed Mater Res* 2002;61:109-120.
28. Li SH, De Wijn JR, Layrolle P, De Groot K. Novel method to manufacture porous hydroxyapatite by dual-phase mixing. *J. Am. Ceram. Soc.* 2003;86[1]:65-72.
29. Amato I, Martorana.D. The rheological properties of alumina colloidal dispersions. *Materials Science and Engineering* 1973;12:23-27.
30. Conway BE. Electrical double layer and Ion adsorption at solid/solution interfaces; 2002. 1658-681
31. Zhu XW, Jiang DL, Tan SH. Improvement in the strength of reticulateed porous ceramics by vacuum degassing. *Materials Letters* 2001;51:363-367.
32. Liao J, Zhang B. Porous materials of powder metallurgy: Metallurgy Industry Press,China; 1978.
33. Petzoldt F, Eifert H, Hartwig T, Veltl G. *Advances in powder metallurgy and particulate materials*. Princeton, NJ: MPIF; 1995.
34. Madorsky SL, Straus S. High temperature resistance and thermal degradation of polymers. London: Society of Chemical Industry; 1961. 64.
35. Madorsky SL. *Thermal degradation of organic polymers*. New York: Interscience; 1964.
36. Vankrevelen DW. *Properties of polymers*. Amsterdam: Elsevier; 1990. 641-653.

Chapter 3

A novel porous Ti6Al4V: characterization and cell attachment

J.P. Li¹ S.H. Li², C.A. van Blitterswijk¹, K. de Groot^{1,2}

¹Institute for Biomedical Technology, University of Twente, The Netherlands.

²CAM Implants. B.V, The Netherlands.

Abstract

For the first time a highly porous strong Ti6Al4V was produced by using a “polymeric sponge replication” method. A polymeric sponge, impregnated with a Ti6Al4V slurry prepared from Ti6Al4V powders and binders was subjected to drying and pyrolyzing to remove polymeric sponge and binders. After sintering at a high temperature and under high vacuum, a porous Ti6Al4V scaffold was produced. Optical microscopical observation, ESEM with energy-dispersive micro X-ray (EDX), mechanical tests and metallurgical analyses were performed in order to characterize the obtained porous scaffold with regard to the porous structure (both macropores and micropores), mechanical properties, chemical composition, phase compositions and cell attachment behaviour. The porous Ti6Al4V made by this method had a three dimensional trabecular porous structure with interconnected pores mainly ranging from 400 to 700 μm and a total porosity of about 90%. The compressive strength was 10.3 ± 3.3 MPa and the Young's modulus 0.8 ± 0.3 GPa. MC3T3-E1 cells attached and spread well in the inner surface of pores. Being similar to cancellous bone with regard to both interconnected porous structure and mechanical properties, the resulting porous Ti6Al4V is expected to be a promising biomaterial for biomedical applications.

Key words: Ti6Al4V, scaffold, porosity, sintering, mechanical properties, in vitro.

1. Introduction

Titanium and its alloys have been widely used in orthopaedic and dental devices because of their excellent properties: 1) good biocompatibility, 2) high ratio of strength to weight, 3) relative low Young's modulus. 4) superior corrosion resistance as compared with other metallic biomaterials, such as cobalt alloy and stainless steel [1-3]. Up to present most implants of titanium (and its alloys) are in dense forms, however, with dense forms, problems, such as interfacial instability with host tissues, biomechanical mismatch of Young's modulus and lacking biological anchorage for tissue ingrowth, may occur [4,5]. Regarding the long-term load-bearing implant, a successful performance of implants requires reliable anchoring of implants into host tissue. The advantage of porous materials is their ability to provide biological anchorage for the surrounding bony tissue via the ingrowth of mineralised tissue into the pore space [6-10]. Several factors may affect ingrowth of bone into the pore spaces of these implants, such as the porous structure (pore size, pore shape, porosity and interconnectivity) of the implant material, the duration of implantation, biocompatibility, implant stiffness, the micromotion between the implant and adjacent bone etc [11-15]. It has been shown in the literature that the architecture of a porous implant has a great effect on the bone ingrowth into the pore space [16,17]. For instance, optimal pore size for bone ingrowth is between 100-500 μm , and the pores must be interconnected in order to maintain the vascular system required for continuing bone development. A three dimensional open porous structure is particularly suitable for implant fixation by tissue ingrowth [7,18].

There are two types of porous implants: either they have a porous surface or they are completely porous (porous bulk implant).

As for orthopaedic and dental implants, the need for mechanical interlock of bone or other connective tissues with an implant surface that gives secure implant fixation, is the primary reason for using porous surfaced implants. Porous surface coating was developed for orthopaedic replacement devices in the early 1970s [19-21]. Generally, porous coatings are obtained by sintering uniform-sized beads or fibres by isostatic pressing sintering or loosely packing sintering [22-27] on the dense cores. The solid cast or machined core provides necessary mechanical strength while the porous surface allows for bone ingrowth.

A brief description and comparison of methods to produce porous bulk titanium and its alloys are summarized in Table 1. The successful clinical applications were attributed to the advantages of these methods [25,28]. However, their remaining drawbacks led scientists to investigate better porous structures, especially where better control over interconnectivity and porosity is concerned.

Table 1 Comparison of the merits and drawbacks of the porous titanium made by powder metallurgy

Method	Material	Advantages	Drawbacks
Pressure shaping	Ti beads [22,29,30]	Practical easiness to make Interconnected pores Narrow pore size distribution	low porosity (<45%) pore size as function of the particle size
	Ti mesh [20,31-33]	Interconnected pores	Difficult to form low porosity
	Ti powder+ pore space[34,35]	Easy method in principle Porosity up to 80% Controllable pore size and porosity	Difficult to control pore interconnectivity and open pore
Pressure-less shaping	Ti beads [4,36]	easiness to make Interconnected pores Narrow pore size distribution	Low porosity (<45%) pore size as function of the particle size
Special shaping -Plasma spray	Ti powder [19]	Commercially most successful for surface-coating	Lack of interconnected pore small pore size varied porosity

To meet practical requirements of bone ingrowth and long term implantation, there is a need to manufacture an implant that mimics the architecture of natural bone, encourages bone to grow into the pore spaces, and provides a biological interlock between the implant and surrounding bone.

The purpose of this study therefore is to develop a new method to produce porous Ti6Al4V with a reticulate structure that has the following features: 1) all the

pores open and interconnected in any direction; 2) the structure similar to that of natural cancellous bone; 3) relative high compressive strength with its high porosity. 4) good cell attachment.

2. Materials and methods

2.1. Raw materials

Ti6Al4V powders with a mean diameter of 45 μ m (Bongen Titanium (China) Co, Ltd) were used in this study, together with polyurethane (PU) sponge with the specification of 3.31R45 (Calligen Europe B.V, the Netherlands). Cancellous bone samples were obtained by boiling goat cancellous bone for one week to remove collagen and other components.

2.2. Porous Ti6Al4V from polymeric sponge replication

- **Preparation of Ti6Al4V slurry**

The Ti6Al4V powders (75 wt.%) were mixed with H₂O (18.5 wt.%). Polyethylene glycol 4000(PEG4000, Fluka Chemie GmbH, Germany) and Methylcellulose (MC, Fisher Scientific B.V, The Netherlands) were employed as binders (3.5wt.%). 1 wt.% Dolapix (Aschimmer&Schwarz GmbH Germany) ,1wt.% ammonia solution(25 wt.%, Merck) and 1 wt.% 1-octanol (ACROS ORGANICS, USA) were mixed to improve the rheological property of the slurry.

- **Shaping**

Porous Ti6Al4V green bodies were made by thoroughly dipping the polymeric sponges into Ti6Al4V slurry. This dipping process was repeated several times so that the struts of the polyurethane sponge could be covered with slurry as more as possible. Excess slurry was removed by using a roller-pressing device. The samples were then dried for 3hrs at 80°C and for at least 24hrs at room temperature.

An equivalent model for measuring surface roughness was made together with the sample batch because of difficulties in measuring directly the surface roughness inside the pores of porous Ti6Al4V made by polymeric sponge replication. To that purpose, a Ti6Al4V plate, covered with Ti6Al4V slurry was sintered under the same conditions as for the real porous samples. We assumed the surface roughness of this model to be an indication of that of the inner walls of the porous Ti6Al4V made via sponge replication process.

- **Removal of sponge and binder**

Before the samples were put into the furnace chamber, 1.0 wt.% of titanium hydride of the total sample weight was placed on both the bottom and the top of the samples and in different locations in the furnace. Prior to debinding, the vacuum pump was used to remove air from the furnace chamber. As the first step, argon gas was flushed into the chamber and subsequently removed by the vacuum pump. This process was repeated twice to prevent potential chemical contamination from atmospheric impurities. Removal of binders and sponge was performed while pressurized argon gas flowed through the furnace under a controlled heating rate. Thermogravimetric analysis (TGA, Perkin Elmer, software of Pyris windows) of the sponge and binder was used as the base for the design of an optimized heating profile. The final heating profile was as follows:

RT 150 min → 150 °C 720 min → 400 °C 150 min → 500°C 120 min → 500°C 600 min → RT

- **Sintering**

The samples after the removal of sponge and binders were eventually sintered in a high vacuum furnace (10^{-5} mbar) with heating profile as followings:

RT 600 min → 500 °C 450 min → 1250 °C 120 min → 1250°C furnace cooling → 25°C

2.3. Characterization

- **General**

Porous Ti6Al4V prepared in the present study was characterized for geometry and porosity, chemical composition, microstructure and mechanical properties, using a stereo optical microscopy (Nikon SMZ-10A with Sony progressive 3CCD color video camera), and environmental scanning electron microscopy (ESEM, Model XL-30, Philips, Eindhoven, The Netherlands) together with energy dispersive micro X-ray analysis (EDX), and a mechanical testing machine (Zwick50, Germany).

- **Pore structure**

The characterization of the porous structure included: mean pore size, uniformity of porous structure, porosity, interconnectivity and inner surface pattern of pores.

To measure the pore size, 10 samples were cut from different porous Ti6Al4V blocks using a WOCO50 sawing machine and a WOCO 997 sawing blade (Wolfgang Conrad), and then the cross sections were polished with a series of SiC papers. After being cleaned in an ultrasonic water bath and dried, the samples were put directly into the ESEM. Under the same magnification (15x), ten (10) random

pores in each sample were measured and imaged, and then used for calculating the mean pore size, standard deviation and pore size distribution indication. Micro pores on the inner surface were measured similarly to determine mean pore size. A sample was put in the ESEM, and under high magnification (500x), surface within a pore was clearly visible, allowing micro pore size to be measured.

Porosity (in % of volume) was calculated by two methods: (1) Porosity (ρ) was calculated by measuring the apparent density (ρ_b = weight of sample/ volume of sample) of sample by using the formula: $\rho = (1 - \rho_b / \rho_s) \times 100$, where ρ_s is the density of 100% dense material. A total of 10 samples were measured. (2) Porosity was estimated using quantitative analysis. The cross-sectioned sample was prepared and cleaned to remove any shaving trapped in the cutting process. After cleaning, the sample was embedded in a viscous epoxy and then evacuated to insure that the epoxy fully penetrated the open cell structure. Next, it was prepared through standard metallographical procedures, and photographed using an inverted stage reflecting light microscope. A selected region of the image was analysed and two counts were made, one of the black pixels and one of the total pixels in the region. The ratio of the number of black pixels to the total pixels in the region represented the factory porosity of the porous body.

Microstructure of inner surface wall of the pores: An inner surface roughness profile was scanned by a non contact Laser Profilometer (UBM measurement system A538, The Netherlands) and surface roughness was calculated according to DIN4768. In addition, we used an equivalent model sample, consisting of a Ti6Al4V plate with a powder layer, for three reasons: 1) to compare inside of porous Ti6Al4V with bead surface coating, 2) to conveniently look at a surface, 3) to easily measure surface roughness.

- **Chemical analysis**

An EDX spectrum of porous Ti6Al4V sample was made to determine the spectrum of porous Ti6Al4V. The oxygen, carbon, and nitrogen contents were analyzed for the raw Ti6Al4V powders, the debinded Ti6Al4V powders (after removal of sponge and binders) and sintered Ti6Al4V. The carbon and nitrogen contents were measured according to ASTM D5271, and the hydrogen and oxygen contents were measured according to JGKJ121.18-2001(Chinese standard).

- **Mechanical properties**

A total of fifteen porous Ti6Al4V samples with a size of $\varnothing 10 \times 11$ mm were prepared using a wire electrical discharge machine. The compressive strength was determined using a mechanical testing machine at a crosshead speed of 1mm/min.

- **Metallurgical Analysis**

Standard metallurgical techniques were applied with the porous Ti6Al4V samples to analyze the microstructure generated by heat treatment. Samples were sectioned by using a WOCO50 sawing machine. Primary polishing was accomplished by grinding with #320 SiC paper, followed by #600, #1200 and #2000 SiC papers respectively. Fine polishing was accomplished by using one micron diamond paste, followed by a 0.05 μm alumina as its final step. Etching was performed using the following solution: 95% distilled water, and 5% hydrofluoric acid. The etchant was applied on the sample surface by swabbing with cotton for 3-5 sec. Samples were then rinsed with water, and dried by blowing air onto the surface.

2.4. Cell attachment study

MC3T3-E1 osteoblast-like cells were used for cell attachment study. The culture medium used was α -MEM supplemented with 10% fetal bovine serum (FBS, Life Technologies, The Netherlands), antibiotics, 1% sodium pyruvate. The cells were seeded on porous Ti6Al4V samples placed in 20-well plates at 1.2×10^6 cells/per sample in 4ml of medium, and cultured at 37°C in a humidified atmosphere with 5% CO₂ and 95% air. After being cultured for 4hrs and 3 days, respectively, the samples (n=2) were fixed and then rinsed with PBS, dehydrated in a graded ethanol series, critical point dried, sputter coated with carbon and examined with ESEM. Other samples (n=3) were digested with proteinase K (Sigma, The Netherlands), added with heparin (Leo Pharm, The Netherlands) and Ribonu-lease A (Sigma, The Netherlands), then shaken and incubated at 56°C for 16hrs. A volume of 100 μm solution of each sample was mixed with 100 μm Cyquant GRDye (Molecular Probe, Poland), and the fluorescence with fluorimeter (Perkin Helmer) was measured at emission wavelength 520nm and excitation 480nm. The DNA content of cells attached on the porous samples was counted through a pre-made standard DNA curve. DNA content was expressed as mean \pm SD.

3. Results

3.1. Raw materials characterization

Fig.1A illustrates an image of Ti6Al4V powder under ESEM. It shows that all powders are spherical in shape. The chemical composition of Ti6Al4V powder and the requirement of ISO5832 standard are listed in Table 2. The distribution of the particle size of Ti6Al4V powder can be seen in Fig. 1B, the majority (~50%) is between 10-30 μm , a range that facilitated the preparation of Ti6Al4V slurry and later its sintering. The smaller the particle size, the lower the sedimentation speed;

on the other hand, fine powders can be sintered more readily than coarse ones. Fig.2 shows that the pores of sponge are well interconnected.

Table 2 Chemical composition of Ti6Al4V powder

Element(wt%)	Al	V	N	H	O	C	Fe	Si	Ti
Ti6Al4V	6.47	4.08	0.025	0.008	0.183	0.02	0.12	0.04	Bal
ISO5832	5.5-6.8	3.5-4.5	0.05	0.015	0.20	0.08	0.3	0.04	Bal

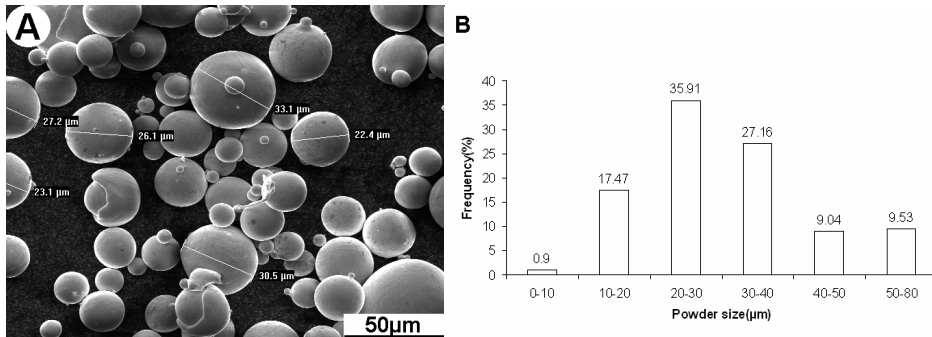


Fig.1 Ti6Al4V particle shape and size distribution of A) Particles under ESEM
B) Particle size distribution

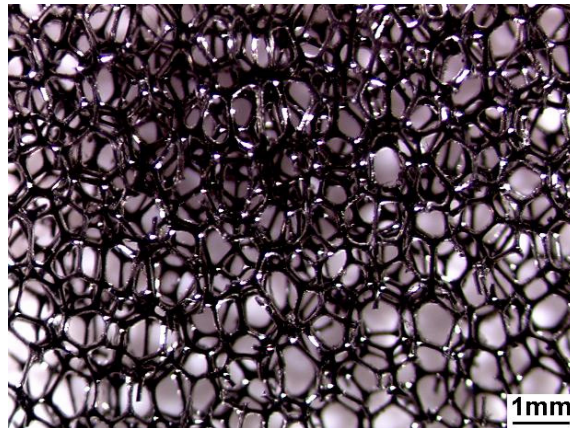


Fig. 2 Polyurethane (PU) sponge under optical micrograph

The results from the removal of sponge and binders by TGA measurement are illustrated in Fig.3. It reveals that most of the sponge and binders pyrolyzed between 150 and 400°C. To complete this pyrolysis process, the debinding temperature was set at 500 °C under flowing argon atmosphere.

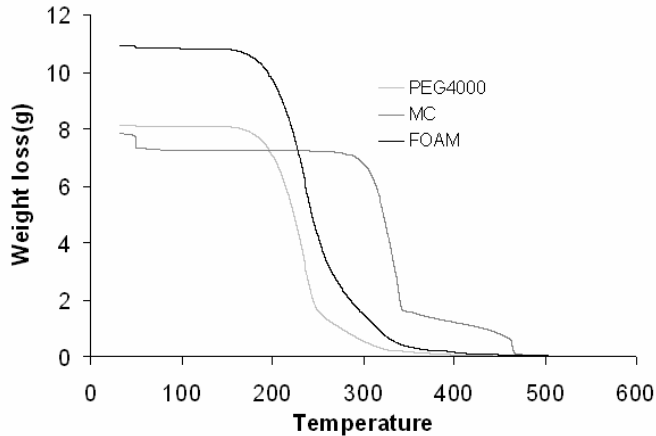


Fig. 3 TGA curves of PEG, MC and PU sponge

3.2. Shrinkage of porous Ti6Al4V

The dimension of a sample was 100X15X30mm before sintering and 91.5X13.7 X 25.6 mm after sintering at 1250°C for 2hrs. Consequently, the horizontal linear shrinkage rate was about 8.5 %, and the vertical linear shrinkage 14.7%, corresponding to a volumetric decrease of 28.7 %.

3.3. Structural analysis

- **Macro porous structure of porous Ti6Al4V and cancellous bone**

Fig.4 (A) and (B) show the macro structures of our porous Ti6Al4V and goat cancellous bone using ESEM. The porous Ti6Al4V reveals a porous, open-cell structure with a sponge-like appearance. The pores are interconnected. Compared with the macrostructure of cancellous bone (shown in Fig. 4(B)), both structures possess similar interconnected porous structures.

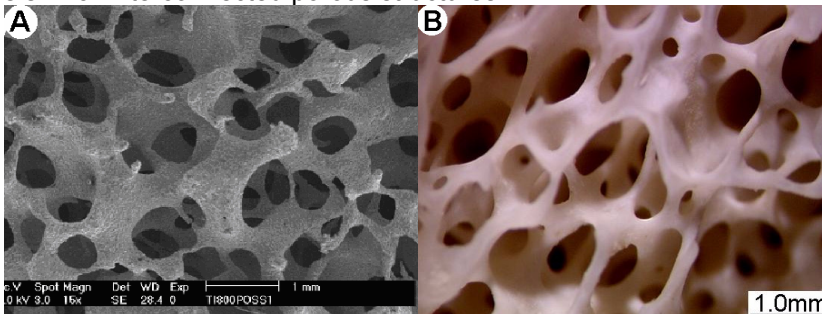


Fig. 4 Macrostructure of porous Ti6Al4V and nature bone from goat. (A) Porous Ti6Al4V. (B) Cancellous bone from goat

- **Mean pore size and pore size distribution indication**

An image of a cross-section of the porous Ti6Al4V is shown in Fig. 5A. The mean pore size was measured on surface pores. The distribution indication of pore size is illustrated in Fig. 5B. A majority of pores are between 400 μm and 700 μm .

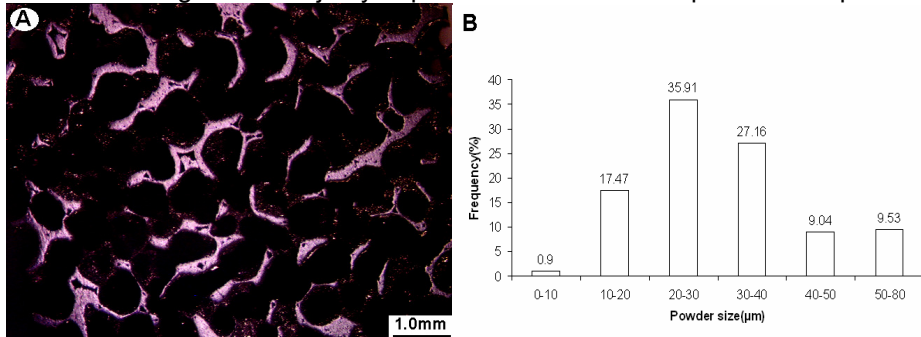


Fig. 5 A) A cross-section of porous Ti6Al4V, B) Pore size distribution of porous Ti6Al4V

- **Density and porosity**

Cylindrical and cubic samples were employed, and their weight and volume were measured. The bulk density was $0.49 \pm 0.1 \text{ g/cm}^3$. Taking the theoretical density of solid Ti6Al4V as 4.45 g/cm^3 , the porosity of porous Ti6Al4V was calculated to be $89 \pm 1.6\%$.

By using image analysis, we estimated that the percent porosity of porous Ti6Al4V to be $91 \pm 1.2\%$. These two methods showed good agreement.

- **Microstructure of inner surface wall**

The microstructure of an inner surface wall is shown in Fig. 6. Fig. 6(A) indicates that powder bonding is achieved by neck growth through a solid state diffusion process. No liquid phase occurs. The measured surface roughness (R_a) was $3.4 \pm 0.3 \mu\text{m}$ by equivalent model. Fig. 6(B) shows a high magnification of the inner surface of a pore. The voids in the rough surface are referred to as micropores, and their size ranges from 1 to 10 μm .

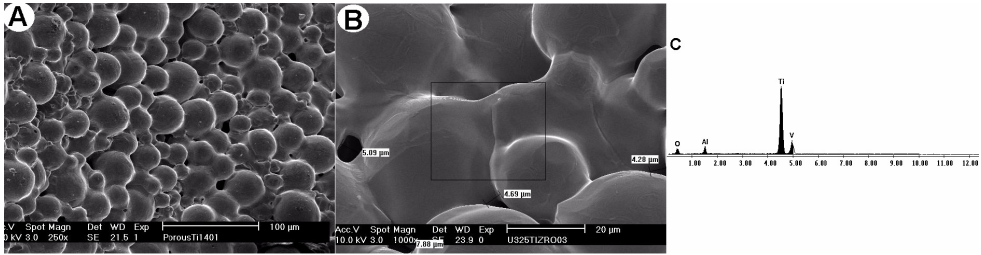


Fig. 6 ESEM images of the inner surface of pores and EDX spectrum acquired from the same area. A) micropore and rough surface structure, B) higher magnification (marked area where EDX was taken), C) EDX spectrum obtained showing a typical spectrum for Ti6Al4V

3.4. Elemental analysis

An EDX spectrum was taken from a sample to determine the chemical composition of porous Ti6Al4V after sintering. Fig. 6B shows the surface (square area) from which the spectrum was acquired and Fig.6C shows the spectrum. We can conclude that porous Ti6Al4V after sintering has a typical spectrum of Ti6Al4V. The chemical analysis results of organic residuals (oxygen, hydrogen, carbon and nitrogen) after the different processing steps are shown in Fig. 7. It can be seen that the contents of oxygen, hydrogen and nitrogen remain nearly unchanged after removal of sponge and binders, the carbon content increases from 0.02% to 0.08%. After sintering, the concentration of carbon, oxygen and nitrogen are all increased. The reason for this behaviour is probably due to residual contaminants in the furnace.

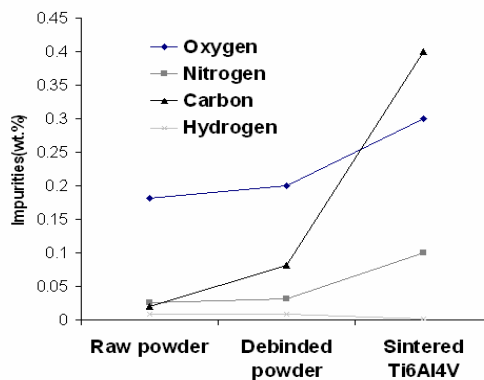


Fig. 7 Chemical analysis of oxygen, carbon, hydrogen and nitrogen contents in Ti6Al4V samples with different steps.

3.5. Mechanical properties

Fig.8 shows the compressive stress-strain curve of the porous Ti6Al4V with a porosity of 90%. The curve was generally characterised by an initial elastic response, followed by decreasing stress, then a long plateau with a little oscillation where the stress is almost independent of strain, finally a region of densification where the stress-strain curve rises slowly. The average compressive strength of porous Ti6Al4V with a porosity of 90% is 10.3 ± 3.3 MPa. The Young's modulus is 0.8 ± 0.3 GPa as calculated from the elastic part of compressive stress-strain curves.

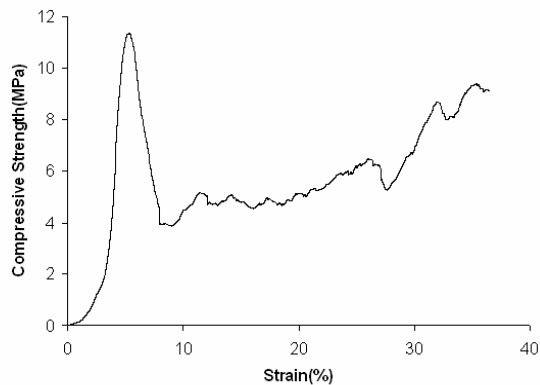


Fig. 8 Compressive stress-strain curve of porous Ti6Al4V with a porosity of 90%.

3.6. Metallography

The Ti6Al4V plate was found to have an equiaxed alpha-beta microstructure. Fig.9 A shows the microstructure of a Ti6Al4V plate without any heat treatment. The matrix is alpha, the small second phase particles are beta. The porous Ti6Al4V was found to have a coarse acicular microstructure, revealing alpha grains with intergranular beta phase (shown in Fig.9B).

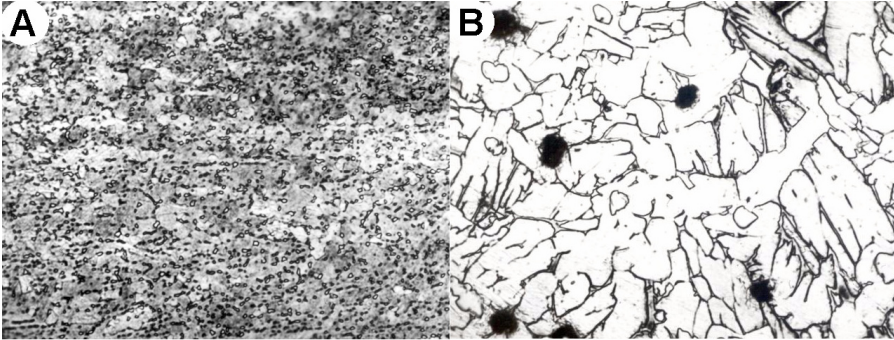


Fig. 9 Light micrograph of section: (A) The raw Ti6Al4V without further heat treatment, revealing an equiaxed alpha-beta microstructure; (B) The porous Ti6Al4V revealing a coarse acicular microstructure.

3.7. Cell attachment test

Fig.10 shows ESEM images of cells cultured on the porous Ti6Al4V samples for 4hrs (Fig.10A) and 3 days (Fig.10B). It can be seen that cells, polygonal and spindle-shaped, attached and spread on the inner surface of porous Ti6Al4V. Meanwhile we can see some cells growing into micropores in the inner surface and the spreading cells maintaining a physical contact with each other by lamellopodia. Cells also formed the extracellular matrix on the surface. No significant difference was found between cells cultured 4hrs and 3 days, but DNA content assay (Table 3, $R^2=0.99$) confirmed that after 3 days culture more cells were found to attach and spread on the porous Ti6Al4V. Cell attachment test reveals that the cells are not only able to attach and spread well on the inner surface of porous Ti6Al4V, but also are able to form an extracellular matrix.

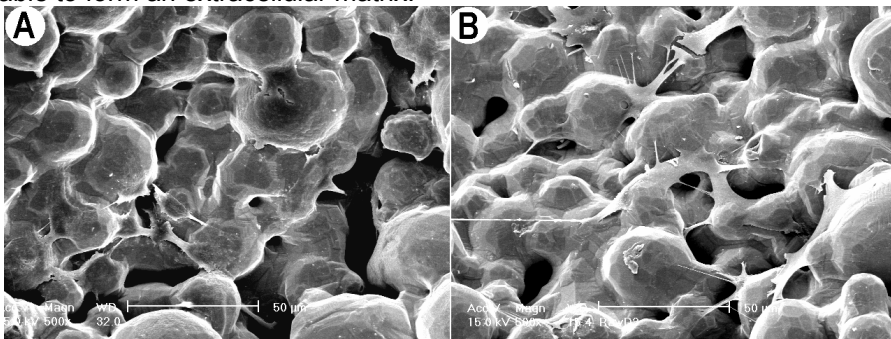


Fig.10 MC3T3-E1 osteoblast-like cells cultured on the porous Ti6Al4V for A) 4hrs, B) 3days.

Table3 DNA content of cells attached on the porous Ti6Al4V

Cultured time	DNA content(ng)
4 hours	5321.56±295.31
3 days	10678.66±1034.31

4. Discussion

The novel feature of the current technique is that the traditional method of “polymeric sponge replication” producing porous ceramics (porous alumina) [37] was successfully applied for making porous Ti6Al4V. The procedure itself is basically simple: dipping polymeric sponge into Ti6Al4V slurry, then debinding to remove binders and sponge struts, and finally sintering to obtain a porous Ti6Al4V body. The structure resembles the original sponge structure. The porosity is up to 90% with complete open structure.

Normally, at 1250°C, titanium powder bonding is achieved through a solid state diffusion process. The driving force during this particle to particle sintering is a reduction of the local surface energy. When the highly reactive metal reacts with oxygen, carbon or nitrogen to form brittle surface layers of titanium oxide, carbide or nitride, this surface energy increases and affects the bonding process as well as ductility and fatigue properties of the final product. To prevent contamination from oxygen, nitrogen and carbon, we applied a novel method by flushing with high purity of argon gas and titanium hydride particles in the process of debinding and sintering. During the debinding and sintering, titanium hydride was first decomposed to pure titanium and hydrogen starting at 400°C, and almost completed around 600°C. Above 700°C, only little TiH₂ remained to be decomposed [38-40]. The titanium generated by decomposing titanium hydride is more reactive than normal pure titanium or Ti6Al4V, thus reacting with nitrogen, oxygen and carbon in the chamber before these impurities can react with porous Ti6Al4V. In addition, hydrogen reacted with oxygen.

As a result, the titanium hydride particles act as a scavenger, protecting porous Ti6Al4V from less desirable compounds. Also the flushing high pure argon gas and sintering under a high vacuum has the further advantage of reducing contaminations. Therefore, our enhanced fusion of Ti6Al4V particles may be caused by the absence of titanium carbide and oxides, resulting in increased mechanical properties of the final porous body. It should be noted that the sintering parameters of porous Ti6Al4V alloys can be optimized by further reducing organic residues: this will be the subject of further studies.

Our porous Ti6Al4V created by “polymeric sponge replication” has a 3D reticulate structure with interconnected pores. As stated before, we need both macro and micro pores, because both types of pores also exist in the solid bony skeleton

(shown in Fig.6A and Fig.6B). Macropores (size and volume) are generated and controlled by sponge characteristics. By selecting different sponges, we can obtain porous Ti6Al4V with varied pore sizes. Micropores are formed by powder sintering and removal of sponge struts. ESEM shows that the micropore size ranged from 1-10 μ m. The surface roughness of the pore walls was estimated by measuring the roughness of a model surface consisting of a powder layer sintered onto a flat solid Ti6Al4V plate. The resulting Ra of 3.4 μ m gives an indication of the “inner” surface roughness of the pores. Recent studies show that microarchitecture plays an important role in the process of bone formation and growth [41,42]. The microarchitecture of the inner surfaces of pores is favourable for cell seeding, cell attachment, proliferation, differentiation and ingrowth of tissue [43].

The porosity of a scaffold influences its mechanical strength according to Gibson and Ashby's model [44] and permeability. Porous Ti6Al4V made by our method has a porosity of 90%, which will be very useful for biomolecules and degraded substances to freely flow into and out of the scaffold. The compressive strength of porous Ti6Al4V in the present study was about 10MPa, slightly higher than that of cancellous bone.

It is clear that where titanium and its alloy is notch sensitive materials the microstructure of these sintered products may well affect mechanical properties like fatigue strength even more. The necking of the powder particles after sintering and possible residual porosity may present discontinuities where stress concentrations will occur. Also, the sintering process causes the microstructure to transform from a fine equiaxed structured to a lamellar, coarse structure as a result of heating the material above its beta phase transition temperature at 992°C with even more detrimental effects on fatigue strength [45]. In loaded application, the fine equiaxed microstructure is certainly preferred in this respect. A number of attempts have been made to transform the microstructure to more favourable forms [46-49]. Cook reported that mechanical properties of the porous coated implant could be improved significantly by the use of post sintering heat treatments directed to reduce alpha grain size [50]. Still, it must be realized that the use of these porous or porous coated implants should be confined to applications where stresses are below the material's fatigue endurance limit and compressive rather than tensile of nature.

All dense metallic alloys used in medical devices have an Young's modulus significantly higher than that of bone, although dense Ti6Al4V has a lower Young's modulus than other metallic biomaterials used for orthopaedic implants [1-3]. The mechanical incompatibility causes implants to be structurally stiffer than bones. The Young's modulus of cancellous bone and cortical bone range from 0.5 GPa to 30GPa. The Young's modulus of porous Ti6Al4V with a porosity of 90% is between

that of cancellous bone and cortical bone. It reveals that porous Ti6Al4V can be made with low Young's modulus thereby reducing stress shielding.

Our experimental result of cell attachment showed that the cells attached and spread well on the surface of porous Ti6Al4V. But in *in vitro* experiments, cell attachment tests only give information on cell attachment and the number of cells in the porous Ti6Al4V. Actually, biomaterials implanted in the bone will encounter complicated conditions compared to that *in vitro*, such as more and different cell types, local strain, and pH changes due to tissue inflammation. Consequently, it is necessary to perform *in vivo* experiments to understand how the bone interacts with our porous Ti6Al4V.

An interesting step in the whole processing route is shaping: the porous Ti6Al4V retained its shape after the supporting sponge was burned out. The reasons can be summarized as following: (1) Powder metallurgy technique was applied for making porous Ti6Al4V. There are some micropores among powders which can overcome collapse during a pyrolysis process, while the polymeric sponge is burning out. There is a space to evaporate gas pyrolyzed by sponge. (2) Binders with two ingredients were used to prepare Ti6Al4V slurry. The two binders were decomposed or evaporated at different temperatures. From TGA curves, it can be seen that first the PEG4000, then the sponge, finally the MC, decomposed to avoid collapsing. (3) The rate of heating was precisely controlled to burn out binders and sponge. As the 'green' part is extremely porous, the sintering temperature must be very strictly controlled in order to retain the shape and prevent from 'slumping'. Removing the binder too fast resulted in blisters, removing it too slowly on the contrary resulted in partial collapsing [51,52].

5. Conclusions

Porous Ti6Al4V was successfully made by integrating a powder metallurgy processing with "polymeric sponge replication". The novel feature of this method lies in the fact that the structure of porous Ti6Al4V body can be directly replicated from that of sponge structure. The porous Ti6Al4V made in such a way possesses a completely open pore, high porosity (~90%), and reticulate porous structure. This structure is similar to that of cancellous bone. The compressive strength is 10.3 ± 3.3 MPa, and the Young's modulus is between that of cancellous bone and cortical bone. *In vitro*, experiments show that the porous Ti6Al4V is not only non-toxic but also favourable for cell attachment. The porous Ti6Al4V fabricated by this method is expected to be a very promising biomaterial for orthopaedic implants.

6. Acknowledgements:

The authors would like to thank IsoTis S.A for the financial support. The authors also thank Fabienne Peters for her enthusiastic help in the TGA experiments and Dr.Jiawei Wang for cell attachment experiments. The discussions with Dr. Huipin Yuan were also very constructive during the preparation of this paper.

Reference

1. Long M, Rack HJ. Review Titanium alloys in total joint replacement materials science perspective. *Biomaterials* 1998;19:1621-1639.
2. Wilke A, Landgraff M, Orth J, Kienapfel H, Grissand P, Franke R. Human bone marrow cell cultures: a sensitive method for determination of the biocompatibility of implant materials. *ATLA* 1999;27:137-151.
3. Gu H, Xu G. *Material Science of Biomedical*. Tianjin: Science Translation Press.; 1993.
4. Pilliar RM. Powder metal-made orthopedic implants with porous surface for fixation by tissue ingrowth. *Clin Orthop* 1983(176):42-51.
5. Pilliar RM, Cameron HU, Welsh RP, Binnington AG. Radiographic and morphologic studies of load-bearing porous-surfaced structured implants. *Clin Orthop* 1981(156):249-57.
6. Pilliar RM, Cameron HU, Macnab I. Porous surface layered prosthetic devices. *Biomed Eng* 1975;10(4):126-31.
7. Murray GA, Semple JC. Transfer of tensile loads from a prosthesis to bone using porous titanium. *J Bone Joint Surg Br* 1981;63-B(1):138-41.
8. Maniatopoulos C, Pilliar RM, Smith DC. Evaluation of shear strength at the cement-endodontic post interface. *J Prosthet Dent* 1988;59(6):662-9.
9. Maniatopoulos C, Pilliar RM, Smith DC. Threaded versus porous-surfaced designs for implant stabilization in bone-endodontic implant model. *J Biomed Mater Res* 1986;20(9):1309-33.
10. Maniatopoulos C, Pilliar RM, Smith DC. Evaluation of the retention of endodontic implants. *J Prosthet Dent* 1988;59(4):438-46.
11. Simmons CA, Valiquette N, Pilliar RM. Osseointegration of sintered porous-surfaced and plasma spray-coated implants: An animal model study of early postimplantation healing response and mechanical stability. *J Biomed Mater Res* 1999;47(2):127-38.
12. Clemow AJ, Weinstein AM, Klawitter JJ, Koeneman J, Anderson J. Interface mechanics of porous titanium implants. *J Biomed Mater Res* 1981;15(1):73-82.
13. Bobynd JD, Pilliar RM, Cameron HU, Weatherly GC, Kent GM. The effect of porous surface configuration on the tensile strength of fixation of implants by bone ingrowth. *Clin Orthop* 1980(149):291-8.

14. Katz JL, Pilliar RM, Berkowitch J, Christel P, Higham P, Kempeneers R, Knox GF, Scott I, Sudanese A. Biomechanical stability and design. Stiffness and remodeling. *Ann N Y Acad Sci* 1988;523:283-6.
15. Cameron HU, Pilliar RM, Macnab I. The rate of bone ingrowth into porous metal. *J Biomed Mater Res* 1976;10(2):295-302.
16. Chen PQ, Turner TM, Ronnigen H, Galante J, Urban R, Rostoker W. A canine cementless total hip prosthesis model. *Clin Orthop* 1983(176):24-33.
17. Landon GC, Galante JO, Maley MM. Noncemented total knee arthroplasty. *Clin Orthop* 1986(205):49-57.
18. Bobyn JD, Cameron HU, Abdulla D, Pilliar RM, Weatherly GC. Biologic fixation and bone modeling with an unconstrained canine total knee prosthesis. *Clin Orthop* 1982(166):301-12.
19. Hahn H, Palich W. Preliminary evaluation of porous metal surfaced titanium for orthopedic implants. *J Biomed Mater Res* 1970;4(4):571-7.
20. Galante J, Rostoker W. Fiber metal composites in the fixation of skeletal prosthesis. *J.Biomed.Mater.Res.* 1973;4:43-61.
21. Welsh RP, Pilliar RM, Macnab I. Surgical implants. The role of surface porosity in fixation to bone and acrylic. *J Bone Joint Surg Am* 1971;53(5):963-77.
22. Wu BD, Cui YF. Research on porous titanium for medical implant material. *Rare Metal Materials Engineering* 1988;4.
23. Wu BD, Guo FH. A study of preparation of man-made hipbone by using composite porous titanium. *The Technology of Powder Metallurgy* 1990;8(4):145-149.
24. Pilliar RM. Overview of surface variability of metallic endosseous dental implants: textured and porous surface-structured designs. *Implant Dent* 1998;7(4):305-14.
25. Pilliar RM, Deporter DA, Watson PA, Todescan R. The endopore implant-enhanced osseointegration with a sintered porous- surfaced design. *Oral Health* 1998;88(7):61-4.
26. Pilliar RM. P/M Processing of Surgical Implants: Sintered Porous Surfaces for Tissue-to-Implant Fixation. *International Journal of Powder Metallurgy* 1998;34(8):33-45.
27. Asaoka K, Kuwayama N, Okuno O, Miura I. Mechanical properties and biomechanical compatibility of porous titanium for dental implants. *J Biomed Mater Res* 1985;19(6):699-713.
28. Pilliar RM. Porous-surfaced metallic implants for orthopedic applications. *J Biomed Mater Res* 1987;21(A1 Suppl):1-33.
29. Oliveira MV, Pereira LC, Cairo CAA. Porous Structure Characterization in Titanium Coating for Surgical Implants. *Materials Research* 2002;5(3):269-273.
30. Oh IH, Nomura N, Masahashi N. Mechanical properties of porous titanium compacts prepared by powder sintering. *Scripta Materialia* 2003;49:1197-1202.

31. Galante J, Rostoker W, Lueck R, Ray RD. Sintered fiber metal composites as a basis for attachment of implants to bone. *J Bone Joint Surg Am* 1971;53(1):101-14.
32. Ducheyne P, Willems G, Martens M, Helsen J. In vivo metal-ion release from porous titanium-fiber material. *J Biomed Mater Res* 1984;18(3):293-308.
33. Kuo KN, Gitelis S, Sim FH. Segmental replacement of long bones using titanium fiber metal composite following tumor resection. *Clin Orthop* 1983;176:108-114.
34. Wen C, Yamata Y, Mabuchi M. Processing and mechanical properties of autogenous titanium implant materials. *J Mater Sci:in medicine* 2002;13:397-401.
35. Matin B, Cornelia S, Bronkremmer HP, Baur H. High-porosity Titanium, Stainless Steel, and Superalloy Parts. *Advance Engineering Materials* 2000;2(4):196-199.
36. Engh CA. Hip arthroplasty with a Moore prosthesis with porous coating. *Clin. Orthop* 1983;176:52-66.
37. Kwon S-H, Jun Y-K, Hong S-H. Calcium Phosphate Bioceramics with Various Porosities and Dissolution Rates. *J Am Ceram Soc* 2002;85(12):3129-31.
38. Akiyama S, Ueno H, Imagawa K, Kitahara A, Nagata, Morimoto SK, Nishikawa T; Foamed metal and method of producing the same. US Patent patent 4,713,277. 1987.
39. Gergely V, Curran DC, Clyne TW. The FOAMCARP process: foaming of aluminium MMCS by the chalk-aluminium reaction in precursors. *Composites Science and Technology* 2003;63(16):2301-2310.
40. Mu W, Deng GZ, Luo FC. *Titanium Metallurgy*. Beijing: Metallurgy Industry Press; 1998.
41. Wilson C, De Bruijn J, Kruijt M, Van Gaalen S, Dhert WV, A. , Van Blitterswijk CA. Design and fabrication of porous hydroxyapatite scaffolds for bone tissue engineering using Rapid prototyping techniques. 2001; San Francisco USA. p 25-28.
42. Yuan H, Kurashina K, de Bruijn JD, Li Y, de Groot K, Zhang X. A preliminary study on osteoinduction of two kinds of calcium phosphate ceramics. *Biomaterials* 1999;20(19):1799-806.
43. Zhang C, Wang J, Zhang X. Osteoinductivity and biomechanics of a porous ceramic with autogenic periosteum. *J Biomed Mater Res* 2000;52:354-59.
44. Gibson LJ, Ashby MF. *Cellular Solids: Structure and Properties*. Cambridge: Cambridge University Press; 1997.
45. Weinstein AM, Klawitter JJ. *Structure Properties Relationship for Porous Ti6Al4V*. 1977; New Orleans. US.
46. Cook SD, Anderson RC, Thongpreda N, Haddad RJ, Jr. The effect of post-sintering heat treatments on the tensile properties of Ti-6Al-4V alloy. *Biomater Med Devices Artif Organs* 1986;14(3-4):167-80.
47. Cook SD, Renz EA, Haddad RJ. Post-sintering heat treatments for porous coated Ti-6Al-4V alloy. *Biomater Med Devices Artif Organs* 1985;13(1-2):37-50.

48. Kohn DH, Ducheyne P. A parametric study of the factors affecting the fatigue strength of porous coated Ti-6Al-4V implant alloy. *J Biomed Mater Res* 1990;24(11):1483-501.
49. Kohn DH, Ducheyne P. "Materials for Bone and joint Replacement" in *Materials Science and Technology. A Comprehensive Treatment*. VCH Publications; 1992. 31 p.
50. Cook SD, Thongpreda N, Anderson RC, Haddad RJ, Jr. The effect of post-sintering heat treatments on the fatigue properties of porous coated Ti-6Al-4V alloy. *J Biomed Mater Res* 1988;22(4):287-302.
51. Lin JY, Zhang Y. Effect of fabrication technology on the structures and properties of TiC ceramics foam. *Powder Metallurgy Technology* 2000;18(1):12-15.
52. Wegmann G, Gerling R, Ebel T, Otto K-H. *Metal injection moulding of Titanium alloys for medical applications*. 2001; Munich, Germany.

Chapter 4

Improvement of mechanical properties of porous Ti6Al4V

J.P. Li¹, S.H. Li², C.A. van Blitterswijk¹, K. de Groot^{1,2}

¹Institute for Biomedical Technology, University of Twente, The Netherlands.

²CAM Implants. B.V, The Netherlands.

Abstract

A highly porous Ti6Al4V with interconnected porous structure has been developed in our previous study. By using a so-called “multiple coating” technique, the porous Ti6Al4V can be tailored to resemble cancellous bone in terms of porous structure and mechanical properties. A thin layer of Ti6Al4V slurry was coated on the struts of base porous Ti6Al4V produced by sponge replication method in order to improve the pore structure. After two additional coatings, pore sizes ranged from 100 μm to 700 μm , and the porosity was decreased from $\sim 90\%$ to $\sim 75\%$, while the compressive strength was increased from 10.3 ± 3.3 MPa to 59.4 ± 20.3 MPa and the Young’s modulus increased from 0.8 ± 0.3 GPa to 1.8 ± 0.3 GPa. The achieved pore size and porosity were similar to that of cancellous bone, the compressive strength is higher than that of cancellous bone. The Young’s modulus lied between that of cancellous and cortical bone. Porosity, pore size and mechanical properties can be controlled using this multiple coating method.

Keywords: Ti6Al4V, porosity, multiple-coating, mechanical properties.

1. Introduction

Development of porous metallic biomaterials associated with their applications in orthopaedics is becoming an increasingly important research project, compared with that of dense metallic biomaterials. Porous metallic biomaterials facilitate bone ingrowth and thereafter improve the interlock between implants and bone. While developing a new porous metallic biomaterial, we have to consider a number of requirements. Firstly, the material must be biocompatible. Secondly, the porous metallic biomaterials should have a high porosity and a porous structure similar to that of human cancellous bone, which therefore can provide sufficient space for tissue ingrowth and exchange of body fluids. A number of research groups have reported porosity and pore size of porous biomaterials are important parameters for bone ingrowth [1-3]. Although there are wide discrepancies regarding the optimal pore size for effective bone ingrowth, a minimum pore size of 100-150 μm is generally considered acceptable for healthy bone ingrowth. Besides porosity and pore size, pore size distribution, pore shape, fenestration size and interconnectivity of the pores [3-5] have also shown their influences on bone formation. Thirdly, the porous metallic material must have suitable mechanical properties [6,7] including a higher compressive strength and an appropriate young's modulus [8].

Due to their excellent biocompatibility and corrosion resistance as compared to conventional stainless steels and cobalt-based alloys [6,9], titanium and its alloy have been widely used as biomaterials in biomedical devices for a long time. Although there are several methods to make porous titanium and its alloy, such as sintering particles and fibres together [10], or processing a mixture of titanium powder and a polymer pore-former [11], the mechanical properties of the resulting porous materials could not be compared with those of human cancellous bone. Accordingly, we developed a new processing technique to make porous Ti6Al4V for biomedical applications.

The porous Ti6Al4V was fabricated by a polymeric sponge replication process, which involves the following steps: impregnation of a polymeric sponge by immersing it in a Ti6Al4V slurry, removal of excess slurry, drying, debinding (the sponge is burned out) and sintering, resulting in a positive replica in Ti6Al4V of the original polymeric sponge [12]. The porous Ti6Al4V obtained possesses a reticulated network with pore size ranging from 100 μm to 1000 μm . After the polymeric sponge was burned out, thin struts, cracks and triangular voids were left inside the structure, which would be sensitive to structural stresses [13,14]. The purpose of this study was to develop a new method to produce porous Ti6Al4V, which may better resemble cancellous bone mechanically and structurally, even assuming biologically.

2. Materials and methods

2.1. Multiple-coating Technique

2.1.1. Materials

Base porous Ti6Al4V with a pore size of 100-1000 μm was fabricated by 'polymeric sponge replication' method as described previously [15]. The samples were subjected to ultrasonic cleaning in acetone, ethanol (70%), and demineralised water for 15 min respectively. The slurry used in this process was termed as "Slurry I [16]". Cancellous bone was obtained through boiling goat cancellous bone for one week to remove collagens and other components.

2.1.2. Thin Ti6Al4V slurry (Slurry I I) for coating

The slurry used has the following chemical composition (in weight percentage wt %): 63.4wt% Ti6Al4V powder (North-west no-ferrous institute, China), 31.7wt% demineralised water, 1.5wt% Polyethyleneglycol4000 (PEG4000, Fluka Chemie GmbH, Germany), 0.4wt% methylcellulose (MC, Fisher Scientific B.V, The Netherlands), 1 % dispersant (Dolapix, Aschimmer&Schwarz GmbH Germany), 1 % ammonia solution (25%, Merck) and 1wt% of 1-Octanol. Firstly, demineralised water was mixed with PEG4000 and MC by stirring for 1h, then Ti6Al4V powder was added and stirring continued for 1.5 h, finally, Dolapix, ammonia solution and 1-octanol were added to improve rheological behaviour. Stirring was subsequently continued for another 1h to achieve homogeneous slurry. The viscosity of the thin Ti6Al4V slurry was measured by viscometry (Brookfield Engineering Labs DV-II+ viscometer) with a spindle of RV4 at the speed of 20 rpm at room temperature

2.1.3. Multiple Coating

The base porous Ti6Al4V was dipped into Slurry II for 30 seconds and then taken out. High-pressure air was used to remove excess slurry to achieve a thin homogenous coating on the struts and to prevent the slurry from blocking the pores. After coating, the samples were dried for 1h at 80°C and for 24hrs at room temperature. Finally, the samples were sintered at 1250°C under high vacuum (10^{-5} mbar) with a dwell time of 2 hrs. The coating procedure can be separated before sintering to obtain samples with multiple coating.

2.2. Characterization

2.2.1. Porosity

The porosity of porous Ti6Al4V sample was calculated from its weight and volume by comparing the bulk density of cylindrical samples (n=10) with the theoretical one of Ti6Al4V: 4.45g/cm³.

2.2.2. Pore size and porous structure

By using an environment scanning electron microscope (ESEM, XL30 ESEM-FEG, Philips, The Netherlands), the structure of porous Ti6Al4V were analysed from cross-sections of the samples. From these cross-sections, estimations of the pore sizes were made by linear measurements. Pieces of porous Ti6Al4V (dimensions Ø10x12mm) were cut off by using a WOCO50 sawing machine and a WOCO 997 sawing blade (Wolfgang Conrad) and polished with a series of SiC sand papers (types from 800, 1200 and 2400). After sawing the samples (n=5, respectively) were cleaned in an ultrasound water bath and dried before ESEM observation.

2.2.3. Permeability

A permeability test was performed with a self-designed permeability-meter [17]. Briefly, a cylindrical sample was mounted in a tube connected to a wide diameter water reservoir which was positioned at a certain constant height. The flow of water through the sample was measured in ml/sec. Normalized for the dimensions of the sample, it provided measure of the sample's permeability. The samples with different porosity (coating times) were tested to study the relationship between permeability and the number of additional coating times.

2.2.4. Mechanical Properties

Before and after coating, micro hardness was measured under a micro hardness tester (SHIMADZU, Japan). Based on the trial testing, a load of 500g applied for 35s to a diamond shaped indents was chosen. Ten samples from each batch were randomly chosen. The compression tests of porous Ti6Al4V samples (Ø10x12mm, n=10) were performed at room temperature with a crosshead speed of 1mm/min (Zwick/Z050, Germany). The Young's modulus was calculated by the load increment and the corresponding deflection increment between the two points on the straight-line part.

3. Results

3.1. Ti6Al4V slurry (Slurry II) for coating

The chemical composition of the two slurries used for sponge replication (Slurry I) and later multiple coating (Slurry II) were listed in Table 1, showing they share the same ingredients but different concentrations of Ti6Al4V powders and binders and therefore resulting in rheological behaviour. Fig.1 shows the viscosity of Slurry I [15] and Slurry II.

Table1 Ti6Al4V slurry composition for polymeric sponge replication and multiple coating

Composition	Slurry I	Slurry II
	Coating foam (wt %)	Multiple-coating (wt %)
Demi water	18.5	31.7
PEG4000	3	1.5
Dolapix	1	1
Ammonia	1	1
Octanol	1	1
Methylcellulose	0.5	0.4
Ti6Al4V powder	75	63.4

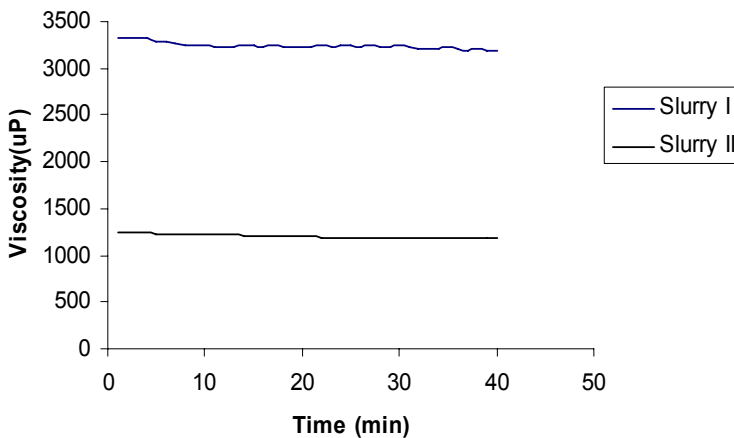


Fig.1 Viscosity of Ti6Al4V slurry I and slurry II

3.2. Pore structure

Fig.2 shows macrostructure of the base porous Ti6Al4V under high magnification. Some large flaws can be seen, such as cracks and triangular voids (denoted by arrows in the figure) in the struts. These flaws and a number of thin struts will contribute significantly to a decrease of the strength. The macrostructure of the base porous Ti6Al4V and after one additional coating are shown in Fig.3(A) and Fig.3(B). As prepared, without extra coating, the porous structure looked too thin. However, these drawbacks were overcome greatly by one extra coating: the cracks being filled by titanium powder turned the porous body denser. It appears that the macro structure of porous Ti6Al4V is not affected significantly by an additional coating treatment. It was found that the pores of porous Ti6Al4V are spherical in shape, and the porous body retains its interconnected porous structure. The struts without or with one additional coating are shown in Fig.3 (C) and Fig.3 (D). Fig.3 (E) shows the macrostructure of cancellous bone, displaying a striking similarity with the structure of Fig.3 (A) and Fig.3 (B).

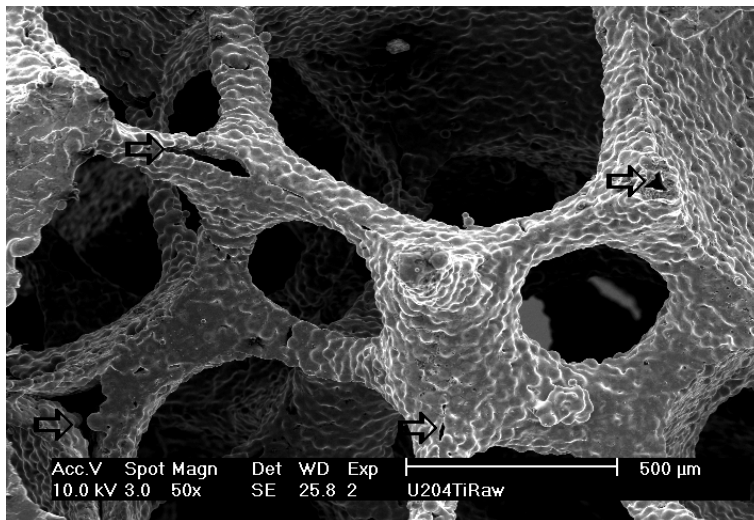


Fig.2 Macrostructure of porous Ti6Al4V(Arrows indicated the crack and triangle hole)

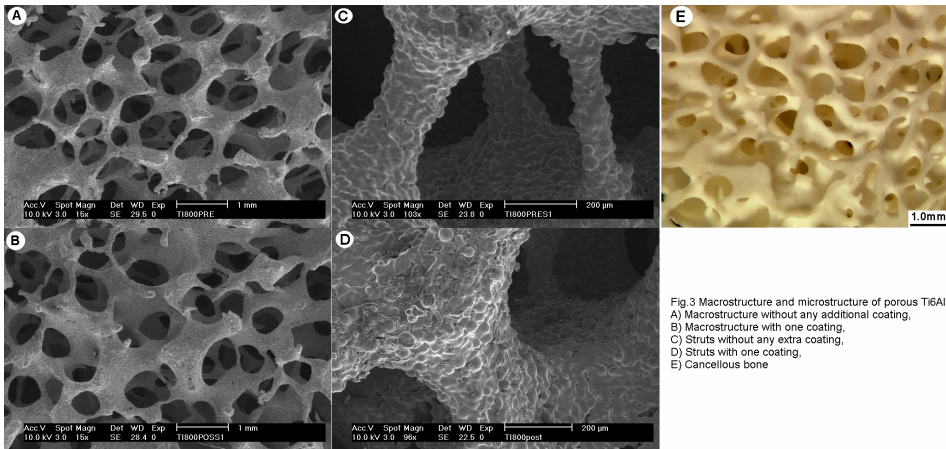


Fig.3 Macrostructure and microstructure of porous Ti6Al4V.
 A) Macrostructure without any additional coating,
 B) Macrostructure with one coating,
 C) Struts without any extra coating,
 D) Struts with one coating,
 E) Cancellous bone

3.3. Porosity and pore size

Fig.4 shows the porosity and pore size versus coating times. It can be seen that the porosity and pore size are dependent on the number of additional coating times, decreasing with increasing coating times. It implies the porosity and pore size of porous Ti6Al4V can be controlled by multiple coating. However, the increase of coating times might result in pore isolation and pore closing.

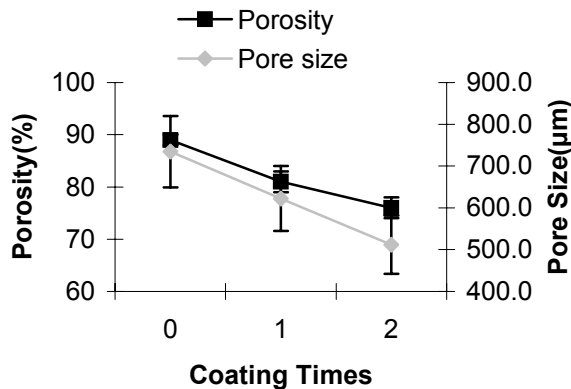


Fig.4 Porosity /Pore size of porous Ti6Al4V as function of coatings

3.4. Permeability

Fig.5 shows the permeability data of porous Ti6Al4V with different porosities and human cancellous bone under transverse direction [18]. It can be seen that the permeability increases with porosity. Porous Ti6Al4V with high porosity has a high value of permeability. The first coating significantly decreased the permeability, additional coating having less effect. It is also clear that porous Ti6Al4V has similar

permeability as human cancellous bone. The permeability test also enables to check repeatability of the coating process. In one batch of samples after coating, the standard deviation in permeability is relative low. The measured porosities (listed in Table 2) also prove the repeatability of the coating process.

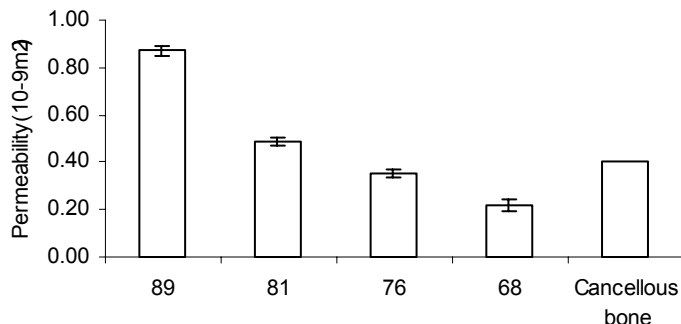


Fig.5 Permeability value of porous Ti6Al4V with various porosities and human cancellous bone.

3.5. Mechanical properties

The mechanical properties of porous Ti6Al4V were evaluated by compressive strength, Young's modulus and micro hardness, and the results are listed in Table 2. Results of Vickers (Hv) micro hardness showed that no difference in micro hardness was caused by additional coating treatment. However, the compressive strength increased from 10 MPa to 35.5 MPa after one extra coating. The young's modulus also increases with the number of extra coating times. This suggests that the compressive strength and young's modulus can be adjusted by the number of additional coating. Fig.6 shows the stress-strain curves of porous Ti6Al4V with different porosities. It can be seen that the plateau stresses increase with decreasing porosity.

Table2 Mechanical properties of porous Ti6Al4V

Sample	Additional Coating Times	Porosity	Compressive Strength (MPa)	Young's modulus (GPa)	Micro Hardness (HV)	Sample Number
PTC0	0	89±1	10.3 ±3.3	0.8± 0.3	373±17	10
PTC1	1	81±2	35.5 ± 7.2	1.5± 0.3	369±14	10
PTC2	2	76±2	59.4± 20.3	1.8± 0.3	379±16	10

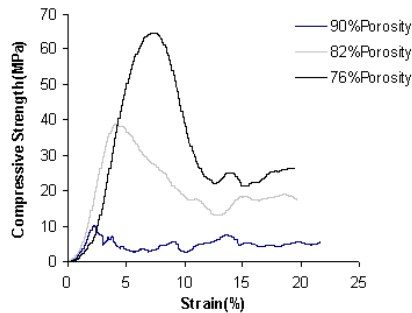


Fig.6 The stress-strain curves of porous Ti6Al4V with different porosities

4. Discussion

4.1. Ti6Al4V slurry for multiple coating (Slurry II)

The base porous Ti6Al4V with interconnected macro and micro structure has a high surface area and high affinity to the slurry, providing the possibility of producing porous Ti6Al4V with higher strength by multiple coating techniques, and further improving the material structure. The viscosity of the Ti6Al4V slurry is an important parameter. It was known that a stable slurry with high solids content and a certain value of viscosity is a prerequisite to an evenly distributed coating on the struts of the sponge [19]. Given the type of the binder, the higher concentration of the binder, the higher the viscosity of the resulting slurry will be. Considering the process of coating a sponge, it is suggested that a thicker coating on the sponge struts is beneficial to maintain the reticulated pre-forms after the sponge substrate is burned out. When coating sponges, the excess slurry can be removed by rolling-pressing while the sponges are immersed in the slurry so that high viscosity slurry can be used. On the other hand, in case of additional coating, the excess slurry has to be removed by high pressure air, so the viscosity of the slurry should be low and possess a good fluidity for going through the network of the base porous Ti6Al4V. However, if the slurry is too thin, only a limited area of the base porous is coated, making it difficult to achieve evenly distributed coating on the struts. Our experimental outcomes show the two slurries which are optimal for fabricating the base body and the additional coating.

4.2. Permeability

The permeability of porous Ti6Al4V after two times extra coating is quite comparable to that of human cancellous bone. It can be seen that not only were

the mechanical properties changed, but also the permeability. In general, when porous materials are studied, two parameters are widely used: porosity and pore size, including mean value and distribution. The other parameters like interconnectivity, interconnection pore sizes are seldom mentioned. It was found that measuring permeability is an easy and effective method to reveal the structural properties of porous materials. Permeability data reflect a combination of (1) porosity, (2) pore size and distribution, (3) interconnectivity, (4) interconnection pore size and distribution, (5) orientation of pores with respect to flow direction. Therefore, permeability can be taken as a comprehensive intrinsic parameter for describing macroporous structure precisely and quantitatively in the future, and probably more relevant than porosity and mean pore size in characterizing porous materials structure.

4.3. Mechanical properties

The mechanical properties of porous Ti6Al4V were studied by compressive strength, which increased significantly as the porosity decreased with the increasing of coating times. For metallic foams, the mechanical parameters are affected by the relative density of foam ($\rho_r = \rho / \rho_s$, the density of the foam ρ divided by that of the solid material ρ_s). Gibson and Ashby[20] suggested a general model, in which the relationship between the relative strength, Young's modulus, and relative density are given by:

$$\sigma_{pl}/\sigma_{ys} = C_1 (\rho / \rho_s)^{N1} \quad (1)$$

$$E/E_s = C_2 (\rho / \rho_s)^{N2} \quad (2)$$

Where σ_{pl} is the plateau stress of the foam; σ_{ys} is the yield stress of solid material; E is the Young's modulus of the foam; E_s is the young's modulus of solid materials, and C_1 , C_2 , $N1$ and $N2$ are constants, depending on cell structure parameters. For the case of aluminium foam with lower density ($\rho_r < 0.2$), Gibson and Ashby found the following coefficients and exponents for the model:

$$\sigma_{pl}/\sigma_{ys} = 0.3(\rho / \rho_s)^{3/2} \quad (3)$$

$$E/E_s = (\rho / \rho_s)^2 \quad (4)$$

With $C1=0.3, N1=3/2$, $C2=1$, $N2=2$. Fig.7 shows the effect of porosity on the compressive strength (shown in Fig.7A) and Young's modulus (shown in Fig.7B) of the porous Ti6Al4V according to the experimental data and theoretical data calculated from Gibson and Ashby's model. The experimental data do not fit the Gibson-Ashby's model. The reason is obviously that the different processing techniques of porous aluminium and porous Ti6Al4V resulted in different pore morphology, and therefore different constitution relationship.

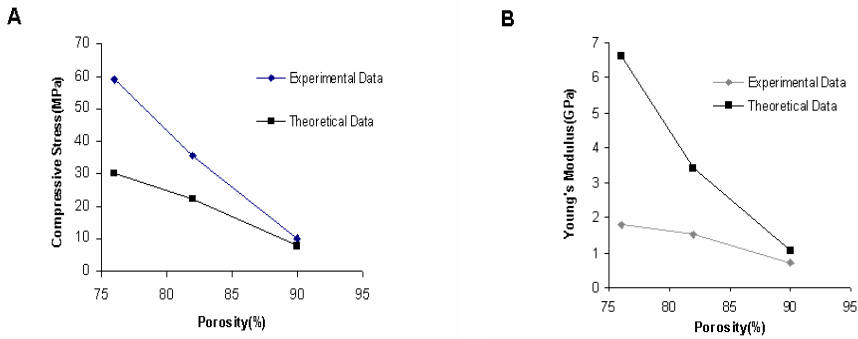


Fig.7 Effect of porosity on the compressive strength and Young's modulus of porous Ti6Al4V (comparison of experimental data and data from theoretical data). A) Effect of porosity on the compressive strength; B) Effect of porosity on the Young's modulus.

With regard to the effect of the relative density on the mechanical properties of porous Ti6Al4V, based on the Gibson and Ashby model expressed in Equation (1) and Equation (2), coefficients fitting our experimental results are calculated as:

$$\sigma_p/\sigma_{ys}=0.5(\rho/\rho_s)^{3/2} \quad (5)$$

$$E/E_s=0.76(\rho/\rho_s) \quad (6)$$

Where $C1=0.5$, $N1=3/2$, $C2=0.78$, $N2=1$, for $E=210\text{GPa}$, and $\sigma_{ys}=827\text{MPa}$ [9].

The main problems of implant materials generally used in load bearing application are twofold: (1) The high Young's Modulus of the dense metallic materials and the low strength of polymers and brittleness of ceramics as compared with human bone. A number of reports showed that lower young's moduli of implants resulted in stresses and strains that are close to those of intact bone, and may better reduce the stress shielding due to too high young's moduli [21-23]. Although dense Ti6Al4V has a young's modulus only about half of those of 316L stainless steel or CoCrMo alloy, it is still about 10-20 times higher than the young's modulus of human bone,. Recently there has been an increasing interest in developing new titanium alloys with lower Young's modulus, such as Ti-15Mo [24], Ti-15Zr-4Nb-2Ta-0.2Pd[25] and Ti-35Nb-5Ta-7Zr [26], but they are still higher than that of human bone. Fig.8 shows the Young's modulus of commonly used implant materials [27,28]. It can be seen that the Young's modulus's of porous Ti6Al4V is between that of cancellous and cortical bone. (2)Although ceramics are good bone substitutes (osteoconductive), they are too brittle and weak to provide sufficient strength for load-bearing condition. Fig.9 shows the compressive strength of various implant materials [27,28]. It can be found that porous Ti6Al4V has much higher compressive strength than that of ceramics and polymers. The porous Ti6Al4V with a porosity of 76% has a strength of 59MPa, the strength of trabecular-bone with 75% porosity is in the range of 10-50MPa. As it is shown previously that

we can adjust the strength and Young's modulus of porous Ti6Al4V by our multiple-coating technique to meet the requirements of porous bone substitute.

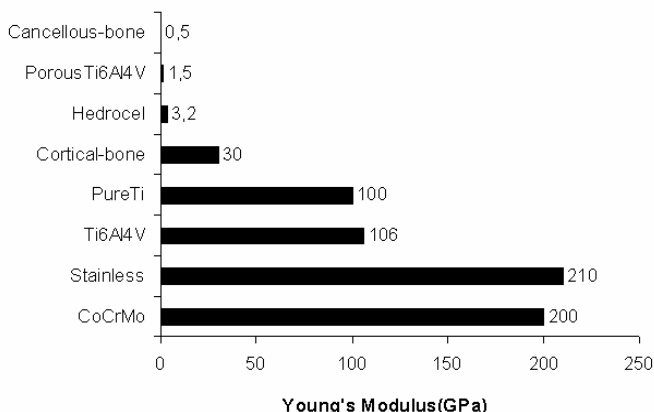


Fig.8 Young's Modulus of Implant biomaterials

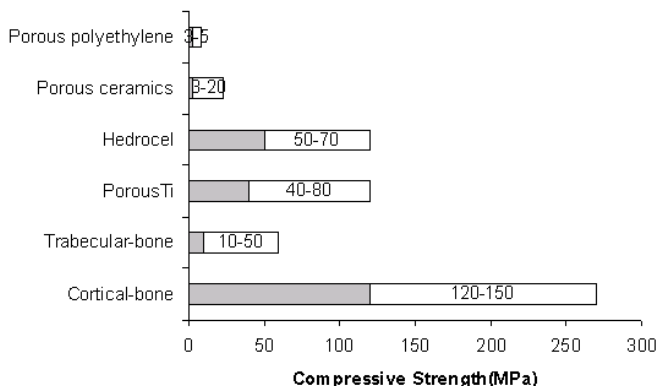


Fig.9 Compressive strength of different porous implant biomaterial comparing with bone

The micro hardness measurements show no significant change after multiple coating. Three mechanisms can be used to explain the improvement of the strength of porous Ti6Al4V by multiple coating. Firstly, some large flaws, such as cracks, were filled with Ti6Al4V powder. Secondly, the additional high vacuum sintering has a further advantage of reducing any contaminations existing on the surface of the powder particle and base body. Therefore, the fusion of Ti6Al4V particles was enhanced by the absence of titanium carbide, titanium nitrides and oxides in the outer surfaces, resulting in increased mechanical properties of the final porous body. Thirdly, the porosity was decreased by multiple coating, as discussed above.

4. Conclusions

Porous Ti6Al4V with cancellous bone properties was successfully made by multiple coating techniques. Porosity, pore size and mechanical properties can be adjusted to correspond with bone. The permeability test proved the repeatability of the multiple coating process. The permeability value increases with porosity of porous Ti6Al4V. Our findings show that both structural and mechanical properties of porous Ti6Al4V are comparable to those of human cancellous bone. This material can be expected to find better practical application for tissue engineering scaffolds and as orthopedic implants

5. Acknowledgements

This study was financially supported by IsoTis S.A. The authors would thank gratefully Dr.Yuan for his helpful discussion.

Reference

1. Cameron HU, Pilliar RM, Macnab I. The rate of bone ingrowth into porous metal. *J Biomed Mater Res* 1976;10(2):295-302.
2. Chang BS, Lee CK, Hong KS, Youn HJ, Ryu HS, Chung SS, Park KW. Osteoconduction at porous hydroxyapatite with various pore configurations. *Biomaterials* 2000;21(12):1291-8.
3. Clemow AJ, Weinstein AM, Klawitter JJ, Koeneman J, Anderson J. Interface mechanics of porous titanium implants. *J Biomed Mater Res* 1981;15(1):73-82.
4. Bobyn JD, Pilliar RM, Cameron HU, Weatherly GC, Kent GM. The effect of porous surface configuration on the tensile strength of fixation of implants by bone ingrowth. *Clin Orthop* 1980(149):291-8.
5. White EW, Weber JN, Roy DM, Owen EL, Chiroff RT, White RA. Replamineform porous biomaterials for hard tissue implant applications. *J Biomed Mater Res* 1975;9(4):23-7.
6. Lemons JE, Lucas LC. Properties of biomaterials. *J Arthroplasty* 1986;1(2):143-7.
7. Crowninshield RD. Mechanical properties of porous metal total hip prostheses. *Instr Course Lect* 1986;35:144-8.
8. Moyle DD, Klawitter JJ, Hulbert SF. Mechanical properties of the bone-porous biomaterial interface: elastic behavior. *J Biomed Mater Res* 1973;7(3):363-82.
9. Long M, Rack HJ. Review Titanium alloys in total joint replacement materials science perspective. *Biomaterials* 1998;19:1621-1639.
10. Pilliar RM. P/M Processing of Surgical implants: sintered porous surfaces for tissue-to-implant fixation. *International Journal of Powder Metallurgy* 1998;34(8):33-45.

11. Matin B, Cornelia S, Bronkremer HP, Baur H. High-porosity Titanium, Stainless Steel, and Superalloy Parts. *Advance Engineering Materials* 2000;2(4):196-199.
12. Li JP, Li SH, Van Blitterswijk CA, De Groot K. A novel porous Ti6Al4V: Characterization and Cell attachment. *J.Biomed.Mat.Res* 2005;73A:223-233.
13. Brezny R, Green DJ. Fracture behavior of Open-Cell Ceramics. *J Am Ceram Soc* 1989;72(7):1145-1152.
14. Lange FF, Metcalf M. Processing related fracture origins:II, Agglomerate motion and crack like internal surfaces caused by differential sintering. *J Am Ceram Soc* 1985(213):225-231.
15. Li JP, Li SH, De Groot K, Layrolle P. Preparation and characterization of porous titanium. *Key Engineering Materials* 2001;218:52-56.
16. Li JP, Van Blitterswijk CA, de Groot K. Factors having influence on the rheological properties of titanium alloy slurry. *J Mat Sci:Mat in Med* 2004;15:951-958.
17. Li SH, De Wijn JR, Li JP, Layrolle P. Biphasic calcium phosphate scaffold with high permeability/porosity ratio. *Tissue Engineering* 2003;9(3):535-548.
18. Grimm MJ, Williams JL. Measurement of permeability in huamn calcaneal trabecular bone. *J.Biomechanics* 1997;30(7):743-745.
19. Lin JY, Zhang Y. Effect of fabrication technology on the structures and properties of TiC ceramics foam. *Powder Metallurgy Technology* 2000;18(1):12-15.
20. Gibson LJ, Ashby MF. *Cellular Solids: Structure and Properties*. Cambridge: Cambridge University Press; 1997.
21. Cheal E, Spector M, Hayes W. Role of loads and prosthesis material properties on the mechanics of the proximal femur after total hip arthroplasty. *J Orthop Res* 1992;10:405-422.
22. Prendergast P, Taylor D. Stress analysis of the proximo-medial femur after total hip replacement. *J Biomed Eng* 1990;12:379-382.
23. Lewis JL, Askew MJ, Wixson RL, Kramer GM, Tarr RR. The influence of prosthetic stem stiffness and of a calcar collar on stresses in the proximal end of the femur with a cemented femoral component. *J Bone Joint Surg* 1984;66-A(280-286).
24. Ho WF, Ju CP, Chern JH. Structure and properties of cast binary Ti-Mo alloys. *Biomaterials* 1999;20:2115-2122.
25. Okazaki Y, Ito Y, Ito A, Tateishi T. *Mater Trans* 1993;34:1217.
26. Ahmed T, Long M, Silvestri J, Ruiz C, Rack HJ. 1995; Birmingham, U.K.
27. Bobyn JD, Hacking SA, Chan SP. Characterization of a new porous tantalum biomaterial for reconstructive orthopaedics.; 1999; Anaheim, CA.
28. Krygier JJ, Bobyn JD, Poggie RA. Mechanical characterization of a new porous tantalum biomaterial for orthopaedic reconstruction.; 1999; Sydney, Australia.

The background of the page is a grayscale image showing several cylindrical porous titanium alloy scaffolds. These scaffolds have a highly porous, interconnected internal structure, characteristic of rapid prototyping techniques. They are arranged in a slightly overlapping, vertical pattern, creating a sense of depth and texture.

Part II

Development of Porous Titanium Alloy by Rapid Prototyping

Chapter 5

Porous Ti6Al4V scaffold directly fabricated by rapid prototyping: preparation and in vitro experiment

Chapter 6

Porous Ti6Al4V scaffolds directly fabricated by 3D fiber deposition technique: effect of nozzle diameter

Chapter 7

The effect of scaffold architecture on properties of direct 3D fiber deposition porous Ti6Al4V for bone tissue engineering and orthopaedic implants

Chapter 5

Porous Ti6Al4V scaffold directly fabricated by rapid prototyping: preparation and in vitro experiment

J.P. Li^{1,2}, J.R. de Wijn¹, C.A. van Blitterswijk¹, K. de Groot^{1,3}

¹Institute for Biomedical Technology, University of Twente, The Netherlands.

²Porogen. B.V, Enschede, The Netherlands.

³CAM Implants. B.V, The Netherlands.

Abstract

Three-dimensional fiber deposition (3DF), a rapid prototyping technology, was successfully directly applied to produce novel 3D porous Ti6Al4V scaffolds with fully interconnected porous networks and highly controllable porosity and pore size. A key feature of this technology is the 3D computer controlled fiber deposition of Ti6Al4V slurry at room temperature to produce a scaffold, consisting of layers of directionally aligned Ti6Al4V fibers. In the present study, the Ti6Al4V slurry was developed for the 3D fiber depositing process, and the parameters for 3D fiber deposition were optimized. The experimental results show how the parameters influence the structure of porous scaffold. The potential of this rapid prototyping 3DP system for fabricating three-dimensional Ti6Al4V scaffolds with regular and reproducible architecture meeting the requirements of tissue engineering and bone graft substitute is demonstrated.

Keywords: Titanium alloy, porosity, scaffold, rapid prototyping-three dimensional fiber deposition

1. Introduction

Scaffolds are of great importance for tissue engineering and orthopedic implants because they enable to provide biological anchorage for the surrounding bony tissue via the ingrowth of mineralized tissue into the pore space[1]. These scaffolds require a specific external shape and a well defined internal structure with interconnectivity[1-3]. Recently, porous ceramics and polymers have been extensively studied to promote bone or tissue ingrowth into pores [4-9]. However, ceramics and polymers are not very strong and can easily transform [10,11], they are less appropriate in load-bearing applications, such as in spinal interbody fusion. Therefore, metals like titanium and its alloys are widely used for orthopaedic and dental implants [12]. They possess low density, good mechanical properties (elastic modulus, toughness, and fatigue strength) and biological and chemical inertness. Recently, there has been an increasing interest in fabricating porous titanium scaffold for bone tissue engineering[13-15]. Porous titanium and its alloys have been used in dental and orthopaedic applications since the end of 1960s[16-18]. Many available methods for producing porous titanium and titanium alloy scaffolds include sintering together of the particles [19] or plasma spraying of the powder on a dense substrate followed by the cutting of the porous layer[20], compressing and sintering of titanium fibers [21,22], solid-state foaming by expansion of argon-filled pores[23] and polymeric sponge replication[24]. However, none of these conventional techniques has allowed for building scaffolds with a completely controlled design of the external shape as well as of the interconnected pore network. The imperfection of the conventional techniques has encouraged the use of a rapid prototyping (RP) technology [25]. Since 1980s RP technologies have emerged as a revolutionary manufacturing process with inherent capability to rapidly make objects in virtually any shape. RP, combining computer aided design (CAD) with computer aided manufacturing (CAM), has the distinct advantage of being able to build objects with predefined microstructure and macrostructure [26,27]. This distinct advantage gives RP the potential for making scaffolds or orthopedic implants with controlled hierarchical structures[28-33]. Until now RP developments mainly focused on polymer and ceramic materials[34-39]. The transfer of RP technologies to metal materials for tissue engineering and orthopedic implants possesses a significant challenge. There are few investigations on making metal scaffold for orthopaedic and tissue engineering application by rapid prototyping techniques [3,40,41]. Two methods were applied to make metal scaffold. One is indirect to make porous scaffolds by invest casting melt metal or metal powder slurry into a mold where the mold was made using RP[40,41,42] , in addition to indirect processing, other researchers have been developing porous titanium scaffolds for tissue engineering using Direct Metal Deposition[3,43,44].

Here, we report the first example of RP Ti6Al4V scaffold with self-supporting features fabricated directly by 3D fiber deposition. In this paper, we investigated the design and fabrication of 3D Ti6Al4V scaffolds and performed in vitro studies to assess cell attachment, cell proliferation and differentiation of the scaffolds.

2. Materials and methods

2.1. Materials

- Ti6Al4V powders with a mean particle diameter of 45 μ m (Bongen Titanium (China) Co, Ltd) were used in this study. The particles are spherical in shape.
- Methylcellulose (MC, Fisher Scientific B.V) and stearic acid (Acros organics, USA) were used as binder and dispersant

2.2. Methods

2.2.1. Preparation of the Ti6Al4V slurry

The Ti6Al4V slurry was prepared as follows: The Ti6Al4V powder (66vol %) was mixed with an aqueous solution of methylcellulose and stearic acid (34vol %). The slurry was stirred for 1 hour at room temperature to obtain homogenous slurry

The concentration of the Ti6Al4V powder in the slurries has influence on the viscosity of the slurry. The effect of powder concentration was studied by utilizing the slurries with Ti6Al4V powder concentrations ranging from 64 to 68 vol%. A powder concentration of 66vol% was used for most studies unless otherwise specified.

2.2.2. 3D fiber deposition

As a 3D fiber depositing device, the “Bioplotter (Envisiontec GmbH, Germany) “was used, which has been reported by Landers and Mülhaupt [45,46]. Fig.1A shows the system, consisting of: (1) a Ti6Al4V slurry dispensing unit consisting of a syringe and nozzle; (2) air pressure plunger to regulate flow of slurry (4) positional control unit linked to a personal computer containing software (PrimCAM) for generating fiber deposition paths.

2.2.3. Scaffold development

The Ti6Al4V slurry was placed in a plastic syringe, through a fixation unit mounted on the “Y”-axis of the apparatus and kept at room temperature. Air pressure (P) was applied to the syringe through a pressurized cap. Rectangular block models

were loaded on the Biplotter CAM software. The process involved depositing continuous fibers of material to produce two-dimensional (2D) layers with alternating $0^\circ/90^\circ$ lay-down patterns of finite thickness and then building the 3D scaffold up layer-by-layer. Fig.1B shows the processing of 3D fiber depositing porous Ti6Al4V scaffold.

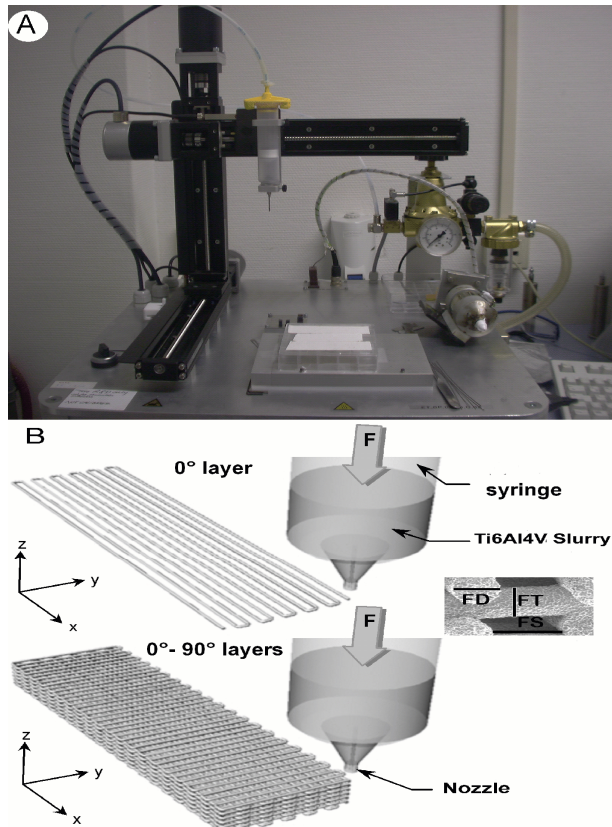


Fig.1 3D fiber depositing system (A) 3D fiber depositing system, (B) 3D fiber depositing scaffold process

The nozzle used to extrude Ti6Al4V slurry fibers is a stainless steel hypodermic needle. The nozzle size is expressed as inner diameter of the nozzle, and a length of 16.1 mm. A nozzle diameter of $400\mu\text{m}$ was used for most studies unless otherwise specified. For all the experiments addressed, fiber spacing was set to 0.5mm to create pore size around $400\mu\text{m}$ since pore size around this range assure a rich blood supply, nutrient and waste exchange and promote in growth of bone[47-49]. and the thickness between fiber layers were kept at 0.35mm which is about $0.85 * \text{nozzle size}$ as discussed previously [46].

After fiber depositing the samples were first dried for 24hrs at RT, then dried for 24hrs at 50°C, and finally sintered in a high vacuum furnace (10^{-5} mbar) applying a heating profile as follows:

RT 600 min → 500 °C 450 min → 1250 °C 120 min → 1250°C furnace cooling → 25°C

2.2.4. Optimization of 3D fiber depositing parameters for fabrication scaffold

The principle of 3D fiber deposition is similar to that of fused deposition modeling (FDM). Many groups have applied FDM to fabricate scaffold for tissue engineering [10,50-52]. The optimized FDM process involves complex interactions between the hardware, software and material properties as discussed previously [39,53,54]. Before fabricating a 3D Ti6Al4V scaffold, experiments were focused on understanding the influence of concentration of powder, air pressure, the feeding speed of fiber depositing and the initial height of fiber depositing on the output quality of the processed scaffold. These four primary parameters, together with the experimented values in brackets, include: (1) the concentration of Ti6Al4V powder; (2) the fiber depositing pressure, P (i.e. 2, 2.5 and 3 bars); (3) the speed of feeding, S (i.e. 210, 280, 350 and 420 mm/min); and (4) the initial height of fiber depositing (i.e. initial distance between the tip and the platform), H (i.e. 0.1, 0.25 and 0.4 mm). Different scaffolds were produced at various settings for the fiber depositing air pressure and feeding speed.

2.2.5. Characterization

The shape of Ti6Al4V powders was analyzed by environmental scanning electron microscope (ESEM, XL-30, Philips, Eindhoven, The Netherlands). Particle size distributions were measured by Retsch Technology in Germany, using a CRYSTALSIZER® which is based on using incoherent light diffraction.

The rheological behavior of Ti6Al4V slurries was measured at room temperature by viscometer (Brookfield engineering labs DV-II+ viscometer) with interval time at a speed of 10 rpm with a RV0 spindle.

The dispensability of Ti slurry was measured in terms of flow rate. Flow rate can be defined as weight of slurry extruded from nozzle per minute. The average of 3 measurements was used to represent the flow rate at experimental machine setting.

3D fiber depositing scaffolds were characterized under ESEM to measure the diameter of fiber and to select the potential settings of fiber depositing parameters. Since the primary concern was to produce consistent and uniform fibers, the fiber diameter from nozzle (FD), the spreading tendency (standard deviation) of the fiber

spacing (FS) and thickness of the fibers (FT) produced by the potential settings were then measured and compared to pick out an optimized setting of parameters (shown in Fig.1B).

The porosity of the Ti6Al4V scaffolds was calculated from the ratio of weight and volume by comparing the bulk density of samples (n=10) with the theoretical density of Ti6Al4V: 4.45 g/cm^3 .

Five samples from each kind of scaffold produced at various settings for the fiber depositing air pressure and feeding speed were randomly chosen. Compression tests of porous Ti6Al4V samples (4x4x6mm, n=5) were performed at room temperature with a crosshead speed of 1mm/min (Zwick/Z050, Germany). The loading direction is in the Z-direction of the deposition process.

2.2.6. In vitro experiment

2.2.6.1. Cell attachment and Proliferation

MC3T3-E1 osteoblast-like cells were used for the cell attachment study. The culture medium used was α -MEM supplemented with 10% fetal bovine serum (FBS, Life Technologies, The Netherlands), antibiotics, and 1% sodium pyruvate. The cells were seeded on porous Ti6Al4V samples placed in a 25-well plate at 0.6×10^6 cells/per sample in 4ml of medium, and cultured at 37°C in a humidified atmosphere with 5% CO₂ and 95% air. After being cultured for 1 day, 3 days and 7 days respectively, the samples (n=2) were fixed and then rinsed with PBS, dehydrated in a graded ethanol series, critical point dried, sputter coated with carbon and examined with ESEM. Other samples (n=3) were digested with proteinase K (Sigma, The Netherlands), added with heparin (Leo Pharm, The Netherlands) and Ribonu-lease A (Sigma, The Netherlands), then shaken and incubated at 56°C for 16hrs. A volume of 100 μ l solution of each sample was mixed with 100 μ l Cyquant GRDye (Molecular Probe, Poland), and the fluorescence was measured with fluorimeter (Perkin Helmer) at emission wavelength 520nm and excitation 480nm. The DNA content of cells attached on the porous samples was counted through a pre-made standard DNA curve.

2.2.6.2. ALP/DNA analysis

The alkaline phosphatase (ALP) activity expressed as a function of cell DNA content was determined using the Cyquant kit (Molecular Probes, C7026, Leiden, The Netherlands). After 4 days and 7 days culture in the presence of dexamethasone, 3 cell-seeded samples were washed with Phosphate Buffered Saline (PBS; Life Technologies) and stored at -80C for at least 24 hours. After thawing on the ice, the cells were sonicated (Branson 250) in PBS with 0.2% Triton

X-100(Sigma) for 10 seconds. The supernatant was employed for the determination of ALP activity according to Lowry's method [55] using *p*-nitrophenyl phosphate (Merck, Germany). A volume of 100 μ l solution of each sample was mixed with 100 μ l Paranitrophenyl phosphate substrate (Sigma) solution on 96-well microplate reader, and then ALP activity was assayed by measuring the amount of release of *p*-nitrophenol from *p*-nitrophenyl phosphate as previously described [56,57]. A standard curve was generated using known concentrations of *p*-nitrophenol. All samples and standards were measured on a BIO-TEK automated microplate reader (New York, USA) at 405nm. To measure the DNA contents, a cyquant assay kit (Molecular Probes) and a LS-50B fluorimeter were used.

2.2.6.3. Protein content of cells layers

The protein content of cell layers was determined using a commercially available kit (Micro/Macro BCA, Pierce chemical Co, Rockford, IL, USA) as previously described [58]. The assay was performed within 96-well microreader plates. The absorbance at a wavelength of 570nm being monitored using a microplate reader (Dynatech, MR 7000, Billingham, UK). Bovine serum albumin was used as standard.

3. Results

3.1. Ti6Al4V powder and slurry

Fig.2A illustrates an image of Ti6Al4V powder under ESEM. It shows that the particles have both a highly spherical shape and smooth surface. The distribution of the particle size of Ti6Al4V powder is given in Fig. 2B, the majority (~50%) being in the range of 10-30 μ m. Of significant importance for the 3D fiber deposition of Ti6Al4V scaffolds are the rheological properties of the slurry. Landers reported the rheological properties must be balanced to achieve flow during dispensing and preferably high thixotropy [59]. Fig.3 shows the viscosity as function of time. The viscosity of slurries with different powder concentrations is shown in Fig.3A. It can be seen that the viscosity decreased with increasing time, revealing the slurry is non-Newtonian. When the measurement is repeated on slurry with a concentration of 66.vol% after 20 mins, the same tendency of decreasing viscosity is observed (Fig.3B). The experimental result reveals that the slurry displays a thixotropic behavior [60]. A reduction in viscosity occurs when shaken, stirred, or otherwise mechanically disturbed, but at rest the slurry recovers in time, eventually reaching its original viscosity.

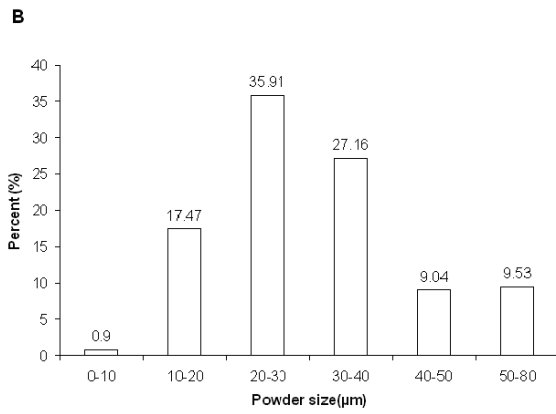
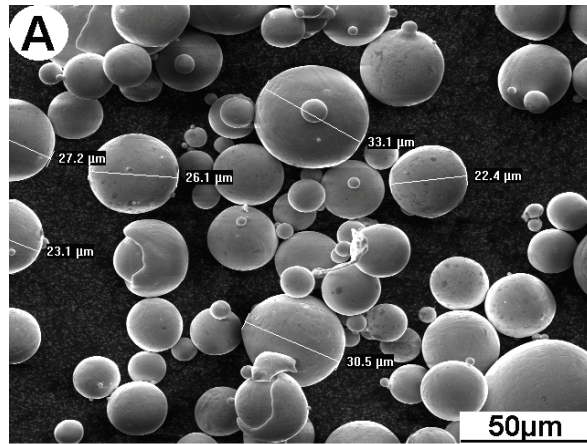


Fig.2 Ti6Al4V powder (A) morphology of powder, (B) distribution of powder

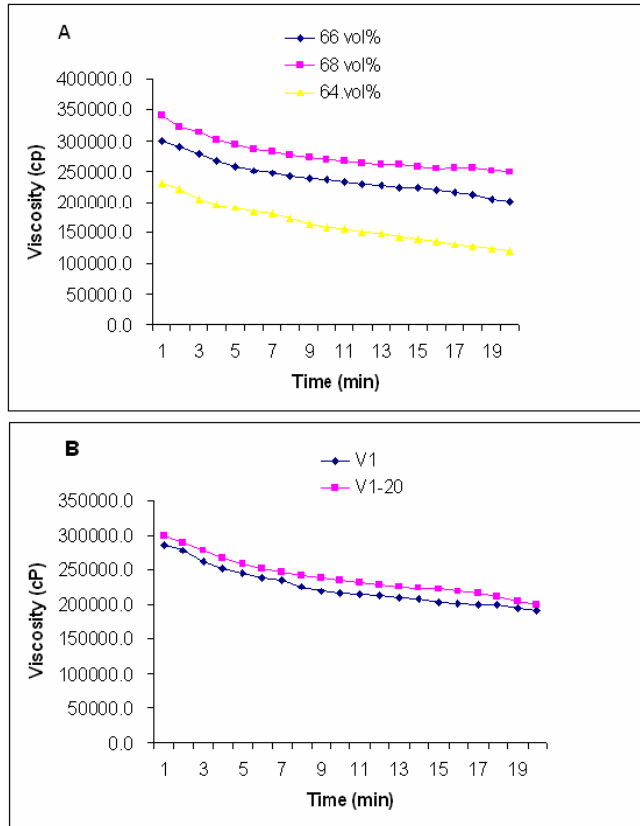


Fig.3 (A) Viscosity of Ti6Al4V slurry with different concentration of powder. (B) Viscosity of slurry with 66vol% concentration, V1-20 means measurement after 20mins of the first measurement.

3.2. Concentration of powder

The viscosity is related to the concentration of the powder in the slurry while binder is at a constant concentration. The higher the powder concentration, the higher the viscosity is. Apparently, a lower viscosity will result in deformation of the deposited fiber, and a higher viscosity of a material will cause a greater resistance against flowing and affect the quality of scaffold. The powder concentration is an important factor which affects the architecture of scaffold, as reflected in Fig.4. It can be seen that the use of a low concentration of powder has undesirably resulted in gravity induced flow subsequent to depositing (Fig.4A). Where slurry with a high concentration of 68ol% was used, there is little or no attachment between the layers (Fig.4C). Slurry with a concentration of 66vol% shows a good attachment between layers (Fig.4B), and has a consistency high enough to withstand flow

under its own weight. Therefore, slurry with a concentration of 66.vol% was applied for later experiment.

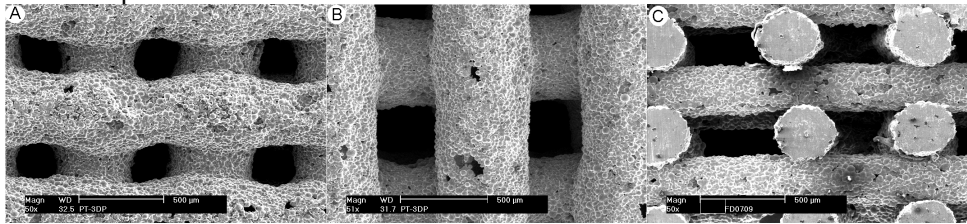


Fig.4 Effect of concentration of powder on the scaffold processing; (A) Low concentration shows the fiber is deformed. (64 vol% Ti6Al4V powder used). (B) Optimal concentration (66vol%). (C) When the powder concentration is high (i.e. 68 vol% Ti6Al4V powder used), there is no adhesion and attachment between the layers

3.3. Viscosity, nozzle diameter and air pressure on the flow rate

The fiber extruded from the FDM nozzle depends on the viscosity of material, the nozzle diameter and geometry, the pressure drop(ΔP) and the flow rate [61-63] For Newtonian behavior of a fluid, the Hagen–Poiseuille equation expressed that the flow rate of a fluid through a circular tube (such as a nozzle) as [64]:

$$Q = \frac{\pi \Delta P}{128 L \eta} d^4$$

Q is the flow rate of fluid through the nozzle direct (diameter d and Length L), η is the viscosity of the fluid, and ΔP is the pressure between the tip of the nozzle and the fluid in the syringe. It can be seen that the flow rate of such a fluid is directly proportional to the pressure across the syringe and nozzle tip at constant nozzle diameter (d), and inversely proportional to nozzle length (L) and viscosity (η). Different nozzles were used to determine the flow rate as a function of viscosity, nozzle size and pressure. In Fig. 5A-5C the increased flow rate is deposited against P, d^4 and $1/\eta$ respectively, showing non linearity except possibly at the lowest flow rate. As can be expected, the behavior of the slurry is non-Newtonian.

It is of importance to control flow rate of slurry. If the flow rate is too high, over-deposition of the fiber, causing draping between fibers and reducing porosity will occur. On the other hand, if Q is too low, this will reduce the fiber diameter at a certain feeding speed, thus forming less contact area between the underlying fibers and affecting the strength of scaffold. In our study, a stainless needle shaped nozzle was used to prevent the depositing material from adhering and accumulating around its tip during fiber deposition. The air regulator was used to vary and set the applied pressure for fiber deposition while the PrimCAM software was used to control the fiber depositing system to achieve the required speed and initial height of fiber depositing.

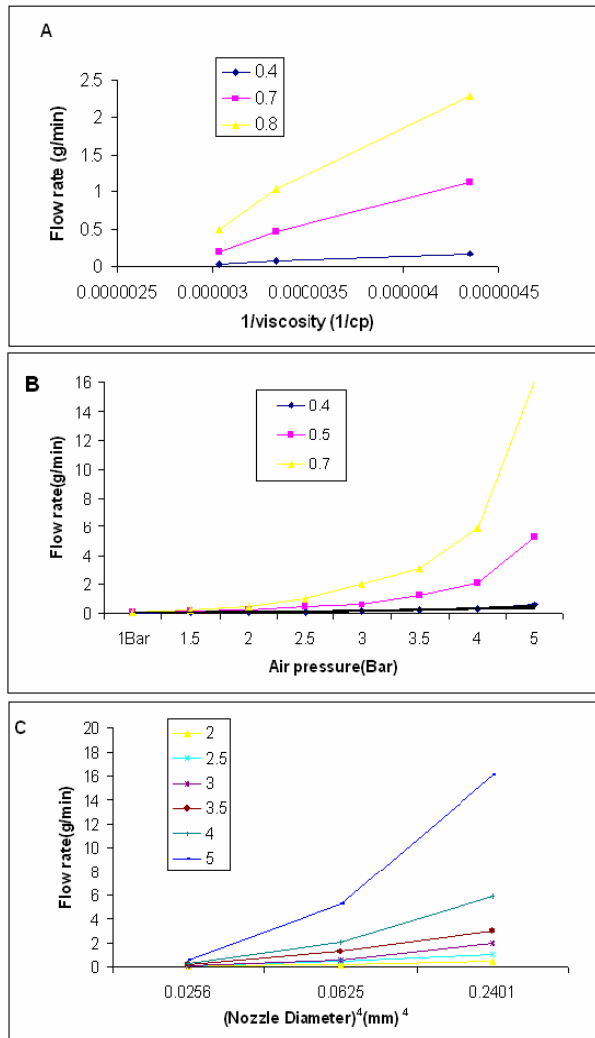


Fig.5 The flow rate as a function of $1/\text{viscosity}$, pressure and $(\text{nozzle diameter})^4$
 (A) Flow rate varied with $1/\text{viscosity}$ at a nozzle diameter of 0.4mm and a pressure of 2.5bar, (B) Flow rate varied with $(\text{nozzle diameter})^4$ at different pressure; (C) Flow rate varied with pressure with different nozzle diameter

3.4. Air pressure, feeding speed and initial height on the scaffold structure

At constant flow rate, it is clear that with a relative low feeding speed rate too much slurry is deposited and the fiber starts to swell. In this case, the solution is to increase the feeding speed or and reduce the pressure slightly to change the flow rate. On the other hand, if the feeding speed is too fast, the fiber is stretched after it

has been deposited and it touches the previous layer much later and affects the contact area between layers. Therefore the material flow rate through the nozzle and the feeding speed must be coordinated with each other. The optimum situation is when the material leaves the nozzle and is immediately pressed against and bonded to the fibers of the previous layer, being only slightly deformed. Fig. 6 shows the effect of air pressure on the scaffold processing at constant feeding speed. With low pressure, there is less adhesion and attachment between the layers (Fig.6A); with higher pressures, the diameter of fiber becomes large (Fig. 6C); optimal air pressure causes the fibers to have a good attachment to each other with minimal deformation (Fig.6B). In a similar way, the feeding speeds affect the scaffold structure at constant pressure as shown in Fig.7. At low speed, the slurry flow rate from the nozzle is too high, and the scaffold becomes denser (Fig.7A). At high feeding speed, the fibers become thinner (Fig.7B to Fig.7D), and dragging of the dispensed material from preceding fibers easily occurs. Table 1 shows the fiber diameter and total porosity of scaffold as function of the fiber depositing pressure and feeding speed. It can be seen that the diameter increased with pressure and decreasing of feeding speed, and the porosity of scaffold increased with the feeding speed and decreasing of pressure.

Table 1 Measurement of Ti6Al4V scaffold by different pressure and feeding speed from ESEM micrographs.

Specimen group	FD	FS	Porosity
F-210	518± 21.5	249±9.9	50±2
F-280	454± 12.7	339±12.3	54±1
F-350	415±14.9	369±11.9	58±1
F-400	364±10.3	419±33.5	64±1.5
P-2 Bar	320±6.9	477±7.4	74±1
P-2.5Bar	415±14.9	369±11.9	58±1
P-3Bar	477±4.4	352±4.9	49±2

FD: Fiber diameter, FS: Fiber spacing, P: porosity

The initial height of the nozzle head above the platform is also important for scaffold construction. It was observed that a large initial height reduced the attachment area of the first layer with the platform, resulting in the instability of the scaffold during fiber depositing and the possible dragging of material. Conversely, a very low height made the first layer becomes denser because of the fibers being spread out to large diameters. Fig.8 shows the effect of the initial distance between nozzle tip and platform on the scaffold processing.

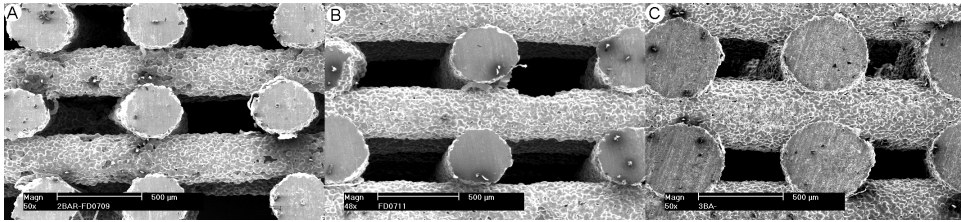


Fig.6 Effect of fiber depositing pressure on the scaffold processing; (A) 2Bar, (B) 2.5Bar, C) 3 Bar.

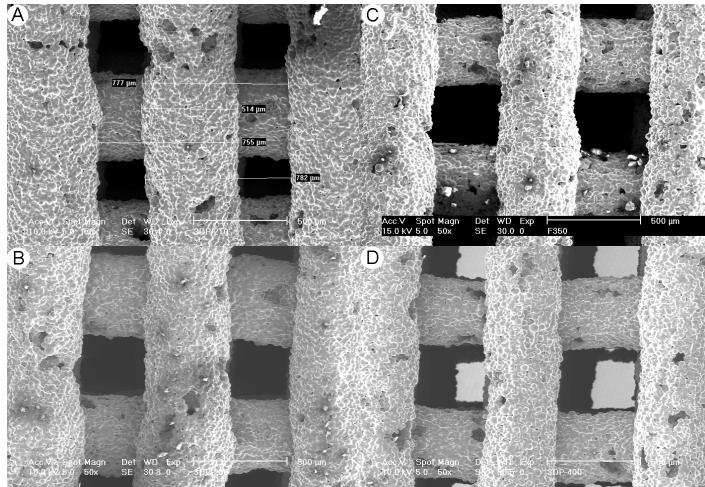


Fig.7 Effect of feeding speed on the scaffold processing; (A) 210mm/min, (B) 280mm/min, (C) 350mm/min, D) 420mm/min

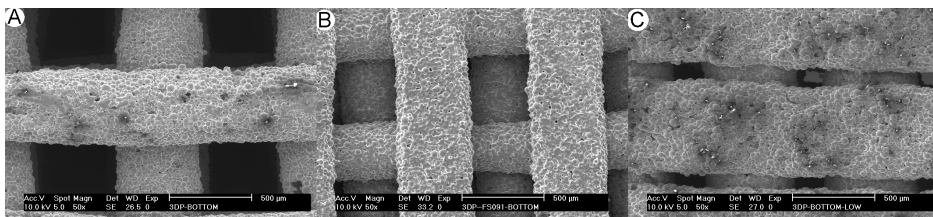


Fig. 8 Effect of the initial height of nozzle head and platform on the scaffold processing; (A) initial height is 0.4mm, (B) initial height is 0.25mm, (C) initial height is 0.1mm.

The quality of the bonding between the layers is equally important. The thickness of layer in the z-direction is of importance to guarantee the contact area between the fibers. Lander reported the thickness of a layer should be 80% to 90% of the diameter of the nozzle so that a sufficient contact area between the layers can be obtained to stick them together, and the material of the overlapping area is deposited lateral to the contact area [46]. Obviously, it is no use if the thickness is equal and larger than the diameter of fiber because the layers would only just

touch, and the bonding is inadequate. If a too low thickness is chosen, the fibers are deformed in the overlapping area and the porosity drops considerably. With a nozzle diameter of 400 μ m, a fiber depositing pressure (P) of 2.5 bars, feeding speed (F) of 350 mm/min and initial height of fiber depositing (H) of 0.25mm, were found to be optimal for fabricating the scaffolds. Fig.9 shows the resulting scaffold under these conditions.

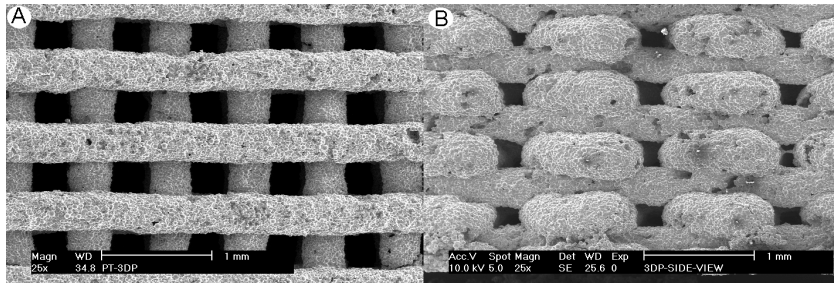


Fig.9 Ti6Al4V scaffold by 3D fiber depositing; (A) Top-view (B) side –view

3.5. Shrinkage of porous Ti6Al4V

Due to high concentration of powder in the slurry almost up to maximum packing density, the shrinkage of sample after drying is neglectable. During sintering, however, shrinkage occurs due to interfusion (necking) of the spherical particles. A sample measuring 20X20X10mm before sintering measured 19.2X19.15 X 9.1 mm after sintering under 1250°C for 2hrs. Consequently, the horizontal linear shrinkage is about 8.5% and the vertical linear shrinkage 9%, corresponding to a volumetric decrease of 16.5 %.

3.6. Macrostructure and microstructure

The macrostructure of the scaffolds obtained by 3D fiber depositing presents a fully interconnected pore network (Fig.9A). The microstructure of a separate fiber is shown in Fig.10A. It shows that particle bonding is achieved by neck growth through a solid state diffusion process. The formation of necks between particles is evidence of good sintering conditions. It can be seen that both macro and micro pores exist in the scaffold. Macro pores are generated and controlled by fiber spacing and layer thickness. Micro pores are left after powder sintering. ESEM shows that the micropore size ranges from 1-10 μ m. Fig.10B shows a cross-section that reveals attachment between layers of the scaffold, as a result of the solid diffusion process. The dimensions as shown in Table 1 prove that fiber diameter, fiber space and porosity have little variation. It means the scaffold made by 3D fiber deposition possess a uniform structure.

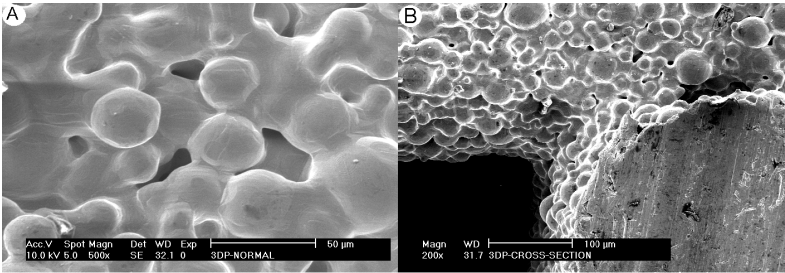


Fig.10 Microstructure of 3D porous Ti6Al4V; (A) high magnification of fiber surface, (B) interface between layers

3.6. Mechanical properties

The compressive strength of scaffolds made with different pressure and feeding speed is shown in Fig.11. It can be seen that the compressive strength increases with the pressure (Fig.11A) and decreases with increasing feeding speed (Fig.11B). As shown in Table 1, the porosity of scaffold was changed by different pressure and feeding speed. Therefore, the compressive strength was affected by porosity. It is in agreement with Gibson and Ashby's model which the stress varies with porosity [65].

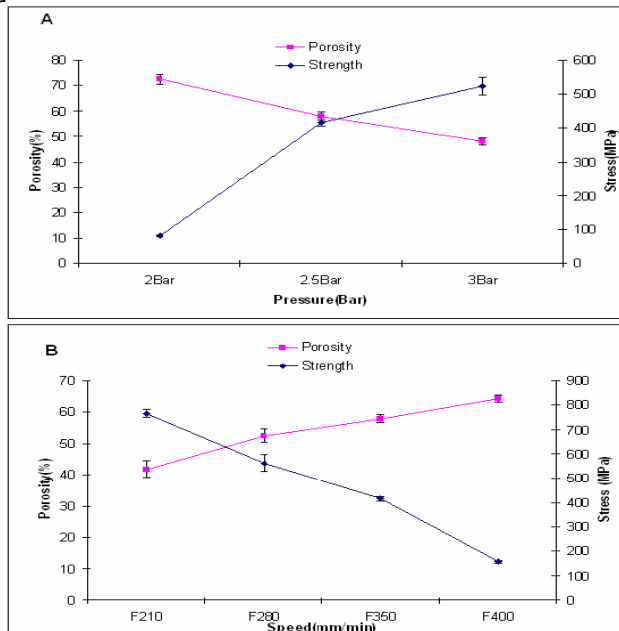


Fig.11 Compressive strength of scaffold varied with different pressure and feeding speed. A) Compressive strength as function of air pressure. B) Compressive strength as function of feeding speed.

3.7. In vitro experiment

Fig.12 shows ESEM images of cells cultured on the porous Ti6Al4V samples for 1 days (Fig.12A), 3 days (Fig.12B) and 7 days (Fig.12C). Polygonal and spindle-shaped cells attached and spread on porous surface of the fibers. Also some cells were found growing via micropores into the inner surface. The spreading cells maintained a physical contact with each other by lamellopodia. Significant cell growth was found over culture period of 7 days. After 1 days culture, only a few cells were seen on the surface (Fig.12A), however, increasing amounts of cells were found after 3days and 7 days culture (Fig.12B and Fig.12C), A DNA content assay (Table 2, $R^2=0.99$) also confirmed that with increasing of culture time, more cells were found to attach and spread on the 3D porous scaffold.

Table 2 DNA content of cells attached on the porous Ti6Al4V

Cultured time	DNA content (ng)
1 day	475±36
3 days	1308±105
7 days	2307±87

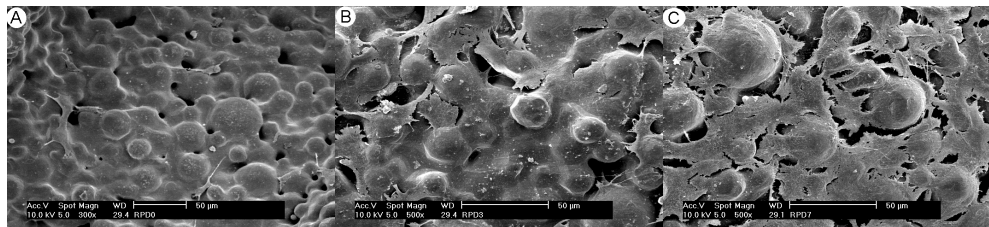


Fig.12 Morphology of MC3T3-E1 osteoblast-like cells cultured on the porous Ti6Al4V for (A) 1day, (B) 3days, (C)7days.

Fig.13A shows amount of protein produced by osteoblast-like cells. The amount of protein increased with the incubation of time. The ALP/DNA activity of cell layers grown on the 3D fiber scaffold also increased as function of culturing time (Fig.13B). The results in vitro show that the cells are not only able to attach and spread well on the surface of porous Ti6Al4V fibers, but also be able to form an extracellular matrix on the surface.

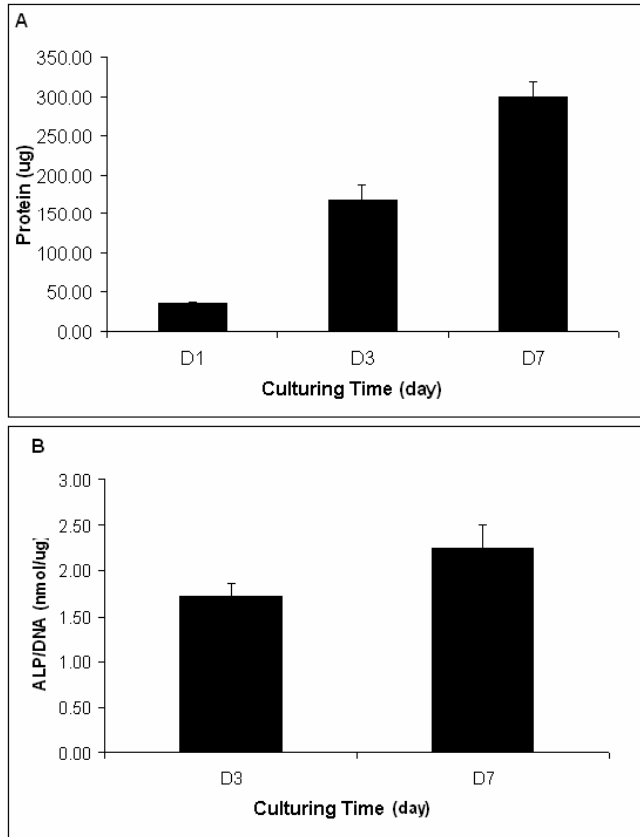


Fig.13 A) Protein content of MC3T3-E1 osteoblast-like cells grown on porous Ti6Al4V scaffold varied with the culturing time. B) ALP/DNA activity of MC3T3-E1 monitored on the scaffold of 3days and 7days

4. Discussion

4.1. Ti6Al4V powder

The used Ti6Al4V powder shows applicability for fiber depositing 3D scaffold. There are four reasons for choosing this powder system. First, the broad distribution of particle size allows a high packing density of powders so that slurries with higher concentrations of powder can be prepared [66]. The optional concentration of powder in the slurry was found to be high as compared to some metal slurries such as with stainless steel (56vol%) [66]. Second, the small powder diameter allows for using small diameter nozzle and reduction of minimum thickness of layer. Third, fine powders can be sintered more readily than coarse ones due to large surface area [67,68]. Finally, the smooth surface of the particles

will enhance powder flowability enabling them to readily flow through small nozzle head without blocking [69].

4.2. Slurry

A high viscosity of the slurry is unavoidable at the concentration levels necessary for enough consistency immediately after extrusion and acceptable shrinkage percentage during drying and sintering. Too high viscosity, on the other hand, will hamper the flow of the slurry through fine nozzles. Fortunately, these slurries show thixotropic behavior, meaning lower apparent viscosity at high shear rates, thus facilitating flow through the nozzle canal, when, after extrusion the slurry is at rest and zero shear rate, the viscosity increases giving the extra enough consistency to prevent flow under gravity force.

4.3. Advantages of 3D fiber depositing porous Ti6Al4V

Several significant advantages of 3D fiber depositing over other processes in porous scaffold fabrication include:

(1) Ti6Al4V scaffolds can be fabricated directly by 3D fiber deposition. It is easy to produce complex geometry with small dimensional defects, which is difficult with casting or milling of titanium, by the setting of parameters, such as fiber spacing, layer thickness and fiber direction. Meanwhile, the nozzles of this fiber depositing system are derived from hypodermic needles and thus disposable, and very cheap. Different diameters of these nozzles are readily available. Therefore, it is possible to assign nozzles of different diameter to different parts to make a functional scaffold.

(2) In most methods of RP, special support structures are needed to support overhanging features of the scaffold. For powder-based methods, like selective laser sintering (SLS) and 3D printing, no support structures are typically required to create complex shapes. But in these methods powder is locally consolidated and the remaining powders serve as support for over hanging structure [34,70]. It is obvious that the support powder in the inner structure is difficult to be removed completely later. SEM images showed that the deposited Ti6Al4V fibers were able to suspend themselves as overhanging fibers with little or no slack (Fig.5). It reveals that these fibers after depositing and solidifying have sufficient strength to hold the shape.

(3) There are some limitations for the variety of materials in conventional RP systems [70,71]. The fiber depositing system described here maybe operated at both high temperature and room temperature offering the versatility and possibility

to apply a wide variety of materials, such as polymers, metal, ceramics and multiple material combinations.

4.3. Limitations of 3D fiber depositing porous Ti6Al4V

Firstly, there is a lower limit of the nozzle size. According to the Hagen–Poiseuille equation, a minor decrease in nozzle diameter will dramatically decrease flow rate and require considerably, greater pressures to deposit suitable fibers. For very small nozzle diameter, even complete blocking of the flow by bridge forming of the particles can be expected. Second, the deposited structures will show some anisotropy, the pore size in z-direction is not necessarily the same as that in x and y-direction but depends on the thickness of the layers. Finally, some pore occlusion at boundaries may occur because of fiber depositing path (Fig.9B) due to continuous fiber depositing.

4. Conclusion

Porous Ti6Al4V scaffolds were successfully fabricated directly by a rapid prototyping technique, 3D fiber deposition. It is shown that Ti6Al4V slurry is a key point for building 3D scaffolds. Three main parameters of the fiber depositing process: the dispensing pressure, feeding speed and initial height between nozzle and platform were investigated for its effect on the integrity of scaffold fabricated. Through a series of experiments, for a nozzle diameter of 0.4mm, a concentration of 66 vol% powders, a fiber depositing pressure of 2.5bar, a feeding speed of 350mm/min and an initial height 0.25mm, were found to be optimal for fabrication of Ti6Al4V scaffolds. The scaffolds have a good attachment between layers, and a fully interconnected porous structure. By varying the direction of fiber depositing and the space between the fibers, scaffolds with highly uniform internal honeycomb-like structures, controllable pore morphology and complete pore interconnectivity can be obtained. Results of in vitro studies revealed the biocompatibility of these scaffolds, which are not only non-toxic but also favorable for cell attachment, proliferation and differentiation. The results of this study demonstrate the potential application in rapid fabrication of 3D Ti6Al4V scaffolds with regular and reproducible architecture for tissue engineering scaffolds and orthopedic implants.

5. Acknowledgements

The authors thank Lorenzo Moroni for his enthusiastic help in the 3D-fiber depositing. The discussions with Dr.Yuan were very constructive during the preparation of this paper.

Reference

1. Vacanti JP, Vacanti CA. The history and scope of tissue engineering, in Principles of Tissue Engineering, 2nd Edition, : Academic Press; 2000. 3-8 p.
2. Yang S, Leong KF, Du Z, Chua CK. The design of scaffolds for use in tissue engineering. Part I. Traditional Factors. Tissue Eng 2001;7(6):679-689.
3. Hollister S, Lin C, Saito E, Schek R, Taboas J, Williams J, Partee B, Flanagan C, Diggs A, Wilke E and others. Engineering craniofacial scaffolds. Orthod Craniofac Res 2005;8(3):162-73.
4. Chang BS, Lee CK, Hong KS, Youn HJ, Ryu HS, Chung SS, Park KW. Osteoconduction at porous hydroxyapatite with various pore configurations. Biomaterials 2000;21(12):1291-8.
5. Nagashima T, Ohshima Y, Takeuchi H. Osteoconduction in porous hydroxyapatite ceramics grafted into the defect of the lamina in experimental expansive open-door laminoplasty in the spinal canal. Nippon Seikeigeka Gakkai Zasshi 1995;69(4):222-30.
6. Tamai N, Myoui A, Tomita T, Nakase T, Tanaka J, Ochi T, Yoshikawa H. Novel hydroxyapatite ceramics with an interconnective porous structure exhibit superior osteoconduction in vivo. J Biomed Mater Res 2002;59(1):110-7.
7. Simske SJ, Ayers RA, Bateman TA. Porous materials for bone engineering. Mater Sci Forum 1997;250:151-182.
8. Ciapetti G, Ambrosio L, Savarino L, Granchi D, Cenni E, Baldini N, Pagani S, Guizzardi S, Causa F, Giunti A. Osteoblast growth and function in porous poly epsilon-caprolactone matrices for bone repair: a preliminary study. Biomaterials 2003;24(21):3815-24.
9. Du C, Meijer GJ, van de Valk C, Haan RE, Bezemer JM, Hesseling SC, Cui FZ, de Groot K, Layrolle P. Bone growth in biomimetic apatite coated porous Polyactive 1000PEGT70PBT30 implants. Biomaterials 2002;23(23):4649-56.
10. Kalita SJ, Bose S, Hosick HL, Bandyopadhyay A. Development of controlled porosity polymer-ceramics composite scaffolds via fused deposition modeling. Mater Sci and Eng (C) 2003;23:611-620.
11. Zhang R, Ma PX. Poly(a-hydroxyl acids)/hydroxyapatite porous composites for bone-tissue engineering. I. Preparation and morphology. J Biomed Mater Res 1999;44:446-455.
12. Williams DF. in Titanium in Medicine: Springer-Verlag, Heidelberg, Germany; 2001. 13 p.
13. Wen C, Yamata Y, Mabuchi M. Processing and mechanical properties of autogenous titanium implant materials. J Mater Sci:in medicine 2002;13:397-401.

14. Holtorf HL, Jansen JA, Mikos AG. Ectopic bone formation in rat marrow stromal cell/titanium fiber mesh scaffold constructs: Effect of initial cell phenotype. *Biomaterials* 2005;26(31):6208-16.
15. Walboomers XF, Jansen JA. Bone tissue induction, using a COLLOSS-filled titanium fibre mesh-scaffolding material. *Biomaterials* 2005;26(23):4779-85.
16. Lueck RA, Galante JO, Rostoker W, Ray RD. Development of an open pore metallic implant to permit attachment to bone. *Surg Forum* 1969;20:456-457.
17. Welsh RP, Pilliar RM, Macnab I. Surgical implants. The role of surface porosity in fixation to bone and acrylic. *J Bone Joint Surg Am* 1971;53(5):963-77.
18. Hahn H, Palich W. Preliminary evaluation of porous metal surfaced titanium for orthopedic implants. *J Biomed Mater Res* 1970;4(4):571-7.
19. Wu BD, Cui YF. Research on Porous Titanium for Medical Implant Material. *Rare Metal Materials Engineering* 1988;4.
20. Fujibayashi S, Neo M, Kim HM, Kokubo T, Nakamura T. Osteoinduction of porous bioactive titanium metal. *Biomaterials* 2004;25(3):443-50.
21. Galante J, Rostoker W. Fiber metal composites in the fixation of skeletal prosthesis. *J.Biomed.Mater.Res.* 1973;4:43-61.
22. Galante J, Rostoker W, Lueck R. Sintered fibre metal composites as a basis for attachment of implants to bone. *J.Bone Joint Surg.* 1971;53A(1):101-114.
23. Davis NG, Teisen J, Schuh C, Dunand DC. Solid-state foaming of titanium by superplastic expansion of argon-filled pores. *J Mater Res* 2001;16:1508-1539.
24. Li JP, Li SH, Van Blitterswijk CA, De Groot K. A novel porous Ti6Al4V: Characterization and Cell attachment. *J.Biomed.Mat.Res* 2005;73A:223-233.
25. Yang S, Leong KF, Du Z, Chua CK. The design of scaffolds for use in tissue engineering. Part II. Rapid prototyping techniques. *Tissue Eng* 2002;8(1):1-11.
26. Sachlos E, Czernuszka JT. Making tissue engineering scaffolds work. Review: the application of solid freeform fabrication technology to the production of tissue engineering scaffolds. *Eur Cell Mater* 2003;5:29-39; discussion 39-40.
27. Sachlos E, Reis N, Ainsley C, Derby B, Czernuszka JT. Novel collagen scaffolds with predefined internal morphology made by solid freeform fabrication. *Biomaterials* 2003;24(8):1487-97.
28. Webb PA. A review of rapid prototyping (RP) techniques in the medical and biomedical sector. *J Med Eng Technol* 2000;24(4):149-53.
29. Hollister SJ. Porous scaffold design for tissue engineering. *Nat Mater* 2005;4(7):518-24.
30. Yeong WY, Chua CK, Leong KF, Chandrasekaran M. Rapid prototyping in tissue engineering: challenges and potential. *Trends Biotechnol* 2004;22(12):643-52.

31. Hutmacher DW, Sittinger M, Risbud MV. Scaffold-based tissue engineering: rationale for computer-aided design and solid free-form fabrication systems. *Trends Biotechnol* 2004;22(7):354-62.
32. Hutmacher DW. Scaffolds in tissue engineering bone and cartilage. *Biomaterials* 2000;21(24):2529-43.
33. Hutmacher DW. Scaffold design and fabrication technologies for engineering tissues- state of the art and future perspectives. *J Biomater Sci Polym Ed* 2001;12(1):107-24.
34. Seitz H, Rieder W, Irsen S, Leukers B, Tille C. Three-dimensional printing of porous ceramic scaffolds for bone tissue engineering. *J Biomed Mater Res B Appl Biomater* 2005;74B(2):782-788.
35. Tan KH, Chua CK, Leong KF, Naing MW, Cheah CM. Fabrication and characterization of three-dimensional poly(ether- ether- ketone)/-hydroxyapatite biocomposite scaffolds using laser sintering. *Proc Inst Mech Eng [H]* 2005;219(3):183-94.
36. Dhariwala B, Hunt E, Boland T. Rapid prototyping of tissue-engineering constructs, using photopolymerizable hydrogels and stereolithography. *Tissue Eng* 2004;10(9-10):1316-22.
37. Woodfield TB, Malda J, de Wijn J, Peters F, Riesle J, van Blitterswijk CA. Design of porous scaffolds for cartilage tissue engineering using a three-dimensional fiber-deposition technique. *Biomaterials* 2004;25(18):4149-61
38. Wilson CE, de Bruijn JD, van Blitterswijk CA, Verbout AJ, Dhert WJ. Design and fabrication of standardized hydroxyapatite scaffolds with a defined macro-architecture by rapid prototyping for bone-tissue-engineering research. *J Biomed Mater Res A* 2004;68(1):123-32.
39. Zein I, Hutmacher DW, Tan KC, Teoh SH. Fused deposition modeling of novel scaffold architectures for tissue engineering applications. *Biomaterials* 2002;23(4):1169-85.
40. Curodeau A, Sachs E, Caldarise S. Design and fabrication of cast orthopedic implants with freeform surface textures from 3-D printed ceramic shell. *J Biomed Mater Res* 2000;53(5):525-35.
41. Melican MC, Zimmerman MC, Dhillon MS, Ponnambalam AR, Parsons JR. Three-dimensional printing and porous metallic surfaces: a new orthopedic application. *J Biomed Mater Res* 2001;55(2):94-202.
42. Wu M, Tinschert J, Augthun M, Wagner I, Schadlich-Stubenrauch J, Sahn PR, Spiekermann H. Application of laser measuring, numerical simulation and rapid prototyping to titanium dental castings. *Dent Mater* 2001;17(2):102-8.
43. Mazumder J, Dutta JD, Kikuchi N, Ghosh A. Closed loop direct metal deposition: art to part. *Optics and Lasers in Engineering* 2000;34:397-414.

44. Mazumder J, Qi H. Fabrication of 3D components by laser-aided direct metal deposition. In: Proceedings of the International Society for Optical Engineering Thomas Schriempf J, editor; 2005; San Jose, CA, USA. p 38-59.
45. Landers R, Hubner U, Schmelzeisen R, Mulhaupt R. Rapid prototyping of scaffolds derived from thermoreversible hydrogels and tailored for applications in tissue engineering. *Biomaterials* 2002;23(23):4437-47.
46. Landers R, pfister A, John.H, Hubner U, Schmelzeisen R, Mulhaupt R. Fabrication of soft tissue engineering scaffolds by means of rapid prototyping techniques. *J.Mat.Sci* 2002;37:3107-3116.
47. Klawitter JJ, Hulbert SF. Application of porous ceramics for the attachment of load bearing orthopedic applications. *J Biomed Mater Res Symp* 1971;2:161-167.
48. Bobyn JD, Pilliar RM, Cameron HU, Weatherly GC. The optimum pore size for the fixation of porous-surfaced metal implants by the ingrowth of bone. *Clin Orthop* 1980(150):263-70.
49. Yuan H, Kurashina K, de Bruijn JD, Li Y, de Groot K, Zhang X. A preliminary study on osteoinduction of two kinds of calcium phosphate ceramics. *Biomaterials* 1999;20(19):1799-806.
50. Bose S, Darsell J, Hosick HL, Yang L, Sarkar DK, Bandyopadhyay A. Processing and characterization of porous alumina scaffolds. *J Mater Sci Mater Med* 2002;13(1):23-28.
51. Hutmacher DW, Schantz T, Zein I, Ng KW, Teoh SH, Tan KC. Mechanical properties and cell cultural response of polycaprolactone scaffolds designed and fabricated via fused deposition modeling. *J Biomed Mater Res* 2001;55(2):203-16.
52. Yedavalli RV, Loth F, Yardimci A, Pritchard WF, Oshinski JN, Sadler L, Charbel F, Alperin N. Construction of a physical model of the human carotid artery based upon in vivo magnetic resonance images. *J Biomech Eng* 2001;123(4):372-6.
53. Comb JW, Priedeman WR, Turley PW. Layered Manufacturing Control Parameters and Material Selection Criteria, *Manufacturing Science and Engineering: Production Engineering Division, ASME*; 1994. 547-556 p.
54. Yardimci AM, Gucerli SI, Danforth SC, Agarwala M, Safari A. Numerical Modelling of Fused Deposition Modelling,. 1995; San Francisco, USA. p part 2.
55. Lowry OH. Micromethods for assay of enzyme. II. Specific procedures. *Alkaline phosphatase*; 1955. 371 p.
56. Boyan BD, Bonewald LF, Swain LD. Localization of 1,25-(OH)₂ D₃ responsive alkaline phosphatase in osteoblast-like cells (ROS 17/2,8, MG 63., and MC 3T3) and growth cartilage cells in culture. *J Biol Chem.* 1989;264:11879.
57. Bretaudiere JP, Spillman T. Alkaline phosphatase, In *Methods of Enzymatic Analysis*, Verlag Chemica: Weinheim,Germany; 1984. 75-92 p.

58. Liu Y, Hunziker EB, de Groot K. BMP-2 incorporated into biomimetic coatings retains its biological activity. *Tissue Eng* 2004;10.
59. Landers R, Mulhaupt R. Desktop manufacturing of complex objects, prototypes and biomedical scaffolds by means of computer-assisted design combined with computer-guided 3D plotting of polymers and reactive oligomers. *Macromol.Mater.Eng* 2000;282:17-21.
60. More solutions to sticky problems-A guide to getting more from your Bronkfield viscometer. U.S: Brookfield Engineering Labs.,Inc.; 2000. 16 p.
61. Benhow J, Bridgwater J. *Pater flow and extrusion*. Oxford: Clarendon Press; 1993.
62. Grida I, Evans JRG. Extrusion freeforming of ceramics through fine nozzles. *Journal of the European Ceramic Society* 2003;23:629-635.
63. Rangarajan S, Qi G, Venkataraman N, Safari A, Danforth SC. Powder Processing, Rheology, and Mechanical Properties of Feedstock for Fused Deposition of Si3N4 Ceramic. *J. Am. Ceram. Soc.* 2000;83(7):1663-1669.
64. Vozzi G. Microsyringe-based deposition of two-dimensional and three-dimensional polymer scaffolds with a well-defined geometry for application to tissue engineering. *Tissue Eng* 2003;8(6):1089-1098.
65. Gibson LJ, Ashby MF. *Cellular solids: structure and properties*. Cambridge: Cambridge University Press; 1997.
66. Liao J, Zhang B. *Porous Materials of Powder Metallurgy*: Metallurgy Industry Press,China; 1978.
67. Oh IH, Nomura N, Masahashi N. Mechanical properties of porous titanium compacts prepared by powder sintering. *Scripta Materialia* 2003;49:1197-1202.
68. Mu W, Deng GZ, Luo FC. *Titanium Metallurgy*. Beijing: Metallurgy Industry Press; 1998.
69. Hong SB, Eliaz N, Leisk GG, Sach EM, Latanision RM, Allen SM. A new Ti-5Ag alloy for customized prostheses by three-dimensional printing (3DP). *J Dent Res* 2001;80(3):860-3.
70. Leong KF, Cheah CM, Chua CK. Solid freeform fabrication of three-dimensional scaffolds for engineering replacement tissues and organs. *Biomaterials* 2003;24(13):2363-78.
71. Lee M, Dunn JC, Wu BM. Scaffold fabrication by indirect three-dimensional printing. *Biomaterials* 2005;26(20):4281-9.

Chapter 6

Porous Ti6Al4V scaffolds directly fabricated by 3D fiber deposition technique: effect of nozzle diameter

J.P. Li^{1,2}, J.R. de Wijn¹, C.A. van Blitterswijk¹, K. de Groot^{1,3}

¹Institute for Biomedical Technology, University of Twente, The Netherlands.

²Porogen. B.V, Enschede, The Netherlands.

³CAM Implants. B.V, The Netherlands.

Abstract

3D porous Ti6Al4V scaffolds were successfully directly fabricated by a rapid prototyping technology: 3D fibre deposition. In this study, the rheological properties of Ti6Al4V slurry were studied and the flow rate was analyzed at various pressures and nozzle diameters. Scaffolds with different fibre diameter and porosity were fabricated. ESEM observation and mechanical tests were performed on the obtained porous Ti6Al4V scaffolds with regard to the porous structure and mechanical properties. The results show that these scaffolds have 3D interconnected porous structure and a compressive strength which depends on porosity at constant fibre diameters and on the fibre diameter at constant porosity. These Ti6Al4V scaffolds are expected to be constructs for biomedical applications.

Keywords: Titanium alloy, porosity, scaffold, 3D fiber deposition

1. Introduction

Titanium and its alloys are widely used in biomedical application for two reasons: their good corrosion resistance and their high strength-to-density ratio [1]. Therefore, various processing techniques have been used to make porous titanium scaffolds, such as: sintering of powders [2], electro sparking Ti6Al4V powder [3], or plasma spraying of powder on a dense substrate followed by cutting off the porous layer [4], compressing and sintering of titanium fibres [5,6] and polymeric sponge replication [7]. Most of these processes form structures with randomly arranged pores with a wide range of sizes, and have limited flexibility to control the pore architecture such as size distribution or interconnectivity and porosity.

During the past decade, rapid prototyping (RP) technologies have emerged as a revolutionary manufacturing process to build objects with predefined microstructure as well as macrostructure [2]. RP allowed researchers to design and fabricate regular and reproducible scaffolds with a completely interconnected pore network. Generally, polymer scaffolds can be directly fabricated by this technique for ceramic and metal scaffolds, a negative replica of the desired structure within a polymeric mould was created first by RP where after the scaffold is produced by casting with molten metal or ceramics suspensions, drying the structure, removing the organic mould by thermal decomposition, followed by sintering. Normally these are time consuming processes [8,9]. Although, selective laser sintering has been used to make ceramics and metal scaffolds directly, the material resolution is relatively low and supporting materials, necessary in overhanging structure, are not easy to remove completely [10].

Directly fabricating scaffolds by using a concentrated Ti6Al4V slurry and 3D fibre deposition offers a new approach for creating Ti6Al4V scaffolds. Development of porous scaffolds via 3D fibre deposition involves three major steps. The first step includes the selection of a Ti6Al4V powder slurry which can be extruded. The second step is feedstock development. The final step involves the 3D deposition of Ti6Al4V fibres. In this study, a 3D-plotting machine [11,12] (Bioplotter, Envisiontec GmbH, Germany) was used. A syringe containing slurry was mounted, and 3 axis motions are independently controlled by a computer system. By setting of the fibre diameter (FD), the length thickness (LT), fibre space (FS) and the fibre lay-down pattern, the elementary structure can be created. Fig.1 shows this fabrication process of computer controlled 3D fibre deposition in the case of a simple "cross-bar" structure.

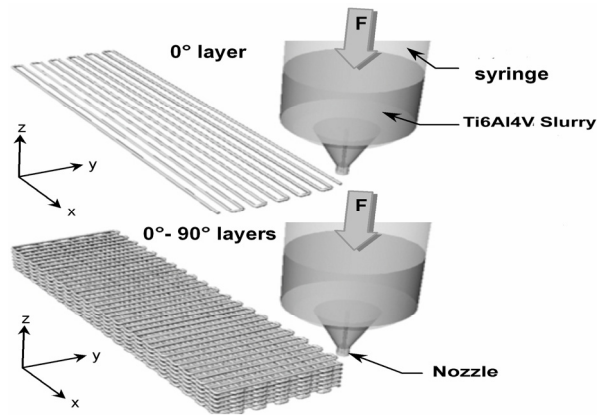


Fig.1 Fabrication process of computer controlled 3D fibre deposition

In a previous study, parameters of 3D fibre deposition were optimized and influences on the scaffold structure were discussed [13].

The purpose of this study was to fabricate scaffolds using different nozzle diameters and determine the result for the scaffold properties.

2. Materials and Methods

2.1. Materials

Ti6Al4V powders (Bongen Titanium (China) Co, Ltd) with a mean diameter of $45\mu\text{m}$ were used in this study. The Ti6Al4V powder (66.vol %) was mixed with an aqueous solution of binders (Methylcellulose (MC, Fisher Scientific B.V) and Stearic acid (Acros organics, USA)). The nozzle used to extrude the Ti6Al4V slurry fibres is a stainless steel hypodermic needle, shorted to a length of 16.1 mm. The nozzle size is expressed as an inner diameter of the nozzle. Nozzle diameters of $250\mu\text{m}$, $400\mu\text{m}$, $500\mu\text{m}$ and $700\mu\text{m}$ were used for this study.

2.2. Scaffold fabrication

Air pressure (pressure 3-5bar) was applied to the syringe through a pressurized cap. The Ti6Al4V slurry is forced through the nozzle to be deposited on a stage as a fibre, which rapidly dries on the air, and the scaffold is fabricated by layering a 0° - 90° pattern of these fibres. Rectangular block models of $20 \times 20 \times 10\text{mm}$ were loaded on the Bioplotter CAM software. After the porous Ti6Al4V scaffolds were dried for 24hrs at room temperature (RT), they were debinded and sintered under high vacuum at 1200°C for 2hrs.

Ti6Al4V scaffolds were fabricated for three experiments. The first experiment (Experiment I) was to investigate the structure of scaffolds with different nozzle

sizes and porosities. In this experiment, nozzle diameters of 250 μ m, 400 μ m, 500 μ m and 700 μ m were used. The second experiment (Experiment II) was to study the effect of fibre diameter at constant porosity on the scaffold mechanical properties. Nozzle diameters of 400 μ m, 500 μ m and 700 μ m were chosen (EII-1, EII-2, EII-3). The third experiment (Experiment III) was to study the effect of porosity on the scaffolds' mechanical properties. A nozzle diameter of 500 μ m was used to make scaffold with different porosities (EIII-1, EIII-2 and EIII-3) by varying the fibre space (200 μ m, 500 μ m and 800 μ m). Table 1 shows the scaffold group for this experiment. To ensure adhesion between the fibres in adjacent layers, the layer thickness was set invariably at about 0.8 * nozzle size [14].

The parameters which determine the geometry and porosity of the 0°-90° cross fibre structure are LT, FD and FS as defined before. Based on a pilot experiment, the parameters of scaffolds with different diameters but equal porosity were estimated (Table 1) so that the influence of each parameter on mechanical properties, for instance, can be determined.

Table1 Scaffold groups for experiment

Specimen group	Nozzle size(mm)	Lay-down pattern(mm)	Fibre space (mm)	Layer thickness(mm)
EII-1	0.4	0/90 ⁰	0.5	0.35
EII-2	0.5	0/90 ⁰	0.6	0.4
EII-3	0.7	0/90 ⁰	0.8	0.5
EIII-1	0.5	0/90 ⁰	0.2	0.4
EIII-2	0.5	0/90 ⁰	0.6	0.4
EIII-3	0.5	0/90 ⁰	0.8	0.4

2.3. Characterization

2.3.1. Viscosity

The rheological behavior of Ti6Al4V slurries was measured at RT with a viscometer (Brookfield Engineering Labs DV-II+ viscometer) with interval time at a speed of 10 rpm with a RV0 spindle.

2.3.2. Morphology

The structure was characterized by environmental scanning electron microscope (ESEM, XL-30, Philips, Eindhoven, The Netherlands), enabling the measurement of the actual of obtained values for FD, FS and LT.

2.3.3. Porosity

The actual Porosity (P) was calculated by measuring the apparent density (ρ_b =weight of sample/ volume of sample) of sample by using the formula: $\rho = (1 - \rho_b / \rho_s) \times 100$, where ρ_s is the density of 100% dense material(4.5g/cm^3). A total of 5 samples were measured.

2.3.4. Mechanical properties

Five samples from each kind of scaffold were randomly chosen. The compression tests of porous Ti6Al4V samples (4x4x6mm, n=10) were performed at room temperature with a crosshead speed of 1mm/min (Zwick/Z050, Germany). The loading direction is in the Z-direction of the deposition process.

3. Results and Discussion:

3.1. Viscosity

The viscosity of Ti6Al4V slurry is shown in Fig.2. The viscosity decreases with increase of time. It can be seen that when the measurement is repeated after 20 mins, the same tendency of decreasing viscosity is observed. It reveals that the slurry displays a thixotropic behaviour. It is of importance to be able to deposit a fibre without supporting material when bridging gaps and this is favoured by the thixotropic behaviour of the slurry which means that a reduction in viscosity occurs when shaken, stirred, or otherwise mechanically disturbed, but at rest the slurry recovers in time, eventually reaching its original viscosity. Fig. 3 shows the flow rate as a function of nozzle diameter and pressure. It appears that the flow rate is not linearly proportional to the pressure, and thus not in agreement with the Hagen–Poiseuille equation [14]. This is to be expected due to non Newtonian behaviour of particulate slurries.

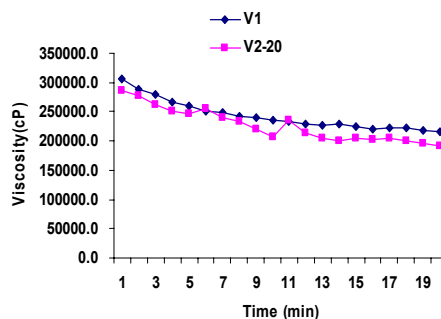


Fig.2 Viscosity of Ti6Al4V slurry with 80 wt% concentration of powder. V2-20 means measurement after 20mins of the first measurement.

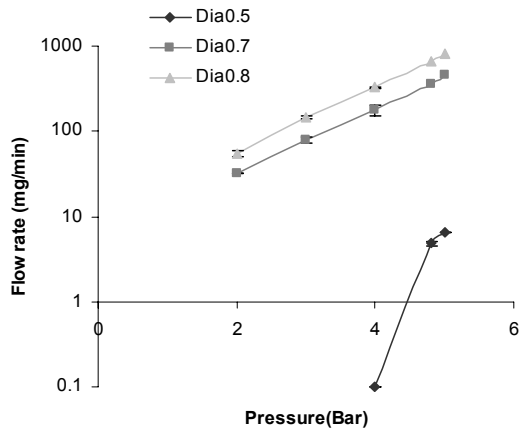


Fig.3 Flow rate varied with nozzle diameter at different pressure

3.2. Morphology

Fig.4 shows the scaffold made at different nozzle diameters. The use of a finer nozzle allowed the fabrication of scaffolds with a larger pore size, under similar setting of the fibre space, and having a higher surface area to volume ratio which may be of importance for cell adhesion in tissue engineering application.

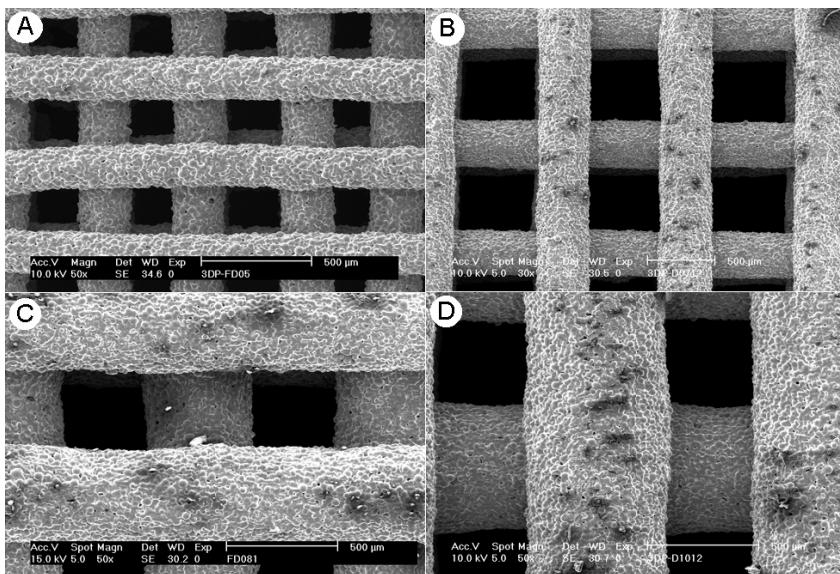


Fig.4 Ti6Al4V scaffold made by different nozzle diameter provide the unity measure for the diameters indicated in a) 250, b) 400, c) 500, d) 700.

Fig.5 shows the scaffolds with varying porosity as result of changing fibre space (FS) at constant fibre diameter (FD). It can be seen that with decreasing the fibre space the structure becomes denser so that porosity of scaffold decreases. To increase the porosity, the FS can be increased but not indefinitely as slacking will occur when the strength of the extruded fibre becomes insufficient to bridge a wide gap.

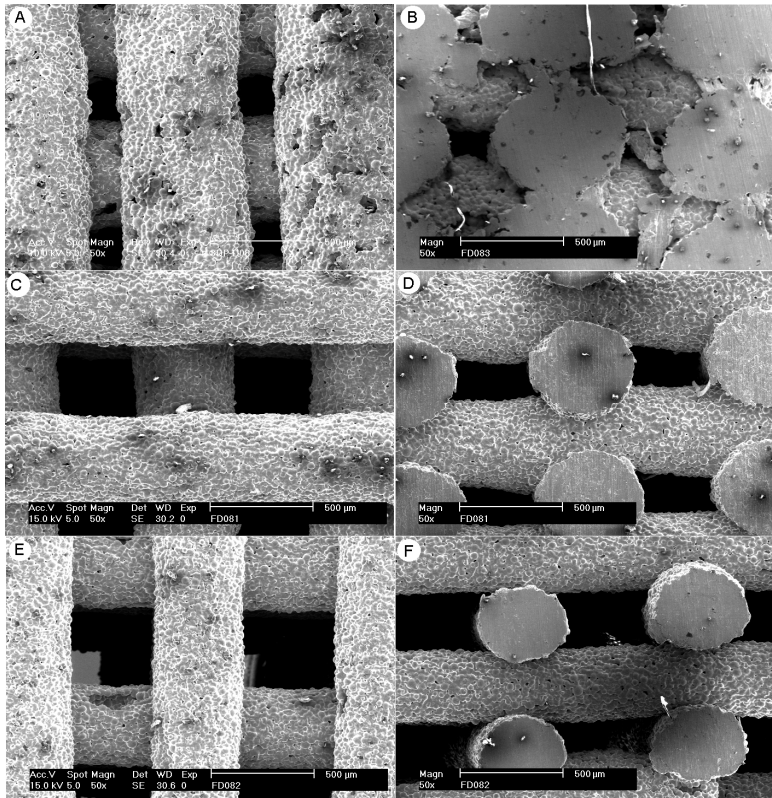


Fig.5 Effect of fibre space on the scaffold processing (a) 200, top-view, (b) 200, side view of cross-section, c) 500, top-view, d) 500, side view of cross-section, e) 800, top-view, f) 800, side view of cross-section.

Based on the ESEM measurement, features of the obtained scaffold are given in Table 2. Compared with the original setting (Table 1). FD is near to the inner size of nozzle, but FS and LT deviate more as a result of the sintering process at elevated temperature.

Table 2 Measurement of structural features of Ti6Al4V scaffold

Specimen group	Fibre Diameter(μm)	Fibre space (μm)	Layer thickness(μm)	Porosity (%)
EII-1	369 \pm 13	381 \pm 16	284 \pm 22	56 \pm 1.5
EII-2	478 \pm 18	374 \pm 18	352 \pm 25	55.5 \pm 1.2
EII-3	570 \pm 19	402 \pm 9	402 \pm 29	55 \pm 1.1
EIII-1	455 \pm 18	176 \pm 14	343 \pm 29	36 \pm 2.2
EIII-2	465 \pm 15	391 \pm 5	347 \pm 26	55 \pm 1.4
EIII-3	485 \pm 13	556 \pm 13	358 \pm 31	62 \pm 0.7

3.3. Porosity

The porosity of the scaffolds in Experiment II showed little variations under measurement (Table 2). The results showed that 3D fibre deposition enables the production of highly reproducible scaffold.

3.4. Mechanical properties

The compressive strength of scaffolds made with different nozzle sizes is shown in Fig.6. In the porosity range of 54-58% scaffolds with the smallest fibre diameter had the highest compressive strength (432 \pm 30MPa). As compressed under z-direction, it is the fibre joint of adjacent layers that bear the loading force. A larger number of fibre joints can indeed be expected to strengthen the scaffold structure. Fig.7 shows the compressive strength of scaffolds at different fibre space. It can be seen that the compressive strength decreases with increasing fibre spacing. It reveals that the compressive strength varies as function of porosity and consequently increasing porosity at constant fibre diameter. This is in agreement with Gibson and Ashby's model which gives an exponential relationship between porosity and mechanical strength [15]. It appears, however, that also a structural component like the fiber diameters in these scaffolds are of influence on its mechanical properties.

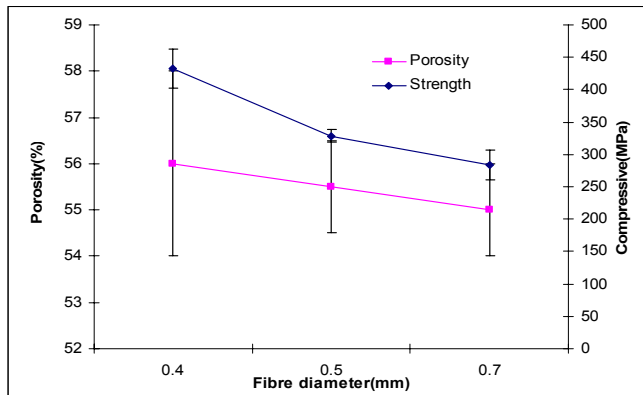


Fig.6 Strength varies with fiber size

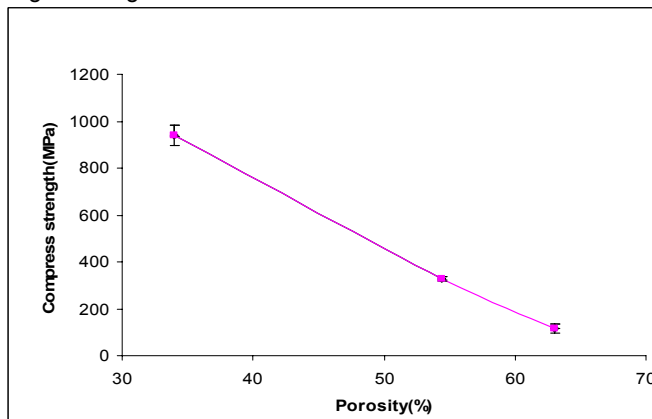


Fig.7 Strength varies with fiber space (porosity)

4. Conclusion

Porous Ti6Al4V scaffolds were successfully directly made by a 3D fibre deposition technology. The scaffold possesses in principal fully interconnected pore networks, and highly controllable porosity and pore size. Scaffolds with different morphology can be made by this technique. The compressive strength was found to be higher in scaffolds with finer fibres under similar porosity. At equal fibre diameter, the strength decreases rapidly with increasing porosity. This technique offer attractive opportunities for designing and desktop manufacturing of biomedical scaffolds and applications in tissue engineering and orthopaedic implants.

Reference

1. Long M, Rack HJ. Review Titanium alloys in total joint replacement materials science perspective. *Biomaterials* 1998;19:1621-1639.

2. Wu BD, Cui YF. Research on Porous Titanium for Medical Implant Material. *Rare Metal Materials Engineering* 1988;4.
3. Okazaki K, Lee WH, Kim DK, Kopczyk RA. Physical characteristics of Ti-6Al-4V implants fabricated by electrodischarge compaction. *J Biomed Mater Res* 1991;25(12):1417-29.
4. Fujibayashi S, Neo M, Kim HM, Kokubo T, Nakamura T. Osteoinduction of porous bioactive titanium metal. *Biomaterials* 2004;25(3):443-50.
5. Galante J, Rostoker W. Fiber metal composites in the fixation of skeletal prosthesis. *J.Biomed.Mater.Res.* 1973;4:43-61.
6. Galante J, Rostoker W, Lueck R. Sintered fibre metal composites as a basis for attachment of implants to bone. *J.Bone Joint Surg.* 1971;53A(1):101-114.
7. Li JP, Li SH, Van Blitterswijk CA, De Groot K. A novel porous Ti6Al4V: Characterization and Cell attachment. *J.Biomed.Mat.Res* 2005;73A:223-233.
8. Wilson C, De Bruijn J, Kruijt M, Van Gaalen S, Dhert WV, A. , Van Blitterswijk CA. Design and fabrication of porous hydroxyapatite scaffolds for bone tissue engineering using Rapid prototyping techniques. 2001; San Francisco USA. p 25-28.
9. Melican MC, Zimmerman MC, Dhillon MS, Ponnambalam AR, Parsons JR. Three-dimensional printing and porous metallic surfaces: a new orthopedic application. *J Biomed Mater Res* 2001;55(2):94-202.
10. Leong KF, Cheah CM, Chua CK. Solid freeform fabrication of three-dimensional scaffolds for engineering replacement tissues and organs. *Biomaterials* 2003;24(13):2363-78.
11. Landers R, Mulhaupt R. Desktop manufacturing of complex objects, prototypes and biomedical scaffolds by means of computer-assisted design combined with computer-guided 3D plotting of polymers and reactive oligomers. *Macromol.Mater.Eng* 2000;282:17-21.
12. Landers R, pfister A, John.H, Hubner U, Schmelzeisen R, Mulhaupt R. Fabrication of soft tissue engineering scaffolds by means of rapid prototyping techniques. *J.Mat.Sci* 2002;37:3107-3116.
13. Li JP, de Wijn JR, Van Blitterswijk CA, de Groot K. Porous Ti6Al4V scaffold directly fabricating by rapid prototyping: Preparation and In Vitro experiment. *Biomaterials.* 2006;27(8):1223-35.
14. Vozzi G. Microsyringe-based deposition of two-dimensional and three-dimensional polymer scaffolds with a well-defined geometry for application to tissue engineering. *Tissue Eng* 2003;8(6):1089-1098.
15. Gibson LJ, Ashby MF. *Cellular Solids: Structure and Properties.* Cambridge: Cambridge University Press; 1997

Chapter 7

The effect of scaffold architecture on properties of direct 3D fiber deposition porous Ti6Al4V for orthopaedic implants

J.P. Li^{1,2}, J.R. de Wijn¹, C.A. van Blitterswijk¹, K. de Groot^{1,3}

¹Institute for Biomedical Technology, University of Twente, The Netherlands.

²Porogen. B.V, The Netherlands.

³CAM Implants. B.V, The Netherlands.

Abstract

3D porous Ti6Al4V scaffolds were directly fabricated by a rapid prototyping technology, 3D fiber deposition (3DF). In this study, scaffolds with different structures were fabricated by changing fiber spacing and fiber orientation. The influence of different architectures on mechanical properties and permeability of the scaffold were investigated. Mechanical analysis revealed that compressive strength and E-modulus increase while decreasing the porosity. The permeability measurement showed that not only the total porosity but also the porous structure can influence the permeability. 3D fiber deposition was found to provide good control and reproducibility of the desired degree of porosity and 3D structure. Results of this study demonstrate that the 3D fiber deposition of Ti6Al4V give us flexibility and versatility to fabricate and improve scaffolds to better mimic the architecture and properties of natural bone and meet the requirements of bone graft substitute and orthopedic and dental implants.

Keywords: Porous Ti6Al4V; scaffold, 3D fiber deposition, mechanical properties, porosity.

1. Introduction

At present, we are evaluating a porous Ti6Al4V to act as a scaffold for tissue engineering and orthopaedic implants, which can, subsequently, be implanted in a bone defect for load bearing sites. Investigators have identified that porous scaffolds for such applications should have the following characteristics[1-6]: (1) 3D and highly porous with an interconnected pore network, enabling cells to enter, attach, and migrate through the scaffold; (2) biocompatibility;(3) suitable surface structure and chemistry for cell attachment, proliferation, and differentiation; (4) mechanical properties to match those of the tissues at the site of implantation, and (5) easy to process into a variety of shapes and sizes. Recently, it has also been shown that mismatches in geometry and mechanical stiffness of repair tissue as compared with the surrounding native tissues causes large stress levels, which may accelerate further joint degeneration [7-9].

During the last 30 years, different processing techniques have been developed to make porous titanium and Ti alloys to be used in dental and orthopedic applications. These conventional techniques include sintering together of particles or plasma spraying of powder [10], pressing and sintering of Ti fibers [11,12], mixing powders with space-holder [13,14], solid-state foaming by expansion of argon-filled pores [15] and polymeric sponge replication [16]. Unfortunately, all of these processes form structures with randomly arranged pores with a wide variety of sizes and offer limited flexibility to control pore volumes and porosity distribution in the final structure. With such scaffolds, it is difficult to achieve the requirements of (1) to (5), and none of these conventional techniques enabled the production of scaffolds with a completely interconnected pore network. Not only the internal structure but also the external shape of implants should be tailored according to customer requirements. The imperfection of the conventional techniques has encouraged the use of a rapid prototyping (RP) technology [17]. RP, combining computer aided design (CAD) with computer aided manufacturing (CAM), has the distinct advantage of enabling the building of objects with predefined microstructure and macrostructure, such as porosity, interconnectivity and pore size. Until now most investigators focused on polymer and ceramic materials[18-23]. Recently, new 3D porous Ti6Al4V scaffolds were successfully developed in our group, which were directly fabricated by a rapid prototyping technology, 3D fiber deposition (3DF) using “bioplotter (Envisiontec GmbH, Germany)”. Fig.1 shows a schematic of a porous prototype made with 3DF deposition. 3D fiber deposition, being a layer-by-layer manufacturing techniques, can be used to manufacture prototypes in which each layer may have a different fiber diameter, thickness, fiber space and fiber orientation. In a previous study, the preparation of

porous Ti6Al4V scaffolds and the optimization of processing parameters of 3DF deposition was discussed [24].

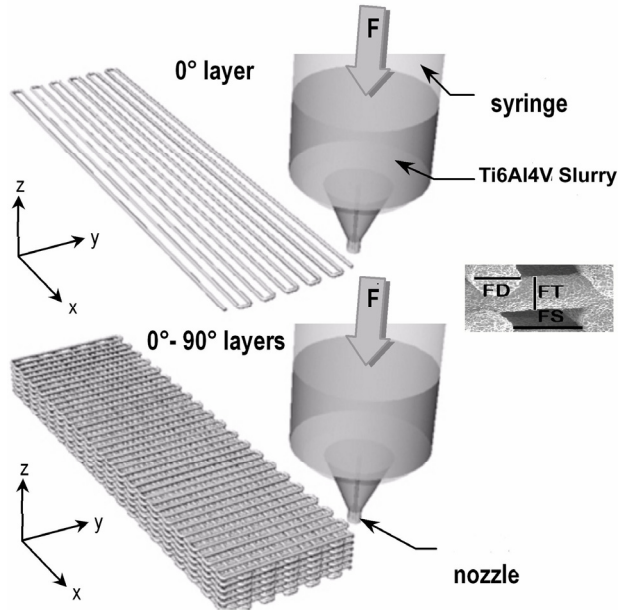


Fig.1 a schematic of a porous prototype made with 3D fiber deposition

To meet practical requirements of bone ingrowth and long term implantation, there is a need to manufacture an implant that mimics the architecture and properties of natural bone, encourages bone and tissue to grow into the pore spaces, and which provides a mechanical and biological interlock between the implant and surrounding bone [25].

In this study, porous Ti6Al4V scaffolds with different structures were directly fabricated by changing fiber orientation and fiber spacing. Studies were conducted to investigate the influences of layer orientation and fiber spacing on the porosity, pore diameter and the mechanical properties of various structures. These studies will determine the suitability of 3DF process for providing an effective and high degree of control over the sizes generated, and uniformity of their structure.

2. Materials and method

2.1. Materials

Ti6Al4V powders (Bongen Titanium (China) Co, Ltd) with a mean diameter of $45\mu\text{m}$ and spherical shape were used in this study. A Ti6Al4V slurry was prepared as follows: The Ti6Al4V powders (68 vol%) were mixed with an aqueous solution of

methylcellulose (0.3 wt.%) as binder and stearic acid (0.2 wt %) to improve the rheological properties of the slurry.

2.2. Processing parameters of 3D fiber deposition

Optimized 3DF process parameters were studied in the previous study. In this study, an inner nozzle diameter of 0.4mm, a deposition pressure of 2.5Bar, a feeding speed of 350mm/min, and an initial height between nozzle head and platform of 0.25mm, were employed to fabricate different scaffolds for testing.

2.3. Scaffold design and fabrication

Ti6Al4V scaffolds were fabricated for three experiments. The first experiment (Experiment I) was to investigate scaffolds with different internal structure. The second experiment (Experiment II) was to study the effect of structure and porosity on the scaffold mechanical properties. The third experiment (Experiment III) was to study the effect of structure and porosity on the permeability of the scaffold as compared to that of human cancellous bone.

For the scaffolds with different structures, four kinds of models were designed and made: with a fiber spacing of 0.5mm, a fiber diameter of 0.4mm and layer thickness of 0.35mm; four lay-down patterns of $0/90^0$, $0/0/90^0/90^0$, $0/45^0$ and $0/90^0$ with staggered space(S1,S2,S3 and S4 corresponded different structure).

For scaffolds with different porosity, a single design was used with variable fiber spacing (0.3mm, 0.4mm,0.5mm,0.6mm,0.7mm,0.8mm, lay-down pattern: $0/90^0$) (P03,P04,P05,P06,P07 and P08 in Table I).

Table1 Scaffold groups for experiment

Specimen group	Nozzle size(mm)	Lay-down pattern(mm)	Fiber space (mm)	Layer thickness(mm)
S1	0.4	$0/90^0$	0.5	0.32
S2	0.4	$0/0/90^0/90^0$	0.5	0.32
S3	0.4	$0/90^0$ stagger	0.5	0.32
S4	0.4	$0/45^0$	0.5	0.32
P03	0.4	$0/90^0$	0.3	0.32
P04	0.4	$0/90^0$	0.4	0.32
P05	0.4	$0/90^0$	0.5	0.32
P06	0.4	$0/90^0$	0.6	0.32
P07	0.4	$0/90^0$	0.7	0.32
P08	0.4	$0/90^0$	0.8	0.32

For all experiments, a total 50 blocks (3 blocks, per condition) were produced. The block size is 22x22x10mm.

2.4. Sintering of scaffolds

After fiber deposition, the samples were first dried for at least 24hrs at room temperature, then for 3hrs at 80°C, and eventually sintered in a high vacuum furnace (10^{-5} mbar) with a heating profile as followings:

RT 600 min → 500 °C 450 min → 1200 °C 120 min → 1200°C furnace cooling → 25°C

2.5. Preparation of samples for properties test

The porosity of the sintered blocks was first calculated by measuring length, width and height as described in the following section. After calculating the porosity, each block was machined by an electrical discharge machine to obtain Ø 7mm by 9mm cylinders for mechanical test and permeability. The samples were labeled for two directions: the Z direction and X- or Y- directions with respect to the lay-down pattern of 0/90° and 0/45°. The structure in X-and Y- direction was considered to be the same.

2.6. Characterization of scaffold

2.6.1. Porosity

Porosity (ρ) was calculated by measuring the apparent density (ρ_b =weight of sample/ volume of sample) and using the formula: $\rho = (1 - \rho_b / \rho_s) \times 100$, where ρ_s is the density of 100% dense material(4.5g/cm³). A total of 5 samples per structure were measured.

2.6.2. Morphology

The scaffold morphology was studied with environmental scanning electron microscopy (ESEM, Model XL-30, Philips, Eindhoven, The Netherlands). The ESEM micrographs were used to measure the fiber space (FS), fiber diameter (FD) and layer thickness (LT) besides studying the scaffold morphology. FS was defined as the edge-to-edge distance between two fibers. LT was defined as the edge-to-edge distance between two layers. FS and FD values were measured from layer top views, which showed the lay-down pattern. LT value was measured from the cross-section views of scaffold specimens, which showed the stacked layers. The dimensions FS, LT and FD are illustrated in Fig.1.

2.6.3. Mechanical test

Five samples from each kind of scaffold were randomly chosen. The compression tests of porous Ti6Al4V samples ($\varnothing 7 \times 9 \text{mm}$, $n=6$) were performed at room temperature with a crosshead speed of 1mm/min (Zwick/Z050, Germany). The E-modulus was calculated by the load increment and the corresponding crosshead displacement between the two points on the straight-line part. Due to the much higher stiffness of the load cell of test machine, the increment of the crosshead displacement was assumed to be equal to the deformation of the sample.

2.6.4. Permeability

A permeability test was performed with a self-designed permeability-meter [26]. Briefly, a cylindrical sample ($\varnothing 7 \times 9 \text{mm}$) was mounted in a tube connected to a wide diameter water reservoir which was positioned at a certain constant height. The flow of water through the sample was measured in ml/sec. Normalized for the dimensions of the sample, it provided a measure for the sample's permeability. The samples with different structure and porosity were tested to study the relationship between permeability and structure or porosity. Two samples under Z- direction of each condition were tested.

2.7. Acetabular cup design and fabrication

In order to provide an example of 3DF concept, an acetabular cup was designed using image-based techniques. The scaffold macrostructure, consisting of interconnected pores, was created using 3D fiber deposition technique. The final result was a porous, anatomically shaped acetabular cup that can be used for total hip joint system.

3. Results

3.1. Morphology

Fig.2 shows the scaffolds with different structures. It can be seen that the scaffold has two patterns under Z-direction view. One group with square pores as a result of $0/90^\circ$ the lay down pattern (Fig.2A-F), and the other with triangular pores as a result of a $0/45^\circ$ lay down pattern (Fig.2G-H). When the scaffolds are viewed under the X- or Y- direction of the fabrication process, more differences between the four scaffolds become overt.

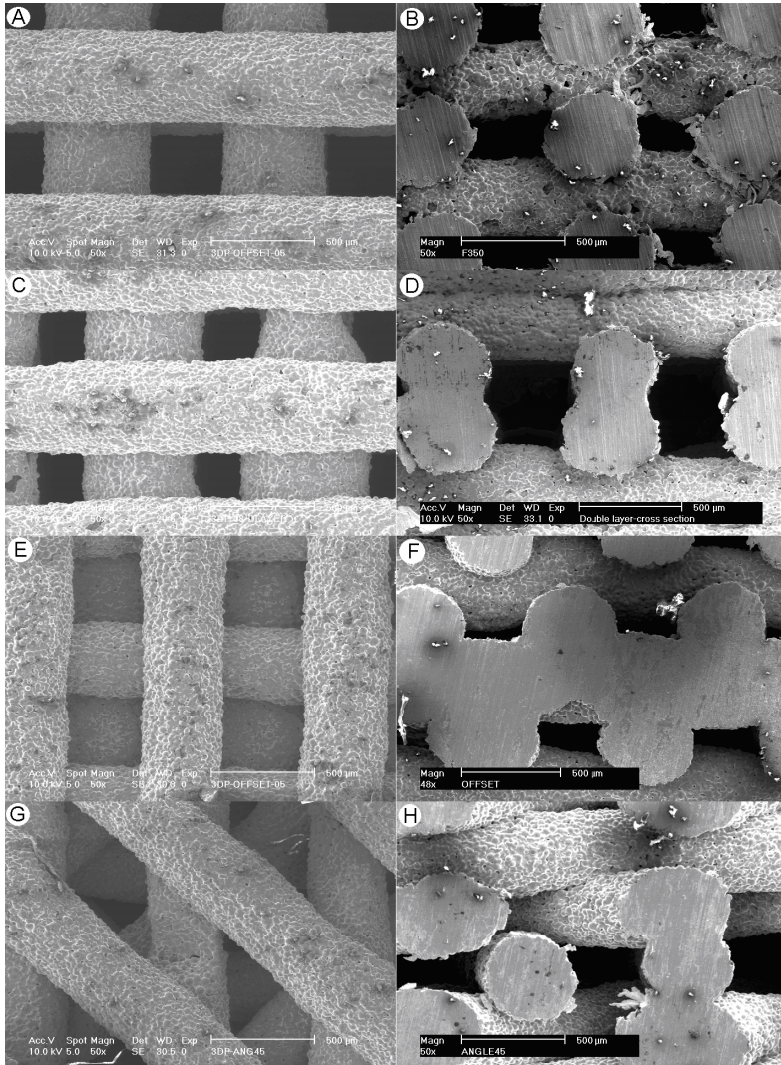


Fig.2 Scaffold with different lay-down pattern. A) lay-down patterns of $0/90^{\circ}$ B) cross-section of $0/90^{\circ}$,C) lay-down patterns of $0/0/90^{\circ}/90^{\circ}$ D) cross-section of $0/0/90^{\circ}/90^{\circ}$, E) lay-down patterns of $0/90^{\circ}$ with stagger ,F) cross-section of $0/90^{\circ}$ with stagger ,G) lay-down patterns of $0/45^{\circ}$,H) cross-section of $0/45^{\circ}$.

Fig.3 shows a series of surface morphologies of scaffolds built with varying fiber spacing from 0.2 to 0.7mm in increments of 0.1mm at constant layer thickness and fiber diameter of 0.32mm and 0.4mm, respectively. It can be seen that with decreasing the fiber space the structure becomes denser and the porosity decreased.

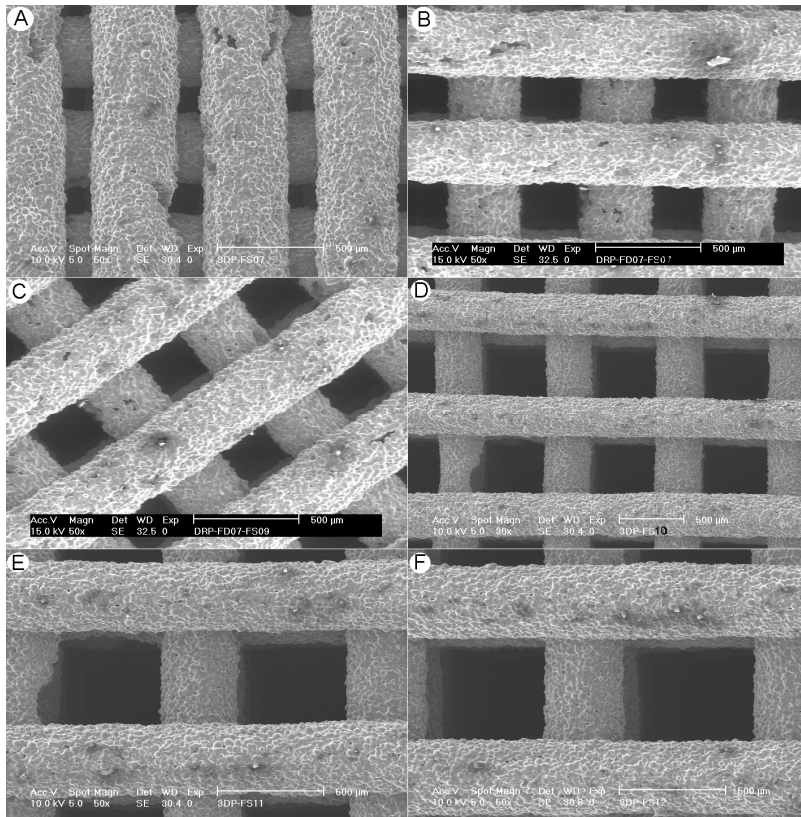


Fig.3 Scaffold with different fiber spacing. A) FS02, B) FS03, C) FS04, D) FS05, E) FS06, F) FS07.

Based on the ESEM measurement, features of scaffolds made by 3D fiber deposition are shown in Table 2. It can be seen that by changing the lay-down pattern and the fiber space, scaffolds with different pore structure and porosity are obtained. Due to sintering at a temperature of 1200°C, some shrinkage has to be expected due to the process of necking of the particles. It can be found in the Table 2, as compared to the machine settings (Table 1), that the shrinkage in the scaffolds is apparently not homogenous and ranges from a few % to sometimes 20%. The fiber diameter (FD) is near to the inner size of nozzle, but fiber spacing (FS) changes significantly. Measurements of fiber space and fiber thickness (FT) showed that pore size ranged between 160 to 680µm (horizontal) and 300 µm (vertical).

Table 2 Measurement of structural features of Ti6Al4V scaffold

Specimen group	FD (μm)	Shrinkage of Fiber (%)	FS (μm)	LT (μm)	Shrinkage of LT(%)	Porosity (%)
S1	369 \pm 12	7.7	381 \pm 15	301 \pm 20	5.9	54.5 \pm 3.5
S2	388 \pm 16	3	394 \pm 18	282 \pm 21	11.8	53.5 \pm 2.2
S3	370 \pm 16	7.7	402 \pm 7	302 \pm 28	5.6	53 \pm 2.1
S4	388 \pm 25	3	405 \pm 17	293 \pm 15	8.4	55 \pm 1.4
P1	368 \pm 22	8	160 \pm 34	275 \pm 24	14	39 \pm 2.1
P2	375 \pm 17	6.2	261 \pm 26	286 \pm 17	10.6	45 \pm 2.8
P3	355 \pm 10	11	396 \pm 16	263 \pm 29	17.8	54 \pm 2.2
P4	365 \pm 18	8.7	465 \pm 7	277 \pm 27	13.4	58 \pm 1.4
P5	385 \pm 14	3.7	556 \pm 12	258 \pm 32	19.3	62 \pm 0.7
P6	381 \pm 7	4.7	679 \pm 10	301 \pm 14	5.9	70 \pm 1

3.2. Porosity

The porosity of the scaffold showed little variations. It can be seen that scaffolds made by different lay-down patterns have similar porosity when the setting for FD, FS and LT become the same (Table 2). Actually, this porosity consists of macro porosity and micro porosity. Macro porosity results from fiber spacing and fiber thickness. Micro porosity results from necking of the particles during powder sintering and residual gas in the starting titanium slurry. High magnification evaluation of fiber surface proves this (Fig.4).

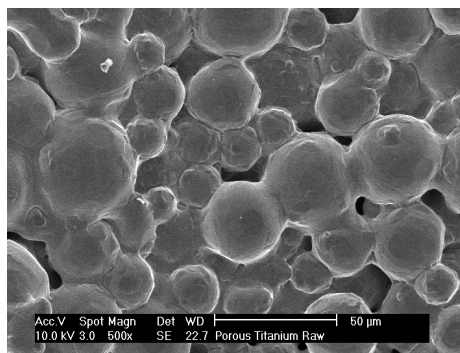


Fig.4 High magnification of fiber surface

3.3. Mechanical properties

The mechanical properties of scaffolds were evaluated by measuring compressive strength and the E-modulus.

3.3.1 Compressive strength

The average values of compressive strength of different scaffolds are plotted against structure and FS setting, as shown in Fig.5. Fig.5A shows the compressive strength of scaffold with different structure in Z-direction and X- or Y- direction. Scaffolds with a $0/90^0$ and $0/45^0$ lay-down pattern had higher compressive strength in Z-direction compared to other patterns. In X- or Y- direction scaffolds with a $0/90^0$ lay- down pattern had the highest compressive strength. Fig.5B shows the compressive strength of scaffolds with different fiber space in Z-direction and X- or Y- direction. It can be seen that the compressive strength decreases with increasing fiber space. This is due to the decrease of the number of fibers within each layer, due to the use of high FS setting, resulting in a decrease of the amount of loading area. In other words, the compressive strength of porous scaffolds depends on the porosity or relative density. There is no significant difference among the compressive strength of scaffold with $0/90^0$ lay-down pattern when measured in two directions. Only with $0/45^0$ patterns significant differences of the compressive strength was found for measurement in (xy) or direction..

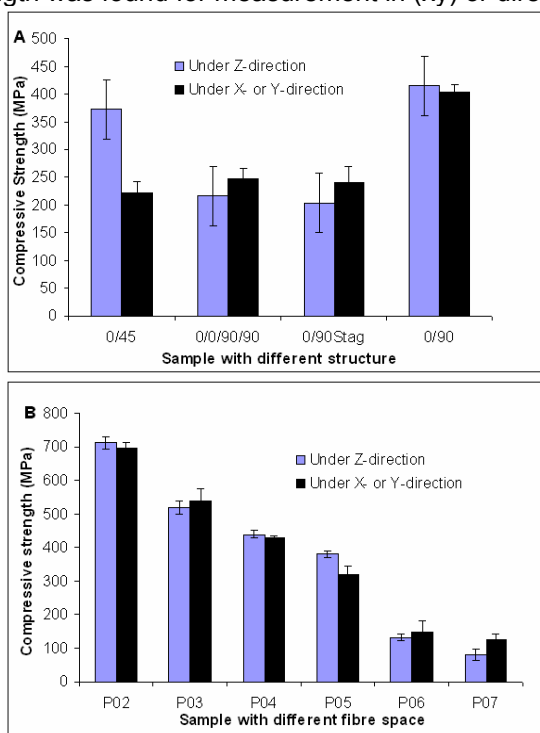


Fig .5 Comparison of compressive strength under Z-direction and X- or Y- direction. A) scaffold with different structure (fiber spacing:500µm, porosity:55%); B) Scaffolds with different porosity(lay-down pattern:0/90⁰).

3.3.2 E-modulus

The calculated E-modulus of different scaffolds was shown in Fig.6A and Fig.6B. Fig.6A shows the E-modulus of scaffolds with different structure under z-direction and X- or Y- direction. Scaffolds with a $0/45^0$ lay-down pattern had the lowest E-modulus in two directions as compared to other scaffolds, and scaffold with different lay- down pattern showed little variation of E-modulus under Z- direction. However, there is significant difference between E-modulus of scaffolds with a $0/45^0$ lay-down pattern under Z-direction and X- or Y- direction. Fig.6B shows the E-modulus of scaffolds with different fiber space in Z-direction and X- or Y- direction. It can be seen that the E-modulus of different scaffolds decrease with increasing fiber space. There is significant difference while fiber space is below P04 under two directions but no such evidence was seen with fiber space above P05.

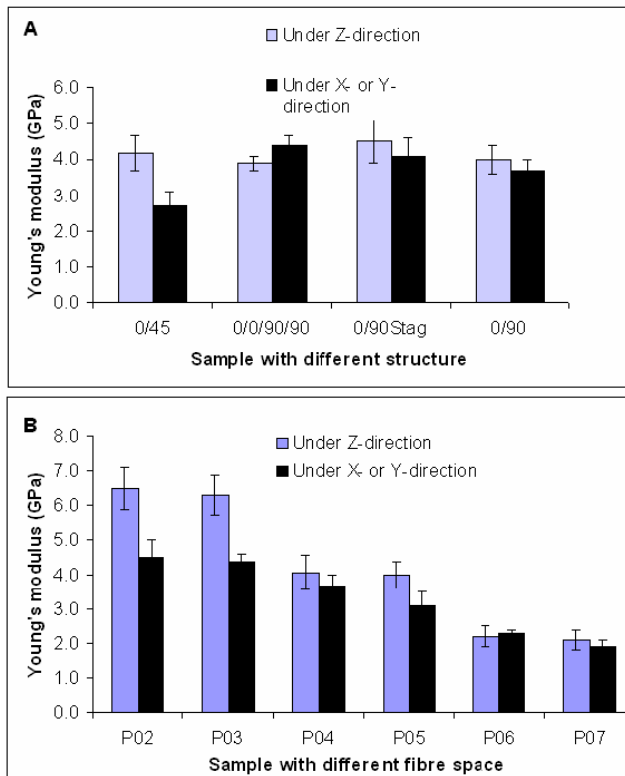


Fig .6 Comparison of Elastic constant under Z-direction and X- or Y- direction
 A) Scaffold with different structure (fibre spacing:500um, porosity:55%); B) Scaffold with different porosity (lay pattern:0/90⁰)

3.3.2. Permeability

Fig.7 shows the permeability data in the two direction of porous Ti6Al4V with different structure and porosity as compared with human cancellous bone under transverse direction [27]. It can be seen that pore structure affects the permeability of scaffold. The permeability of scaffolds with lay down pattern $0/45^{\circ}$ and $0/90^{\circ}$ with staggered spacing as measured in the two direction is similar to that of human cancellous bone. It is clear that the porosity affected the permeability greatly. The permeability data show that permeability increases with increasing porosity. Moreover, the permeability test enables us to prove repeatability of the 3D fiber deposition process. In one batch of samples, the standard deviation in permeability is relative low. The measured porosities (listed in Table 2) also prove the repeatability of this process.

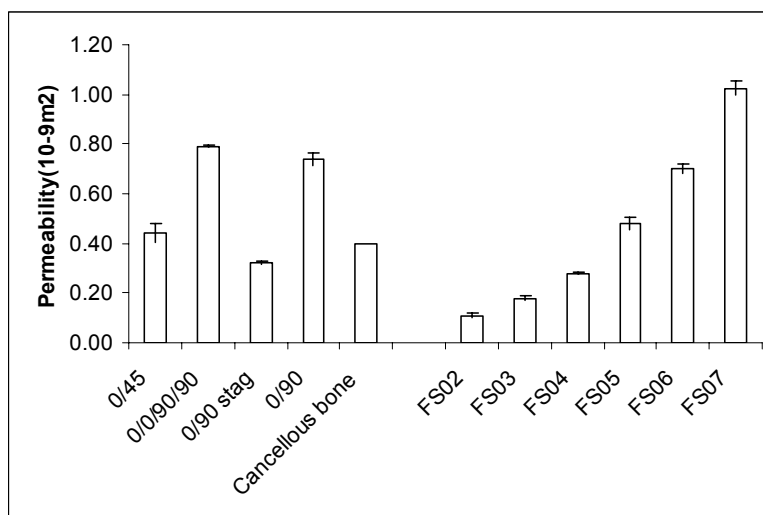


Fig. 7 Permeability as function of different structure constant porosity and porosity compared with that of cancellous bone

3.4. Acetabular cup design and fabrication

The 3D fiber deposition fabrication technique successfully built acetabular cup scaffolds designed using image-based design techniques. In briefly, a cup with a diameter of 50mm and a wall thickness of 5mm was designed using Rhinoceros software 3D (Fig. 8A), then dataset of cup was transported to 3D bioplotter. The fiber space was set to 500 μm ; the layer thickness is 320 μm , resulting pore size of cup (Fig. 8B and 8C) around 400 μm . It can be seen that resulting acetabular cup replicated the design well

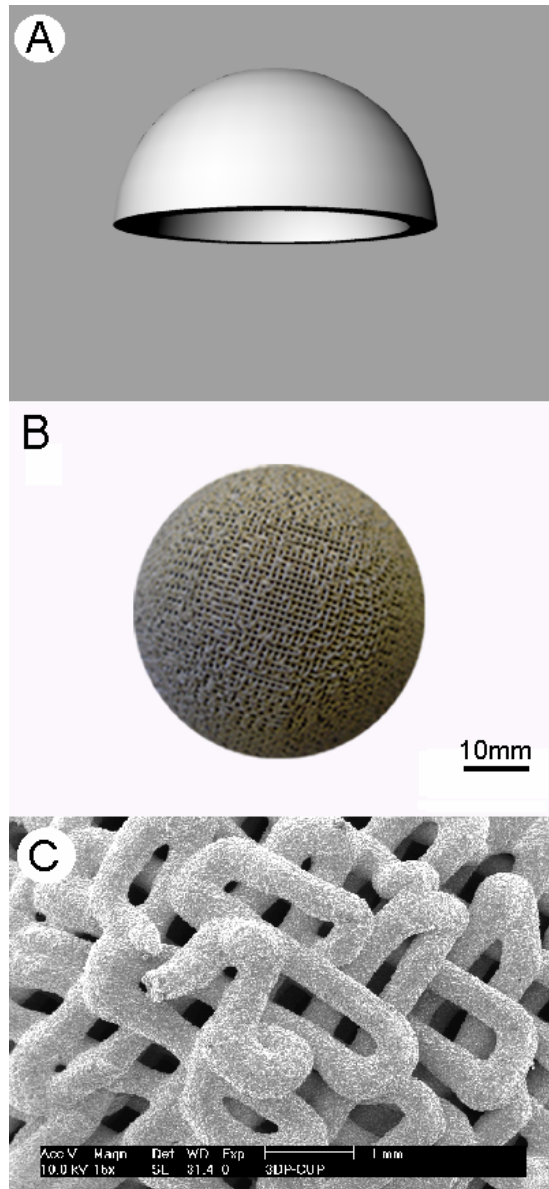


Fig.8 Prototype of acetabular cup. A) Image design by CAD software, B) Porous acetabular cup by 3DF, C) High magnification of acetabular cup surface.

4. Discussion

The results show that FS value played an important role in the porosity for each scaffold. Since a pore is the space created between successive strands within a layer, the pore formed in the scaffold increases in size by increasing the value of

FS. However, this value can not be increased indefinitely as slacking will occur when there is insufficient strength for an extruded fiber to bridge a gap [23,28,29]. It was essential that every layer is well deposited as the preceding layer served as the foundation for the next layer. In the previous study, we knew the parameters of 3D fiber deposition affect the porosity of scaffold, especially feeding speed and air pressure on the slurry, however, by increasing speed to stretch the extruded fiber or changing pressure to reduce amount of Ti slurry, the stability and reproducibility of scaffold might be affected. The flexibility of 3D fiber deposition for changing the FS setting allows highly consistent, controllable and reproducible pore size and arrangement. In this study, FS was set from 200 μm to 800 μm , resulting in pore size ranging from 160 to 680 μm , meeting the requirements for bony ingrowth.

When scaffolds were viewed in the Z direction and the X- or Y- direction, the 3D interconnectivity of pores was observed to be as exemplification in Fig.2 and Fig.3, and the structure of 3D scaffolds designed and fabricated using 3D fiber deposition was not unlike to the honeycomb of bees with a regular array. It reveals that 3D fiber deposition is capable of producing a matrix-like structure or scaffold that is consistently controllable, with reproducible porosity and uniform pore arrangement. The consistency and repeatability of the extruded fibers, fiber arrangement and FS setting enables the production of matrix –like structures with intended and predictable macrostructure. These conditions are highly favorable, since they allow the user to predict parameters accurately and produce structures with known pore sizes and arrangement.

Apparently, by increasing the number of layers with different fiber orientation in a multi-layered scaffold, it is possible to make a porous 3D scaffold with various degrees of channel dimensions. Meanwhile, the use of a finer nozzle diameter allow the fabrication of scaffolds with finer architecture, and a higher surface area to volume ratio can be obtained compared with the scaffold made with a large nozzle [23].

When compressed under z- direction, it was the fiber joint of adjacent layers that bears the loading force. It is clear that a larger number of fiber joints would be expected to strengthen the scaffold structure. When compressed under X- or Y- direction, it was the axially fiber that bears the loading strength, the compressive strength is dependent on the number of fibers aligned in the loading direction and angles of lay down patter. Our results of changing fiber space confirm this. The strength of scaffold is expected to be stronger when compressed in the direction with a higher degree of fiber alignment compared to 0/45⁰ lay down pattern.

For metallic foams, the mechanical parameters are affected by the relative density of the foam ($\rho_r = \rho / \rho_s$, the density of the foam ρ divided by that of the solid material ρ_s). Gibson and Ashby [30] suggested a general model, in which the

relationship between the relative strength, E-modulus, and relative density are given by a power-law relationship of the form:

$$\sigma_{pl}/\sigma_{ys} = C_1 (\rho / \rho_s)^{N1} \quad (1)$$

$$E/E_s = C_2 (\rho / \rho_s)^{N2} \quad (2)$$

Where σ_{pl} is the plateau stress of the foam; σ_{ys} is the yield stress of solid material; E is the Young's modulus of the foam; E_s is the young's modulus of solid materials, and $C1$, $C2$, $N1$ and $N2$ are constants, depending on cell structure parameters. For the case of aluminium foam with lower density ($\rho_r < 0.2$), Gibson and Ashby found the following coefficients and exponents for the model:

$$\sigma_{pl}/\sigma_{ys} = 0.3(\rho / \rho_s)^{3/2} \quad (3)$$

$$E/E_s = (\rho / \rho_s)^2 \quad (4)$$

With $C1=0.3$, $N1=3/2$, $C2=1$, $N2=2$.

Comparing all the sample groups of 3D-fiber deposition scaffolds, the compressive strength and E-modulus were found to decrease with increasing porosity regardless of the lay down pattern and loading direction.

Fig.9 shows the effect of porosity on the compressive strength and E-modulus of scaffolds under two directions according to the experimental data and theoretical predictions by Gibson and Ashby for open cell foams. It shows scaffold compressive strength and E-modulus decreased significantly as the porosity increased,. It can be seen that compressive strength under Z direction and X-or Y-direction is higher than experimental data and E-modulus is lower than experimental data,. The experimental data do not fit the Gibson-Ashby's model well. The reason is probably that the different processing techniques of porous aluminum and porous Ti6Al4V resulted in different pore morphology, and therefore different constitution relationship. It also should be noticed that the theoretical predictions of Gibson and Ashby are based on generic regular structures and take only local yielding into account for limiting the linear elastic regime. Local instability phenomena are not considered. Although ceramics are good bone substitutes, they are not able to provide sufficient strength for load-bearing condition. Ti6Al4V scaffolds made by 3D fiber deposition have a compressive strength ranging from 110MPa to 650 MPa while porosity ranged from 70 to 30%. The compressive strength is higher than that of cancellous bone and comparable to that of cortical bone [31]. It is known that implants with high elastic modulus result in stress shielding, which leads to bone resorption and eventual loosening of the implant[32-34]. Although dense Ti6Al4V has a young's modulus only about half of those of 316L stainless steel or CoCrMo alloy [35,36], it is still about 10-20 times higher than the E-modulus of human bone. The E-modulus of 3DF scaffolds with porosities of 39-70% ranged from 1.9-4.5GPa, that is between that of cancellous bone and cortical bone[35,36].

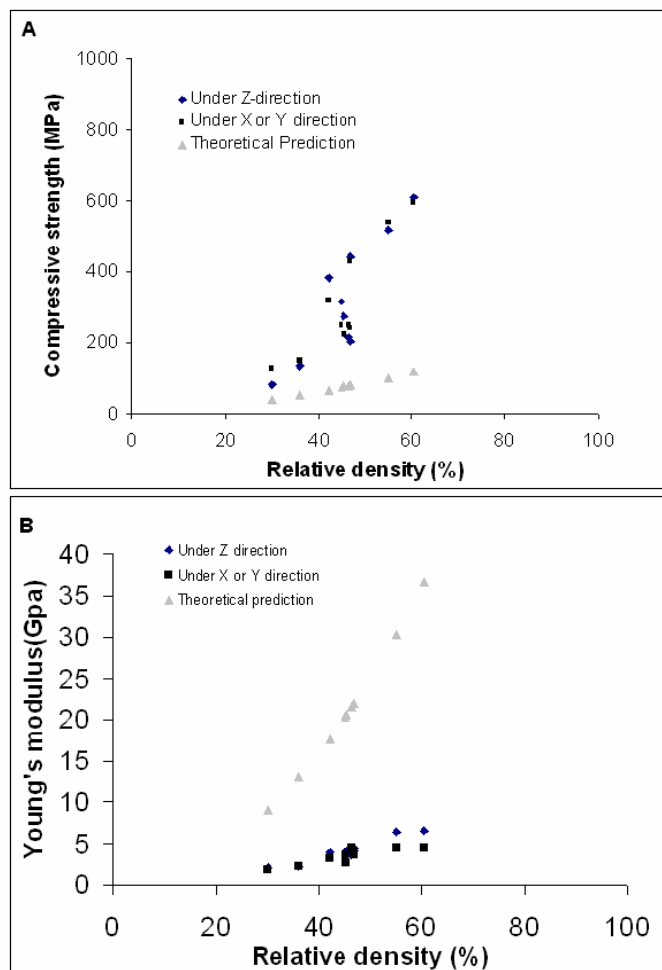


Fig. 9 Compressive strength and elastic constant as function of porosity Under z-direction and x- or Y- direction. A) Compressive strength as function of porosity; B) Elastic modulus as function of porosity

The permeability of scaffolds with $0/45^{\circ}$ and $0/90^{\circ}$ with staggered lay down pattern is quite comparable to that of human cancellous bone. Therefore the scaffold made by 3D fiber deposition might be a promising biomaterial for biomedical applications since a higher metabolic exchange rate of bone cells as well as minerals can be achieved by its interconnected pore structure and a high surface to volume ratio. Since high permeability could prove highly beneficial for cell seeding and tissue formation, allowing the cells to diffuse into the centre of the scaffold and will provide space for the ingrowth of tissue and subsequent vascularisation, thus increasing its osteoconductive potential[37,38]. In general, when porous materials are studied, two parameters are widely used: porosity and

pore size, including mean value and distribution. In our experiment, although the porosity and pore size are similar, the permeability is not the same due to difference in pore shape and interconnectivity. It was found that permeability is an easy, additional method to reveal the structural properties of open porous materials. Permeability data reflect a combination of (1) porosity, (2) pore size and distribution, (3) interconnectivity, (4) interconnection pore size and distribution, (5) orientation of pores with respect to flow direction. Therefore, in the future permeability can be taken as a comprehensive intrinsic parameter for describing macro porous structure precisely and quantitatively, and probably more relevant than porosity and mean pore size in characterizing porous materials structure.

It can be seen that there are several advantages of this scaffold. First, the structure of scaffold is highly regular and repeatable and all macro pores are interconnective. Second, scaffolds with regular architecture will presumably permit cells to be seeded in the core region easily than with random architecture scaffolds and create environments, which encouraging uniform conditions for free of flowing nutrients to the interior of implant and promoting cell viability. Third, scaffolds with regular architecture could permit parametric analyses to be conducted in terms of nutrient concentration and local environments. It is essential in scientific investigations to identify and predict optimal cell environments and to know how scaffolds and material affect tissue regeneration. Fourth, the technique allows us to design and fabricate scaffold with designed properties that can balance the requirements of load bearing and cell nutrition for tissue in growth.

5. Conclusion

3D fiber deposition was successfully applied to fabricate porous Ti6Al4V scaffold with a fully interconnected network, highly controllable porosity and pore size. The scaffold can be made with different structures and porosity by controlling process parameters, such as fiber spacing, layer thickness and fiber orientation. The characteristics of resulting scaffolds were analyzed. Experimental results show that the fiber spacing has a profound effect on the porosity, pore size and thus on compressive strength and elastic's constant of the built scaffolds. The resulting scaffold can mimic the properties of both the cancellous bone and cortical bone. This method provides a control of external shape to match graft geometry and internal architecture with pore structure in 3D space to provide control over interconnectivity, geometry, fiber diameter and orientation, mechanical properties. Therefore, 3D fiber deposition is an interesting new technique for design and fabrication of tailor-made or custom-made Ti6Al4V scaffold architectures for tissue engineering scaffolds and orthopaedic implant application.

References

1. Yang S, Leong KF, Du Z, Chua CK. The design of scaffolds for use in tissue engineering. Part I. Traditional Factors. *Tissue Eng* 2001;7(6):679-689.
2. Vacanti JP, Vacanti CA. The history and scope of tissue engineering, in *Principles of Tissue Engineering*, 2nd Edition, : Academic Press; 2000. 3-8 p.
3. Hollister S, Lin C, Saito E, Schek R, Taboas J, Williams J, Partee B, Flanagan C, Diggs A, Wilke E and others. Engineering craniofacial scaffolds. *Orthod Craniofac Res* 2005;8(3):162-73.
4. Hutmacher DW, Schantz T, Zein I, Ng KW, Teoh SH, Tan KC. Mechanical properties and cell cultural response of polycaprolactone scaffolds designed and fabricated via fused deposition modeling. *J Biomed Mater Res* 2001;55(2):203-16.
5. Hutmacher DW. Scaffold design and fabrication technologies for engineering tissues--state of the art and future perspectives. *J Biomater Sci Polym Ed* 2001;12(1):107-24.
6. Hutmacher DW. Scaffolds in tissue engineering bone and cartilage. *Biomaterials* 2000;21(24):2529-43.
7. Pompe W, Worch H, Epple M, Friess W, Gelinsky M, Greil P, Hempele U, Scharnweber D, Schulte K. Functionally graded materials for biomedical applications. *Mate.Sci. and Eng A* 2003;362:40-60.
8. Simske SJ, Ayers RA, Bateman TA. Porous materials for bone engineering. *Mater Sci Forum* 1997;250:151-182.
9. McNamara BP, Cristofolini L, Toni A, Taylor D. Relationship between bone prosthesis bonding and load transfer in total hip reconstruction. *J Biomech* 1997;30(6):621-630.
10. Fujibayashi S, Neo M, Kim HM, Kokubo T, Nakamura T. Osteoinduction of porous bioactive titanium metal. *Biomaterials* 2004;25(3):443-50.
11. Galante J, Rostoker W. Fiber metal composites in the fixation of skeletal prosthesis. *J.Biomed.Mater.Res.* 1973;4:43-61.
12. Galante J, Rostoker W, Lueck R, Ray RD. Sintered fiber metal composites as a basis for attachment of implants to bone. *J Bone Joint Surg Am* 1971;53(1):101-14.
13. Wen C, Yamata Y, Mabuchi M. Processing and mechanical properties of autogenous titanium implant materials. *J Mater Sci:in medicine* 2002;13:397-401.
14. Matin B, Cornelia S, Bronkremer HP, Baur H. High-porosity Titanium, Stainless Steel, and Superalloy Parts. *Advance Engineering Materials* 2000;2(4):196-199.
15. Davis NG, Teisen J, Schuh C, Dunand DC. Solid-state foaming of titanium by superplastic expansion of argon-filled pores. *J Mater Res* 2001;16:1508-1539.
16. Li JP, Li SH, Van Blitterswijk CA, De Groot K. A novel porous Ti6Al4V: Characterization and Cell attachment. *J.Biomed.Mat.Res* 2005;73A:223-233.
17. Yang S, Leong KF, Du Z, Chua CK. The design of scaffolds for use in tissue engineering. Part II. Rapid prototyping techniques. *Tissue Eng* 2002;8(1):1-11.

18. Seitz H, Rieder W, Irsen S, Leukers B, Tille C. Three-dimensional printing of porous ceramic scaffolds for bone tissue engineering. *J Biomed Mater Res B Appl Biomater* 2005;74B(2):782-788.
19. Tan KH, Chua CK, Leong KF, Naing MW, Cheah CM. Fabrication and characterization of three-dimensional poly(ether- ether- ketone)/-hydroxyapatite biocomposite scaffolds using laser sintering. *Proc Inst Mech Eng [H]* 2005;219(3):183-94.
20. Dhariwala B, Hunt E, Boland T. Rapid prototyping of tissue-engineering constructs, using photopolymerizable hydrogels and stereolithography. *Tissue Eng* 2004;10(9-10):1316-22.
21. Chua CK, Leong KF, Tan KH, Wiria FE, Cheah CM. Development of tissue scaffolds using selective laser sintering of polyvinyl alcohol/hydroxyapatite biocomposite for craniofacial and joint defects. *J Mater Sci Mater Med* 2004;15(10):1113-21.
22. Wilson CE, de Bruijn JD, van Blitterswijk CA, Verbout AJ, Dhert WJ. Design and fabrication of standardized hydroxyapatite scaffolds with a defined macro-architecture by rapid prototyping for bone-tissue-engineering research. *J Biomed Mater Res A* 2004;68(1):123-32.
23. Zein I, Hutmacher DW, Tan KC, Teoh SH. Fused deposition modeling of novel scaffold architectures for tissue engineering applications. *Biomaterials* 2002;23(4):1169-85.
24. Datta N, Holtorf HL, Sikavitsas VI, Jansen JA, Mikos AG. Effect of bone extracellular matrix synthesized in vitro on the osteoblastic differentiation of marrow stromal cells. *Biomaterials* 2005;26(9):971-7.
25. Sun W, Starly B, Nam J, Darling A. Bio-CAD modeling and its applications in computer-aided tissue engineering. *Computer-Aided Design* 2005;37:1097-114.
26. Li SH, De Wijn JR, Li JP, Layrolle P. Biphasic calcium phosphate scaffold with high permeability/porosity ratio. *Tissue Engineering* 2003;9(3):535-548.
27. Grimm MJ, Williams JL. Measurement of permeability in human calcaneal trabecular bone. *J Biomechanics* 1997;30(7):743-745.
28. Landers R, Mulhaupt R. Desktop manufacturing of complex objects, prototypes and biomedical scaffolds by means of computer-assisted design combined with computer-guided 3D plotting of polymers and reactive oligomers. *Macromol.Mater.Eng* 2000;282:17-21.
29. Landers R, Pfister A, John H, Hubner U, Schmelzeisen R, Mulhaupt R. Fabrication of soft tissue engineering scaffolds by means of rapid prototyping techniques. *J.Mat.Sci* 2002;37:3107-3116.
30. Gibson LJ, Ashby MF. *Cellular Solids: Structure and Properties*. Cambridge: Cambridge University Press; 1997.

31. Li JP, S.H.Li, Van Blitterswijk CA, de Groot K. Cancellous Bone from Porous Ti6Al4V by Multiple Coating Technique. *J Mat Sci:Mat in Med* 2005;16:in press.
32. Cheal E, Spector M, Hayes W. Role of loads and prosthesis material properties on the mechanics of the proximal femur after total hip arthroplasty. *J Orthop Res* 1992;10:405-422.
33. Prendergast P, Taylor D. Stress analysis of the proximo-medial femur after total hip replacement. *J Biomed Eng* 1990;12:379-382.
34. Lewis JL, Askew MJ, Wixson RL, Kramer GM, Tarr RR. The influence of prosthetic stem stiffness and of a calcar collar on stresses in the proximal end of the femur with a cemented femoral component. *J Bone Joint Surg* 1984;66-A(280-286).
35. Bobynd JD, Hacking SA, Chan SP. Characterization of a new porous tantalum biomaterial for reconstructive orthopaedics.; 1999; Anaheim, CA.
36. Krygier JJ, Bobynd JD, Poggie RA. Mechanical characterization of a new porous tantalum biomaterial for orthopaedic reconstruction.; 1999; Sydney, Australia.
37. Hui PW, Leung PC, Sher A. Fluid conductance of cancellous bone graft as a predictor for graft-host interface healing. *J Biomech* 1996;29(1):123-32.
38. Shimko DA, Shimko VF, Sander EA, Dickson KF, Nauman EA. Effect of porosity on the fluid flow characteristics and mechanical properties of tantalum scaffolds. *J Biomed Mater Res B Appl Biomater* 2005;73(2):315-24.



Part III

Biological Properties of Porous Titanium Scaffold

Chapter 8
Comparison of porous titanium alloy made by sponge replication and 3D fiber deposition

Chapter 9
Bone ingrowth in porous titanium alloy implants produced by 3D fiber deposition

Chapter 10
Bone tissue reconstruction using porous titanium alloy combined with biphasic calcium phosphate ceramic: in vivo study in goats

Chapter 8

Comparison of porous Ti6Al4V made by sponge replication and 3D fiber deposition

J.P. Li^{1,2}, J.R. de Wijn¹, C.A. van Blitterswijk¹, K. de Groot^{1,3}

¹Institute for Biomedical Technology, University of Twente, The Netherlands.

²Porogen. B.V, The Netherlands.

³CAM Implants. B.V, The Netherlands.

Abstract

In the present study we compared porous Ti6Al4V made by sponge replication (FT) with porous Ti6Al4V made by direct 3D fiber deposition (3DFT) and cancellous bone in terms of structural properties, permeability, mechanical properties and osteoconductivity. Both FT and 3DFT were highly macroporous. While 3DFT exhibited a very regular open porous structure, FT's pore structure was more complex and similar to that of cancellous bone. Microstructure of the two alloy types was similar. Due to these structural differences, mechanical properties of the two scaffold types, such as stiffness or strength were different too. The compressive strength and Young's modulus of both types of porous Ti6Al4V scaffolds were higher than that of cancellous bone, while their permeability was comparable to the permeability of bone. In vivo result showed a larger amount of newly formed bone in FT than in 3DFT scaffolds.

Key words: Ti6Al4V alloy, sponge replication, 3D fiber deposition, porosity, osteoconductivity

1. Introduction

The materials of choice for fabricating load bearing permanent orthopedic and craniofacial implants are titanium and its alloys due to their excellent mechanical properties and biocompatibility [1-3]. Porous titanium and its alloys are currently considered one of the most promising materials for application in orthopaedic and dental surgery since porosity allows for bone ingrowth inside the material resulting in good mechanical interlocking between the implant and surrounding bone and better long-term fixation of the implant [4-6].

The function of human bone is to provide the human body with the required structural stiffness and strength of the human body. Bone consists of cancellous and compact bone. Cancellous bone has an open porous structure for bone marrow and metabolic exchange of cells and minerals among others. When designing synthetic materials for bone repair and replacement, one is logically trying to mimic the properties of bone as closely as possible.

The aim of the present study was to give a comparison between two types of porous Ti6Al4V scaffolds developed in our group, i.e. sponge replication porous Ti6Al4V (FT) and 3D fiber deposition porous Ti6Al4V (3DFT) [7-9], and human bone with regard to structure, strength and stiffness, and permeability for fluids. In addition, bone formation and conduction capacity of the two titanium alloy types was investigated in vivo.

2. Materials and methods

2.1. Materials

3DFT: A Ti6Al4V slurry (80 wt% of Ti6Al4V powder in 0.5wt% aqueous water methylcellulose solution) was forced through a syringe nozzle by using a 3D-biplotter machine (Envisiontec GmbH, Germany) [9]. The slurry was plotted on a stage as a fiber, which rapidly solidified, and the scaffold was fabricated by layering a 0°-90° pattern of fibers. After deposition, the obtained Ti6Al4V scaffolds were dried at RT for 24 hours, followed by the sintering of scaffolds under high vacuum (10^{-5} mbar) at 1200°C for 2 hours. The fiber diameter was around 400µm. The porosity of the scaffolds was varied by changing the fiber spacing.

FT: The fabrication process of FT consisted of two steps. In step 1, base porous Ti6Al4V was fabricated by a polymeric sponge replication process consisting of impregnation of a polymeric sponge by immersing it in a Ti6Al4V slurry, removal of excess slurry, drying, debinding (the sponge is burned out) and sintering, resulting in a positive replica in Ti6Al4V of the original polymeric sponge [7]. In step 2, this base porous Ti6Al4V was dipped into a thinner slurry for 30 seconds after which

high-pressure air was used to remove excess slurry to achieve a homogenous coating on the struts and to prevent the slurry from blocking the pores [8,10]. After coating, the samples were dried at 80°C for 1 hour, followed by drying at RT for 24 hours. Finally, the scaffolds were sintered at 1200°C under high vacuum (10^{-5} mbar) with a dwell time of 2 hours. Different porosities were obtained by changing the coating time [8,10].

Characteristics: Mechanical properties were measured on cylinders with a diameter of 10 mm and a height of 12 mm using a Zwick testing machine with a cross-head speed of 1 mm/min. Permeability was determined using a home-made device to measure the constant in the Darcy law formula [11].

2.2. In vivo study

In this study 10 adult Dutch milk goats, with an average weight of 65 ± 8.5 kg, were used. Animals were housed at Central Animal Laboratory Institute (GDL), Utrecht, The Netherlands, at least 4 weeks prior to surgeries. The study was approved by Dutch Animal Care and Use Committee.

3DFT and FT implants ($7\times 8\times 4$ mm³) were implanted bilaterally on the transverse processes of the L4 and L5 vertebrae of each goat using polymeric cages (Fig.1). Cage design and fabrication were described previously [12]. To monitor bone formation over time, fluorochrome markers were administered 3, 6 and 9 weeks and the animals were sacrificed 12 weeks after implantation. Spinal cages were retrieved by sawing off a piece of the transverse processes. Bone formation into porous titanium implants was investigated by histology and histomorphometry of non-decalcified sections using epifluorescent and light microscopy. The following parameters were investigated:

1. %b. ROI: the percentage of bone area in the total implant area [(bone area / total implant area) x 100%];
2. Depth of bone ingrowth: bone ingrowth depth from the host bone bed into the implant.

For statistical analysis ANOVA for randomized complete block design with a post hoc Tukey's HSD ($p=0.05$) test was used in SPSS (Chicago, IL) 11.5 software.

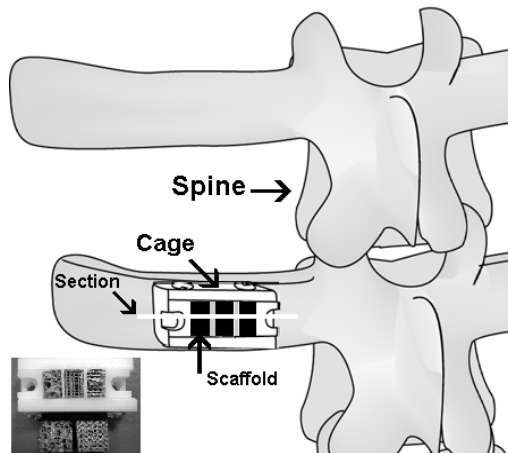


Fig.1: Schematic drawing of the implantation on goat's transverse process. The lower left is the cage with three implants

3. Results and discussion

3.1. Structure

One of the most important functions of orthopaedic implants is to provide structural stiffness in the original defect area. Porous material is needed to provide biological anchorage for the surrounding bone tissue via the ingrowth of new bone into the pores of the implant. Macrostructure of FT was similar to that of cancellous bone (Fig.2A and 2B), with the difference that triangle-shaped holes were left in the core of the struts of metallic implant due to processing technique (Fig.3A). Unlike FT and cancellous bone, 3DFT possessed a very regular porous structure, as determined by the lay-down pattern of the fibers (Fig.2C). Closer investigation revealed that FT implants had thinner struts as compared with cancellous bone, whereas the diameter of the fibers of 3DFT was constant throughout the implant. Microstructure of the two scaffold types was similar (Fig.4), as they were produced from the same raw Ti6Al4V powder and underwent a similar sintering procedure.

The length to thickness ratio of the individual trabecular struts of cancellous bone is about 4 [4]. Although the structure of FT was similar to that of cancellous bone, the length to diameter ratio of the FT struts was about 10, making these scaffolds imperfection sensitive and susceptible to micro-buckling. Structural fiber length to diameter ratio of the 3DFT was $1000/400 \mu\text{m} = 2.5$.

Human bone and porous titanium also show a different behavior with respect to anisotropy. The axial stiffness of cancellous bone is 2-3 times higher than the stiffness in the transverse direction. This is a result of the process of functional

adaptation. While FT can be considered an isotropic material, 3DFT showed anisotropy due to the layered structure (shown in Fig.3B).

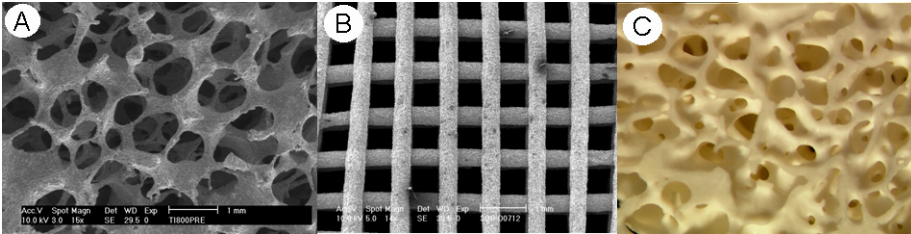


Fig.2 Macrostructure of FT (A), 3DFT (B) and cancellous bone (C)

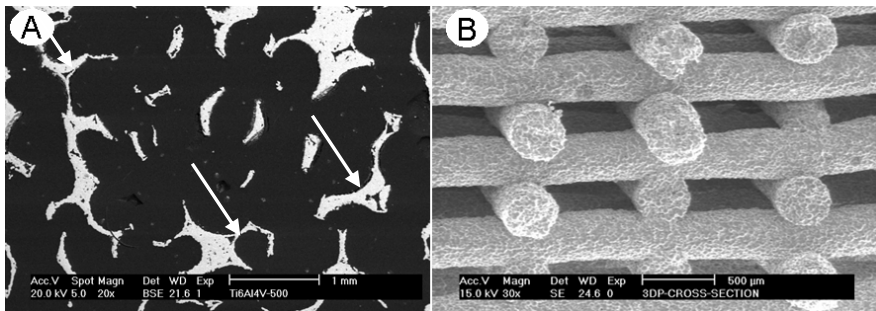


Fig.3 Cross-section of FT (A) and 3DFT (B). Due to production process, holes are present in the struts of FT (arrows)

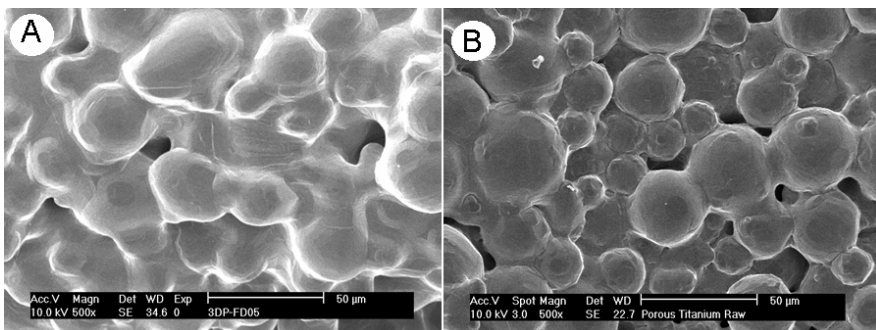


Fig.4 Microstructure of FT (A) and 3DFT (B)

3.2. Mechanical properties

It is well known that both stiffness and strength of a porous material strongly depends on its apparent density. Theoretical predictions of the effective mechanical properties of a porous material, based on mechanical properties of equally dense materials and apparent density were given by Gibson and Ashby for open- and closed pore forms [5].

Fig.5A shows the measurements of Young's modulus and compressive strength as a function of relative density for FT, 3DFT and cancellous bone as well as the predicted theoretical values ($E/E_s = C (\rho/\rho_s)^2$ assuming $C=1$, $E_s=5000$ MPa, $\rho_s=2.0$ g/cm³) [13]. The measured Young's modulus values of both porous Ti6Al4V types were lower than the analytical predictions by Gibson and Ashby for open porous structures, but higher than the values measured for cancellous bone. Only high porosity titanium alloy structures showed Young's modulus close to the theoretical predictions. An explanation for the fact that measured Young's moduli were generally lower than theoretically predicted values might be found material's microstructure. Imperfections like curved cell walls, triangle holes, and inhomogeneities like nodal inclusions or large voids in the fiber generally reduce the stiffness, while theoretical considerations of Gibson and Ashby are based on regular microstructures.

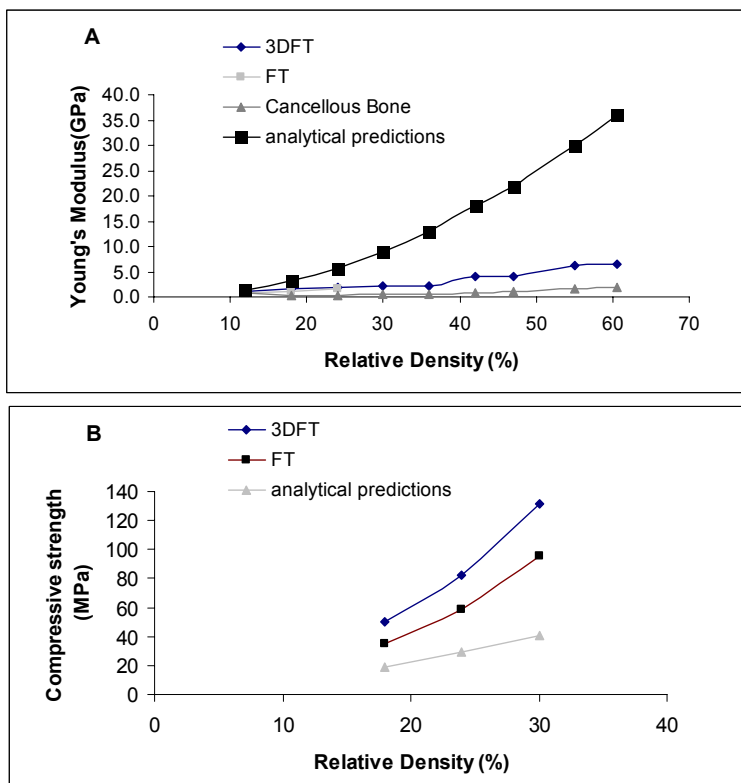


Fig.5 Young's modulus (A) and compressive strength (B) of FT, 3DFT, cancellous bone and theoretically predicted values

Besides the Young's modulus, the strength is an important property of orthopaedic implants, in particular in load bearing applications. Compressive strength of FT and 3DFT and predicted theoretical values for open porous material

are given in Fig.5B. It can be seen that the measured values for both FT and 3DFT were higher than the analytical predictions by Gibson and Ashby and compressive strength of cancellous bone (10-50MPa). The compressive strength values of 3DFT were higher than those of FT, probably due to a more uniform structure and constant fiber diameter of 3DFT.

3.3. Permeability

The permeability of FT and 3DFT scaffolds compared with cancellous bone is shown in Fig.6. While permeability of FT was comparable to that of human cancellous bone [6], 3DFT had a much higher permeability due to its 0/90 fiber lay-down pattern. Based on permeability values, it is expected that high metabolic exchange rate of bone cells as well as minerals can be achieved in both FT and 3DFT due to their interconnected porous structure and a high surface to volume ratio.

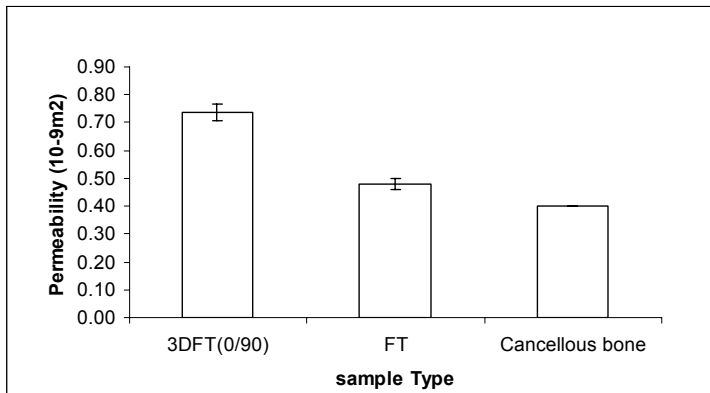


Fig.6 Permeability of 3DFT and FT compared with cancellous bone

3.4. In vivo

In all implants bone ingrowth started from the host bone bed towards the center of the implant. Fluorescent microscopy of the sequential fluorochrome labels revealed the dynamics of bone formation in different implants (Fig.7). In most implants, all three labels were present, suggesting start of bone formation before the third week of implantation. In some implants, however, the 3-week label could not be detected, indicating a delayed start of new bone formation. This delay was not directly related to certain implant type, but rather to individual animals.

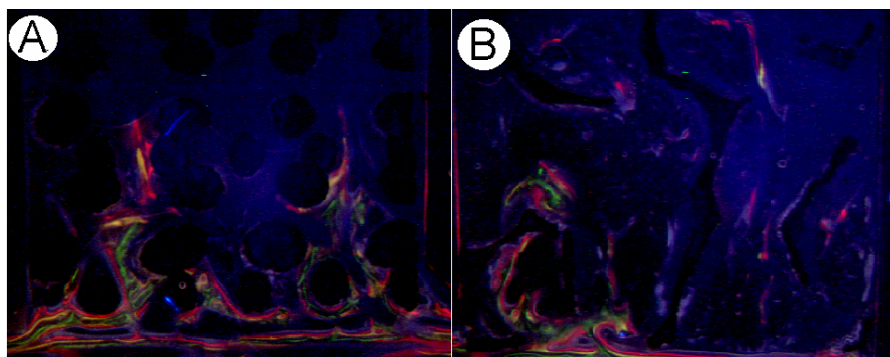


Fig. 7 Epifluorescent microscopy images of fluorochrome markers in 3DFT (A) and FT (B). In all images the earliest label is green (3 weeks, calcein green), the middle label is yellow (6 weeks, oxytetracycline) and the final label is orange (9 weeks, xylenol orange). The dark areas indicate scaffold.

Fig. 8 is an example of histological sections showing bone ingrowth from transverse process into the pores of the implants on orthotopic implantation site. Bone is stained pink/red and Ti alloy black. The transverse process can be seen at the bottom of the implants and Teflon plates are visible between the implants. It can be seen that FT implant has a big pore and very open compared to 3DFT with small pore in this model.

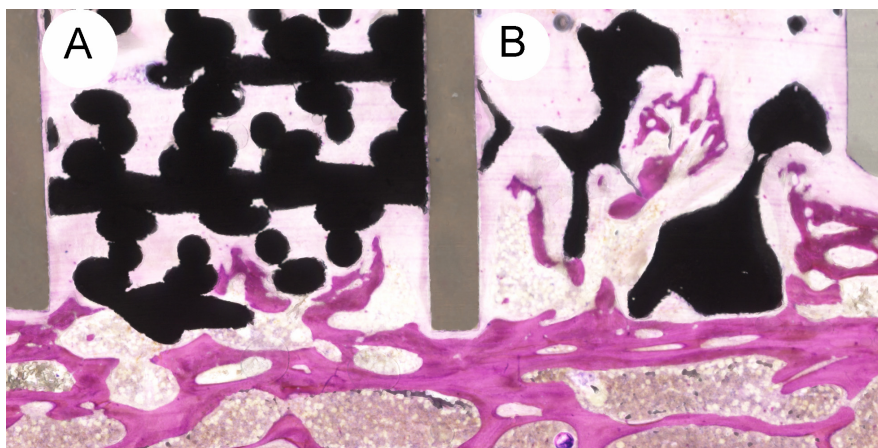


Fig. 8 Digital photographs of stained (methylene blue/basic fuchsin) histological sections of 3DFT (A) and FT (B)

Histomorphometrical analysis revealed that in all implants a relatively low amount of bone was formed (about 2-3% of the total area of 3DFT and about 5-7% of total area of FT was filled with new bone). Fig. 9 represents histomorphometrical data of

bone area in the total region of interest after 12 weeks of implantation. Significantly more bone was formed in FT than in 3DFT implants.

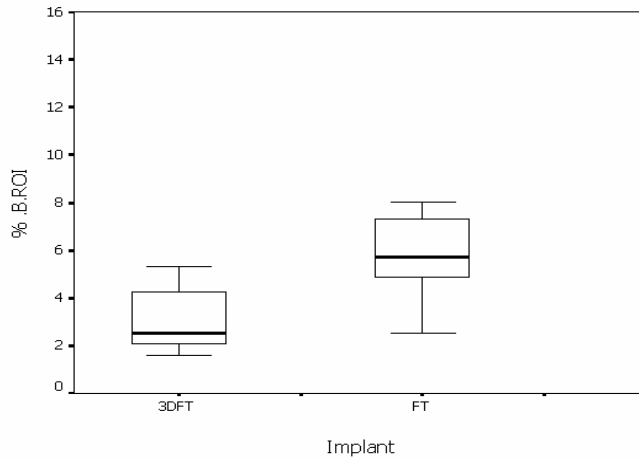


Fig.9 Histomorphometrical results: boxplots (mean and interquartile values) of bone formation in the total implant area.

Similar to the measured bone area, the value of the depth of bone ingrowth after 12 weeks of implantation was significantly higher ($p=0.001$) for FT than for 3DFT implants (Fig. 10).

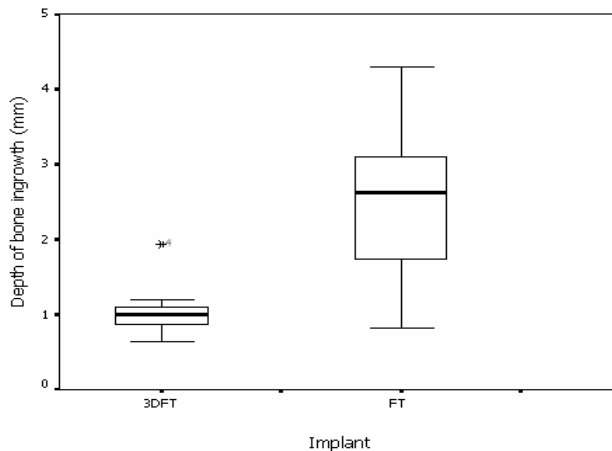


Fig. 10 Box plots of bone ingrowth depth at 12 weeks of implantation, measured on stained histological sections. (“ж” indicates an extreme outlier)

Main differences between FT and 3DFT that may explain differences in the amount of newly formed bone after implantation on transverse processes are

porosity and pore shape. The porosity of FT was 20-30% higher than that of 3DFT. In addition, porous structure of the FT was more complex than that of 3DFT, resulting in a slightly lower permeability. The high porosity and larger surface area may result in promoting precipitation of calcium-phosphate layer onto the surface from body fluids and possible integration of inducing factors in the implant surface [14], which in turn may have a positive effect on attachment, proliferation and differentiation of osteogenic cells. This has been discussed in a previous study on titanium mesh and porous ceramics [15]. FT possessed a higher specific surface area, which may be beneficial for cell seeding, cell attachment, nutrient supply and tissue formation [14-18].

4. Conclusion

In this study, we successfully developed two types of porous Ti6Al4V scaffolds. FT scaffolds, produced by sponge replication method had an open macroporous structure similar to that of cancellous bone. 3D Fiber deposition scaffolds had a very regular highly interconnected macroporous structure, achieved by direct deposition of Ti6Al4V slurry fibers in a predesigned lay-down pattern. Mechanical properties of the two scaffold types differed due to the differences in their macrostructure, however, both scaffold types had higher Young's modulus and compressive strength than cancellous bone. Pore size and permeability of the two porous titanium scaffold types were comparable with those of cancellous bone. The in vivo results showed that bone could grow into the porous structure of both implant types, and that more bone was found in FT than in 3DFT implants, probably due to a higher porosity and a more complex porous structure.

Reference

1. Sedel L, Nizard R, Meunier A. Orthopedic biomaterials. *Bull Acad Natl Med* 1995;179(3):497-505; discussion 505-6.
2. Pilliar RM. Modern metal processing for improved load-bearing surgical implants. *Biomaterials* 1991;12(2):95-100.
3. Frosch KH, Sturmer KM. Metallic biomaterials in skeletal repair. *European Journal of Trauma* 2006;2:149-159.
4. Pilliar RM. Porous-surfaced metallic implants for orthopedic applications. *J Biomed Mater Res* 1987;21(A1 Suppl):1-33.
5. Pilliar RM. Powder metal-made orthopedic implants with porous surface for fixation by tissue ingrowth. *Clin Orthop* 1983(176):42-51.
6. Pilliar RM. P/M Processing of Surgical Implants: Sintered Porous Surfaces for Tissue-to-Implant Fixation. *International Journal of Powder Metallurgy* 1998;34(8):33-45.

7. Li JP, Li SH, Van Blitterswijk CA, De Groot K. A novel porous Ti6Al4V: Characterization and Cell attachment. *J.Biomed Mat Res* 2005;73A:223-233.
8. Li JP, Li SH, De Groot K, Layrolle P. Improvement of Porous titanium with thicker struts. *Key Engineering Materials* 2002;240:547-550.
9. Li JP, de Wijn JR, Van Blitterswijk CA, de Groot K. Porous Ti6Al4V scaffold directly fabricating by rapid prototyping: preparation and in vitro experiment. *Biomaterials* 2006;27(8):1223-35.
10. Li JP, S.H.Li, Van Blitterswijk CA, de Groot K. Cancellous Bone from Porous Ti6Al4V by Multiple Coating Technique. *J Mat Sci:Mat in Med* 2005;16:in press.
11. Li SH, De Wijn JR, Li JP, Layrolle P. Biphasic calcium phosphate scaffold with high permeability/porosity ratio. *Tissue Engineering* 2003;9(3):535-548.
12. Wilson CE, Kruyt MC, de Bruijn JD, van Blitterswijk CA, Oner FC, Verbout AJ, Dhert WJ. A new in vivo screening model for posterior spinal bone formation: comparison of ten calcium phosphate ceramic material treatments. *Biomaterials* 2006;27(3):302-14.
13. Gibson LJ, Ashby MF. *Cellular solids: structure and properties*. Cambridge: Cambridge University Press; 1997.
14. Yuan H, Kurashina K, de Bruijn JD, Li Y, de Groot K, Zhang X. A preliminary study on osteoinduction of two kinds of calcium phosphate ceramics. *Biomaterials* 1999;20(19):1799-806.
15. Habibovic P, Yuan H, van der Valk CM, Meijer G, van Blitterswijk CA, de Groot K. 3D microenvironment as essential element for osteoinduction by biomaterials. *Biomaterials* 2005;26(17):3565-75.
16. Hing KA, Annaz B, Saeed S, Revell PA, Buckland T. Microporosity enhances bioactivity of synthetic bone graft substitutes. *J Mater Sci Mater Med* 2005;16(5):467-75.
17. Chu TM, Orton DG, Hollister SJ, Feinberg SE, Halloran JW. Mechanical and in vivo performance of hydroxyapatite implants with controlled architectures. *Biomaterials* 2002;23(5):1283-93.
18. Chang BS, Lee CK, Hong KS, Youn HJ, Ryu HS, Chung SS, Park KW. Osteoconduction at porous hydroxyapatite with various pore configurations. *Biomaterials* 2000;21(12):1291-8.

Chapter 9

Bone ingrowth in porous titanium alloys implants produced by 3D fiber deposition

J.P. Li^{1,2}, P. Habibovic¹, M. van den Doel³, C. E. Wilson², J.R. de Wijn¹, C.A. van Blitterswijk¹, K. de Groot^{1,4}

¹Institute for Biomedical Technology, University of Twente, The Netherlands.

²Porogen. B.V, The Netherlands.

³CellTec. B.V, The Netherlands.

⁴CAM Implants. B.V, The Netherlands.

Abstract

3D fiber deposition is a technique that allows the development of metallic scaffolds with accurately controlled pore size, porosity and interconnecting pore size, which in turn permits a more precise investigation of the effect of structural properties on the in vivo behavior of biomaterials.

This study analyzed the in vivo performance of titanium alloy scaffolds fabricated using 3D fiber deposition. The titanium alloy scaffolds with different structural properties, such as pore size, porosity and interconnecting pore size were implanted on the decorticated transverse processes of the posterior lumbar spine of 10 goats. Prior to implantation, implant structure and permeability were characterized. To monitor the bone formation over time, fluorochrome markers were administered at 3, 6 and 9 weeks and the animals were sacrificed at 12 weeks after implantation. Bone formation in the scaffolds was investigated by histology and histomorphometry of non-decalcified sections using traditional light- and epifluorescent microscopy. In vivo results showed that increase of porosity and pore size, and thus increase of permeability of titanium alloy implants positively influenced their osteoconductive properties.

Keywords: osteoconduction, porous Ti6Al4V, scaffold, 3D fiber deposition.

1. Introduction

At present, most widely used clinical therapies for bone replacement and regeneration employ autologous- and allogeneic bone grafts. It is well known that autologous bone graft is considered to be the golden standard in spinal fusions, i.e. for achieving a bony bridge between transverse processes. However, treatments with both autografts and allografts exhibit a number of limitations. The harvest of the autologous graft requires an additional invasive surgical procedure that may lead to donor site morbidity, chronic post-operative pain, hypersensitivity and infection [1-5]. Another important drawback of the use of autograft is the limited availability. Unlike autologous bone, allogeneic grafts are widely available and do not require an additional surgery on the patient. However, allogeneic bone has to undergo processing techniques such as lyophilization, irradiation or freeze-drying to remove immunogenic proteins in order to avoid any risk of immunogenic reaction[6]. In turn, these processing techniques have a negative effect on osteoinductive and osteoconductive potential of the allograft [7], which consequently decreases its biological performance as compared to autografts [8].

Therefore, the use of synthetic biomaterials for orthopaedic reconstructive surgery as a means of replacing autografts and allografts is of increasing interest and the large number of scientific reports confirms this trend. Calcium-phosphate based biomaterials, such as ceramics and cements and polymeric biomaterials are attractive as they can be produced in such a way that they mimic the mineral composition and/or the porous structure of bone. However, although ceramics show excellent corrosion resistance and good bioactive properties, porous ceramic structures, as they are available today, are limited to non load-bearing applications, due to their intrinsic brittleness. Likewise, porous polymeric systems are deemed to be ductile with insufficient rigidity and inability to sustain the mechanical forces present in bone replacement surgery.

Metals have so far shown the greatest potential to be the basis of implants for long-term load-bearing orthopedic applications, owing to their excellent mechanical strength and resilience when compared to alternative biomaterials, such as polymers and ceramics. Particularly, titanium and its alloys have been widely used in orthopaedic and dental devices because of their excellent mechanical properties and biocompatibility [9].

Several factors have shown their influence on bone ingrowth into porous implants, such as porous structure (pore size, pore shape, porosity and interconnecting pore size) of the implant, duration of implantation, biocompatibility, implant stiffness, micromotion between the implant and adjacent bone etc [10-22]. The architecture of a porous implant has been suggested to have a great effect on implant integration by newly grown bone [23,24]. However, up to now, porous structures of

most metallic implants are not very well controlled due to their production techniques, involving porogens and replication methods. These techniques mostly result in porous structures with a certain pore size range, rather than structures with an accurately defined pore size.

Recently, rapid prototyping, such as fused deposition modeling and 3D printing, has been employed to fabricate 3D scaffolds with accurately designed structure [25,26], which allowed investigation of architectural influences on tissue regeneration. However, these studies focused on porous scaffolds made of ceramics and polymers [12,27,28], while very little is known about porous titanium scaffolds with precisely controlled pore structure.

Because there is hardly consensus regarding the optimal pore size for effective bone ingrowth, researchers have created scaffolds with pore sizes between 150-300 μm and 500-710 μm to promote bone formation [29]. A minimum pore size of 100-150 μm is generally considered acceptable for bone ingrowth [20,30-33].

3D porous Ti6Al4V scaffolds were successfully fabricated in our group by a rapid prototyping technology, named 3D fiber deposition (3DF) [34]. 3D fiber deposition, being a layer-by-layer manufacturing technique, can be used to manufacture prototypes in which each layer may have a different fiber diameter, thickness, fiber space and fiber orientation. This technique therefore provides a possibility to develop scaffolds with well-controlled pore size, porosity and interconnecting pore size. The advantage of scaffolds produced by 3DF is that they permit parametric analyses to be conducted, which is essential in investigations of how scaffolds perform as a function of their physical characteristics.

In the present study, implants with different pore size, porosity and interconnecting pore size were fabricated by 3DF technique. Influence of the structural characteristics on the bone ingrowth was screened by using the well-established multi-channel cage model [35-38], that was adapted to use on the transverse process of the goat lumbar spine.

2. Materials and methods

2.1. Implants

5 different porous Ti6Al4V scaffolds made by 3D fiber deposition were used in this study. Porous Ti6Al4V scaffolds made by 3D fiber deposition were used in this study. The preparation procedure of these scaffolds was described earlier [2]. In short, Ti6Al4V slurry (80 wt% of powder Ti6Al4V with a mean particle diameter of 45 μm (AP&C Inc. Canada) in 0.5wt% aqueous water methylcellulose solution) is forced through the syringe nozzle by using a 3D-bioplotter machine (Envisiontec GmbH, Germany). The slurry is plotted on a stage as a fiber, which rapidly

solidifies by drying, and the scaffold is fabricated by layering a pattern of fibers. After deposition, the obtained Ti6Al4V scaffolds were dried for 24hrs at RT, and sintered under high vacuum at 1200^oC for 2hrs. By varying spacing and fiber lay-down pattern, 5 different Ti alloy scaffolds (low porosity (3DFL), middle porosity (3DF), high porosity (3DFH), double-layered (3DFDL) and gradient porosity (3DFG)) were produced as is specified in Table 1.

Table 1 3D fiber deposition conditions for different implants

Implant	Fiber space (μm)	Lay down angle	Layer thickness (μm)
3DFL	200	0/45	320
3DF	500	0/45	320
3DFH	800	0/45	320
3DFDL	500	0/0/45/45	320
3DFG	800-200(bottom to top)	0/90	320

2.2. Cage

A cage design and its fabrication were described previously [38]. In brief, polyacetal cages were designed for fixation to the transverse process of the goat lumbar spine. Each cage consisted of two side walls, two end pieces, four stainless steel machine screws for cage assembly and two self-tapping bone screws to attach the cage to the transverse process. Three scaffolds (4x7x8 mm) were plugged into a cage and separated by thin Teflon plates (0.5x7x8 mm). These scaffolds were open to both the underlying bone and the overlying soft tissues, had cross sections of 4x7.0 mm² and were 8.0 mm in length (Fig.1). The scaffolds, polyacetal components of the cages and the metal screws were sterilized by autoclaving.

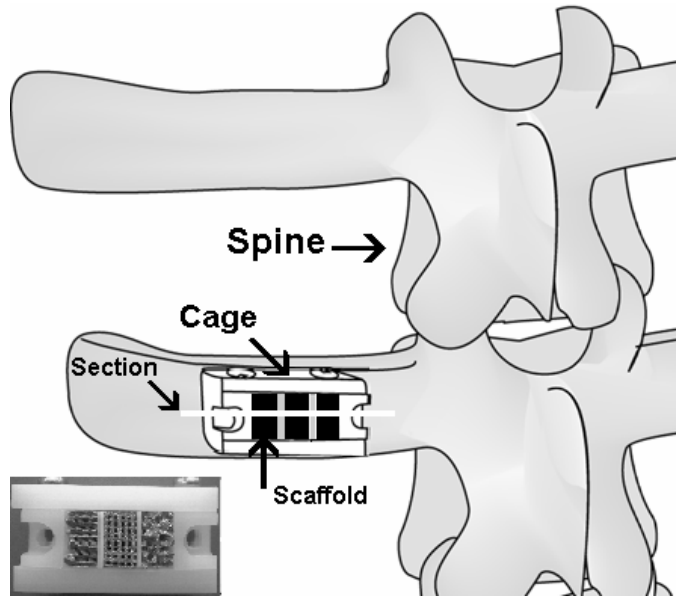


Fig.1 Schematic drawing of the implantation on the goat's transverse process. The lower left is a cage with three implants.

2.3. Implant characterization

Cubical implants (4x7x8 mm) were machined by using a wire electric discharge machine, with demineralized water as medium. The structure of different implants was characterized by using an environmental scanning electron microscope (ESEM; XL30, ESEM-FEG, Philips, The Netherlands) in the secondary electron mode. The porosity of the material was determined by volume/weight method (n=10) and the following calculation: $100\% - [(weight\ of\ the\ porous\ implant / the\ weight\ of\ a\ dense\ implant\ with\ the\ same\ size) * 100\%]$. A permeability test was performed with a self-designed permeability-meter [39]. Briefly, a cylindrical sample was mounted in a tube connected to a wide diameter water reservoir which was positioned at a certain constant height. The flow of water through the sample was measured in ml/sec. Normalized for the dimensions of the sample, it provided measure of the sample's permeability. Two samples for each condition were tested

2.4. Animal study

2.4.1. Experimental design

Total of 10 adult Dutch milk goats were used following the approval of the institutional animal care committee. Four spinal cages containing a total of twelve different Ti implants (three per cage), were implanted bilaterally on the transverse processes of the L4 and L5 vertebrae of each goat according to a randomized complete block design. To monitor the bone formation over time, fluorochrome markers were administered at 3, 6 and 9 weeks and the animals were sacrificed at 12 weeks after implantation. Bone formation into the porous titanium scaffolds was investigated by histology and histomorphometry of non-decalcified sections using epifluorescent and light microscopy. In this paper, scaffolds with different pore size, porosity and interconnecting pore size were studied. Other Ti scaffolds implanted in these animals will be discussed and published separately.

2.4.2. Implantation procedure

The goats, which were 2–4 years of age with a body weight ranging from 64–75 kg, were housed at the Central Animal Laboratory Institute (GDL), Utrecht, The Netherlands, at least 4 weeks prior to surgery.

Before the surgical procedure, a dose of 0.1mL in 5mL of physiologic saline solution (\pm 1mL/25kg body weight) of Domosedan (Pfizer Animal Health BV, Capelle a/d IJssel, The Netherlands) was administered by intravenous injection. The surgical procedure itself was performed under general inhalation anesthesia of the animals. Thiopental (Nesdonal, \pm 400mg/70kg of body weight, on indication, Rhone Merieux, Amstelveen, The Netherlands) was injected intravenously, and anesthesia was maintained with a gas mixture of nitrous oxide, oxygen and Halothane (ICI-Farma, Rotterdam, The Netherlands).

Prior to the surgical procedure, four spinal cages for each animal were aseptically assembled with the twelve titanium scaffolds conditions arranged according to a randomized complete block design. These cages were implanted bilaterally on the transverse processes of the L4 and L5 vertebrae of each goat according to a randomized complete block design. In addition to the 5 conditions that are discussed in this paper, another seven Ti alloy conditions were evaluated which findings will be presented separately. The orthotopic scaffolds were open to both the underlying bone and the overlying soft tissues.

The surgical procedure was described previously [38]. After shaving and disinfecting the thoracolumbar region, a central skin incision, from approximately T8 to L1, was made to expose the muscle fascia. This incision supported

implantation of both spinal implants and intramuscular implants which are not discussed in the present manuscript. Bilateral muscle incisions were then made and retracted to expose both transverse processes of the L4 and L5 vertebrae. The processes were decorticated using an angled bone drill by dental driller. Care was taken to ensure an even decortication of a flat surface with an area sufficient for placement of a cage. One cage was placed on each transverse process and pilot holes were drilled under saline irrigation. Two stainless steel self-tapping screws were then inserted to firmly attach each cage. Light finger pressure was applied to the top of each cage just prior to muscle closure to ensure the scaffolds were in contact with the underlying bone (Fig.2). The muscle fascia was closed with non-resorbable sutures and the skin was closed in two layers with resorbable sutures. Durogesic 25 (fentanyl transdermal CII patches; Janssen-Cilag EMEA, Beerse, Belgium) was administered for postoperative pain relief.

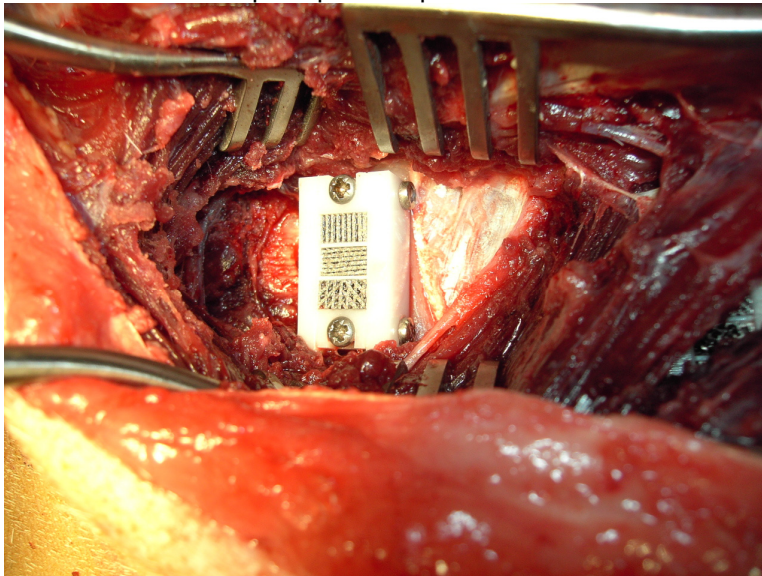


Fig.2 Conduction cage placed on a transverse process of a goat lumbar spine.

2.5. Fluorochrome labeling

Sequential fluorochrome markers were administered at 3, 6 and 9 weeks after implantation. Calcein Green (10 mg/kg intravenously, Sigma, The Netherlands) was administered at 3 weeks, Oxytetracyclin (Engemycin 32 mg/kg intramuscularly, Mycofarm, The Netherlands) at 6 weeks and Xylenol Orange (80 mg/kg intravenously, Sigma, The Netherlands) at 9 weeks after implantation. At 12 weeks, the animals were sacrificed by an overdose of pentobarbital (Euthasaat, Organon, The Netherlands) and the implants retrieved.

2.6. Histological processing and histomorphometry

The explanted samples were fixated in a solution of 5% glutaraldehyde and 4% paraformaldehyde at 4°C. They were then dehydrated by ethanol series (70%-100%) and transferred into a methylmethacrylate (MMA) solution that polymerized at 37°C within one week. Three centrally located longitudinal 10-15 µm thick sections were cut from each sample using a sawing microtome (Leica, Germany). The second section remained unstained for epifluorescence microscopy and the other two sections were stained with 1% methylene blue and 0.3% basic fuchsin after etching with HCl/ethanol mixture for histology. High-resolution digital scans of the stained sections were made for histomorphometry using a photographic film scanner (Dimage Scan Elite 5400, Minolta, Japan). The general tissue response, bone formation and fluorochrome markers were evaluated using a light/fluorescence microscope (E600, Nikon, Japan) equipped with a quadruple filter block (XF57, dichroic mirror 400, 485, 558 and 640 nm, Omega Optics, The Netherlands). Prior to histomorphometry analysis, using Adobe Photoshop 6.0, bone and material were pseudocoloured, red and green respectively. Image analysis was performed using a PC-based system with the KS400 software (version 3, Zeiss, Germany). Before measurements the system was geometrically calibrated with an image of a block of known dimensions. A custom macro program was developed to measure the bone area and contact between new bone and implant surface. These parameters were measured in both total implant area, and 25% of the implant area closest to host bone bed. Following parameters were investigated:

1. %b. ROI: the percentage of bone area in total implant area $[(\text{bone area} / \text{total implant area}) \times 100\%]$;
2. %b. pore total: the percentage of bone area in total available pore space $[(\text{bone area} / (\text{total implant area} - \text{total scaffold area})) \times 100\%]$;
3. %b. pore low: the percentage of bone area in available pore space in the 25% of the scaffold closest to host bone bed;
4. %b.cont. total: percentage of length of contact between bone and available scaffold surface in the total implant area: $[(\text{bone contact scaffold length} / \text{scaffold outline length}) \times 100\%]$;

In addition, bone ingrowth depth was effectively measured at 3, 6 and 9 weeks by measuring the maximum height of each fluorochrome marker and at 12 weeks by measuring the maximum bone height on the stained sections.

2.7. Statistics

Statistical calculations were done with the SPSS (Chicago, IL) 11.5 software. Statistical analyses were performed on histomorphometrical results of bone area, bone contact and bone ingrowth depth by ANOVA for randomized complete block design with a post hoc Tukey's HSD ($p=0.05$) to determine differences between scaffold conditions.

3. Results

3.1. Implant characterization

The pore size and porous structure were analyzed by ESEM and porosity was calculated by the volume / weight method. The porous structures of different Ti alloy samples are shown in Fig. 3. It can be seen that the pores of the implants are completely interconnected. Table 2 gives a summary of pore sizes and porosities. The first three implant types, 3DFL, 3DF and 3DFH were produced by a similar lay down pattern of the fibers (0/45) but with increasing spacing between fibers, which resulted in an identical structure but increasing pore size and porosity. The porosity of 3DFDL was similar to that of 3DF, however, because of double layering of the fibers, the distance between the layers of 3DFDL was larger as compared to 3DF resulting in a larger interconnecting pore size. 3DFG also had a similar porosity to that of 3DF and 3DFDL. The pore sizes of five implant types varied. Fig. 4 shows the results of the permeability test. All implants were found to be highly permeable. It can be seen that permeability increases with increasing pore size and interconnecting pore size.

Table 2 Implant pore size, interconnecting pore size and porosity

implant	Pore size Z(μm)	under Interconnecting pore size (μm)	porosity
3DFL	160 \pm 11	~160x280	39 \pm 1.3
3DF	396 \pm 16	~400x280	55 \pm 1.1
3DFH	680 \pm 36	~680x280	68 \pm 2.5
3DFDL	400 \pm 22	~400x400	56 \pm 1.7
3DFG	160-660	~160x280-680x280	53 \pm 3.5

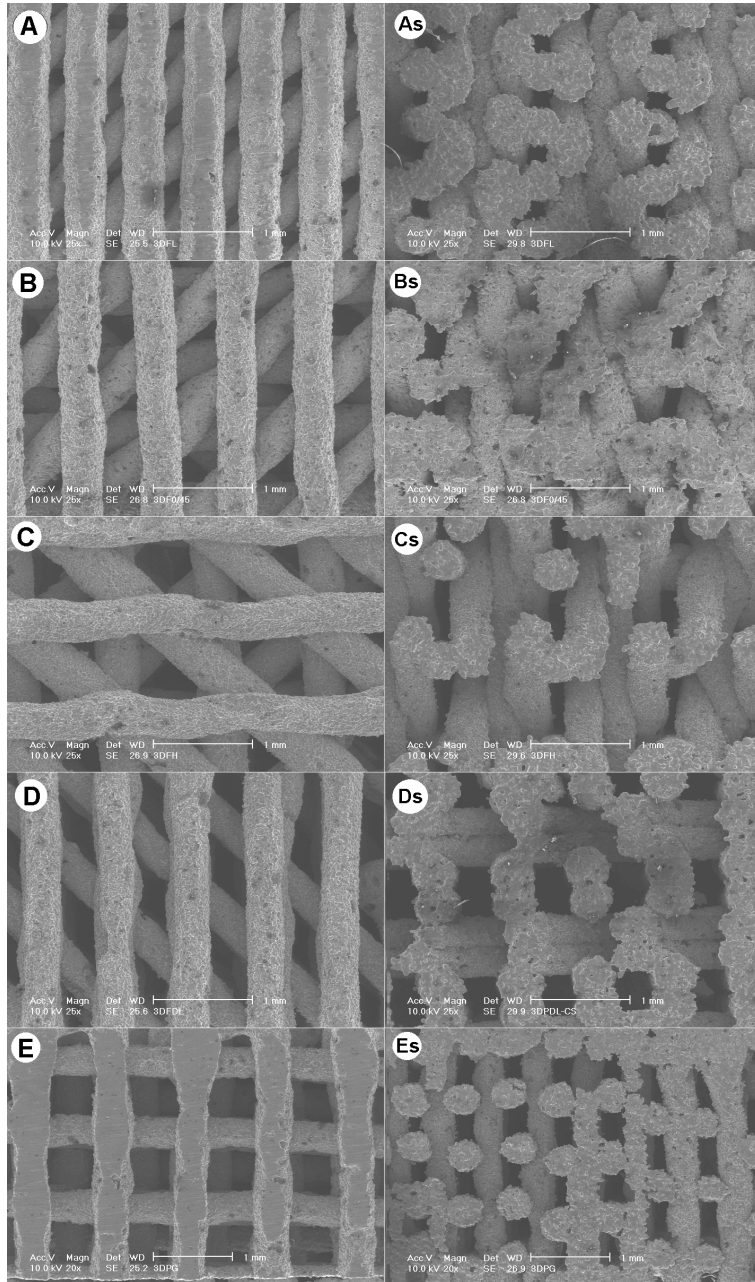


Fig.3 ESEM photographs of Ti alloy scaffolds (magnification 25x): 3DFL top view (A) and side view (As), 3DF top view (B) and side view (Bs), 3DFH top view (C) and side view (Cs), 3DFDL top view (D) and side view (Ds) and 3DFG top view (E) and side view (Es). Refer to Table 1 for preparation conditions.

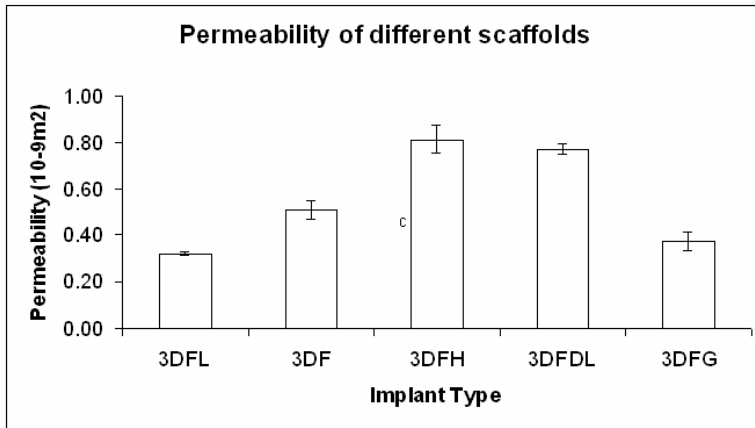


Fig.4 Permeability results of different scaffolds.

3.2. In vivo results

One goat had to be euthanized before the end of the study due to complications not directly related to the performed surgery and was replaced by another goat. In total 10 goats were included in the study. There were no surgical complications and all cages were firmly attached to the underlying transverse process at retrieval. No macroscopic or microscopic signs of infection were found. In total, 50 titanium implants were examined.

In all implants bone ingrowth started from the host bone bed towards the implant. New bone did not completely fill any of the scaffolds, so the final amount of bone in the scaffolds could be used for measuring the effect of various conditions to new bone formation.

Fluorescent microscopy of the sequential fluorochrome labels revealed the dynamics of bone formation in different implants (Fig.5). In most implants, all three labels were present, suggesting start of bone formation before the third week of implantation. In some implants, however, the 3-weeks label could not be detected, most likely indicating a delayed start of new bone formation. This delay was not directly related to a certain implant type, but more to individual animals.

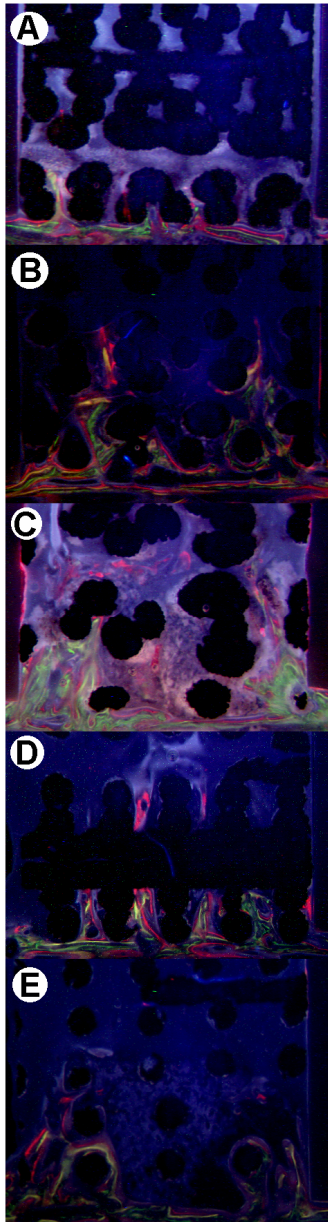


Fig. 5. Epifluorescent microscopy images of fluorochrome markers in 3DFL (A), 3DF (B), 3DFH (C), 3DFDL (D) and 3DFG (E). In all images the earliest label is green (3 weeks, calcein green), the middle label is yellow (6 weeks, oxytetracyclin) and the final label is orange (9 weeks, xylenol orange). The dark blue areas indicate scaffold.

Histological observations of stained sections revealed bone formation in all different scaffolds. The newly formed bone was in close contact with the Ti alloy

surface (Fig.6). The results showed that in all implants a relatively low amount of bone was formed (about 2-4.5% of the total area of implants and about 5-10% of total available pore space was filled with new bone).

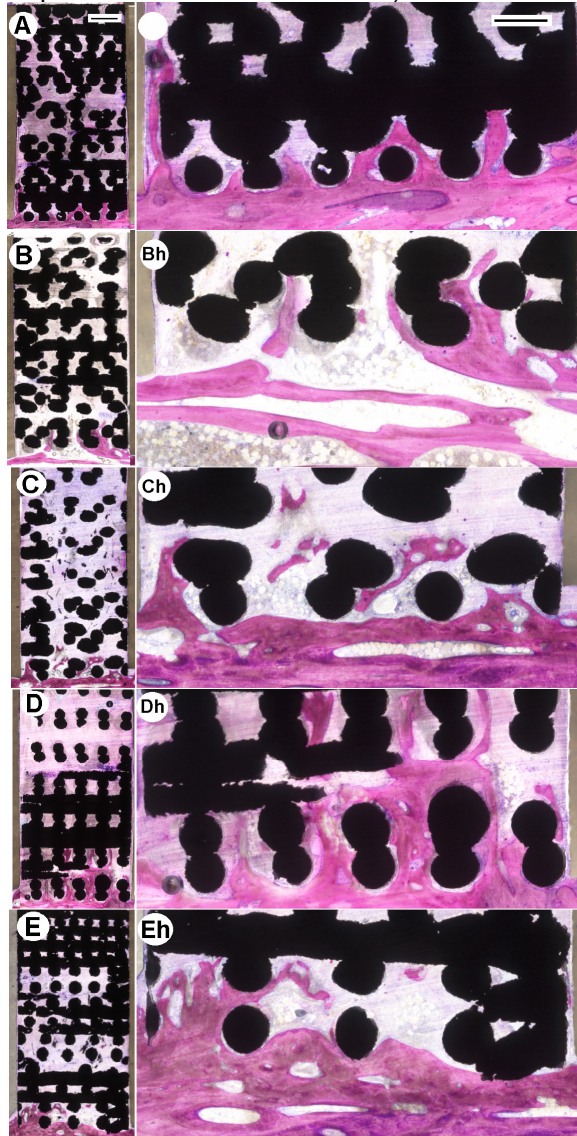


Fig. 6. Digital photographs of stained (methylene blue/basic fuchsin) histological sections. Bone is stained pink/red and Ti alloy black. The transverse process can be seen at the bottom of the implants and Teflon plates are visible between the implants. Implant in the image is A= 3DFL, B=3DF, C=3DFH, D=3DFDL, E=3DFG. Bar=1mm. The high magnification of interface between bone and implant is shown in Ah to Eh (correspond to 3DFL, 3DF, 3DFH, 3DFDL and 3DFG, respectively).

Fig. 7 represents histomorphometrical data of the bone area in the total region of interest after 12 weeks of implantation. As can be observed, the general trend is that the amount of bone increased with both increasing porosity and increasing pore size. 3DFL showed less bone than 3DF, while 3DFH had more bone as compared to 3DF. 3DFDL showed a similar amount of bone as 3DFH, while the amount of bone in 3DFG was between that of 3DFL and 3DF. Due to relatively high variations in the amount of formed bone between individual animals, and with the relatively low number of animals, significant differences were only observed between 3DFL and 3DFH ($p < 0.01$) and between 3DFL and 3DFDL ($p < 0.01$).

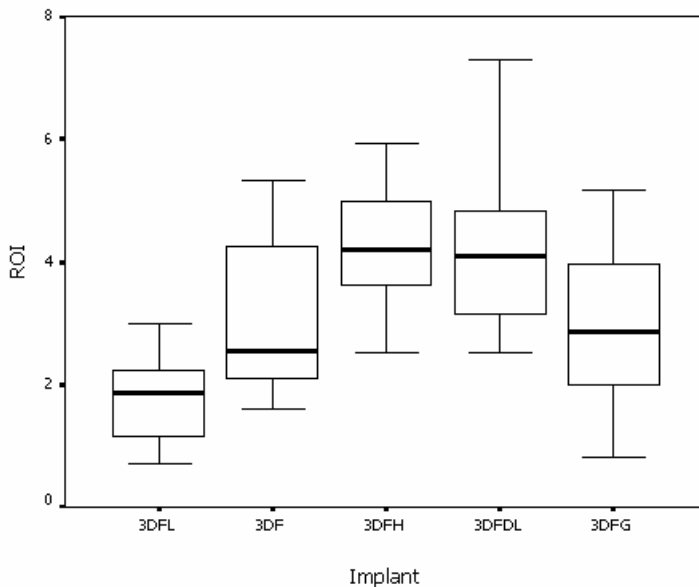


Fig.7 Histomorphometrical results: boxplots (mean and interquartile values) of bone area in the total implant area (region of interest).

Concerning the bone formation in the available pore space inside the implants (Fig.8a), a similar trend was observed to the one in the total region of interest. Significant differences were found between 3DFL and 3DFDL ($p < 0.01$) and between 3DFG and 3DFDL ($p = 0.035$).

Analysis of the area of new bone in the available pore space in the quarter of the implant closest to the host bone bed showed no significant differences between the five material types (Fig. 8b), indicating differences in the bone ingrowth depth inside the implants.

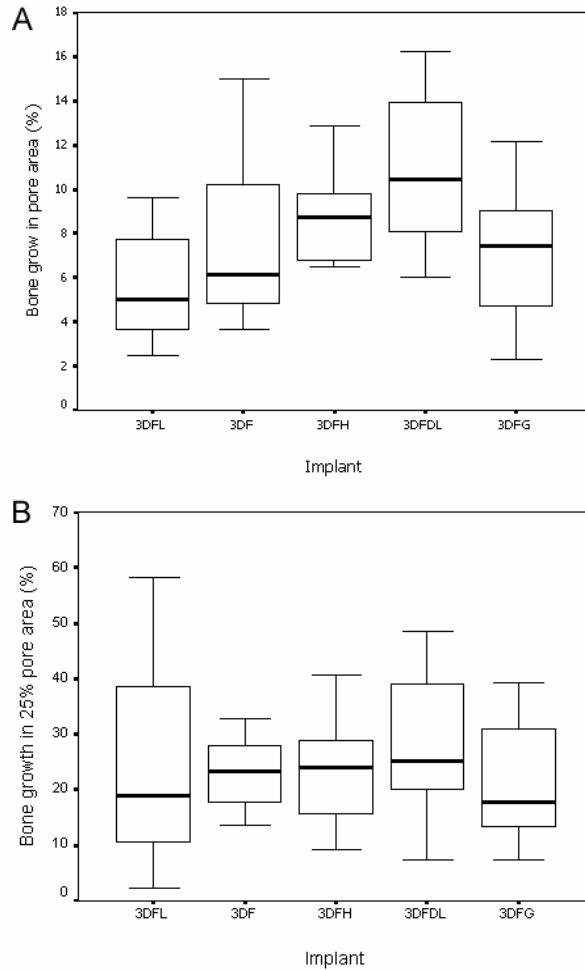


Fig.8 Histomorphometrical results: boxplots (mean and interquartile values) of bone formation in available pore space (A) and in 25% of the implant closest to host bone bed (B).

Boxplots with data of the depth of bone ingrowth after 3, 6, 9 and 12 weeks of implantation, based either on fluorochrome labels (for 3, 6 and 9 weeks) or histological analysis (12 weeks) are shown in figure 9. Bone growth in all implants progressively increased in the first 9 weeks, after which no significant increase was observed, indicating the start of a bone remodeling process. As expected, increasing porosity and pore size resulted in an increase of the depth of bone ingrowth. At 3, 6 and 9 weeks, 3DFDL showed the highest and 3DFL the lowest bone ingrowth. Significant difference was found at 9 weeks between the 3DFL and 3DFDL ($p=0.001$). At 12 weeks, 3DFDL showed a lower value for bone depth than 3DFH, which might suggest a different phase of bone remodeling. Both 3DFH and

3DFDL showed significantly deeper bone ingrowth as compared to 3DFL ($p=0.013$ and 0.031 , respectively) at 12 weeks of implantation.

Measurements of contact between bone and implant surface showed similar results to the bone area measurements (data not shown).

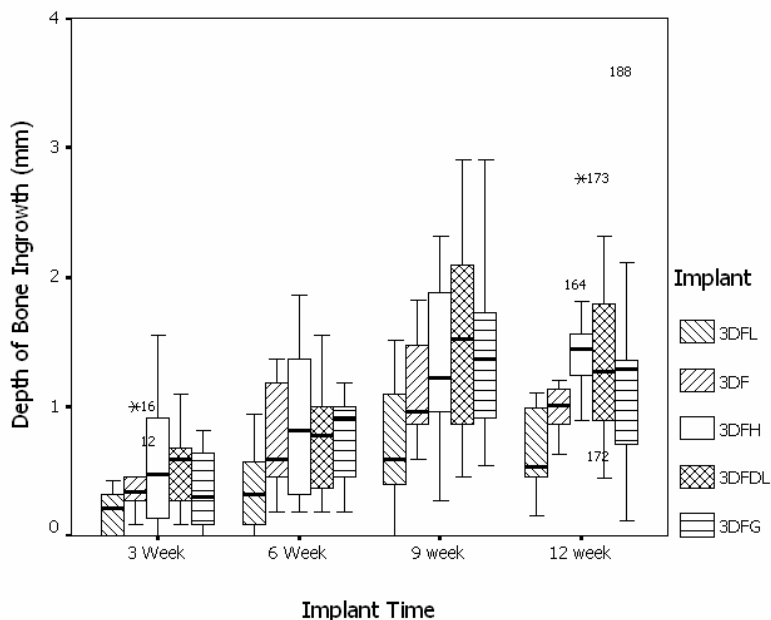


Fig. 9 Box plots of bone height at 3, 6 and 9 weeks, measured on fluorescent microscope images, and at 12 weeks, measured on stained histological sections. The symbol “O” indicates outlier and the symbol “x” indicates an extreme outlier.

4. Discussion

Characterization of the porous structure of the materials indicated that 3D fiber deposition allows fabrication of scaffolds with well-controlled porous structure. Fiber spacing between fibers, layer thickness between two layers as well as the angle of fiber deposition is parameters that can be used to control porosity, pore size and spatial arrangement. This control over architecture permits testing of the influences of specific geometrical parameters on biological performance of biomaterials, such as their osteoconductive properties.

New bone growth into porous metal implant depends on several factors, including pore size and porosity of the implant, interconnecting pore size, stability and degree of micromotion between the implant and bone, and presence of gaps between the implant and the bone surface [16,20,40]. In the present study, in order

to minimize gapping and micromotion of the implant, care was taken to ensure an even decortication of the surface of transverse processes. Tight press was applied to the top of each cage to ensure that bottom of each implant was in contact with the underlying bone while two stainless steel self-tapping screws were then inserted to firmly attach each cage onto bone.

There are a vast number of studies in which the influence of porosity and pore size on the biological behaviour of bone graft substitutes has been investigated; however, no consensus has been reached yet with regard to the optimum pore size. Recently, Holister et al [29] examined pore size and geometry using HA scaffolds with well controlled architecture. Their results demonstrated that overall bone ingrowth was not dependent on the pore sizes between 400 and 1200 μm . Also the shape of the pores, often defined by pore aspect ratio did not influence the bone growth. In contrast, many other studies [32-34, 43, 44] suggested that changes in pore size and shape can radically affect the success of bone development. The optimal pore size for bone ingrowth has been reported to be in the range of 150–600 μm . It should however be noted that this optimal pore size range was determined in studies with either porous-coated metallic implants or porous calcium-phosphate implants. Furthermore, scaffolds used in these studies did not have a well controlled architecture. In the present study, in which fully porous metallic implants with precisely controlled pore size were used, the optimal pore size (range) may be different.

The pore sizes of implants evaluated in the present study were between the lower and the upper limit of this “optimal pore range” for porous materials. Data showed that scaffold with smallest pore size and lowest porosity had significantly less bone ingrowth. And further, the implant with the largest pore size and highest porosity conducted most new bone formation. There were statistical differences in the amount of newly formed bone between 3DFL and 3DFH. However, although the trend of positive effect of increasing porosity on bone growth was observed, no significant difference between 3DF and 3DFH was found. These data suggest that, for the implants investigated in the present study, bone conduction is definitely influenced by, but not highly sensitive to changes in porosity.

Apart from the pore size and porosity of the implant, interconnecting pore size of porous implant also affects osteoconductivity. In our study, the 3DF and 3DFDL implants had similar porosities, but their interconnecting pore sizes were different. 3DFDL showed better results for all measured parameters as compared to 3DF. Due to double layers, the amount of surface available for bone ingrowth inside 3DFDL was larger as compared to 3DF. The permeability test proved that 3DFDL had a higher permeability compared to 3DF. This high permeability is apparently beneficial for cell attachment and tissue formation, presumably allowing the cells to

diffuse into the centre of the scaffold and provide space for the ingrowth of tissue and subsequent vascularisation [43,44]. These results are in agreement with many studies suggesting that good interconnecting fenestrations in porous implants are essential to provide the space for vascular tissue ingrowth followed by new bone formation [13,27,45].

It should be noted that the amount of formed bone as well as bone contact between bone and Ti alloy surface in this study were relatively low. As it is well known, Ti and its alloys are bioinert, but not bioactive materials. Therefore, in order to improve their biological performance it might be necessary to either combine them with other, more bioactive biomaterial types or to improve their bioactivity by surface modification. Coating Ti alloy surfaces with CaP ceramic and chemical and thermal treatments of the surface have been reported to be successful ways of increasing metal bioactivity [46,47].

Although increased porosity and pore size are obviously preferential for new bone growth facilitation in Ti alloy implants, it should be kept in mind that another consequence of the porosity and pore size increase is reduction of the implant mechanical properties. Thus depending on the intended application, a balance between mechanical properties and the biological performance should be found. This is again simplified by the use of 3D fiber deposition technique.

It is interesting that bone growth in all implants progressively increased in the first 9 weeks, after which this increase leveled off. This behavior is related to the bone-healing mechanism. After a bone fracture occurs, formation of a hematoma, regeneration, and maturation by modeling and remodeling are generally recognized as the three stages of bone healing. At the early stage, there is a fast ingrowth of bone into the porous implant. After that, bone modeling and remodeling are restructured in response to stress and strain (Wolff's Law) [48]. In our study, no mechanical loading was applied on the implant, resulting in the start of resorption after 9 weeks of implantation.

Although not as realistic as a load-bearing model, the screening model of transverse process of goat lumbar spine as used in the present study is very useful for the initial characterization of new porous biomaterials. Using the appropriate instruments, a flat plane on which the implant is attached to bone can be made ensuring a uniform initial fit of all implants.

In this study, we have demonstrated the capability to control scaffold architecture variables of the metallic implants by using 3D fiber deposition technique. Design and fabrication of a bone graft substitute should find a balance between mechanical function and biological performance. The versatility and possibility provided by 3D fiber deposition technique allows the fabrication of implants with different porosities, pore sizes and thus different mechanical properties. In addition,

bone structures at specific implantation sites can be mimicked in order to optimize bone tissue regeneration in the intended application.

5. Conclusion

Bone ingrowth into porous titanium alloy implants with varying pore size, porosity and interconnecting pore size, produced by 3D fiber deposition was evaluated in a goat lumbar spine model. Increase of porosity and pore size, and hence permeability of the 3D fiber deposition Ti6Al4V implants had a positive effect on the amount of new bone growth. 3D fiber deposition is a rapid prototyping technique that allows the development of porous implants with accurately controlled structural properties and therewith the investigation of the effect of structural parameters on the in vivo behaviour of biomaterials

6. Acknowledgements

Authors would like to thank Dr. Maarten Terlou from the Image Analysis Department of the University Utrecht for developing the software used for the histomorphometry and Dr. Kruyt for the kind help for spine image.

This study was financially supported in part by CAM Implants B.V., Leiden, The Netherlands.

References

1. Brown KL, Cruess RL. Bone and cartilage transplantation in orthopaedic surgery. A review. *J Bone Joint Surg Am* 1982;64(2):270-9.
2. Damien CJ, Parsons JR. Bone graft and bone graft substitutes: a review of current technology and applications. *J Appl Biomater* 1991;2(3):187-208.
3. Lane JM, Tomin E, Bostrom MP. Biosynthetic bone grafting. *Clin Orthop Relat Res* 1999(367 Suppl):S107-17.
4. Arrington ED, Smith WJ, Chambers HG, Bucknell AL, Davino NA. Complications of iliac crest bone graft harvesting. *Clin Orthop Relat Res* 1996(329):300-9.
5. Mendicino RW, Leonheart E, Shromoff P. Techniques for harvesting autogenous bone graft of the lower extremity. *J Foot Ankle Surg* 1996;35(5):428-35.
6. Brantigan JW, Cunningham BW, Warden K, McAfee PC, Steffee AD. Compression strength of donor bone for posterior lumbar interbody fusion. *Spine* 1993;18(9):1213-21.
7. Lane JM, Sandhu HS. Current approaches to experimental bone grafting. *Orthop Clin North Am* 1987;18(2):213-25.
8. Prolo DJ, Rodrigo JJ. Contemporary bone graft physiology and surgery. *Clin Orthop Relat Res* 1985(200):322-42.

9. Long M, Rack HJ. Review Titanium alloys in total joint replacement materials science perspective. *Biomaterials* 1998;19:1621-1639.
10. Nishikawa M, Myoui A, Ohgushi H, Ikeuchi M, Tamai N, Yoshikawa H. Bone tissue engineering using novel interconnected porous hydroxyapatite ceramics combined with marrow mesenchymal cells: quantitative and three-dimensional image analysis. *Cell Transplant* 2004;13(4):367-76.
11. Kujala S, Ryhanen J, Danilov A, Tuukkanen J. Effect of porosity on the osteointegration and bone ingrowth of a weight-bearing nickel-titanium bone graft substitute. *Biomaterials* 2003;24(25):4691-7.
12. Simon JL, Roy TD, Parsons JR, Rekow ED, Thompson VP, Kemnitzer J, Ricci JL. Engineered cellular response to scaffold architecture in a rabbit trephine defect. *J Biomed Mater Res A* 2003;66(2):275-82.
13. Mastrogiacomo M, Scaglione S, Martinetti R, Dolcini L, Beltrame F, Cancedda R, Quarto R. Role of scaffold internal structure on in vivo bone formation in macroporous calcium phosphate bioceramics. *Biomaterials* 2006;27(17):3230-7.
14. Konttinen YT, Zhao D, Beklen A, Ma G, Takagi M, Kivela-Rajamaki M, Ashammakhi N, Santavirta S. The microenvironment around total hip replacement prostheses. *Clin Orthop Relat Res* 2005(430):28-38.
15. Whiteside LA, White SE, Engh CA, Head W. Mechanical evaluation of cadaver retrieval specimens of cementless bone-ingrown total hip arthroplasty femoral components. *J Arthroplasty* 1993;8(2):147-55.
16. Cameron HU, Pilliar RM, MacNab I. The effect of movement on the bonding of porous metal to bone. *J Biomed Mater Res* 1973;7(4):301-11.
17. Deporter DA, Watson PA, Pilliar RM, Howley TP, Winslow J. A histological evaluation of a functional endosseous, porous-surfaced, titanium alloy dental implant system in the dog. *J Dent Res* 1988;67(9):1190-5.
18. Du C, Meijer GJ, van de Valk C, Haan RE, Bezemer JM, Hesseling SC, Cui FZ, de Groot K, Layrolle P. Bone growth in biomimetic apatite coated porous Polyactive 1000PEGT70PBT30 implants. *Biomaterials* 2002;23(23):4649-56.
19. Pilliar RM. Porous-surfaced metallic implants for orthopedic applications. *J Biomed Mater Res* 1987;21(A1 Suppl):1-33.
20. Pilliar RM. P/M Processing of Surgical Implants: Sintered Porous Surfaces for Tissue-to-Implant Fixation. *International Journal of Powder Metallurgy* 1998;34(8):33-45.
21. Simmons CA, Valiquette N, Pilliar RM. Osseointegration of sintered porous-surfaced and plasma spray-coated implants: An animal model study of early postimplantation healing response and mechanical stability. *J Biomed Mater Res* 1999;47(2):127-38.
22. Clemow AJ, Weinstein AM, Klawitter JJ, Koeneman J, Anderson J. Interface mechanics of porous titanium implants. *J Biomed Mater Res* 1981;15(1):73-82.

23. Chen PQ, Turner TM, Ronnigen H, Galante J, Urban R, Rostoker W. A canine cementless total hip prosthesis model. *Clin Orthop* 1983(176):24-33.
24. Nasca RJ, Montgomery RD, Moeini SM, Lemons JE. Intervertebral spacer as an adjunct to anterior lumbar fusion. Part II. Six-month implantation in baboons. *J Spinal Disord* 1998;11(2):136-41.
25. Woodfield TB, Van Blitterswijk CA, De Wijn J, Sims TJ, Hollander AP, Riesle J. Polymer scaffolds fabricated with pore-size gradients as a model for studying the zonal organization within tissue-engineered cartilage constructs. *Tissue Eng* 2005;11(9-10):1297-311.
26. Tan KH, Chua CK, Leong KF, Naing MW, Cheah CM. Fabrication and characterization of three-dimensional poly(ether- ether- ketone)/-hydroxyapatite biocomposite scaffolds using laser sintering. *Proc Inst Mech Eng [H]* 2005;219(3):183-94.
27. Hollister S, Lin C, Saito E, Schek R, Taboas J, Williams J, Partee B, Flanagan C, Diggs A, Wilke E and others. Engineering craniofacial scaffolds. *Orthod Craniofac Res* 2005;8(3):162-73.
28. Hollister SJ. Porous scaffold design for tissue engineering. *Nat Mater* 2005;4(7):518-24.
29. Ishaug-Riley SL, Crane-Kruger GM, Yaszemski MJ, Mikos AG. Three-dimensional culture of rat calvarial osteoblasts in porous biodegradable polymers. *Biomaterials* 1998;19(15):1405-12.
30. Bobyn JD, Pilliar RM, Cameron HU, Weatherly GC. The optimum pore size for the fixation of porous-surfaced metal implants by the ingrowth of bone. *Clin Orthop* 1980(150):263-70.
31. Bobyn JD, Hacking SA, Chan SP. Characterization of a new porous tantalum biomaterial for reconstructive orthopaedics.; 1999; Anaheim, CA.
32. Bobyn JD, Wilson GJ, MacGregor DC, Pilliar RM, Weatherly GC. Effect of pore size on the peel strength of attachment of fibrous tissue to porous-surfaced implants. *J Biomed Mater Res* 1982;16(5):571-84.
33. Pilliar RM. Overview of surface variability of metallic endosseous dental implants: textured and porous surface-structured designs. *Implant Dent* 1998;7(4):305-14.
34. Li JP, de Wijn JR, Van Blitterswijk CA, de Groot K. Porous Ti6Al4V scaffold directly fabricating by rapid prototyping: preparation and in vitro experiment. *Biomaterials* 2006;27(8):1223-35.
35. Frenkel SR, Jaffe WL, Dimaano F, Iesaka K, Hua T. Bone response to a novel highly porous surface in a canine implantable chamber. *J Biomed Mater Res B Appl Biomater* 2004;71(2):387-91.

36. Spivak JM, Ricci JL, Blumenthal NC, Alexander H. A new canine model to evaluate the biological response of intramedullary bone to implant materials and surfaces. *J Biomed Mater Res* 1990;24(9):1121-49.
37. Frenkel SR, Simon J, Alexander H, Dennis M, Ricci JL. Osseointegration on metallic implant surfaces: effects of microgeometry and growth factor treatment. *J Biomed Mater Res* 2002;63(6):706-13.
38. Wilson CE, Kruyt MC, de Bruijn JD, van Blitterswijk CA, Oner FC, Verbout AJ, Dhert WJ. A new in vivo screening model for posterior spinal bone formation: comparison of ten calcium phosphate ceramic material treatments. *Biomaterials* 2006;27(3):302-14.
39. Li SH, De Wijn JR, Li JP, Layrolle P. Biphasic calcium phosphate scaffold with high permeability/porosity ratio. *Tissue Engineering* 2003;9(3):535-548.
40. Pilliar RM, Lee JM, Maniopoulos C. Observations on the effect of movement on bone ingrowth into porous- surfaced implants. *Clin Orthop* 1986(208):108-13.
41. Chang BS, Lee CK, Hong KS, Youn HJ, Ryu HS, Chung SS, Park KW. Osteoconduction at porous hydroxyapatite with various pore configurations. *Biomaterials* 2000;21(12):1291-8.
42. Boyde A, Corsi A, Quarto R, Cancedda R, Bianco P. Osteoconduction in large macroporous hydroxyapatite ceramic implants: evidence for a complementary integration and disintegration mechanism. *Bone* 1999;24(6):579-89.
43. Eckert M, Wittmann I, Rollinghoff M, Gessner A, Schnare M. Endotoxin-induced expression of murine bactericidal permeability/increasing protein is mediated exclusively by toll/IL-1 receptor domain-containing adaptor inducing IFN-beta-dependent pathways. *J Immunol* 2006;176(1):522-8.
44. Kuo SM, Chang SJ, Chen TW, Kuan TC. Guided tissue regeneration for using a chitosan membrane: an experimental study in rats. *J Biomed Mater Res A* 2006;76(2):408-15.
45. Shimko DA, Shimko VF, Sander EA, Dickson KF, Nauman EA. Effect of porosity on the fluid flow characteristics and mechanical properties of tantalum scaffolds. *J Biomed Mater Res B Appl Biomater* 2005;73(2):315-24.
46. Spoerke ED, Murray NG, Li H, Brinson LC, Dunand DC, Stupp SI. A bioactive titanium foam scaffold for bone repair. *Acta Biomater* 2005;1(5):523-33.
47. Habibovic P, Li J, Van Der Valk CM, Meijer G, Layrolle P, Van Blitterswijk CA, De Groot K. Biological performance of uncoated and octacalcium phosphate-coated Ti6Al4V. *Biomaterials* 2005;26(1):23-36.
48. Buckwalter JA, Glimcher MJ, Cooper RR, Recker R. Bone biology. II: Formation, form, modeling, remodeling, and regulation of cell function. *Instr Course Lect* 1996;45:387-99.

Chapter 10

Biological performance of porous composite implants based on titanium alloy and biphasic calcium phosphate ceramic: in vivo study in goats

J.P. Li^{1,2}, P. Habibovic¹, H.P. Yuan¹, C. E. Wilson², J.R. de Wijn¹, C.A. van Blitterswijk¹, K. de Groot^{1,3}

¹Institute for Biomedical Technology, University of Twente, The Netherlands.

²Porogen. B.V, The Netherlands.

³CAM Implants. B.V, The Netherlands.

Abstract

In this study, porous 3D fiber deposition titanium (3DFT) and 3DFT combined with porous biphasic calcium phosphate ceramic (3DFT+BCP) implants, both bare and one week cultured with autologous bone marrow stromal cells (TE: Tissue engineered), were implanted intramuscularly and orthotopically in 10 goats. To assess the dynamics of bone formation over time, fluorochrome markers were administered at 3, 6 and 9 weeks and the animals were sacrificed at 12 weeks after implantation. New bone in the implants was investigated by histology and histomorphometry of non-decalcified sections.

Intramuscularly, no bone formation was found in any of the 3DFT implants, while a very limited amount of bone was observed in 2 out of 10 TE 3DFT implants. Both 3DFT+BCP and TE 3DFT+BCP implants showed ectopic bone formation, in 8 and 10 animals, respectively. The amount of formed bone was significantly higher in TE 3DFT+BCP as compared to 3DFT+BCP implants.

Implantation on transverse processes resulted in significantly more bone formation in composites implants as compared to titanium alloy alone, both with and without cells. Unlike intramuscularly, no significant effect on the amount of new bone was observed in composite implants with/without bone marrow stromal cells. The performance of 3DFT and TE 3DFT implants was also similar.

In conclusion, titanium alloy scaffolds combined with BCP ceramic showed higher osteoinductive and osteoconductive potential than the metal alone. Although the 3DFT is inferior to BCP for bone growth, the reinforcement of the brittle BCP with a 3DFT cage did not negatively influence osteogenesis, osteoinduction and osteoconduction as previously shown for the BCP alone. The positive effect of

bone marrow stromal cells was observed ectopically, while it was not significant orthotopically.

Keywords: Porous Ti6Al4V, Biphasic calcium phosphate (BCP), BMSCs, osteoconduction.

1. Introduction

Bone grafts and bone graft substitutes are essential for replacement and repair of damaged and degraded skeletal tissue. Classical methods for bone repair employ autografts and allografts, which have good osteoinductive and osteoconductive properties. However, their use is often associated with important drawbacks such as limited availability and possible donor site morbidity for autografts [1,2] and disease transmission and immunologic incompatibility for allografts. [3]. Synthetic bone graft substitutes, the design of which is based on mimicking the mineral composition of bone, such as hydroxyapatite (HA), tricalcium phosphate (TCP) and biphasic calcium phosphate (BCP) ceramics, also possess satisfying bone healing properties. However, these materials are very stiff and brittle, have low impact resistance and relatively low tensile strength [4]. In particular in large bone defects, which are unable to heal spontaneously, it is important to restore the structural integrity of the bone, as well as its function (i.e. load-bearing capacity) in an as short as possible period of time. Due to poor mechanical properties of the above mentioned bone fillers; their application in critical-sized bone defects is often associated with the use of some kind of external fixation. In order to decrease patient's discomfort during the healing process, ideally, bone fillers should be able to temporarily take over the mechanical function of the bone.

Metals possess mechanical properties suitable for load-bearing applications. However, the high stiffness of the metals often leads to stress-shielding from the residual bone, which may result in detrimental resorptive bone remodeling, and consequently to a poor fixation of the implant. Recent developments in metallic implant design therefore focus on adapting the mechanical properties of metals to those of biological systems by for example, applying a porous structure whereby mechanical interlocking may enhance the integration process.

Recently, porous titanium and titanium alloys gained interest as they have been shown to possess excellent mechanical properties as permanent orthopaedic implants under load-bearing conditions [5,6]. While titanium is generally considered as a bioinert material and thus its bioactivity is inferior to that of calcium-phosphates, different approaches to improve the bioactivity of titanium and its alloys have been published. Fujibayashi et.al used chemical and thermal treatments to enhance the bioactivity of porous titanium implants [7]; Habibovic and coworkers applied biomimetic octacalcium phosphate (OCP) coatings to show improved osteoconductive and osteoinductive properties of porous titanium [8]; Vehof et.al. and van den Dolder and colleagues performed different studies in which they attempted to improve the biological properties of porous titanium mesh by combining scaffolds with either osteogenic cells or osteogenic growth factors [9-11].

In this present study, we produced composites consisting of 3D fiber deposition Ti6Al4V (3DFT) and BCP ceramic in order to investigate the bone formation of composite construct and whether peripheral 3DFT of the BCP influenced BCP bioactivity. In addition, we combined these implants with autologous bone marrow stromal cells (BMSCs). 3DFT was produced by rapid prototyping [12], a method that allows for fabrication of precisely defined porous structures. In the previous reports, it has been reported that a scaffold with different geometry may affect the surrounding cells and tissue ingrowth [13,14]. Highly interconnected porous structures provide a large surface area, enabling cells to migrate, proliferate, and differentiate [15,16]. The in-house produced BCP ceramic had a highly interconnected macro- and microporous structure, and was previously shown to be both osteoconductive and osteoinductive [17-20].

Therefore, we filled the 3DFT metallic implant with the BCP ceramic to form a composite, and alone or in combination with BMSCs to investigate the bone formation of construct. These implants were inserted both intramuscularly and on spinal transverse processes of 10 goats for 12 weeks.

2. Materials and methods

2.1. Experimental design

This study was approved by institutional animal care committee approval, and 10 adult Dutch milk goats were used.

BMSCs were obtained, culture expanded and cryopreserved. Ten days before surgery the cells were thawed, allowed to acclimate for 3 days, seeded on 3DFT and 3DFT+BCP scaffolds and cultured in osteogenic medium. Bare scaffolds and the constructs with Autologous BMSCs were implanted ectopically in the paraspinal muscles. Orthotopically, polymeric cages containing three conditions were implanted bilaterally on the L4 and L5 transverse processes according to a randomized complete block design (Figure.1) .. To monitor bone formation over time, fluorochrome markers were administered at 3, 6 and 9 weeks and the animals were sacrificed at 12 weeks after implantation. Bone formation was investigated by histology and histomorphometry of non-decalcified sections using epifluorescent and light microscopy.

2.2. Implants

3DFT: Porous Ti6Al4V scaffolds made by 3D fiber deposition were used in this study. The compressive strength of 3DFT was higher than that of cancellous bone, and the Young's modulus value lied between that of cancellous and cortical bone. The permeability is comparable to that of cancellous bone. The preparation

procedure of these scaffolds was described earlier [12]. In short, Ti6Al4V slurry (80 wt% of powder Ti6Al4V in 0.5% aqueous water methylcellulose solution) is forced by gas pressure through a syringe nozzle of a 3D-biplotter machine (Envisiontec GmbH, Germany). The slurry is deposited on a stage as a fiber, which rapidly solidifies by drying, and the scaffold is fabricated by layering a 0°-45° pattern of fibers. After deposition, the obtained Ti6Al4V scaffolds were dried for 24hrs at room temperature, and sintered under high vacuum at 1200°C for 2hrs. Both the fiber diameter and the space between fibers were around 400µm. The scaffolds were machined into the following implants: blocks with dimensions 4x7x8 mm (metal alone) and 4x7x8 mm with an inner hole of 4x4x4 mm (composite) for orthotopic implantation (Fig 1). Blocks with dimensions of 4x7x8 mm (metal alone) and Ø8x8 mm cylinders with a central hole of Ø5x8 mm for intramuscular implantation (Fig.1).

For composite scaffolds porous biphasic calcium phosphate (BCP) ceramic was prepared by using the so-called H₂O₂ method as published earlier [21]. For the preparation of the ceramic, in-house made BCP powder was used. Porous green bodies were produced by mixing this powder with 2% H₂O₂ solution (1.0g powder / 1.2 ± 0.05ml solution) and naphthalene (Fluka Chemie, The Netherlands) particles (710 - 1400 µm; 100g powder/ 30g particles) at 60°C. The naphthalene was then removed by sublimation at 80°C and the green porous bodies were dried. Finally, the bodies were sintered at 1200°C for 8 hours. Blocks with the dimensions of 4x4x4 mm and cylinders of Ø5 x 8 mm were machined and fitted into relative 3DFT bodies to make the composites

The microstructure of different implants was characterized by using an environmental scanning electron microscope (ESEM; XL30, ESEM-FEG, Philips, The Netherlands) in the secondary electron mode.

The BCP ceramic composition and crystal structure were determined by Fourier Transform Infra Red Spectroscopy (FTIR; Spectrum100, Perkin Elmer Analytical Instruments, Norwalk, CT) and X-Ray Diffraction (XRD; Miniflex, Rigaku, Japan). HA/β-TCP weight ratio in the BCP was calculated by comparing the XRD pattern to the calibration patterns prepared from the powders with the known HA/β-TCP weight ratios. Each type of scaffold was left without or cultured with BMSCs. BMSC constructs were never placed next to unseeded scaffolds in the transverse process cages.

For intramuscular and orthotopic implantation, four types of implants were prepared:

- 1: 3DFT: 3DFT scaffolds without cells
- 2: TE 3DFT: 3DFT scaffolds with cells
- 3: 3DFT+BCP: 3DFT+BCP scaffolds without cells
- 4: TE 3DFT+BCP: 3DFT+BCP scaffolds with cells.

2.3. Cages for orthotopic implantation on transverse processes

Cage design and fabrication were described previously [22] The scaffolds, polyacetal components of the cages and the metal screws were sterilized by autoclaving. Three scaffolds (4x7x8 mm) were plugged into a cage and separated by thin Teflon plates (0.5x7x8 mm). Four spinal cages were implanted bilaterally on the transverse processes of the L4 and L5 vertebrae of each goat according to a randomized complete block design. In addition to the four conditions that are discussed in this paper, another eight Ti alloy conditions were evaluated which findings will be presented separately. The orthotopic scaffolds were open to both the underlying bone and the overlying soft tissues. Implant and cage are shown in Fig.1.

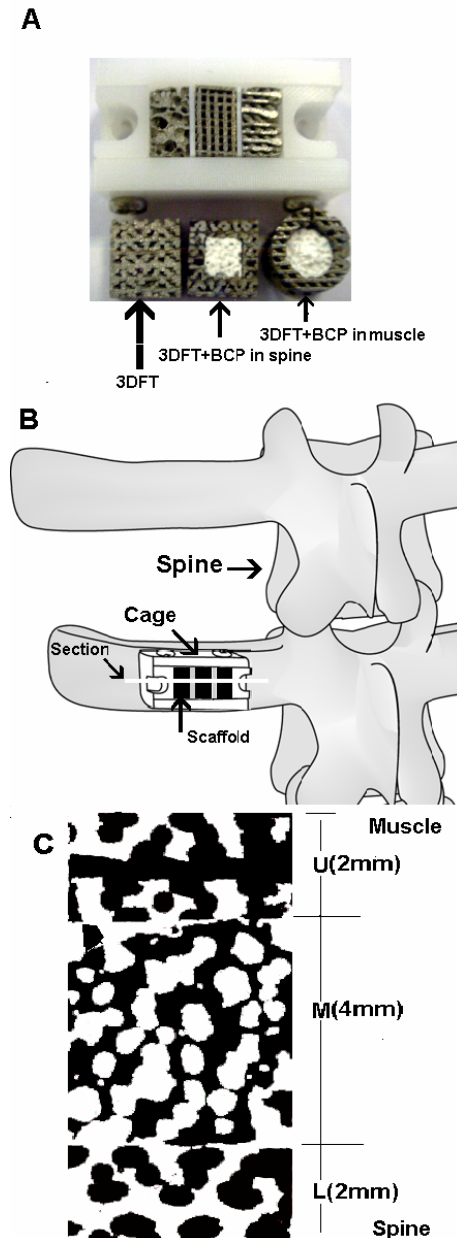


Fig.1: (A) Implants for intramuscular and spinal implantation. (B) Schematic drawing of spinal cage mounted on a transverse process. (C) Central slide through 3DFT+BCP. Division of the implant area on histological sections as used for histomorphometry for studying bone ingrowth from host bone bed. Dotted lines indicate the upper (U) quarter, middle (M) half and lower (L) quarter.

2.4. BMSC culture and seeding conditions

Autologous serum (AS) was derived from 100 ml venous blood that was taken at the time of bone marrow aspiration [23]. The BMSCs were derived from 30 ml bone marrow obtained from the iliac wings of each goat according to a previously described procedure [24]. After 7-10 days of culture in standard culture medium containing 15% of fetal bovine serum (FBS, Gibco, Paisly, Scotland) in T300 flasks, firstly, medium containing non adherent cells was removed after 2-3 days and replaced by fresh medium. Then, the adherent cells were expanded according to previously described method [25]. Finally, cells were trypsinized and concentrated by centrifugation at 1500 rpm for 4 minutes followed by resuspension in 10 ml of fresh medium containing 30% FBS and 10% dimethylsulfoxide (DMSO, Sigma, The Netherlands) for cryopreservation. 10 days before surgery, the cells were thawed in pure FBS, centrifuged at 1500 rpm for 4 minutes and after washing with culture medium, replated in medium containing 10% FBS. After 3 days of culture, cells were washed with PBS, then detached and centrifuged before resuspension at a concentration of 5×10^6 cells/ml in medium containing 15% AS. 3 of 9 TE scaffolds in per goat were immersed in 4 ml of this suspension respectively, and incubated for 2 hours. After the cell-seeding period, each construct was placed in a well of a 25-well plate. The constructs were pre-cultured for 1 week under static conditions in 3 ml of medium containing 15% AS and 10mM β -Glycerophosphate (BGP, Sigma, Zwijndrecht, The Netherlands) and 10nM Dexamethasone (DEX, Sigma).

The control scaffolds (without cells) were placed in the same medium for the same period of time as the TE constructs. The medium was changed every 2 to 3 days. At the end of the incubation period, implants were transported to surgery in serum-free medium.

2.5. In vitro analysis of constructs

Two extra implants of each implant type were used to determine cell proliferation and viability by Alamar blue assay at day 1, 4 and 6. The Alamar blue solution was diluted 1:10 in culture medium, and the constructs were cultured for 2 hours. 200 μ l of Alamar blue solution from each well was transferred into 96-well plates, and fluorescence was measured using a Perkin Elmer Luminescence Spectrometer LS50B. Results were recorded by FL Winlab software.

2.6. Implantation

10 adult Dutch milk goats, weighing 45-75kg (mean weight: 65 ± 8.5 kg), were housed at the Central Animal Laboratory Institute (GDL), Utrecht, The Netherlands, at least 4 weeks prior to surgery.

The surgical procedures were performed under standard conditions [19,22]. After shaving and disinfection of the dorsal thoracolumbar area, a midline skin incision from T8-L5 was made to expose the paraspinal muscles that were separated longitudinally to expose the transverse processes of the L4 and L5 vertebrae. The processes were decorticated using an angled bone rasp. One cage was screwed to each process. Finger pressure was applied to the top of the blocks in the cage prior to muscle closure to ensure direct contact of all blocks with the underlying bone. After spinal cage implantation, using blunt dissection, separate intramuscular pockets were created in the T8-L3 paraspinal muscles and filled with one of the intramuscular conditions according to a randomized scheme. Subsequently, the fascia was closed with a nonresorbable suture to facilitate implant localization at explantation. The skin was closed in two layers. Durogesic 25 (fentanyl transdermal CII patches; Janssen-Cilag EMEA, Beerse, Belgium) was administered for postoperative pain relief.

Sequential fluorochrome markers were administered at 3 weeks (CalceinGreen, 10 mg/kg, Sigma, The Netherlands), 6 weeks (Oxytetracyclin, Engemycin 32 mg/kg, Mycofarm, The Netherlands) and 9 weeks (Xylenol Orange, 80 mg/kg Sigma) in order to visualize bone growth dynamics.

At 12 weeks, the animals were euthanized by an overdose of pentobarbital (Organon, Oss, The Netherlands). Spinal cages were retrieved by sawing off the transverse processes, while intramuscular implants were removed with some surrounding muscle tissue.

2.7. Histological processing and histomorphometry

The explanted samples were fixed in a solution of 5% glutaraldehyde and 4% paraformaldehyde at 4°C. Fixed samples were dehydrated by ethanol series (70%-100%) and transferred into a methylmethacrylate (MMA) solution that polymerized at 37°C within 1 week. Three centrally located longitudinal 10-15 µm thick sections were cut from each sample using a sawing microtome. Two sections were stained with 1% methylene blue and 0.3% basic fuchsin after etching with HCl/ethanol mixture for histology. The third section remained unstained for epifluorescence microscopy of the fluorochrome markers.

Implanted materials were qualitative analyzed using a light microscope (E600 Nikon, Japan). The presence of fluorochrome markers were evaluated using a light/fluorescence microscope (E600, Nikon, Japan) equipped with a quadruple filter block (XF57, dichroic mirror 400, 485, 558 and 640 nm, Omega Optics, The Netherlands). High-resolution digital scans of the stained sections of spinal cage implants were made for histomorphometry using a photographic film scanner (Dimage Scan Elite 5400, Minolta, Japan). Prior to histomorphometrical analysis,

bone and material were pseudocoloured, red and green respectively, by using Adobe Photoshop 6.0. Image analysis was performed using a PC-based system with the KS400 software (version 3, Zeiss, Germany). Prior to measurements the system was geometrically calibrated with an image of a block of known dimensions to analysis the area of implant. A custom made macro was developed to measure area of interest, area of scaffold, area of bone, scaffold outline available for bone apposition, contact length of bone and scaffold [13]. The following parameters were investigated:

1. %b. ROI: the percentage of bone area in total implant area $[(\text{bone area} / \text{total implant area}) \times 100\%]$;
2. %b. pore total: the percentage of bone area in total available pore space $[(\text{bone area} / (\text{total implant area} - \text{total scaffold area})) \times 100\%]$;
3. %b. pore low: the percentage of bone area in available pore space in the low quarter of the implant closest to host bone bed (L area in Fig.1C; only applicable for orthotopic implantation);
4. %b. pore middle: the percentage of bone area in available pore space in the middle half of the implant (M area in Fig.1C; only applicable for orthotopic implantation);
5. %b. pore upper: the percentage of bone area in available pore space in the upper quarter of the implant (U area in Fig.1C; only applicable for orthotopic implantation);
6. %b. cont. total: percentage of length of contact between bone and scaffold outline relative to total available scaffold outline in the total implant area: $[(\text{bone contact scaffold length} / \text{scaffold outline length}) \times 100\%]$;

2.7. Statistics

Statistical calculations were done with SPSS (Chicago, IL) 11.5 software. Statistical analyses were performed on histomorphometrical results on bone area, bone contact and bone ingrowth depth by ANOVA for randomized complete block design with a post hoc Tukey's HSD ($p=0.05$) to determine differences between scaffold conditions.

3. Results

3.1. Material characterization and in vitro results

XRD and FTIR analysis confirmed the biphasic nature of the BCP ceramic, consisting of $80 \pm 5\%$ HA and $20 \pm 5\%$ β -TCP (data not shown). Macro- and microstructures of 3DFT and 3DFT+BCP implants are shown in Figure 2. As

observed by the ESEM, 3DFT implants consisted of a well interconnected macroporous structure, with a pore size of around $400\mu\text{m}$. The porosity of 3DFT is $55\pm 3\%$. BCP scaffolds also possessed an interconnected macroporous structure with pore sizes varying between $100\mu\text{m}$ and $800\mu\text{m}$. The porosity of BCP is $60\pm 4\%$. At high magnification micropores (pore size $< 10\mu\text{m}$) became visible in the structure of both scaffolds, 3DFT and BCP (Fig.2C and 2D).

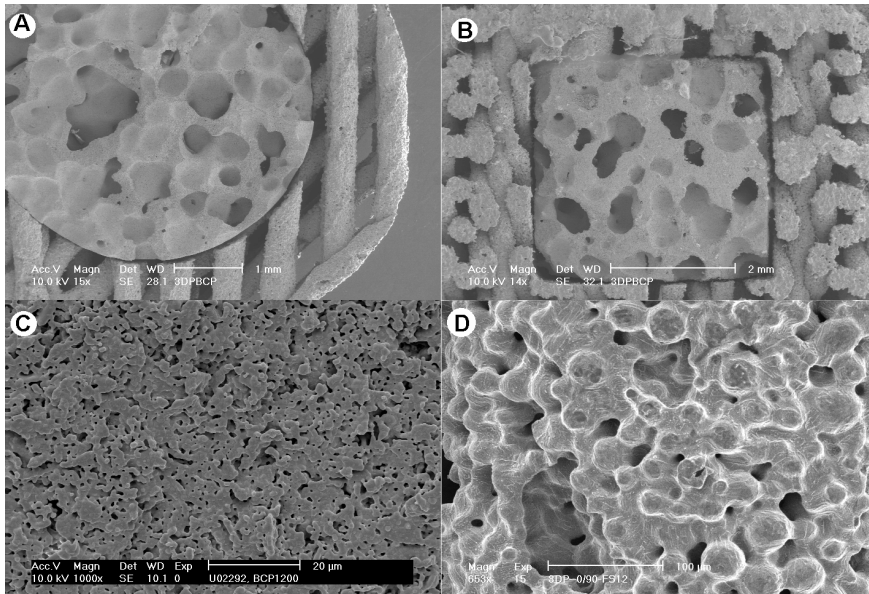


Fig.2: ESEM photographs of the scaffolds. Macrostructure of implants for intramuscular (A) and orthotopic (B) implantation and microstructure of BCP (C) and 3DFT surface (D).

Results of Alamar blue assay on day 1, 4 and 6 are shown in Fig.3. Between day 1 and 4, an increase in cellular activity for all implant types was observed, suggesting cell proliferation or cell metabolism was increased. After day 4, a decrease in cellular activity suggested that the cells stop to grow and cell metabolism decreased due to limitation of oxygen. At day 1 and 4, metabolic activity on metal alone was lower than on BCP containing implants; this difference disappeared after 6 days of culture.

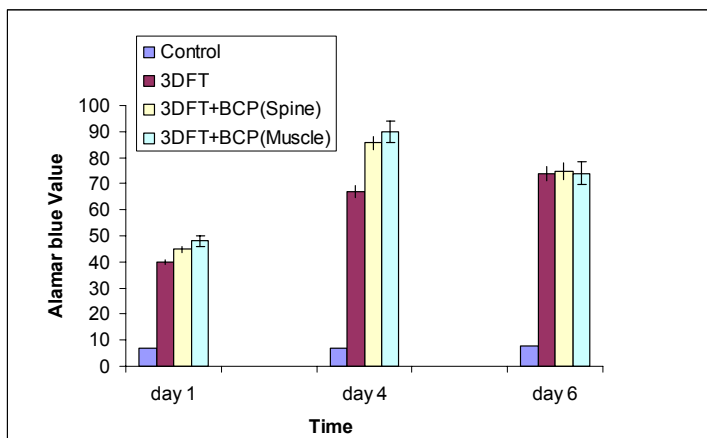


Fig.3: Alamar blue value for implants different implant types at 1, 4 and 6 days of culture. Up to 4 days, increased metabolism is observed, followed leveling off.

3.2. In vivo results

3.2.1. Intramuscular implantation

At retrieval, all implants were surrounded by well-vascularized muscle tissue. Histology showed no indications for toxicity of the implants nor were signs of an inflammatory tissue response directly related to the implants observed.

Table 1 shows bone incidence in different implants after 12 weeks of intramuscular implantation.. None of the bare titanium alloy implants showed bone formation. They were filled with fibrous tissue containing capillaries, and occasionally showed fatty tissue in the presence of growth.(Fig.4A). Two of the TE 3DFT implants showed bone formation albeit to a limited extend (Fig.4B). In one of these implants the Xylenol orange fluorochrome label was observed, indicating that bone was formed between 6th and 9th week of implantation (data not shown). In the other implant, none of the labels was found, suggesting that the start of bone formation had taken place after 9 weeks.

Table 1 Bone incidence intramuscular in goat

Implant	Bone incidence after 12 weeks
3DFT	0/10
TE 3DFT	2/10
3DFT+BCP	8/10
TE+3DFT+BCP	10/10

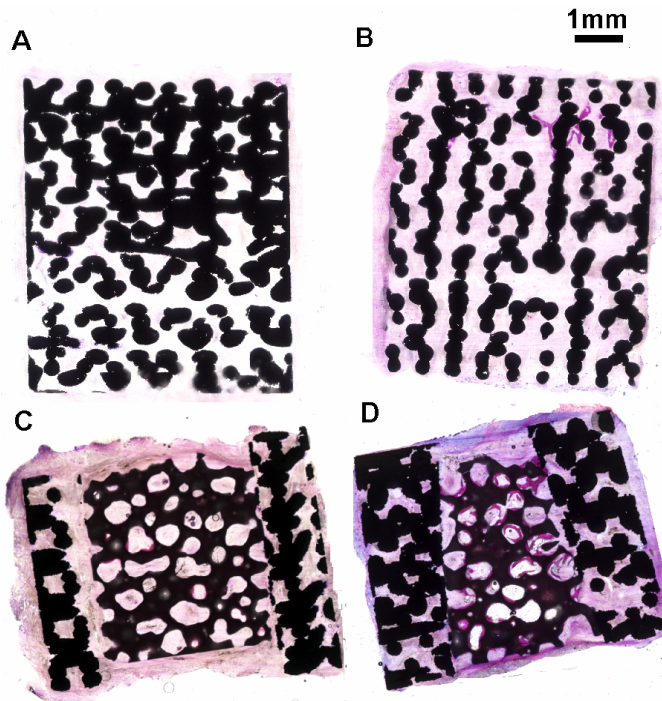


Fig.4: Digital photographs of of stained (methylene blue/basic fuchisine) histological sections of 3DFT (A), TE 3DFT (B), 3DFT+BCP (C) and TE 3DFT+BCP (D) implants after 12 weeks of implantation in paraspinal muscles.

Fig.4B, 4C and 4D illustrate bone formation in TE 3DFT, 3DFT+BCP and TE 3DFT+BCP implants. In both BCP implant types, bone was only observed in the pores of the BCP ceramic, rather than in the titanium alloy area of the implant. In the TE 3DFT+BCP implants, bone was found in all implants after 12 weeks of implantation. All three fluorochrome markers were found in TE 3DFT+BCP implants suggesting an early start of bone formation before the 3rd week of implantation.

Histomorphometrical analysis of the amount of bone formed in the available pore area indicated significantly more bone formation in TE 3DFT+BCP as compared to 3DFT+BCP implants ($p < 0.001$; Fig.5). Similar results were obtained for bone contact measurements (data not shown).

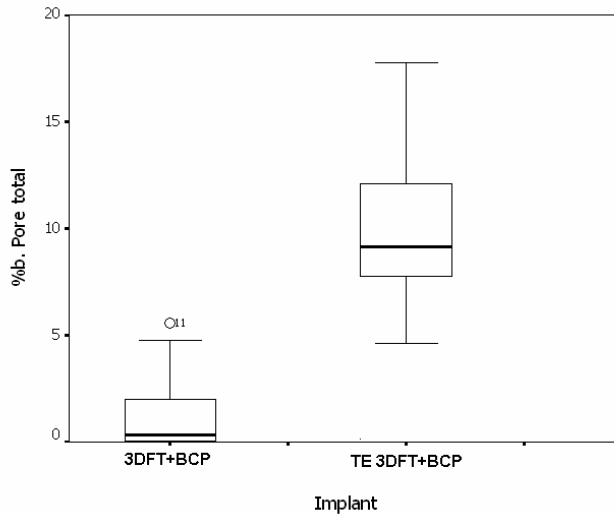


Fig.5: Histomorphometrical results: boxplots (mean and interquartile values) of bone formation in total available pore space in 3DFT+BCP and TE 3DFT+BCP implants after 12 weeks of intramuscular implantation. ("o" indicates outliers)

3.2.2. Orthotopic implantation

Upon explantation, no macroscopic or microscopic signs of infection were found. All cages were found firmly attached to the underlying transverse processes, even after removing the bone screws.

In all implants bone ingrowth started from the host bone bed towards the implant. New bone did not completely fill any of the implants, so the final amount of bone in the implants could be used for measuring the effect of various implants to new bone formation.

In the 3DFT and TE 3DFT, bone formation was obviously the result of ingrowth from the underlying bone (osteoconduction) as in both 3DFT and TE 3DFT bone was predominantly found in the lower part of the implants adjacent to the underlying transverse processes (Fig.6A and 6C). In contrast to 3DFT implants, in both 3DFT+BCP and TE 3DFT+BCP implants bone had reached the top of the middle part of the implant (Fig.6B and 6D).

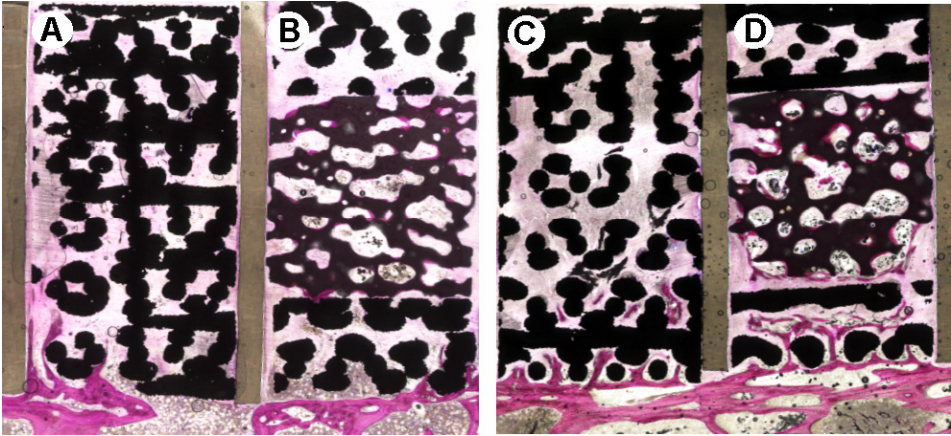


Fig.6: Digital photographs of stained (methylene blue/basic fuchsiene) histological sections of 3DFT (A), 3DFT+BCP (B), TE 3DFT (C) and TE 3DFT+BCP (D). after 12 weeks of implantation on lumbar transverse process. Bone is stained pink/red, Ti alloy black and BCP ceramic dark brown. The transverse process can be seen at the bottom of the implants and Teflon plates are visible between the implants.

Histomorphometrical analysis confirmed the histological observations revealing that a relatively low amount of bone was formed in 3DFT and TE 3DFT implant (about 2-3% of the total implant area was new bone). Significantly more bone was found in 3DFT+BCP and TE 3DFT+BCP implants (about 8-10% of total implant area). Fig.7 represents histomorphometrical data of bone area in the total implant area (i.e. region of interest) after 12 weeks of implantation. Significant difference was found between 3DFT and 3DFT+BCP ($p < 0.05$) and between 3DFT and TE 3DFT+BCP ($p < 0.002$) as well as between TE 3DFT and 3DFT+BCP ($p < 0.05$) and between TE 3DFT and TE 3DFT+BCP ($p < 0.002$). Significant difference was found neither between 3DFT and TE 3DFT nor between 3DFT+BCP and TE 3DFT+BCP implants. As can be observed, the general phenomenon is that the amount of bone was dependent on the implant type rather than on the presence of cells. Measurements of bone contact with the implant outline showed similar results as ROI for all implant types (Fig.8).

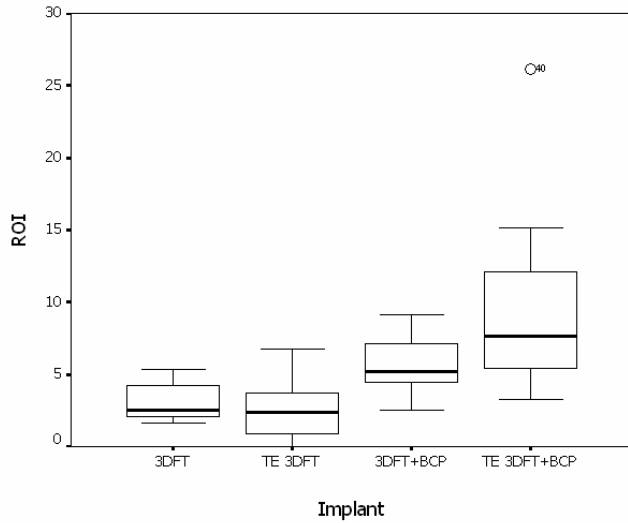


Fig.7: Histomorphometrical results: boxplots (mean and interquartile values) of the percentage of new bone area in the total implant area (region of interest) after 12 weeks of implantation on lumbar transverse process. ("o" indicates outliers) .

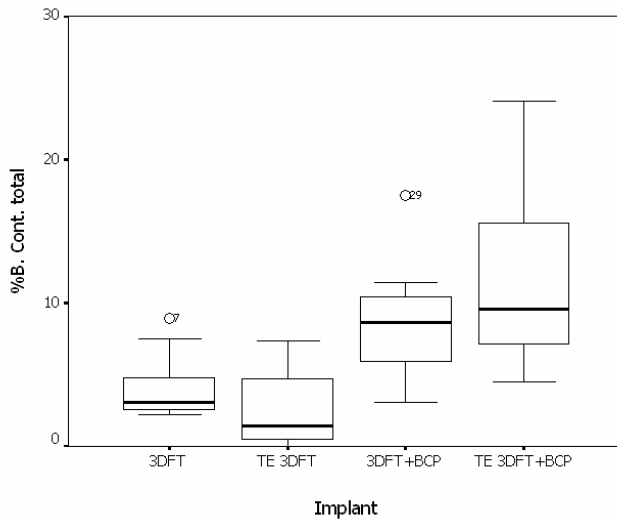


Fig.8: Histomorphometrical results: boxplots (mean and interquartile values) of the percentatge of the total length of available scaffold outline in contact with bone in the total implant area. ("o" indicates outliers).

Regarding the bone ingrowth into different area of implants in the available pore space, no significant difference was found between different implant types (Fig.9A) in the third of the implant closest to the host bone bed (L area in Fig.1C). In contrast, the bone area in the middle half of both 3DFT+BCP and TE 3DFT+BCP (M area in Fig.1C) was significantly higher as compared to the implants consisting of metal alone (Fig.9B). No bone formation was found on the upper part of implant (U area in Fig.1C).

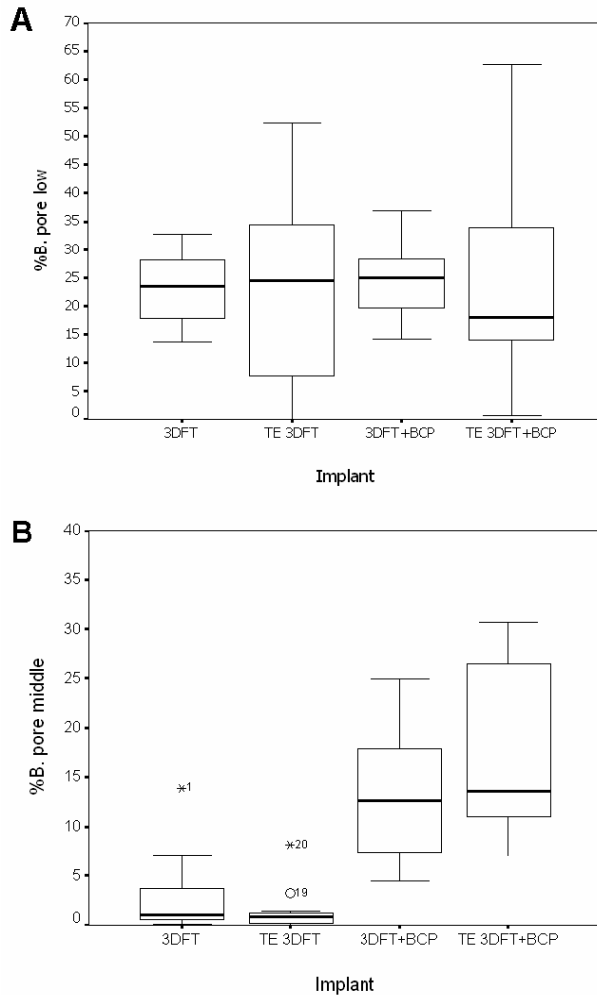


Fig.9: Histomorphometrical results of bone area in the available pore space in (A) the quarter of the implant closest to transverse process (L area in Figure 1C) and (B) the middle half of the implant (M area in Figure 1C) (“o” and “x” indicate outliers and extreme outliers respectively).

Fluorescent microscopy of the sequential fluorochrome labels revealed the dynamics of bone formation in different implants. In most implants, all three labels were present at the lower part of implants, closest to transverse process as is illustrated by TE 3DFT+BCP micrograph in Fig.10A, suggesting the start of new bone formation before the 3rd week of implantation. In the middle part, all three markers were also found in the TE 3DFT+BCP implants (Fig.10B), unlike for the other implant types. It suggested that there is an osteogenic effect of the cells. In the middle half of the 3DFT+BCP implants, only the oxytetracycline (6-week) and xylenol orange (9-week) markers were observed, while there were no markers in 3DFT and TE 3DFT implants, confirming the histological observation of lack of bone formation in the deeper regions of metallic implants. Another remarkable observation was that in the middle part of 3DFT+BCP and TE 3DFT+BCP implants, early fluorochrome markers were observed predominantly on the BCP to Ti alloy interface both on the lower and on upper interface.

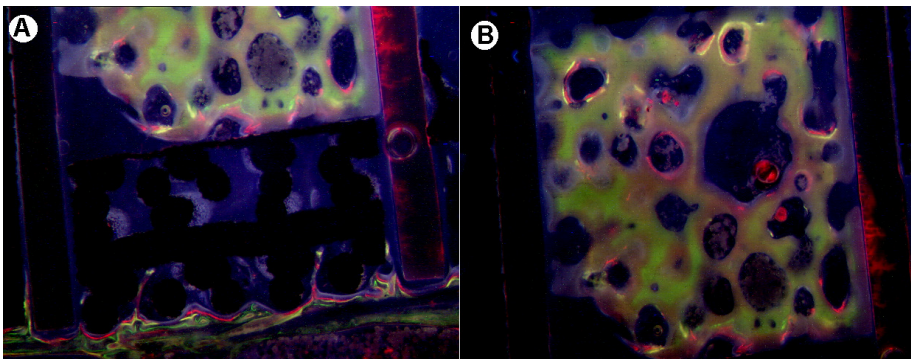


Fig.10: Epifluorescent microscopy images of fluorochrome markers in the low part of implant (A) and BCP part (B) of TE 3DFT+BCP implant after 12 weeks of implantation on lumbar transverse process. In all images the earliest label is green (3 weeks, calcein green), the middle label is yellow (6 weeks, oxytetracycline) and the final label is orange (9 weeks, xylenol orange).

4. Discussion

In this *in vivo* study in goats, we investigated the behavior of 3DFT metallic implants and 3DFT+BCP composites either as such or as tissue-engineered constructs loaded with autologous BMSCs by implanting them in paraspinal muscles and on lumbar transverse processes. The goal of the study was to combine BCP and 3DFT to make benefit of the advantageous characteristics of both materials [8]. By incorporating BCP inside a 3DFT cage, optimal bioactivity was combined with optimal biomechanical characteristics since 3DFT retaining its

mechanical properties and BCP retaining its bioactivity. BCP ceramic was chosen for the preparation of composite implants, since previous animal studies have shown that this material has a high osteoinductive and osteoconductive potential and is apt for cell based bone formation [17,26].

As we did not find signs of foreign body reaction related to the implants, we can conclude that 3DFT and 3DFT+BCP have an acceptable biocompatibility to be used as bone graft substitute.

Intramuscularly, no bone formation was observed in 3DFT implants, while only 2 out of 10 implants showed a very limited amount of bone in TE 3DFT implants. In contrast to metallic implants, bone incidence in composite implants was 80% and 100% for 3DFT+BCP and TE 3DFT+BCP, respectively. The amount of bone formed in tissue-engineered constructs based on composite material was significantly higher as compared to bare composite implants.

The observed differences in bone formation between titanium alloy and titanium alloy combined with BCP ceramic can be explained by the well-known bioactivity of BCP. In view of this, biphasic CaP ceramics, composed of hydroxyapatite and tricalcium phosphate, are considered to be even more bioactive than hydroxyapatite alone [19,27], possibly due to higher resorbability. Moreover, BCP ceramics have been shown to induce ectopic bone formation without addition of osteogenic factors.

The difference in bone formation between 3DFT+BCP and TE 3DFT+BCP is most probably caused by the presence of osteogenic cells in TE construct. During the culturing of cells on the scaffolds in order to produce constructs for the implantation, BGF and dexamethasone were added into culturing medium, which maybe stimulated osteogenic differentiation. After 7 days of culture, the extracellular matrix was formed in the scaffolds. This extracellular matrix may be useful for bone formation as reported previously [25]. It can be seen that BMSCs did have a significantly positive effect on ectopic bone formation when seeded on composite implants, and lacked the ability to do so on metallic implants. The reason might be explained by the difference in the interaction with cells and endogenous growth factors between the BCP and Ti6Al4V surface. This is conceivable, based on earlier reports of favorable behavior of CaP-ceramics due to preferential binding of growth factors and / or bone marrow cells to their surfaces [9,28,29]. Our results are in agreement with earlier studies with titanium fiber mesh in which more bone formation was shown when metallic implants were coated with calcium-phosphate and loaded cells[9,30].

Similar to intramuscular results, the presence of BCP ceramic has a significantly positive effect on bone formation at the orthotopic implantation site. Even though BCP ceramic was not in direct contact with either underlying bone of the transverse

process or with the muscles covering the cage, its bioactivity was apparent in both the amount and the rate of new bone formation.

Unlike intramuscularly, BMSCs did not have a significant effect on orthotopic bone formation in neither metallic nor in composite implants although there are indications for cell derived (early) osteogenesis. This observation is in accordance with a previous study of the effect of orthotopic BCP TE constructs in goats [20]. A few reasons can be given as possible explanation for the lack of effect of tissue engineering orthotopically. Bone is one of the few types of tissues that have the potential to repair itself completely and to reconstitute its original structure. In the study, the surface of transverse process was removed by a rasp. The resultant surgical trauma unavoidably caused primary mechanical damage to the vasculature, cells, matrix, and bone marrow, possibly resulting in impaired circulation, exudates, and hemorrhage. Taken that the success of tissue engineering for a large part lies in the communication of the implanted cells with their surroundings, damage caused by the surgical procedure may be the reason for the poor effect of tissue engineering on the implants on the transverse processes as compared to intramuscular implantation, where the surgical trauma is much less severe.

Another possible reason for the lack of the effect of tissue engineering orthotopically may be the effect of the endogenous cells. It is well-known that stromal stem cells exist in the bone marrow, and under specified conditions can proliferate and differentiate into osteoblastic cells, resulting in the formation of bone [31-33]. Perhaps, in combination with the materials with high osteoconductive and osteoinductive potential such as BCP ceramic, the effect of endogenous cells and growth factors is strong enough to overrule that of the implanted cells, in particular after a longer implantation time. Although we could not find differences in the amount of formed bone between TE 3DFT+BCP and 3DFT+BCP implant, the fluorochrome labels showed that TE 3DFT+BCP induced earlier start of bone formation than 3DFT+BCP. Similar observations of the temporary effect of tissue engineering when appropriate osteoconductive / osteoinductive implants are used has been reported previously [20]. A better understanding of the processes involved in the osteogenicity of tissue-engineered constructs is needed to give the exact explanation of the results observed in our study.

Another interesting observation of this study was that in composite implants early fluorochrome labels (calcein green or oxytetracycline) often appeared on the interface between BCP and titanium alloy both on the side of overlying muscle or underlying bone, rather than in the middle of the BCP part. This is likely the result of oxygen supply and nutrient diffusion from the overlying muscle or underlying bone, which suggested that bone only forms early in the presence of vasculature

and proved that osteoconductivity of the BCP ceramic plays a role orthotopically too as earlier suggested [17]. In the middle part, the lack of nutrient delivery and waste removal delayed the bone growth. This is in agreement with a previous study of different ceramics on the transverse process model in goats [19] and contradictory to the hypothesis that cell survival should have been restricted to only a superficial 300–500µm layer of the implant since high depth of bone ingrowth was obtained (around 2000 µm) [34,35].

5. Conclusion

In the current study, 3DFT and 3DFT+BCP scaffolds, bare and seeded with goat BMSCs were implanted intramuscularly and orthotopically in goats. Implantation of composites of 3DFT with BCP ceramic resulted in significantly more bone formation both intramuscularly and orthotopically. The effect of BMSCs administration was more pronounced ectopically than orthotopically. Although this is not a posterior spinal fusion model, it is very useful for the screening of different materials as it illustrates their performance in the bone formation processes that are relevant for posterior spinal fusion. Porous titanium combined with BCP is a promising biomaterial for spine fusion applications.

6. Acknowledgements

Authors would like to thank Dr. Maarten Terlou from the Image Analysis Department of the University Utrecht for developing the software used for the histomorphometry and helpful discussion with Dr. Kruyt.

This study was financially supported in part by CAM Implants B.V., Leiden, The Netherlands.

References

1. Damien CJ, Parsons JR. Bone graft and bone graft substitutes: a review of current technology and applications. *J Appl Biomater* 1991;2(3):187-208.
2. Arrington ED, Smith WJ, Chambers HG, Bucknell AL, Davino NA. Complications of iliac crest bone graft harvesting. *Clin Orthop Relat Res* 1996(329):300-9.
3. Brantigan JW, Cunningham BW, Warden K, McAfee PC, Steffee AD. Compression strength of donor bone for posterior lumbar interbody fusion. *Spine* 1993;18(9):1213-21.
4. Rezwan K, Chen QZ, Blaker JJ, Boccaccini AR. Biodegradable and bioactive porous polymer/inorganic composite scaffolds for bone tissue engineering. *Biomaterials* 2006;27(18):3413-31.

5. Ryan G, Pandit A, Apatsidis DP. Fabrication methods of porous metals for use in orthopaedic applications. *Biomaterials* 2006;27(13):2651-70.
6. Crowninshield RD. Mechanical properties of porous metal total hip prostheses. *Instr Course Lect* 1986;35:144-8.
7. Fujibayashi S, Neo M, Kim HM, Kokubo T, Nakamura T. Osteoinduction of porous bioactive titanium metal. *Biomaterials* 2004;25(3):443-50.
8. Habibovic P, Li J, Van Der Valk CM, Meijer G, Layrolle P, Van Blitterswijk CA, De Groot K. Biological performance of uncoated and octacalcium phosphate-coated Ti6Al4V. *Biomaterials* 2005;26(1):23-36.
9. Vehof JW, Spauwen PH, Jansen JA. Bone formation in calcium-phosphate-coated titanium mesh. *Biomaterials* 2000;21(19):2003-9.
10. van den Dolder J, Farber E, Spauwen PH, Jansen JA. Bone tissue reconstruction using titanium fiber mesh combined with rat bone marrow stromal cells. *Biomaterials* 2003;24(10):1745-50.
11. Vehof JW, Mahmood J, Takita H, van't Hof MA, Kuboki Y, Spauwen PH, Jansen JA. Ectopic bone formation in titanium mesh loaded with bone morphogenetic protein and coated with calcium phosphate. *Plast Reconstr Surg* 2001;108(2):434-43.
12. Li JP, de Wijn JR, Van Blitterswijk CA, de Groot K. Porous Ti6Al4V scaffold directly fabricating by rapid prototyping: preparation and in vitro experiment. *Biomaterials* 2006;27(8):1223-35.
13. Tsuruga E, Takita H, Itoh H, Wakisaka Y, Kuboki Y. Pore size of porous hydroxyapatite as the cell-substratum controls BMP-induced osteogenesis. *J Biochem (Tokyo)* 1997;121(2):317-24.
14. Jin QM, Takita H, Kohgo T, Atsumi K, Itoh H, Kuboki Y. Effects of geometry of hydroxyapatite as a cell substratum in BMP-induced ectopic bone formation. *J Biomed Mater Res* 2000;51(3):491-9.
15. Chang BS, Lee CK, Hong KS, Youn HJ, Ryu HS, Chung SS, Park KW. Osteoconduction at porous hydroxyapatite with various pore configurations. *Biomaterials* 2000;21(12):1291-8.
16. Du C, Meijer GJ, van de Valk C, Haan RE, Bezemer JM, Hesseling SC, Cui FZ, de Groot K, Layrolle P. Bone growth in biomimetic apatite coated porous Polyactive 1000PEGT70PBT30 implants. *Biomaterials* 2002;23(23):4649-56.
17. Habibovic P, Yuan H, van den Doel M, Sees TM, van Blitterswijk CA, de Groot K. Relevance of osteoinductive biomaterials in critical-sized orthotopic defect. *J Orthop Res* 2006;24(5):867-76.
18. Habibovic P, Yuan H, van der Valk CM, Meijer G, van Blitterswijk CA, de Groot K. 3D microenvironment as essential element for osteoinduction by biomaterials. *Biomaterials* 2005;26(17):3565-75.

19. Kruyt MC, Wilson CE, de Bruijn JD, van Blitterswijk CA, Oner CF, Verbout AJ, Dhert WJ. The effect of cell-based bone tissue engineering in a goat transverse process model. *Biomaterials* 2006;27(29):5099-106.
20. Kruyt MC, Dhert WJ, Yuan H, Wilson CE, van Blitterswijk CA, Verbout AJ, de Bruijn JD. Bone tissue engineering in a critical size defect compared to ectopic implantations in the goat. *J Orthop Res* 2004;22(3):544-51.
21. Yuan H, Kurashina K, de Bruijn JD, Li Y, de Groot K, Zhang X. A preliminary study on osteoinduction of two kinds of calcium phosphate ceramics. *Biomaterials* 1999;20(19):1799-806.
22. Wilson CE, Kruyt MC, de Bruijn JD, van Blitterswijk CA, Oner FC, Verbout AJ, Dhert WJ. A new in vivo screening model for posterior spinal bone formation: comparison of ten calcium phosphate ceramic material treatments. *Biomaterials* 2006;27(3):302-14.
23. Kruyt MC, de Bruijn JD, Wilson CE, Oner FC, van Blitterswijk CA, Verbout AJ, Dhert WJ. Viable osteogenic cells are obligatory for tissue-engineered ectopic bone formation in goats. *Tissue Eng* 2003;9(2):327-36.
24. Kruyt MC, de Bruijn JD, Yuan H, van Blitterswijk CA, Verbout AJ, Oner FC, Dhert WJ. Optimization of bone tissue engineering in goats: a peroperative seeding method using cryopreserved cells and localized bone formation in calcium phosphate scaffolds. *Transplantation* 2004;77(3):359-65.
25. Kruyt MC, Dhert WJ, Oner C, van Blitterswijk CA, Verbout AJ, de Bruijn JD. Optimization of bone-tissue engineering in goats. *J Biomed Mater Res B Appl Biomater* 2004;69(2):113-20.
26. Yang Z, Yuan H, Tong W, Zou P, Chen W, Zhang X. Osteogenesis in extraskelally implanted porous calcium phosphate ceramics: variability among different kinds of animals. *Biomaterials* 1996;17(22):2131-7.
27. Kruyt MC, van Gaalen SM, Oner FC, Verbout AJ, de Bruijn JD, Dhert WJ. Bone tissue engineering and spinal fusion: the potential of hybrid constructs by combining osteoprogenitor cells and scaffolds. *Biomaterials* 2004;25(9):1463-73.
28. Ohgushi H, Goldberg VM, Caplan AI. Heterotopic osteogenesis in porous ceramics induced by marrow cells. *J Orthop Res* 1989;7(4):568-78.
29. Ohgushi H, Goldberg VM, Caplan AI. Repair of bone defects with marrow cells and porous ceramic. Experiments in rats. *Acta Orthop Scand* 1989;60(3):334-9.
30. Vehof JW, van den Dolder J, de Ruijter JE, Spauwen PH, Jansen JA. Bone formation in CaP-coated and noncoated titanium fiber mesh. *J Biomed Mater Res* 2003;64A(3):417-26.
31. Buckwalter JA, Glimcher MJ, Cooper RR, Recker R. Bone biology. II: Formation, form, modeling, remodeling, and regulation of cell function. *Instr Course Lect* 1996;45:387-99.

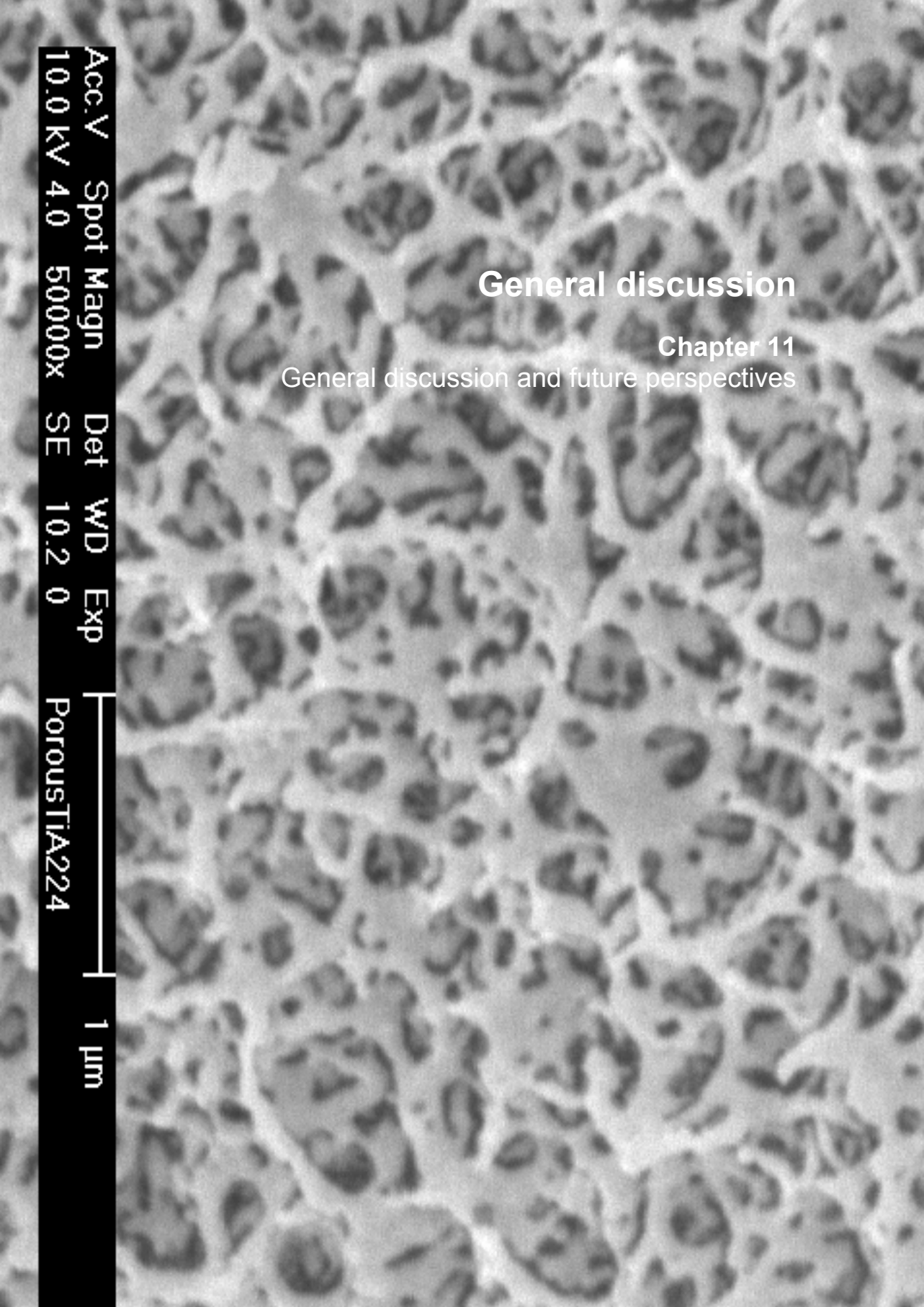
32. Haynesworth SE, Goshima J, Goldberg VM, Caplan AI. Characterization of cells with osteogenic potential from human marrow. *Bone* 1992;13(1):81-8.
33. Yong-Shun Chang, Hai-Ou Gu, Masanori Kobayashi, Oka M. Influence of Various Structure Treatments on Histological Fixation of Titanium Implants. *The Journal of Arthroplasty* 1998;816-824(7).
34. Ishaug-Riley SL, Crane-Kruger GM, Yaszemski MJ, Mikos AG. Three-dimensional culture of rat calvarial osteoblasts in porous biodegradable polymers. *Biomaterials* 1998;19(15):1405-12.
35. Heslop BF, Zeiss IM, Nisbet NW. Studies on transference of bone. I. A comparison of autologous and homologous bone implants with reference to osteocyte survival, osteogenesis and host reaction. *Br J Exp Pathol* 1960;41:269-87.

General discussion

Chapter 11

General discussion and future perspectives

Acc.V 10.0kV Spot 4.0 Magn 500000x Det SE WD 10.2 Exp 0
PorousTiA224 1 μ m



Chapter 11

General discussion and future perspectives

1. General discussion

Metallic biomaterials are of importance in skeletal repair. A brief overview of metallic implant materials currently used in trauma-, orthopedic- and maxillofacial surgery is given in **Chapter 1**. Currently, titanium, titanium alloys, stainless steels and cobalt-chromium alloys are often used for production of bone graft substitutes. In particular titanium and its alloys are currently receiving more attention in both the medical and the dental field owing to excellent biocompatibility, light weight, good balance of mechanical properties, corrosion resistance, etc. They are mainly used in implant devices for replacement of failed hard tissue, for example, artificial hip joints, artificial knee joints, bone plates, dental implants, etc. [1-7]. The increasing demand for synthetic bone graft substitutes is accompanied by the need to develop synthetic biomaterials which have the ability to better adopt to the *in vivo* environment both from biological and mechanical point of view. Implant stability is not only a function of its strength but is also dependent upon the degree of fixation within the surrounding tissues. In the past, such implant stability was primarily achieved using screws [8-11] and bone cement [9,12,13], but in many instances it is preferred to achieve some measure of biological union, that is to permit tissue growth to actively bond the implant to the living structures.

Porous metallic systems possess a large potential to advance the current generation of prostheses and to address unresolved clinical applications [4,14-18]. The Young's modulus of porous systems can be tailored by changing the level of porosity in such a way that it matches the Young's modulus of natural bone. Adaptation of Young's modulus of the implant to that of the surrounding tissue is important in order to avoid problems of stress shielding that often occur in solid metallic implants. Implantations of porous implants based on materials such as titanium and cobalt chromium have shown a high degree of bone ingrowth and body fluid transport through their three-dimensional interconnected array of pores [19-23]. A review of the current methods for fabricating porous titanium and its alloy, as well as advantages and limitations of various methods are also presented **Chapter 1**. In the past years, the value of implant systems exhibiting surface or total bulk porosity have led researchers to conduct investigations aimed at clarifying some fundamental aspects of porous implant/tissue interactions. In the

first chapter of this thesis critical requirements and challenges in development of these implants to facilitate bone ingrowth are also outlined and discussed.

To improve performance and longevity of metallic orthopedic implants, research described in this thesis aimed at developing porous titanium alloy structures that allow for bone ingrowth, fixation of the implant within surrounding tissue and provide a satisfying mechanical support. In **Chapters 2-10**, attempts to design, develop and fabricate new porous titanium alloy structures and to evaluate their biological properties in vitro and in vivo are described. The achievements of the research described in this thesis will be attended by answering the following questions:

1. How can we develop porous titanium to mimic cancellous bone structure?
2. How can we design porous titanium that meets various requirements to be used as successful orthopaedic implant?
3. What are the similarities and differences between porous titanium alloy made by sponge replication and 3D fiber deposition?
4. What is the influence of pore architecture on bone ingrowth during orthotopic implantation?
5. What is the influence of scaffold composition on bone formation in vivo?

1.1. Mimicking the structure of cancellous bone: porous titanium alloy by sponge replication

In **Chapters 2-4**, the development of porous titanium alloy made by sponge replication is described. The final product of sponge replication method to produce porous titanium alloy scaffolds had a high and interconnected porosity with a regular pore shape and size. The structure was very similar to that of cancellous bone (**Chapter 3**). With regard to the processing route, rheological properties of Ti6Al4V slurry were shown to be a key issue in the preparation of porous Ti6Al4V. Influences on rheological properties were addressed in terms of Ti6Al4V particle size and shape, concentration of powder, type of binder, pH value and presence of air bubbles. Finally, Ti6Al4V slurry was optimized to produce porous Ti6Al4V with desirable sponge structure. In addition, the study described in **Chapter 3** aimed at characterizing porous Ti6Al4V with regard to porous structure, mechanical properties, chemical composition, phase composition during heat treatment etc. Porous Ti6Al4V made by sponge replication method had a three dimensional trabecular porous structure with interconnected pores ranging from 400 μm to 700 μm and a total porosity of about 90%. The compressive strength was 10.3 ± 3.3 MPa and the Young's modulus 0.8 ± 0.3 GPa. An attempt to further improve porous Ti6Al4V to resemble cancellous bone in terms of porous structure and mechanical properties by coating the sponge with multi layers of Ti6Al4V slurry was described

in **Chapter 4**. After two additional coating steps, pore size ranged from 100 μm to 700 μm , and the porosity was decreased from $\sim 90\%$ to $\sim 75\%$, while the compressive strength and the Young's modulus increased from 10.3 ± 3.3 MPa to 59.4 ± 20.3 MPa and from 0.8 ± 0.3 GPa to 1.8 ± 0.3 GPa, respectively. The pore size and porosity of the final scaffold were similar to that of cancellous bone. The compressive strength was higher than that of cancellous bone, and the Young's modulus value lied between that of cancellous and cortical bone.

The conclusion of the first part of this thesis is that sponge replication is a method that can successfully be employed to produce porous titanium alloy implants, and that by applying multiple slurry coatings, the porosity, pore size and mechanical properties of the final scaffold can be controlled. Therefore, sponge replication method can be applied to produce porous metallic implants that match bone properties. We have used sponge replication to produce various porous titanium orthopaedic implant prototypes, such as an acetabular cup for total hip joint replacement (Fig. 1A), and a porous surfaced hip stem and tibia tray (Fig. 1B and 1C).



Fig.1 Prototypes of porous titanium (alloy) orthopaedic implants made by sponge replication: (A) Acetabular cup for total hip joint replacement; (B) Porous Ti6Al4V as coating on hip stem, (C) Porous titanium as coating on tibia tray.

1.2. Producing customized implants: rapid prototyping porous titanium alloy using 3D fiber deposition

In **Chapter 5**, we described the development of porous titanium using a novel 3D fiber deposition technique which allows for design and production of scaffolds with precisely controlled characteristics, such as porosity, pore size and pore interconnectivity.

Based on computer designed 3D geometry, Ti6Al4V scaffolds could directly be fabricated by 3D fiber deposition. A key feature of this RP technology is the three-dimensional dispensing of Ti6Al4V slurry at room temperature to produce porous scaffold made of layers of directionally aligned fibers using a computer controlled process. Scaffolds that are impossible to generate using conventional machining methods can therefore be produced. Material can be deposited over the entire

layer without constraint, and the property of Ti6Al4V slurry to solidify immediately after deposition eliminates geometrical restrictions, allowing different layers to be deposited on top of each other without additional support. 3D fiber deposition can be used for producing different porous structures, such as scaffolds with staggered spacing, different pore shapes, anisotropic scaffolds with pore size gradient, etc. In **Chapters 6** and **7**, the influences of different architectures on mechanical properties and permeability of the scaffold were investigated. Mechanical analysis revealed that compressive strength and Young's modulus increase with decreasing porosity. The permeability results showed that not only total porosity but also porous structure can influence the permeability. It was revealed that 3D fiber deposition method provides a good control and reproducibility of the desired degree of porosity and shape of 3D porous structure. The flexibility and versatility of 3D fiber deposition as described in **Chapter 7** provided an elegant method to further investigate the effects of scaffold architecture on bone formation in vivo.

1.3. Comparison of sponge replication and 3D fiber deposition method for production of porous titanium alloy implants

An investigation of the in vitro behavior of cells on sponge replication and 3D fiber deposition porous Ti6Al4V scaffold is described in **Chapter 3** and **Chapter 5**. The results showed that cells were able to attach and spread on the surfaces of both scaffold types, and to subsequently form extracellular matrix. There was no difference in the behavior of cells between the two scaffold types, as they were produced from the same titanium alloy powder but different process techniques.

In **Chapter 8**, porous titanium scaffolds, produced by sponge replication and 3D fiber deposition respectively, were compared in terms of structure and mechanical properties. Macrostructure of the two scaffold types differed, but their microstructure was similar, probably due to the same post-fabrication sintering procedure. Both scaffolds revealed an open porous structure. The fiber deposited scaffolds consisted of fairly regular open pores in contrast to the sponge replica ones, which exhibited a more irregular pore structure similar to that of cancellous bone. While the length to thickness ratio of the individual trabecular struts of cancellous bone is about 4 [4], sponge replication titanium alloy scaffolds had a length to diameter ratio of the struts of about 10, making these structures imperfection sensitive and susceptible to micro-buckling. 3D fiber deposition titanium scaffolds had a regular pore structure with a structural fiber length to diameter ratio of $1000/400\mu\text{m} = 2.5$. Due to these structural differences, mechanical properties of the two scaffold types, such as stiffness and strength were different. The compressive strength and the Young's modulus of both types of

porous Ti6Al4V scaffolds were higher than that of cancellous bone, while the permeability of both scaffold types was comparable to that of cancellous bone.

The Young's moduli of some commonly used implant materials are shown in Fig.2 [24,25]. It can be seen that the Young's modulus's of sponge replication titanium alloy (Sponge Ti) and 3D fiber deposited titanium alloy (3DF) lies between that of cancellous and cortical bone.

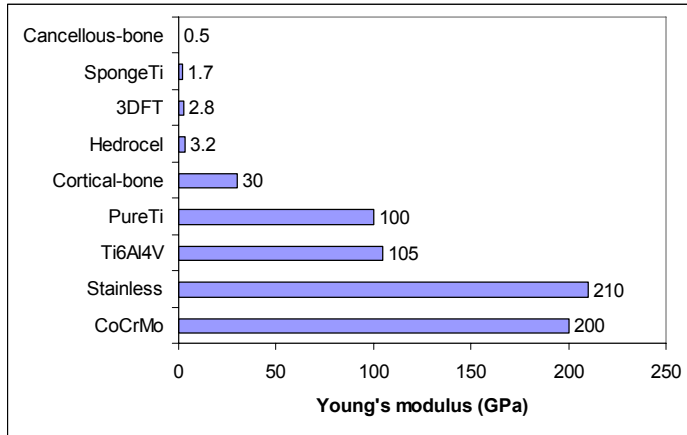


Fig.2 Young's moduli of different biomaterials

Fig.3 exhibits compressive strength of various implant materials [24,25]. Compressive strength of both porous Ti6Al4V types is higher than that of ceramics, polymers and trabecular (cancellous) bone. Sponge replication porous titanium has a compressive strength similar to the commercially available Hydrocel made of tantalum, while compressive strength of fiber deposited titanium alloy lies between that of cancellous and cortical bone.

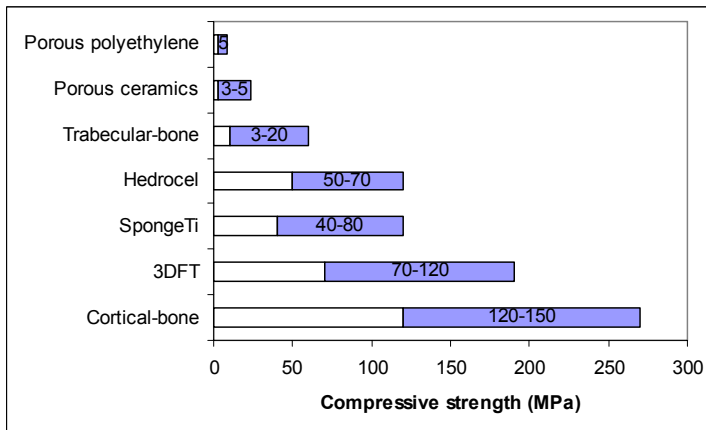


Fig.3 Compressive strength of different porous materials

From the biomechanical point of view, it is desirable to have an implant with the Young's modulus comparable to that of natural bone in order to achieve a good load transfer from the implant to the surrounding bone, leading to a continuous stimulation of new bone formation [26]. As earlier mentioned, the Young's modulus of porous material is dependent on its porosity [27]; the higher the porosity, the lower the Young's Modulus. However, with the increasing porosity, the compressive strength of porous material is decreased too. Therefore, a compromise should be reached between mechanical properties and porosity of material in order to design an optimally functioning orthopedic implant.

In an *in vivo* study, sponge replication porous Ti6Al4V and 3D fiber deposited porous Ti6Al4V were implanted on decorticated transverse processes of goat lumbar spine. Total amount of newly formed bone was higher in sponge replication scaffolds than in 3D fiber deposited ones, probably due to the larger pore size and a higher porosity of former scaffold, which is considered beneficial for cell attachment and diffusion, vascularization and subsequent new bone formation [28-31]. With regard to bone formation in the available pore space, no significant difference was found between the two scaffold types, suggesting that pore size and pore shape have a weaker effect on the bone formation when the pore size is above 400 μm , which is in agreement with studies by others [32,33].

1.4. Influence of pore architecture on bone formation

In **Chapter 9**, a study is presented in which, using 3D fiber deposition, Ti6Al4V scaffolds with different structural properties, such as pore size, porosity and interconnecting pore size were fabricated and implanted on the decorticated transverse processes of the posterior lumbar spine of 10 goats for 12 weeks. The designed pore sizes of implants evaluated in this study were between the lower and the upper limit of the generally accepted "optimal pore range" for porous materials [2,22,28,32,34,35]. Data showed that scaffold with a pore size of 200 μm had significantly less bone ingrowth as compared to the scaffolds with larger pore size. And further, implants with a large pore size of 700 μm conducted most new bone formation. The positive effect of increasing pore size was visible up to the diameter of 400 μm , which is in agreement with previously published studies [32,33]. This study also showed that not only pore size but also the interconnecting pore size of the implant significantly affects osteoconductive properties of porous titanium alloy implants. Two scaffolds with similar porosity but different interconnecting pore sizes were compared. Better results were obtained with implants with large interconnecting pore size as compared to the ones with smaller interconnecting pore size. These results are in agreement with many studies suggesting that good interconnecting fenestrations in porous implants are essential

to provide the space for vascular tissue ingrowth followed by new bone formation [28,29,32,35-37].

Although increased porosity and pore size are obviously preferential for new bone growth facilitation in porous titanium alloy implants, it should be kept in mind that another consequence of the porosity and pore size increase is reduction of the implant mechanical properties. Thus depending on the intended application, a balance between mechanical properties and the biological performance should be found.

1.5. Influence of scaffold composition on bone formation

The ability of porous titanium and its alloys to conduct new bone formation is limited since they are considered bioinert, by many. Therefore, in order to improve their biological performance it might be necessary to either combine them with other, more bioactive biomaterials or to improve their bioactivity by surface modification. Coating titanium alloy surfaces with CaP ceramic coatings and chemical and thermal treatments of the surface have been reported to be successful ways of increasing metal bioactivity in vivo [38,39]. Recently, some efforts have been carried out to study the effect of surface treatments on porous titanium. Habibovic et.al [39,40] studied biological performance of uncoated and octacalcium phosphate coated sponge replication Ti6Al4V in goats. The coated implants performed better than the uncoated ones when implanted in a bony defect and intramuscularly, they revealed osteoinductive capacity. Takemoto et.al [41] applied alkali-treatment on the porous titanium. After treatment, porous titanium showed bioactivity in vitro, and osteoconductivity as well as osteoinductivity in vivo.

In the study of **Chapter 10**, we investigated the behavior of 3D fiber deposited Ti6Al4V porous implants and 3D fiber deposited Ti6Al4V porous implants combined with porous biphasic calcium phosphate (BCP) ceramic either alone or as tissue-engineered constructs loaded with autologous bone marrow stromal cells by implanting them in paraspinal muscles and on lumbar transverse processes of goats. BCP ceramic was chosen for the preparation of composite implants, since previous in vivo studies have shown that this material has a high osteoinductive and osteoconductive potential [42,43]. Intramuscularly, there was a significant difference between metallic and composite implants both with and without bone marrow stromal cells. The amount of bone formed intramuscularly in tissue-engineered constructs based on composite material was significantly higher as compared to bare composite implants. In implants without added cells, intramuscular bone formation was found in the ceramic part of the implant, confirming its earlier found osteoinductivity, while no bone was induced by the metallic implants without ceramic. Similar to intramuscular results, the presence of

BCP ceramic had a significantly positive effect on new bone formation at orthotopic implantation sites. Even though BCP ceramic was not in direct contact with either underlying bone of the transverse process or with the muscle covering the cage, its excellent bioactivity was apparent in both the amount and the rate of new bone formation. However, no significant difference was found between tissue-engineered scaffolds and implants without cells.

This study showed that chemical composition of the implant material is very important for its behavior in the role of bone graft substitute. Titanium is considered a bioinert material by many, and even when bone marrow cells are preoperatively seeded on the scaffold, new bone formation is limited. However, when metal is combined with a bioactive material such as calcium phosphate ceramic, both osteoconductive and osteoinductive properties of the implant are significantly improved.

2. Future perspectives

In the work presented by this thesis, we have developed porous titanium alloys with highly interconnected and open porous architecture, as well as satisfying mechanical properties. From the biomechanical point of view, it is probably desirable to have a low Young's modulus comparable to that of surrounding bone at the interface of implant and bone, and a gradually increasing Young's modulus away from this interface in order to achieve a continuous load transfer from the bone to the implant [26]. This can be achieved by introducing gradient porosity into the implant. By using the 3D fiber deposition technique as described in this thesis (**Chapter 6 and 7**), in addition to varying scaffold fiber spacing and lay down pattern, in the future, nozzles and syringe can be varied during processing in order to deposit fibers with different diameter and different composition. As a result, interconnecting pore size, volume fraction, fiber orientation, surface chemistry and mechanical properties could be controlled from one layer to another. In this way, anatomically shaped or customized implants can be produced, which may have a significant impact for clinical applications [44,45]. For example, varying scaffold architectures could be produced based directly on 3D CAD models and/or CT/MRI scans of actual defects.

The ability to control various properties of porous implants using 3D fiber deposition technique provides tools for performing parametric analyses in terms of nutrient concentration and local environments, which is essential in order to identify and predict optimal cell environment and to understand the effect of implant on tissue regeneration. Moreover, finite element diffusion/perfusion studies are more feasible when scaffolds with regular architecture, such as ones produced by fiber deposition, are employed.

The screening model of transverse process of goat lumbar spine as used in the studies presented in this thesis is useful for the initial characterization of new porous biomaterials. However, mechanical conditioning or stimulation of bone formation and remodeling has been shown to be important for the final performance of implants [46-50]. It is therefore important to design a load-bearing model that resembles clinical situation as closely as possible in order to optimize relevant properties of porous implant. To evaluate the success of orthopedic implants in bone repair, long-term functional stability study is necessary. The time needed to clinically evaluate novel scaffold technologies and treatment options limits rapid innovation and development of repair strategies.

Finally, the important issue is how to improve existing medical devices and/or develop new approaches and systems for long term implantation. The new porous titanium scaffolds described in this thesis offer possibility of in-depth study of relationships between physical, mechanical, chemical and biological properties of implants and allow for further optimization as required for the improvement of life quality in the world with increasing life expectancy.

Reference

1. Smith DC, Lugowski S, McHugh A, Deporter D, Watson PA, Chipman M. Systemic metal ion levels in dental implant patients. *Int J Oral Maxillofac Implants* 1997;12(6):828-34.
2. Pilliar RM. Porous-surfaced metallic implants for orthopedic applications. *J Biomed Mater Res* 1987;21(A1 Suppl):1-33.
3. Cook SD, Georgette FS, Skinner HB, Haddad RJ, Jr. Fatigue properties of carbon- and porous-coated Ti-6Al-4V alloy. *J Biomed Mater Res* 1984;18(5):497-512.
4. Hirshorn MS, Holley LK, Hales JR, Money DK, Young FA, Spector M, Wickham GG. Screening of solid and porous materials for pacemaker electrodes. *Pacing Clin Electrophysiol* 1981;4(4):380-90.
5. Hong SB, Eliaz N, Leisk GG, Sach EM, Latanision RM, Allen SM. A new Ti-5Ag alloy for customized prostheses by three-dimensional printing (3DP). *J Dent Res* 2001;80(3):860-3.
6. Pilliar RM, Deporter DA, Watson PA, Valiquette N. Dental implant design--effect on bone remodeling. *J Biomed Mater Res* 1991;25(4):467-83.
7. Long M, Rack HJ. Review Titanium alloys in total joint replacement materials science perspective. *Biomaterials* 1998;19:1621-1639.
8. Li DL, Ferguson SJ, Beutler T, Cochran DL. Biomechanical comparison of the sandblasted and acid-etched and the machined and acid-etched titanium surface for dental implants. *J Biomed Mater Res* 2002;60:325-32.

9. Cameron HU, Jacob R, Macnab I, Pilliar RM. Use of polymethylmethacrylate to enhance screw fixation in bone. *J Bone Joint Surg Am* 1975;57(5):655-6.
10. Bobynd JD, Cameron HU, Abdulla D, Pilliar RM, Weatherly GC. Biologic fixation and bone modeling with an unconstrained canine total knee prosthesis. *Clin Orthop* 1982(166):301-12.
11. Thanner J. The acetabular component in total hip arthroplasty. Evaluation of different fixation principles. *Acta Orthop Scand Suppl* 1999;286:1-41.
12. Ryan G, Pandit A, Apatsidis DP. Fabrication methods of porous metals for use in orthopaedic applications. *Biomaterials* 2006;27(13):2651-70.
13. Fujita H, Iida H, Ido K, Matsuda Y, Oka M, Nakamura T. Porous apatite-wollastonite glass-ceramic as an intramedullary plug. *J Bone Joint Surg Br* 2000;82(4):614-8.
14. Bhardwaj T, Pilliar RM, Grynpas MD, Kandel RA. Effect of material geometry on cartilagenous tissue formation in vitro. *J Biomed Mater Res* 2001;57(2):190-9.
15. Crowninshield RD. Mechanical properties of porous metal total hip prostheses. *Instr Course Lect* 1986;35:144-8.
16. Vehof JW, Spauwen PH, Jansen JA. Bone formation in calcium-phosphate-coated titanium mesh. *Biomaterials* 2000;21(19):2003-9.
17. Orton EC, Polher O, Shenk R, Hohn RB. Comparison of porous titanium-surfaced and standard smooth-surfaced bone plates and screws in an unstable fracture model in dogs. *Am J Vet Res* 1986;47(3):677-82.
18. Colella SM, Miller AG, Stang RG, Stoebe TG, Spengler DM. Fixation of porous titanium implants in cortical bone enhanced by electrical stimulation. *J Biomed Mater Res* 1981;15(1):37-46.
19. Cameron HU, Macnab I, Pilliar RM. A porous metal system for joint replacement surgery. *Int J Artif Organs* 1978;1(2):104-9.
20. Pilliar RM. Dental implants: materials and design. *J Can Dent Assoc* 1990;56(9):857-61.
21. Pilliar RM. Porous surfaced endosseous dental implants: fixation by bone ingrowth. *Univ Tor Dent J* 1988;1(2):10-5.
22. Pilliar RM. P/M Processing of Surgical Implants: Sintered Porous Surfaces for Tissue-to-Implant Fixation. *International Journal of Powder Metallurgy* 1998;34(8):33-45.
23. Pilliar RM, Deporter DA, Watson PA, Todescan R. The Endopore implant-enhanced osseointegration with a sintered porous- surfaced design. *Oral Health* 1998;88(7):61-4.
24. Bobynd JD, Hacking SA, Chan SP. Characterization of a new porous tantalum biomaterial for reconstructive orthopaedics.; 1999; Anaheim, CA.
25. Krygier JJ, Bobynd JD, Poggie RA. Mechanical characterization of a new porous tantalum biomaterial for orthopaedic reconstruction.; 1999; Sydney, Australia.

26. McGovern TE, Black J, Jacobs JJ. In vivo wear of Ti-6Al-4V femoral heads: a retrieval study. *J Biomed Mater Res* 1996;32:447-457.
27. Gibson LJ, Ashby MF. *Cellular Solids: Structure and Properties*. Cambridge: Cambridge University Press; 1997.
28. Karageorgiou V, Kaplan D. Porosity of 3D biomaterial scaffolds and osteogenesis. *Biomaterials* 2005;26(27):5474-91.
29. Mastrogiacomo M, Scaglione S, Martinetti R, Dolcini L, Beltrame F, Cancedda R, Quarto R. Role of scaffold internal structure on in vivo bone formation in macroporous calcium phosphate bioceramics. *Biomaterials* 2006;27(17):3230-7.
30. Pilliar RM. Powder metal-made orthopedic implants with porous surface for fixation by tissue ingrowth. *Clin Orthop* 1983(176):42-51.
31. Schliephake H, Neukam FW, Klosa D. Influence of pore dimensions on bone ingrowth into porous hydroxylapatite blocks used as bone graft substitutes. A histometric study. *Int J Oral Maxillofac Surg* 1991;20(1):53-8.
32. Hollister S, Lin C, Saito E, Schek R, Taboas J, Williams J, Partee B, Flanagan C, Diggs A, Wilke E and others. Engineering craniofacial scaffolds. *Orthod Craniofac Res* 2005;8(3):162-73.
33. Hollister SJ. Porous scaffold design for tissue engineering. *Nat Mater* 2005;4(7):518-24.
34. Bobynd JD, Pilliar RM, Cameron HU, Weatherly GC. The optimum pore size for the fixation of porous-surfaced metal implants by the ingrowth of bone. *Clin Orthop* 1980(150):263-70.
35. Sachlos E, Czernuszka JT. Making tissue engineering scaffolds work. Review: the application of solid freeform fabrication technology to the production of tissue engineering scaffolds. *Eur Cell Mater* 2003;5:29-39; discussion 39-40.
36. Nishikawa M, Myoui A, Ohgushi H, Ikeuchi M, Tamai N, Yoshikawa H. Bone tissue engineering using novel interconnected porous hydroxyapatite ceramics combined with marrow mesenchymal cells: quantitative and three-dimensional image analysis. *Cell Transplant* 2004;13(4):367-76.
37. Shimko DA, Shimko VF, Sander EA, Dickson KF, Nauman EA. Effect of porosity on the fluid flow characteristics and mechanical properties of tantalum scaffolds. *J Biomed Mater Res B Appl Biomater* 2005;73(2):315-24.
38. Spoerke ED, Murray NG, Li H, Brinson LC, Dunand DC, Stupp SI. A bioactive titanium foam scaffold for bone repair. *Acta Biomater* 2005;1(5):523-33.
39. Habibovic P, Li J, Van Der Valk CM, Meijer G, Layrolle P, Van Blitterswijk CA, De Groot K. Biological performance of uncoated and octacalcium phosphate-coated Ti6Al4V. *Biomaterials* 2005;26(1):23-36.

40. Habibovic P, van der Valk CM, van Blitterswijk CA, De Groot K, Meijer G. Influence of octacalcium phosphate coating on osteoinductive properties of biomaterials. *J Mater Sci Mater Med* 2004;15(4):373-80.
41. Takemoto M, Fujibayashi S, Neo M, Suzuki J, Matsushita T, Kokubo T, Nakamura T. Osteoinductive porous titanium implants: effect of sodium removal by dilute HCl treatment. *Biomaterials* 2006;27(13):2682-91.
42. Habibovic P, Yuan H, van den Doel M, Sees TM, van Blitterswijk CA, de Groot K. Relevance of osteoinductive biomaterials in critical-sized orthotopic defect. *J Orthop Res* 2006;24(5):867-76.
43. Yang Z, Yuan H, Tong W, Zou P, Chen W, Zhang X. Osteogenesis in extraskeletally implanted porous calcium phosphate ceramics: variability among different kinds of animals. *Biomaterials* 1996;17(22):2131-7.
44. Schantz JT, Hutmacher DW, Lam CX, Brinkmann M, Wong KM, Lim TC, Chou N, Guldberg RE, Teoh SH. Repair of calvarial defects with customised tissue-engineered bone grafts II. Evaluation of cellular efficiency and efficacy in vivo. *Tissue Eng* 2003;9 Suppl 1:S127-39.
45. Schantz JT, Teoh SH, Lim TC, Endres M, Lam CX, Hutmacher DW. Repair of calvarial defects with customized tissue-engineered bone grafts I. Evaluation of osteogenesis in a three-dimensional culture system. *Tissue Eng* 2003;9 Suppl 1:S113-26.
46. Quinn TM, Grodzinsky AJ, Buschmann MD, Kim YJ, Hunziker EB. Mechanical compression alters proteoglycan deposition and matrix deformation around individual cells in cartilage explants. *J Cell Sci* 1998;111 (Pt 5):573-83.
47. Carver SE, Heath CA. Influence of intermittent pressure, fluid flow, and mixing on the regenerative properties of articular chondrocytes. *Biotechnol Bioeng* 1999;65(3):274-81.
48. Carver SE, Heath CA. Semi-continuous perfusion system for delivering intermittent physiological pressure to regenerating cartilage. *Tissue Eng* 1999;5(1):1-11.
49. Guilak F, Meyer BC, Ratcliffe A, Mow VC. The effects of matrix compression on proteoglycan metabolism in articular cartilage explants. *Osteoarthritis Cartilage* 1994;2(2):91-101.
50. Piscoya JL, Fermor B, Kraus VB, Stabler TV, Guilak F. The influence of mechanical compression on the induction of osteoarthritis-related biomarkers in articular cartilage explants. *Osteoarthritis Cartilage* 2005;13(12):1092-9.

Summary

Metallic biomaterials have so far shown the greatest potential to be the basis of implants for long-term load-bearing orthopedic and dental applications, owing to their excellent mechanical strength when compared to alternative biomaterials, such as polymers and ceramics. Particularly titanium and its alloys are currently receiving much attention because of their biocompatibility, light weight, excellent balance of mechanical properties, corrosion resistance, etc. They are mainly used in implant devices for replacement of failed hard tissue such as artificial hip and knee joints, bone plates and dental implants. In general, failure of joint replacements due to the mechanical failure of materials such as fatigue fracture of the implant seldom occurs. A more common cause of arthroplasty failure is aseptic loosening of the implant that occurs several years after the implant has been in situ and functioning reasonably, due to interfacial instability within host tissues, biomechanical mismatch of Young's modulus and lacking biological anchorage through tissue ingrowth.

The improvement of longevity of orthopedic implants is of great importance for the quality of human life. Continuous increase of life expectancy demands improvement of existing medical devices and/or development of new approaches and systems, which can only be achieved by a more in-depth understanding of relationships between physical, mechanical, chemical and biological properties of biomaterials.

For many applications, strength considerations seem to require the use of the materials in their solid form but at an increasing rate also porous structures are being used, either as a coating or as structural material. The most important advantage of porous implants is that they allow for ingrowth of bone and other tissues into the pores of the implant, resulting in a mechanical interlocking with the surrounding tissue and a better implant fixation. Most existing methods for the production of porous metallic implants exhibit some important drawbacks, such as lack of good pore size control, low porosity and poor pore interconnectivity and there exists therefore the need for new, improved techniques.

This thesis focuses on two main goals: (1) Developing new methods to fabricate porous titanium and titanium alloys that allow for bone ingrowth, fixation of the implant within surrounding tissue and provide a satisfying mechanical support and (2) Investigating biological behavior of different porous titanium scaffolds to address relative influences of various chemical, physical and structural parameters on their performance in the role of bone graft substitute for orthopedic and maxillofacial surgery.

In Chapter 1 we reviewed the current methods for fabricating porous titanium and its alloys, as well as advantages and limitations of various methods. We also described critical requirements and challenges in development of porous titanium implants to optimize their biological performance. Based on these requirements, we developed two methods to fabricate porous Ti6Al4V: sponge replication and 3D fiber deposition.

In Chapters 2-4, we focused on the development of sponge replication porous Ti6Al4V to mimic the structure of cancellous bone. In Chapter 2, the Ti6Al4V slurry for sponge replication process was optimized and influences of rheological properties of the slurry were discussed in detail. In Chapter 3 we characterized sponge replication porous Ti6Al4V with regard to porous structure, mechanical properties, chemical composition etc. The final product of this method to produce porous titanium alloy scaffolds had a three dimensional trabecular porous structure with interconnected pores, which was very similar to that of cancellous bone. In Chapter 4 we made an attempt to further improve porous Ti6Al4V to resemble cancellous bone in terms of porous structure and mechanical properties by coating the sponge with multi layers of Ti6Al4V slurry. The pore size and porosity of the final scaffold were similar to that of cancellous bone. The compressive strength was higher than that of cancellous bone, and the Young's modulus value lied between those of cancellous and cortical bone.

In Chapter 5, we described the development of porous titanium alloy using a novel 3D fiber deposition technique which allows for design and production of scaffolds with precisely controlled characteristics, such as porosity, pore size and pore interconnectivity. We were able to control both the design of the external shape of the implant and its internal porous structure. In Chapters 6 and 7, we investigated the influences of different architectures on mechanical properties and permeability of the scaffold. The results showed that 3D fiber deposition is a good way to produce customized implants with the desired degree of porosity and shape of 3D porous structure. 3D fiber deposition also provides an elegant method to further investigate the effects of scaffold architecture parameters on bone formation *in vivo*.

In Chapter 8, porous titanium alloy scaffolds, produced by sponge replication and 3D fiber deposition respectively, were compared in terms of structure, mechanical properties and permeability. Macrostructure of the two scaffold types differed, but their microstructure was similar. Both scaffolds revealed an open porous structure. The fiber deposited scaffolds consisted of fairly regular open pores in contrast to the sponge replica ones, which exhibited a more irregular pore structure similar to that of cancellous bone. The compressive strength and the Young's modulus of both types of porous Ti6Al4V scaffolds were higher than that of cancellous bone,

while the permeability of both scaffold types was comparable to that of cancellous bone. In an in vivo study, total amount of newly formed bone was higher in sponge replication scaffolds than in 3D fiber deposited ones, which suggested that the larger pore size and a higher porosity degree are beneficial for cell attachment and diffusion, vascularization and subsequent new bone formation.

In Chapter 9 a study is described in which we implanted porous Ti6Al4V scaffolds with different structural properties made by 3D fiber deposition on the decorticated transverse processes of the posterior lumbar spine of goats to investigate influence of pore architecture on bone formation. The results showed that not only pore size and porosity but also the interconnecting pore size of the implant significantly affects osteoconductive properties of porous titanium alloy implants.

Chapter 10 describes a study where we investigated the behavior of 3D fiber deposited Ti6Al4V porous implants and 3D fiber deposited Ti6Al4V porous implants combined with porous biphasic calcium phosphate ceramic either alone or as tissue-engineered constructs loaded with autologous bone marrow stromal cells by implanting them in paraspinal muscles and on lumbar transverse processes of goats. The results showed that chemical composition of the implant material is very important for its behavior in the role of bone graft substitute. Titanium is a bioinert material, and even when bone marrow cells are preoperatively seeded on the scaffold, new bone formation is limited. However, when metal is combined with a bioactive material such as calcium phosphate ceramic, both osteoconductive and osteoinductive properties of the implant are significantly improved.

In conclusion, the work presented in this thesis shows that both sponge replication and 3D fiber deposition are suitable methods for producing porous titanium and titanium alloy scaffolds with well controlled structural and hence mechanical characteristics. Both methods have therefore the potency to be successfully applied for the production of implants for orthopedic and dental surgery.

Samenvatting

Dank zij hun hoge mechanische sterkte vergeleken met polymeren en keramieken zijn metallische biomaterialen tot nu toe het meest geschikt gebleken voor de vervaardiging van mechanisch belaste implantaten voor langdurige toepassing in orthopedie en tandheelkunde. Vooral titanium en legeringen ervan genieten veel belangstelling door hun biocompatibiliteit, lichte gewicht, de goede mix van mechanische eigenschappen, de corrosie weerstand, etc. De voornaamste toepassingen ervan liggen op het gebied van implantaten ter vervanging van ziek of ontbrekend hard weefsel, zoals bij artificiële heup- en kniegewrichten, botplaatjes of tandimplantaten. Het falen van gewrichtsvervangingen door mechanische (vermoeidheids-) breuk komt dan ook zelden voor. Complicaties met arthroplastieën worden meestal veroorzaakt door steriele loslating na een aantal jaren van bevredigend functioneren en door instabiele fixatie, bijvoorbeeld door het ontbreken van weefselingroei, of door een biomechanische mismatch van Young's moduli.

Verbetering van de levensduur van orthopedische implantaten is van groot belang voor verbetering van de kwaliteit van leven. De toename van de levensverwachting van de mens vraagt voortdurende verbetering van de bestaande medische voorzieningen en/of de ontwikkeling van nieuwe methoden en technieken wat alleen bereikt kan worden via meer gedetailleerde kennis van de relaties tussen de fysische, mechanische, chemische en de biologische eigenschappen van biomaterialen.

Voor veel toepassingen vereisen sterkte overwegingen het gebruik van de materialen in massieve vorm zoals bij femur-, knie- en tandprothesen maar steeds vaker worden ook poreuze structuren ingezet, het zij als coating hetzij als structureel materiaal.

Een belangrijk voordeel van poreuze implantaten is dat deze de ingroei van bot en andere weefsel mogelijk maken waardoor een betere implantaat fixatie ontstaat. Voor de productie van poreuze metallische implantaten is het nodig een goede controle te hebben over het porie volume, de porie afmetingen en over de verbinding tussen de poriën afzonderlijk en dat is waar het bij de meeste productiewijzen aan ontbreekt en waarom de ontwikkeling van nieuwe technieken wenselijk is.

Dit proefschrift stelt zich tweeërlei doel: (1) de ontwikkeling van nieuwe methoden ter vervaardiging van poreus titanium en titaniumlegeringen waardoor ingroei van weefsel gecombineerd met een goede mechanische ondersteuning mogelijk wordt en (2) onderzoek naar de biologische reacties op verschillende poreuze "scaffolds" van titanium om de invloed van de diverse chemische, fysische en

structuurparameters op het gedrag ervan in toepassingen als botvervanger in orthopedie en kaakchirurgie te bepalen.

In hoofdstuk 1 wordt een overzicht gegeven van de tot nu toe gebruikelijke technieken om poreus titanium en titaniumlegeringen te vervaardigen tegelijk met de voordelen en beperkingen ervan. Ook beschrijven we de kritische factoren en uitdagingen die er liggen voor optimalisatie van de biologische prestaties. Gebaseerd op deze overwegingen ontwikkelden we twee methoden ter vervaardiging van poreus Ti6Al4V: spons replicatie en “3D fiber deposition”.

In de hoofdstukken 2 – 4 ligt het accent op de ontwikkeling van spons-gerepliceerd poreus Ti6Al4V ter imitatie van de structuur van spongieus bot.

Hoofdstuk 2 beschrijft de optimalisatie van de voor het replicatie proces benodigde Ti6Al4V-dispersie en wordt de rol van de reologische eigenschappen ervan tot in detail besproken. In hoofdstuk 3 wordt het spons gerepliceerde Ti6Al4V gekarakteriseerd voor wat betreft structuur, mechanische eigenschappen, chemische samenstelling, etc. Het product van deze methode vertoont een poreuze structuur die veel lijkt op de structuur van spongieus bot. Hoofdstuk 4 beschrijft pogingen om deze structuur te verbeteren met betrekking tot de mechanische eigenschappen door de spons te coaten met meerdere lagen van de Ti6Al4V-dispersie. Uiteindelijk kwamen poriegrootte en porievolume overeen met die van spongieus bot. De drukkracht was hoger en de Young's modulus lag tussen die van spongieus en corticaal bot.

In hoofdstuk 5 beschrijven we de ontwikkeling van een methode ter vervaardiging van poreus titanium met behulp van een nieuwe “3D fiber deposition” (3DF) techniek waardoor een nauwkeurige controle over parameters als poriegrootte, porositeit en porie-interconnectiviteit mogelijk wordt. We zijn hierdoor in staat zowel de uitwendige vorm als de interne poriestructuur van een implantaat te bepalen. In de hoofdstukken 6 en 7 wordt de invloed van verschillende geometrieën op de mechanische eigenschappen en de permeabiliteit van zulke scaffolds onderzocht. De resultaten bevestigen de geschiktheid van de 3DF techniek voor maatwerk waar het de 3D-poriestructuur betreft. Hierdoor wordt ook een elegante mogelijkheid verkregen om de invloed van zulke structuurparameters op *in-vivo* botvorming te bepalen.

Hoofdstuk 8 omvat een vergelijkende studie naar de structuur, mechanische eigenschappen en permeabiliteit van de met beide methoden verkregen scaffolds. Waar de macrostructuren van de scaffolds verschilden, bleek de microstructuur gelijk te zijn. Beide scaffolds vertoonden een open poreuze structuur. De 3DF scaffolds bezaten een tamelijk regelmatige structuur terwijl de spons gerepliceerde scaffolds de veel onregelmatiger structuur van spongieus bot vertoonden. De druksterkte en Young's modulus van beide soorten scaffolds waren hoger dan die

van spongieus bot maar de permeabiliteit was van een vergelijkbare grootte. Uit een *in-vivo* studie bleek dat de hoeveelheid nieuw gevormd bot in het geval van spons gerepliceerde implantaten hoger lag dan bij 3DF implantaten, waarbij ook bleek dat grotere poriën en een hogere porositeit gunstig zijn voor celhechting en spreiding, vascularisatie en dus voor de vorming van nieuw bot.

In hoofdstuk 9 wordt onderzoek beschreven waarbij poreuze Ti6Al4V scaffolds met verschillende, door 3DF verkregen structuren werden geïmplantéerd op de van cortex ontdane processen van de achterste lumbale wervels van geiten teneinde de invloed van de poriearchitectuur op botvorming te bepalen. De resultaten lieten zien dat niet alleen poriegrootte en porievolume maar ook de diameter van de interconnecties tussen de poriën de osteoconductive eigenschappen van deze titanium implantaten beïnvloeden.

Hoofdstuk 10 beschrijft een studie naar de biologische reacties op 3DF Ti6Al4V implantaten al of niet gecombineerd met poreus bifasisch calcium-fosfaat en al of niet na vooraf te zijn beladen met autologe stromale beenmergcellen ("tissue engineering") die waren geïmplantéerd intramusculair in de rugspieren of op de processen van ruggenwervels van geiten. De resultaten laten zien dat de chemische samenstelling van groot belang is voor het functioneren van een botvervangend materiaal. Titanium is een bioinert materiaal en zelfs wanneer er vooraf beenmergcellen op worden gezaaid treedt er maar in beperkte mate botnieuwvorming op. Wanneer echter het materiaal wordt gecombineerd met een bioactief materiaal als calcium-fosfaat keramiek, heeft dat een sterk verbeterende invloed op de osteoconductive en osteoïnductive van het implantaat.

Het onderzoek dat in dit proefschrift is gepresenteerd toont aan dat zowel spons replicatie als 3D fiber deposition geschikte methoden zijn om van titanium(legeringen) poreuze scaffolds te vervaardigen met goed gecontroleerde structurele karakteristieken en dus mechanische eigenschappen. In potentie zijn beide technieken geschikt voor het succesvol vervaardigen van orthopedische en tandheelkundige implantaten.

Acknowledgements

First of all, my greatest thanks and admiration go to my promoters Prof. Klaas de Groot and Prof. Clemens van Blitterswijk. I am thankful to both of you for giving me the opportunity to pursue my PhD within your group. Dear Klaas and Clemens, you have created a truly unique environment for doing a doctorate. Your strength lies in enabling your students to realize their research ideas by giving them all the freedom, advice and support they need, while accepting the differences between the individuals without judging them. Dear Klaas, I greatly appreciate your availability, guidance and feedback. It is you who introduced me to the, for me completely new area of biomaterials and I am still glad you did so. Dear Clemens, although we did not often discuss things, I appreciate your clear scientific ideas, your enthusiasm, your criticism and your compliments.

I would like to thank my co-promotor, Dr. J. R. de Wijn. Dear Joost, I enjoyed working with you in the lab and talking to you in your office. Numerous discussions we had about my work and your vast knowledge of biomaterials have been proven very valuable for my research. You have millions of ideas and solid practical experience, and you are able to find a solution for almost every problem. Thanks for your patience in correcting my Chinese English.

I would also like to express my gratitude to the colleagues and former colleagues at IsoTis and PhD Pool who made my work a real pleasure and who contributed to this thesis in one way or another. A special thank you goes to Viola van der Lee who took care of many of my personal problems in the Netherlands. Clayton, thanks for your support and helpful discussions. I am glad we worked together and I sincerely hope that PoroGen will be a great success. Other people I would like to thank for their contribution to my work are: Florence, Pierre, Joost, Jens, Jerome, Mirella, Roka, Linda, Jeanine, Inge, Pascal, Paul, Jeroen, Chantal, Tara, Moyo, Fabienne, Peter, Frederic, Remco, Peter Paul, Steven, Tim, Jos, Annette, Janita.

To my fellow colleagues in Twente: Jan, Lorenzo, Aart, Jeroen, Ineke, Audrey, Andre, Hüge, Sanne, Jojanneke, Doreen, Ram, Soledad, Nicolas, Gustavo, Anouk, Anand, Remi, Hemant, thank you all, I really enjoyed the lively, fresh and inspiring atmosphere in the lab. I wish you all the best in your further work.

I am very grateful to my Chinese friends Huipin Yuan, Shihong Li, Jun Liu, Chang Du, Maria Liu, Yanling Xiao, Hongjun Wang, Jiawei Wang, Liang Yang, Feng Bai, Amos Zhao. Thanks for your help and support in many ways.

My special thanks goes to two ladies, Pamela and Zhao Fu. Dear Pamela, thank you for all you have done for me. It was great working with you in the Rainbow team, Ph.D Pool and Twente. Dear Zhao, I am glad we have met in the

Acknowledgements

Netherlands. It is a great feeling to know we can talk about everything and thank you for the beautiful design of the cover of my thesis. Both of you are very kind and great friend.

I greatly appreciate all the unconditional support and continuous motivation from my family and friends in China and abroad.

Last but not least my greatest thanks goes to my wife Kang Sun and my son HaoXuan Li, for their enduring love, support and inspiration.

JiaPing Li

Curriculum Vitae

JiaPing Li was born on Oct 23 1965 in Luan, Anhui province, middle of China. After the graduation from the first middle school of Luan in July of 1984, he went to the department of material science and engineering in Beijing University of aeronautics and astronautics (BUAA) in Beijing, whereby he was awarded a Bachelor degree in material science in July. 1988. Thereafter, he worked as a research technician in casting factory in Hebei province for two years. In Sep. 1990, he went to the department of manufacture engineering in BUAA, where by he was award a Master degree in mechanical engineering in March of 1993. He worked as a lecturer in BUAA since April of 1993. From Mar 2000 until Mar 2003 he worked as a research scientist at IsoTis NV, Bilthoven, The Netherlands on development of porous titanium scaffold. In April 2003 he started as a PhD student at University of Twente, Institute for Biomedical Technology on the 3D hard printing under supervision of Prof. Klaas de Groot and Prof. Clemens A. van Blitterswijk. In Oct. 2004, he also worked for PoroGen. B.V. for development of porous titanium for orthopaedic implant.